AD-A034 788 NAVAL SURFACE WEAPONS CENTER WHITE OAK LAB SILVER SP--ETC F/G 13/13
A GENERALIZED FINITE DIFFERENCE ELEMENT FOR THE THERMOELASTIC S--ETC(U)
JUN 76 R J EDWARDS

UNCLASSIFIED NSWC/WOL/TR-76-66 NL

1 OF 4
AD
A034788



AD A034788

NSWC/WOL/TR 76-66

NSWC/WOL/TR 76-66

NSWC TECHNICAL REPORT

WHITE OAK LABORATORY

A GENERALIZED FINITE DIFFERENCE ELEMENT FOR THE THERMOELASTIC STRUCTURAL RESPONSE OF ANISOTROPIC THIN SHELLS

BY
Robert J. Edwards

JUNE 1976

NAVAL SURFACE WEAPONS CENTER
WHITE OAK LABORATORY
SILVER SPRING, MARYLAND 20910

- Approved for public release; distribution unlimited

DDC
RECEIVED
JAN 26 1977
A

NAVAL SURFACE WEAPONS CENTER
WHITE OAK, SILVER SPRING, MARYLAND 20910

UNCLASSIFIED

SECURITY CLASSIFICATION OF THIS PAGE (When Data Entered)

REPORT DOCUMENTATION PAGE

READ INSTRUCTIONS BEFORE COMPLETING FORM

1. REPORT NUMBER: NSWC/WOL/TR-76-66	2. GOVT ACCESSION NO.
3. RECIPIENT'S CATALOG NUMBER: (9) Technical rept.
4. TITLE (and Subtitle): A Generalized Finite Difference Element for the Thermoelastic Structural Response of Anisotropic Thin Shells.	5. TYPE OF REPORT & PERIOD COVERED
	6. PERFORMING ORG. REPORT NUMBER
7. AUTHOR(s): Robert J. Edwards	8. CONTRACT OR GRANT NUMBER(s): (16) F 32-322; (17) SF 32322 507
9. PERFORMING ORGANIZATION NAME AND ADDRESS: Naval Surface Weapons Center, White Oak Laboratory, Silver Spring, Maryland 20910	10. PROGRAM ELEMENT, PROJECT, TASK AREA & WORK UNIT NUMBERS: SEA 18457/SF32-322-507
11. CONTROLLING OFFICE NAME AND ADDRESS	12. REPORT DATE: June 1976
	13. NUMBER OF PAGES: 312 (12) 314
14. MONITORING AGENCY NAME & ADDRESS (if different from Controlling Office)	15. SECURITY CLASS. (of this report): UNCLASSIFIED
	15a. DECLASSIFICATION/DOWNGRADING SCHEDULE

16. DISTRIBUTION STATEMENT (of this Report)

Approved for public release; distribution unlimited

17. DISTRIBUTION STATEMENT (of the abstract entered in Block 20, if different from Report)

18. SUPPLEMENTARY NOTES

19. KEY WORDS (Continue on reverse side if necessary and identify by block number)

Structural Analysis	Matrix Methods
Thin Shells	Anisotropic Materials
Energy Methods	Thermal Stresses
Finite Elements	Tensor Analysis
Finite Differences	Isoparametric Mapping

391 596

20. ABSTRACT (Continue on reverse side if necessary and identify by block number)

Two well established matrix methods for thin shell structural analysis, the finite element method and the finite difference energy method, have been integrated into one unified analytical approach and have been effectively applied to the thermoelastic analysis of anisotropic thin shells. The finite element method is a widely used tool for structural analysis of thin shells due to its ability to model the complex geometries that occur in

DD FORM 1 JAN 73 1473 EDITION OF 1 NOV 65 IS OBSOLETE S/N 0102-014-6601

UNCLASSIFIED

SECURITY CLASSIFICATION OF THIS PAGE (When Data Entered)

20.

engineering practice. In recent years, it has been demonstrated that the finite difference energy method offers significant advantages over contemporary finite element formulations especially for problems involving geometrical nonlinearities. However, the method suffers from the modeling restrictions imposed by rectangular gridworks which must follow the shell coordinate lines. The results of this research demonstrate that this classic restriction can be removed and that a generalized finite difference energy method can be developed for arbitrary quadrilateral meshes. Furthermore, the formulation is amenable to installation in contemporary, general purpose, finite element computer programs.

The SHEFA generalized finite difference element for the thermoelastic analysis of anisotropic thin shells is developed herein. The term SHEFA is an acronym for SHell Element based on a Finite difference Approach. The shell reference surface geometry is described in terms of curvilinear surface coordinates using tensor notation. The deformation of the shell is described by the linear strain and curvature change tensors of Sanders. A shell wall model has been developed that is sufficiently general to treat a broad range of wall constructions including layered orthotropic walls, filament wound walls and angle ply composite walls as well as more conventional monocoque construction. The model treats the effects of nonlinear temperature gradients through the shell wall, including material property temperature dependence, and also accounts for coupling between membrane and bending action. Isoparametric mapping techniques have been used to establish a finite difference approximation of the strain and curvature tensors in terms of displacement variables at arbitrarily placed discrete nodes on the shell reference surface. The potential energy of the structural system is then formed in terms of the nodal variables and the equations of motion are obtained by use of the Minimum Potential Energy Theorem.

A series of twelve demonstration problems were solved to verify the accuracy and convergence characteristics of the element in a variety of applications and to demonstrate the generality of the element via several problems that are most efficiently modeled with arbitrary meshes. The SHEFA predictions were verified against classical analytical solutions or experimental results, and in some cases, the results obtained with finite element formulations were available for comparison.

NSWC/WOL/TR 76-66 1 June 1976

A GENERALIZED FINITE DIFFERENCE ELEMENT FOR THE THERMOELASTIC STRUCTURAL RESPONSE OF ANISOTROPIC THIN SHELLS

This report describes a newly developed numerical method for predicting the thermoelastic response of anisotropic thin shell structures. The theoretical development and report preparation was sponsored under the Naval Surface Weapons Center Advanced Graduate Study Program. The computer coding and check out of the analysis method was funded under the Structural Technology for Advanced Re-entry Systems (STAR) exploratory development program as one task in the general area of re-entry vehicle structural analysis methods development.

The results of this investigation have been accepted by the University of Maryland as a thesis in partial fulfillment of the requirements of the Doctor of Philosophy Degree in Mechanical Engineering.

The author wishes to acknowledge the programming assistance of Mr. Myles Hurwitz of the Navy Nastran Systems Office, Naval Ship Research and Development Center.

Leon H. Schindel

LEON H. SCHINDEL
By direction

Buff Section
A

TABLE OF CONTENTS

Chapter		Page
I.	INTRODUCTION	19
	A. Discrete Element Analysis	19
	B. Historical Review - Finite Element Method	22
	C. Historical Review - Finite Difference Energy Method	40
	D. Comparison of Finite Element Method and Finite Difference Energy Method	50
	E. Objective and Synopsis of Research	57
II.	SHELL THEORY	59
	A. Surface Geometry	59
	B. Deformation of the Shell	66
III.	GENERAL DESCRIPTION OF THE ANALYSIS METHOD	69
IV.	THEORETICAL DEVELOPMENT OF SHEFA ELEMENT	73
	A. General Remarks	73
	B. Thin Shell Strain Energy	75
	1. Strain Energy Density	75
	2. Shell Wall Model	79
	3. Strain-Displacement and Curvature-Displacement Relations	87
	4. Finite Difference Approximation to Strain and Curvature Change Tensors	90
	5. Coordinate Transformations	106
	6. Element Stiffness Matrix	117
	7. Element Thermal Load Vector	121

Page

C. Potential Energy of Mechanical and Inertial Loads..... 124

1. Total Work Potential..... 124

2. Element Mass Matrix..... 127

3. Element Surface Load Vector..... 133

4. Concentrated Force Vector..... 136

5. Concentrated Moment Vector..... 141

6. Element Gravity Load Vector..... 144

D. Calculation of Structural Response..... 147

E. Boundary Conditions..... 161

V. ANALYTICAL RESULTS..... 166

A. Introduction..... 166

B. Membrane Plate Study..... 170

C. Isotropic Plate Bending Study..... 172

D. Anisotropic Plate Bending Study..... 178

E. Arbitrary Mesh Example - Bending of Rhombic Cantilever Plate..... 181

F. Cylindrical Shell Bending Study..... 183

G. Cylindrical Shell Thermal Stress Study..... 186

H. Arbitrary Mesh Example - Cylindrical Shell With Circular Cutout..... 188

VI. CONCLUSIONS..... 191

APPENDIX A. Tables..... 195

APPENDIX B. Figures..... 205

APPENDIX C. Discussion of Shape Functions..... 249

APPENDIX D. Inverse Functional Relationship Between Surface Coordinates and Parametric Interpolating Coordinates... 259

Page

APPENDIX E. Shell Reference Surface Geometries.... 275

REFERENCES..... 301

LIST OF TABLES

Tables		Page
1	Curved, Thin Shell, Finite Elements With Four Sides	196
2	Curved, Thin Shell, Finite Elements With Three Sides	197
3	Abscissae of Integration Points and Weight Coefficients for the Gaussian Quadrature Formula	198
4	Correspondence Between Element Interpolating Coordinates and Element Connection Number	199
5	Summary of Demonstration Problems	200
6	Flat Plate Membrane Behavior Displacement Solutions	201
7	Flat Plate Membrane Behavior Stress Solutions	202
8	Stress Concentrations in an Axially Loaded Cylindrical Shell With a Circular Hole	203

LIST OF FIGURES

Figures		Page
1	STAGS Finite Difference Mesh Schemes	206
2	Finite Difference Mesh Scheme by Johnson [110]	207
3	Discrete Elements for Comparative Study by Bushnell [114]	208
4	Shell Geometry and Coordinate Systems	209
5	Shell Wall Model	210
6	Temperature Gradient Through Shell Wall	211
7	SHEFA Element Geometry	212
8	Element Edge Coordinate System	213
9	Sign Conventions for Displacements, Rotations and Stresses	214
10	Sign Conventions for Force and Moment Resultants Acting on Reference Surface	215
11	Analysis Conditions for Plate Under Parabolic Edge Load	216
12	Meshes for Membrane Plate Study	217
13	Summary of Analysis Conditions for Plate Bending Problems	218
14	Typical Mesh for Plate Bending Problems With Simply-Supported Edges	219
15	Typical Mesh for Plate Bending Problems With Fixed Edges	220
16	Convergence of Central Deflection vs Mesh Size for Isotropic, Simply-Supported Plate Under Uniform Load	221
17	Convergence of Central Deflection vs Mesh Size for Isotropic, Simply-Supported Plate Under Concentrated Load	222

Figures

		Page
18	Convergence of Central Deflection vs Mesh Size for Isotropic, Clamped Plate Under Uniform Load.....	223
19	Convergence of Central Deflection vs Mesh Size for Isotropic, Clamped Plate Under Concentrated Load.....	224
20	Convergence of Central Deflection vs Degrees of Freedom for Isotropic, Simply-Supported Plate Under Uniform Load.....	225
21	Convergence of Central Deflection vs Degrees of Freedom for Isotropic, Simply-Supported Plate Under Concentrated Load.....	226
22	Convergence of Central Deflection vs Degrees of Freedom for Isotropic, Clamped Plate Under Uniform Load.....	227
23	Convergence of Central Deflection vs Degrees of Freedom for Isotropic, Clamped Plate Under Concentrated Load.....	228
24	Convergence of Central Deflection vs Mesh Size for Simply-Supported Orthotropic Plate Under Uniform Load.....	229
25	Convergence of Central Deflection vs Mesh Size for Anisotropic Plate (10 Layer, $\pm 30^\circ$ Angle-Ply Composite) Under Uniform Load.....	230
26	Convergence of Central Deflection vs Mesh Size for Anisotropic Plate (2 Layer, Cross-Ply Composite) Under Uniform Load.....	231
27	Deflection of Uniformly Loaded Rhombic Cantilever.....	232
28	Cantilevered Rhombic Plate, 13x13 Mesh.....	233
29	Comparison of Predicted Displacements vs Experiment for Cantilevered Rhombic Plate Under Uniform Load.....	234

Figures

		Page
30	Summary of Analysis Conditions for Cylindrical Shell With Circumferential Line Load	235
31	Typical Mesh for Cylindrical Shell Bending Problem	236
32	Convergence of Deflection Under Load vs Mesh Size for Cylindrical Shell With a Load Uniformly Distributed Along a Circular Section	237
33	Displacement Distribution for Cylindrical Shell With a Load Uniformly Distributed Along a Circular Section	238
34	Moment Distribution for Cylindrical Shell With a Load Uniformly Distributed Along a Circular Section	239
35	Summary of Analysis Conditions for Cylindrical Shell With Nonlinear Radial Temperature Gradient	240
36	Cylinder With Nonlinear Radial Temperature Gradient, 3x20 Mesh	241
37	Material Property Temperature Dependence for Cylindrical Shell With Nonlinear Radial Temperature Gradient	242
38	Temperature Distribution Through Shell Wall for Cylindrical Shell With Nonlinear Radial Temperature Gradient	243
39	Stress Distribution Through Shell Wall for Cylindrical Shell With Nonlinear Radial Temperature Gradient	244
40	Summary of Analysis Conditions for Cylindrical Shell With Circular Cutout Loaded in Tension	245
41	Cylindrical Shell With Circular Cutout, 20x20 Mesh	246
42	Cylindrical Shell With Circular Cutout, Enlargement of 20x20 Mesh in Vicinity of Hole	247

LIST OF SYMBOLS

The following is a list of symbols used in the analytical developments of Chapters II through IV:

a	determinant of metric tensor
$a_{\alpha\beta}, a^{\alpha\beta}$	metric tensors
$\vec{a}_\alpha$	base vectors for Gaussian surface coordinates
$[a_M]$	matrix defined by (IV.194)
A	area
A_α	Lame´ parameters
$b_{\alpha\beta}, b^\alpha_\beta, b^{\alpha\beta}$	initial curvature tensors
$[\bar{b}]$	matrix defined by (IV.138)
$[B]$	bending compliances for shell wall
$[C]$	coupling compliances for shell wall
$[D]$	membrane compliances for shell wall
$\vec{e}_\alpha$	unit vectors for Gaussian surface coordinates
$\vec{e}_3$ or $\vec{e}_n$	unit vector along outward normal to shell reference surface
$\vec{e}_t, \vec{e}_s$	unit vectors tangent and normal to an element edge
$\{e\}$	physical strain components at point on shell reference surface
$\{\bar{e}\}$	physical strain components at point off shell reference surface
E_{11}, E_{22}	orthotropic moduli of elasticity
E_{12}	orthotropic shear modulus
$[E]$	matrix relating membrane displacement gradient vector to element displacement vector, see (IV.105)

$\mathbf{E}^{\alpha\beta\lambda\rho}$	elastic material constant tensor relating strain to stress
$[\mathbf{E}]$	matrix form of elastic material constant tensor
$\vec{F}$	externally applied concentrated force
$\vec{F}_g$	gravity force
$[F]$	matrix relating bending displacement gradient vector to element displacement vector, see (IV.84)
$\mathbf{F}_{\alpha\beta\lambda\rho}$	elastic material constant tensor relating stress to strain
$[\mathbf{F}]$	matrix form of elastic material constant tensor
$\vec{g}$	gravity vector
$[G]$	matrix form of physical material constants relating strain to stress
H_i	weighting coefficients for Gaussian quadrature formula
$H_1,\ldots,H_9$	quadratic shape functions
$[H]$	matrix of quadratic shape functions
$\vec{I}_i$	unit vectors for basic coordinates
$[J_1]$	Jacobian matrix for in-plane displacement gradients, see (IV.75)
$[J_2],..,[J_5]$	Jacobian matrices for normal displacement gradients, see (IV.92)
$[\mathbf{K}_e]$	tensor form of element stiffness matrix
$[\overline{\mathbf{K}}_e]$	physical form of element stiffness matrix
$[\overline{\mathbf{K}}]$	system stiffness matrix
$L_1,\ldots,L_4$	linear shape functions
$[L]$	matrix of linear shape functions

$\bar{m}_e$	element mass per unit area
$\bar{m}_{ns}$	non-structural mass per unit area
$\bar{m}_e^C$	first moment of the element mass per unit area
$\bar{m}_e^R$	second moment of the element mass per unit area
$\vec{\bar{M}}$	externally applied edge moment resultant
$\tilde{M}_1, \tilde{M}_2$	components of $\vec{\bar{M}}$ in shell coordinates
$\tilde{M}_t, \tilde{M}_s$	components of $\vec{\bar{M}}$ in edge coordinates
$\{\bar{M}\}$	internal moment resultants
$\{M_T\}$	thermal moments
$[\bar{M}_e^T]$	element mass matrix due to translational inertia
$[\bar{M}_e^R]$	element mass matrix due to rotational inertia
$[\bar{M}_e^C]$	element mass matrix due to coupling between translational and rotational inertia
$[\bar{\mathbf{M}}_e]$	physical form of element mass matrix
$[\bar{\mathbf{M}}]$	system mass matrix
$\vec{\bar{N}}$	externally applied edge force resultant
$\tilde{N}_1, \tilde{N}_2, \tilde{N}_n$	components of $\vec{\bar{N}}$ in shell coordinates
$\tilde{N}_t, \tilde{N}_s, \tilde{N}_n$	components of $\vec{\bar{N}}$ in edge coordinates
$\{\bar{N}\}$	internal force resultants
$\{N_T\}$	thermal forces
$\vec{\bar{p}}$	externally applied surface load
$\{\mathbf{P}_T\}_e$	tensor form of element thermal load vector
$\{\bar{\mathbf{P}}_T\}_e$	physical form of element thermal load vector
$\{\bar{\mathbf{P}}_p\}_e$	element load vector due to surface loading
$\{\bar{\mathbf{P}}_F\}$	load vector due to concentrated force
$\{\bar{\mathbf{P}}_Q\}$	load vector due to concentrated moment

$\{\bar{P}_g\}_e$	element gravity load vector
$\{\bar{P}\}$	system load vector
$\{q\}$	system displacement vector
$\vec{Q}$	externally applied concentrated moment
$\{Q\}$	physical form of thermal stress term in constitutive equation
$\vec{r}$	position vector of a point on shell reference surface
$[R]$	shell geometry matrix relating curvature change vector to bending displacement gradient vector, see (IV.66)
dS_α	incremental arc lengths in surface coordinate directions
dS	incremental arc length
ΔS_α	arc length in surface coordinate directions between two corner nodes of an element
ΔS	length of an element side
$[S]$	shell geometry matrix relating strain vector to membrane displacement gradient vector, see (IV.59)
T_κ	temperature at points through shell wall
ΔT	temperature change from reference state
$[T_E]$	transformation relating covariant displacement vector to element displacement vector, see (IV.114)
$[T^H]$	transformation relating normal displacement gradients to element displacement vector, see (IV.102)
$[T_H]$	partition of $[T^H]$, see (IV.134)
$[\bar{T}_H]$	augmented form of $[T_H]$, see (IV.140)
$[T^L]$	transformation relating in-plane displacement gradients to element displacement vector, see (IV.78)

$[T_L]$	partition of $[T_E]$, see (IV.130)
$[\bar{T}_L]$	augmented form of $[T_L]$, see (IV.139)
$[T_P]$	transformation for rotation of physical elastic constants from material coordinates to shell coordinates
$[T_Q]$	transformation for rotation of physical coefficients of expansion from material coordinates to shell coordinates
$[T_u],[T_w]$	transformations relating covariant displacement vector to physical displacement vector and vice-versa, see (IV.285-IV.288)
$[T^u],[T^w]$	transformations relating contravariant displacement vector to physical displacement vector and vice-versa, see (IV.285-IV.288)
$[T_v]$	partition of $[T_u]$, see (IV.129)
$[T_W]$	transformation relating the tensor and physical forms of the element displacement vector, see (IV.120)
$[T_W^I]$	transformation relating the tensor and physical components of displacement at a node.
$[T_{W_{12}}],[T_{W_3}]$	partitions of $[T_W]$, see (IV.120)
$[T_\gamma],[T_e]$	transformations relating tensor and physical components of strain, see (IV.300-IV.302)
$[T_\omega]$	transformation relating covariant rotation vector to element displacement vector, see (IV.141)
$[T_\vartheta]$	transformation relating physical rotation vector to element displacement vector, see (IV.157)
$[T_\tau],[T_\sigma]$	transformations relating tensor and physical components of stress, see (IV.311-IV.314)
$\vec{u}$	displacement vector at a point on shell reference surface
$\vec{\bar{u}}$	displacement vector at a point off shell reference surface
u^α, u_α	tensor components of in-plane displacement

u_α^K	nodal values of the tensor components of in-plane displacement
$\{u\}$	covariant displacement vector
$\{\tilde{u}\}$	contravariant displacement vector
U	strain energy
U_o	strain energy density
$\bar{U}$	strain energy per unit area
$\bar{U}_o$	strain energy density per unit area
$\{U\}$	membrane displacement gradient vector, see (IV.57)
$\{V\}$	bending displacement gradient vector, see (IV.64)
w	normal component of displacement
$\bar{w}_e$	element weight per unit area
W	potential of externally applied mechanical and inertial loads
$\{w\}$	physical displacement vector
$\{W\}$	tensor form of element displacement vector, see (IV.83)
$\{\bar{W}\}$	physical form of element displacement vector, see (IV.119)
$\{W_1\},\{W_2\}$	nodal point displacement vectors, see (IV.67)
$\{W_{12}\},\{W_3\}$	partitions of $\{W\}$, see (IV.116)
$\{\bar{W}_{12}\}$	partition of $\{\bar{W}\}$, see (IV.119)
x^α	Gaussian surface coordinates
x^3	outward normal to shell reference surface
x_k^M	nodal values of surface coordinates

X^i	basic Cartesian coordinates
z	shell thickness coordinate
α, β	interpolating coordinates for quadratic shape functions
$\{\alpha\}$	physical coefficients of expansion
$\gamma_{\alpha\beta}$	reference surface strain tensor
$\bar{\gamma}_{\alpha\beta}$	strain tensor at a point off the reference surface
$\Gamma^{\alpha}_{\beta\lambda}$	Christoffel symbols of the second kind
$\{\gamma\}$	reference surface strain tensor components
$\{\bar{\gamma}\}$	components of strain tensor at a point off the reference surface
δ^{α}_{β}	Kronecker's delta, see (II.15)
$\epsilon_{\alpha\beta}$	coefficient of expansion tensor
$\{\epsilon\}$	components of coefficient of expansion tensor
$\vec{\theta}$	rotation vector
$\theta_{\alpha}, \theta^{\alpha}$	tensor components of rotation vector
$\vec{\vartheta}$	alternate form of rotation vector
$\{\theta\}$	covariant components of rotation vector
$\{\vartheta\}$	physical components of alternate form of rotation vector
$\{\kappa\}$	physical bending strain components
λ, μ	interpolating coordinates for linear shape functions
ν_{12}, ν_{21}	orthotropic Poisson's ratios
π	potential energy

ρ	mass density
$\{\bar{\sigma}\}$	physical stress components at a point off shell reference surface
$\tau^{\alpha\beta}$	stress tensor at a point on shell reference surface
$\bar{\tau}^{\alpha\beta}$	stress tensor at a point off shell reference surface
$\{\bar{\tau}\}$	tensor stress components at a point off shell reference surface
ϕ	anisotropic material orientation angle
Φ	angle between surface coordinates
$\chi_{\alpha\beta}$	curvature change (bending strain) tensor
$\{\chi\}$	bending strain tensor components
ψ	angle between the unit vector tangent to an element edge, and the surface coordinate x^1
Ψ_α	physical components of rotation vector
$\{\Psi\}$	physical components of rotation vector
$\Omega^{\alpha\beta}$	tensor form of thermal stress term in constitutive equation
$\{\Omega\}$	tensor components of thermal stress term in constitutive equation

SUBSCRIPTS AND SUPERSCRIPTS

B	bending action
C	coupling between membrane and bending action
e	element
F	concentrated force
g	gravity force
I	inner surface or inertial load
m	material coordinates
M	membrane action
n	normal to shell reference surface
O	outer surface
p	surface pressure
Q	concentrated moment
S	shell
T	thermal force
T_B	thermal bending action
T_M	thermal membrane action

CHAPTER I

INTRODUCTION

A. Discrete Element Analysis

In order to obtain solutions to practical problems in structural mechanics, discrete element numerical procedures utilizing the finite element method or the finite difference method are most often used. The classical analysis of continuous systems begins with the establishment of relationships between various quantities associated with small differential elements. Partial differential equations or integral equations governing the behavior of the entire domain are obtained by allowing the dimensions of the differential element to approach zero as the number of elements becomes large. In contrast, discrete element methods begin with the investigation of properties of elements of finite dimensions. The properties are established through direct use of equilibrium and compatibility relationships from the theory of elasticity or by use of variational methods and energy principles. Integrations are replaced by finite summations and the partial differential equations of the continuous domain with infinite degrees of freedom (d.o.f.) are replaced by a system of algebraic equations which have a finite number of degrees of

freedom. If certain continuity, admissibility and completeness conditions [1-7]* are satisfied in the formulation of the discrete element, the behavior of the discrete system converges to that of the continuous system as the number of discrete elements is increased and their dimensions are decreased. Discrete element methods are in principle applicable to the analysis of the static and dynamic, linear and nonlinear deformation and material behavior of anisotropic, nonhomogeneous bodies of any geometrical shape with arbitrary boundary conditions.

This paper is concerned with the analysis of thin shell structures by discrete element methods. Thin shells are widely used as structural elements where lightweight construction is necessary. Prior to the advent of computerized discrete elements, only simple, highly idealized shell problems could be solved. With the evolution of discrete structural analysis methods, the state of the art has advanced dramatically during th e past fifteen years. Solutions to complex shell problems involving geometric and material nonlinearities, anisotropic and inhomogeneous material behavior, discrete stiffening and local reinforcement, arbitrary geometries and boundary conditions and general loadings are now feasible.

Hartung [8,9] has recently conducted assessments of current capability for computer analysis of shell structures.

*Brackets [ ] indicate references and parentheses ( ) indicate equations

As he points out, the analysis of most practical shell problems can only be treated by discrete methods. The only two such methods which have found widespread application are the finite element and finite difference methods, both of which have been extensively developed. The relative advantages and disadvantages of the two methods will be discussed in a later section following an historical review of both methods.

B. Historical Review-Finite Element Method

Since its inception about 20 years ago, the finite element method, in conjunction with the digital computer, has evolved into the numerical procedure most commonly used for many classes of structural analysis problems. The wide use of finite element methods is due in large part to their generality, i.e., their ability to model the complex structural configurations that occur in modern engineering practice.

Oden [10] has reviewed the evolution of the concept of representing continuous functions by piecewise approximations which was followed by the introduction, in the early days of aircraft structural analysis, of the practice of representing a structural system by a collection of discrete elements. He cites the works of Kron, Hrennikoff, Courant, Polya, Prager and Synge, as being important. In 1954, Argyris and his coworkers began a series of papers which generalized, extended and unified the fundamental energy principles for the analysis of elastic structures. Reference [11] summarizes this work and presents in considerable detail methods for analyzing complex, discrete aircraft structures in forms easily adapted to automatic computation. Turner, Clough, Martin and Topp [12] are generally credited with the first presentation of the finite element method together with the direct stiffness method for assembling elements to represent a complex structure. It remained for Clough [13]

in 1960 to first coin the term "finite elements" in a paper which addressed plane stress problems. In the last 15 years hundreds of papers have been published on the subject. References [3,14-22] represent important collections of papers and together with [10,23-26] give a good overview of the evolution of the method.

In the 1960's both the force (flexibility) and displacement (stiffness) methods of matrix structural analysis were in common use for the analysis of discrete element systems [14]. These methods are defined simply as a solution procedure formulated directly in terms of unknown forces for the force method and in terms of unknown displacements for the displacement method.

The matrix force method for the analysis of statically indeterminate structures evolved from indeterminate frame and truss analysis in Civil Engineering which is based on the application of the principles of least work, Castigliano's theorem or virtual work. The force method is characterized by the selection of an internal force system which is in equilibrium with the external loads, but since compatibility conditions are not satisfied for this basic system, it is necessary that a redundant load system be selected which in combination with the basic system produces a state of compatible displacement. In modern practice, a rigorous derivation of elements for the force method is based on complementary energy theorems. The method is still popular in certain segments of the aircraft industry but the

displacement method is far more widely used primarily due to problems associated with automating the selection of a redundant load system.

Initial attempts at element formulation for the displacement method utilized the so-called "direct approach" in which element properties were developed through the direct use of equilibrium and compatibility relationships as defined by the pertinent differential equations of elasticity theory. This approach was found to be unsatisfactory for reasonably complex elements because the method failed to yield symmetric stiffness matrices [14].

A rigorous theoretical basis for the formulation of finite elements was introduced when variational methods came into common use. In this context, the finite element displacement method may be viewed as a generalization of the Rayleigh-Ritz method in the calculus of variations. In both methods the total potential energy is formulated and the displacement pattern is expressed in terms of a set of undetermined parameters, which are defined at discrete nodes in the finite element method. A set of simultaneous equations is formed which minimizes the total potential energy with respect to the undetermined parameters. The difference between the two methods is in the manner in which the displacements are prescribed. In the Rayleigh-Ritz procedure the displacements are usually specified by

admissible displacement functions which satisfy the boundary conditions of the entire structure while in the finite element process this specification is piecewise.

The principle of minimum potential energy states: "Of all admissible displacements satisfying the given boundary conditions, those which satisfy the equations of equilibrium are distinguished by a stationary (extreme) value of the potential energy." The potential energy is a minimum for "actual" displacements only in the neighborhood of the stable equilibrium state, where the strain energy is positive definite [27].

Abstracting the discussion of Gallagher [33], the finite element formulation generally adheres to the following sequence. For stable equilibrium the potential energy (π) is a minimum ; thus

$$\delta\pi = \delta U - \delta W = 0 \qquad \text{(I.1)}$$

where U is the strain energy of the system and W is the potential of the applied loads. The strain energy can be cast in the form,

$$U = \frac{1}{2} \int_V \{e\}^T [E] \{e\} dV \qquad \text{(I.2)}$$

where the integral is taken over the volume (V) of the element, the matrix [E] contains the coefficients of the

the constitutive equations and {e} is a vector of strain measures.

The key operation in the development is then the selection of admissible displacement fields in terms of nodal displacements, {q}. Then by application of the strain-displacement equations, expressions, [D], are obtained which relate the strain vector to the nodal displacement vector. Thus

$$\{e\} = [D]\{q\} \tag{I.3}$$

Substituting (I.3) into (I.2) results in the quadratic form,

$$U = \{q\}^T \int_V [D]^T[E][D]dV \{q\} \tag{I.4}$$

By application of the energy theorem (I.1), the element stiffness matrix, [K], is obtained in the form,

$$[K] = \int_V [D]^T[E][D]dV \tag{I.5}$$

Two significant problems arise in formulating the element stiffness matrix: the choice of admissible displacement functions which preserve the compatibility of displacement in the complete analytical model, and the performance of the integrations required by (I.5), which can be quite difficult in the case of irregular element shapes.

In 1966 a significant innovation in finite element technology, the isoparametric element, was introduced by Irons [28] who recognized the earlier unpublished work of Taig. The essence of the isoparametric concept is the interpolation of both coordinates and displacements by the same interpolation functions which are written in terms of a set of local (mapping) coordinates for the element. The isoparametric mapping leads to two significant advantages. Simple rectangular and triangular shapes can be distorted into irregular shapes (with curved boundaries if desired) which better approximate the complex geometries of practical structures. And the isoparametric formulation permits the element stiffness to be easily established through use of numerical integration.

The isoparametric concept has been extended and successfully applied to a wide range of problems by a number of researchers with Zienkiewicz and his coworkers [23,24,29,30] leading the development. But as Zienkiewicz [30] points out, the isoparametric formulation possesses essential advantages only for the class which embraces all plane and three-dimensional elasticity problems. Its extension to higher-order variational principles is not easy. A useful extension of the method to the plate-shell domain has however been made by Ahmad, et.al. [31,32], who deal with the development of "reduced" solid elements that have been degenerated in the thickness direction to approximate thin and thick shell behavior. The validity

and limitations of this approach will be deferred for later discussion.

A thorough review of the application of the finite element method to general shells* is contained in the papers by Gallagher [33,34] and the paper by Dawe [50].

As Gallagher [34] points out, the analysis of shells via finite elements is approached in one of three alternative forms:

(1) In "faceted" form by use of flat elements to approximate curved surfaces.

(2) By means of "reduced" isoparametric 3-D solid elements which have been specialized to 2-D representations of curved thick or thin shells.

(3) By curved finite elements that have been formulated directly from the theories of shallow or deep thin shells.

The finite element flat plate technology has been well developed over the past ten years. Numerous "facet" elements [35-40], both quadrilateral and triangular, have been in wide use for shell analysis for a number of years. The "facet" type of element is formulated by superposition of membrane and flexural behavior and by application of appropriate coordinate transformations (see for example, Clough and Johnson [45]).

*The term "general shell" refers to shell problems which require discretization in two surface dimensions. The more restrictive class of shell of revolution problems which requires discretization in only the meridional direction is not being addressed in this paper.

Some of the difficulties and shortcomings of the "facet" model as enumerated by Gallagher [33] are as follows:

(1) The behavior represented by the differential equations is not approached in the limit of refinement by the flat plate representation.

(2) The discontinuities of slope between adjacent elements may produce calculated bending moments in regions of the shell where none exist.

(3) The effects of curvature, in the form of the coupling of membrane and flexural behavior, are absent in the interiors of the individual elements.

In the development of degenerated isoparametric solid elements for thin and thick shell analysis, Ahmad, et.al. [31,32] imposed the requirements that the original normals to the middle surface remain straight and inextensible and the elastic modulus in the normal direction be zero to avoid normal stresses. These assumptions are compatible with thin shell theory and since the surface normals can rotate relative to the middle surface of the shell, shear deformations are approximately included.

For shells where membrane stresses are predominant, good results have been obtained with the Ahmad approach, but where bending effects are important the results have been poor when thickness/length ratios of an element become small [30]. The error arises because constant bending moments can be represented by the deformation

patterns of these elements but for a linearly varying moment excessive shear strain energy is stored [41]. Two approaches have been employed to improve this behavior. The use of approximate integration techniques in order to avoid integrating the excess shear strain energy has been successfully applied by several investigators [32,42,43]. However, Wilson [44] points out that convergence is not assured and the technique is difficult to apply in the general case of curved anisotropic elements. Wilson [44] introduced extra displacement modes (which in general violate interelement compatibility) into the element. The extra modes have the same form as the inherent errors and their magnitudes are determined by requiring that the total strain energy of the element be a minimum. This approach can be very effective but must be used with care [41].

In summary, Wilson [44], Bathe [41] and Zienkiewicz [30] discuss the limitations associated with the use of isoparametric solid elements for shell analysis. These include:

(1) Solid elements do not represent well the deformation patterns induced by bending moments except for the cubic isoparametric element with four nodes along each side.

(2) Errors in the shear and normal strains cause the element to be overly stiff.

(3) If the element is relatively thin, the stiffness coefficients corresponding to the transverse displacement are considerably larger than those associated with the in-plane displacements, which results in numerical ill-conditioning of the stiffness equations.

(4) A large number of variables have to be included when compared to more conventional analysis methods and excessive amounts of input data are required.

(5) A single element through the thickness cannot represent a layered, anisotropic shell wall construction.

The first two problems can be treated to some extent by approximate integration techniques or the incompatible mode approach. The alternative of using the cubic element is objectionable due to the relatively large amount of computer time required to form the stiffness equations. Problems three, four and five tend to restrict the application of this method to thick shells.

The development of curved finite elements on the basis of shallow or deep, thin shell theories results in a much more complicated formulation than for the flat plate or "reduced" solid representations previously discussed. Gallagher [33,34] reviews in detail the

following general difficulties:

(1) The choice of an appropriate shell theory from the many shallow and deep shell theories in the literature.

(2) The description of the curved geometry, including the definition of the element curvature from the given coordinate data and the derivation of appropriate transformations for the connection of the elements.

(3) The choice of admissible displacement fields in curvilinear coordinates. Three problems of concern in this respect are the retention of the required interelement continuity of displacement, the representation of all constant states of strain and the assurance of zero-strain energy modes of rigid body displacement.

The representation of rigid body modes by polynomial displacement fields defined in curvilinear coordinates is particularly troublesome, since satisfaction of this condition is approached in the limit only by higher order polynomials [46]. Fonder and Clough [47] have demonstrated that the importance of the zero strain condition under rigid body motion varies significantly with the application.

The net effect of these complications in curved element formulation is that most of those reported in the literature employ higher order polynomial displacement assumptions.

As a consequence, the resulting elements have a relatively large number of degrees of freedom which tends to increase stiffness matrix generation time and the bandwidth of the equations. For higher order facet and curved shell elements, the nodal degrees of freedom frequently exceed six and furthermore do not retain the physical significance that the simpler elements employ; i.e., the degrees of freedom are not translations and physical rotations but are more often translations and their spatial derivatives. This factor complicates their use in general purpose computer programs (see for example [48,49]) both from the standpoint of strategy for assembling the stiffness equations and the need to implement special constraint procedures in order to join the higher order elements to other types of elements with differing nodal degrees of freedom or to join two different surface types. The actual use of higher order shell elements in contemporary general purpose computer codes will be discussed later following a review of the available element technology.

Tables 1 and 2 summarize the major developments in curved, thin shell finite elements using the displacement approach. Many of the developers listed in Tables 1 and 2 have investigated a family of finite elements representing various perturbations on the assumed displacement functions and element assembly procedures. The element description listed in the tables

is for that element in the family which was recommended by the developer as performing best.

Table 1 summarizes the level of sophistication available in four-sided elements [51-63]. There are severe restrictions on the utility of this class of element as regard element shape and surface geometry. Several elements [51-53] are applicable only to cylindrical shells and another [54] is restricted to conical surfaces. Several elements that retain some generality in surface representation [55-60], however, are restricted to regular element shapes whose edges must lie along the curvilinear coordinate lines. The SLADE element by Key and Beisinger [61,62] is an arbitrary curvilinear quadrilateral that treats linear, static and dynamic problems with layered, orthotropic shell walls. The element also treats thermal stresses including material property temperature dependence through the thickness of the shell but the shell geometry is restricted to an axisymmetric reference surface.

The quadrilateral element by Jones [63] is based on the Marguerre shallow shell equations which are equivalent to applying an initial warping to a flat plate to form the curved shell element. This element employs a quadratic form of surface representation which includes cylinders, cones, ellipsoids, hyperboloids and paraboloids. The Jones' element has been developed for problems of small strain, large deflection and nonlinear isotropic, material behavior and hence is probably the most general of the

four-sided elements presently available. It does not however treat layered, anisotropic, shell wall construction or the effects of thermal stresses. Furthermore, Argyris and Scharpf [69], view critically the use of a shallow shell theory in element formulation, particularly with respect to kinematic compatibility between adjoining elements.

Table 2 summarizes the level of sophistication available in three-sided elements [64-72]. The triangular elements possess an inherent generality in shape that makes them quite adaptable to the modeling of irregular domains. However, it takes about twice as many triangular elements to model a structure as it does quadrilateral elements and since element generation times for triangular elements are generally more than half that of a comparable quadrilateral, it will take more computer time to solve a given problem with triangular elements. An optimum modeling would utilize quadrilaterals for the bulk of the mesh with triangular elements being used to fill in irregular regions at the boundaries.

The group of elements [64-68] employ shallow shell theories and generally impose some limitations on surface representation. The shallow shell element by Cowper, et.al. [67,70] appears to be the most useful in this group.

The elements [69-72] are based on deep shell theories, the most sophisticated in this group being the SHEBA element by Argyris and Scharpf [69] and the element by Dupuis and Goel [71]. Both elements satisfy continuity

and rigid-body motion requirements as well as accommodate a completely arbitrary surface geometry. Both element formulations are restricted to isotropic materials and each employ the middle surface as the shell reference surface.

Bushnell [73] presents an excellent review of the behavior of thin shells in practical engineering structures and he reviews modeling requirements for computer codes. As he points out, one of the first requirements of a computer program for shell analysis is the arbitrary location of the reference surface with respect to the wall material and the inclusion of energy coupling between changes in curvature and normal strains. Coupling between membrane and bending energies is present in shells with certain types of composite walls, eccentrically stiffened shells and nonuniformly heated shells with temperature dependent wall materials. Also, the middle surface is often a poor choice for the reference surface, since many practical shells have variable wall thicknesses and local reinforcements which make the middle surface difficult to describe mathematically and which cause its position to change abruptly in space. In such cases, the inner or outer surface of the shell is usually a better choice. Few of the shell elements listed in Tables 1 and 2 have provided for other than single layer wall construction with the reference surface being restricted to the middle surface. Many are restricted to isotropic materials.

A notable exception is the SLADE element by Key and Beisinger [61,62] which permits an arbitrary reference surface with layered, orthotropic walls.

In summarizing the status of curved element development, it is evident that no one element has won wide acceptance and that the quadrilateral elements as a group are not as well developed as the triangular elements. The trend is toward more sophisticated elements with a large number of degrees of freedom and hence increased element generation times. The argument for this approach is that for a given level of accuracy fewer elements will be needed than for the less sophisticated formulations; thus total stiffness matrix generation time and equation solution time will balance out in favor of the sophisticated elements. This argument generally holds up for simple test problems but for the complex structures which occur in engineering practice, the presence of cutouts, stiffeners, thickness variations, severe thermal gradients, and intersections with other components tend to force a minimum level of grid refinement which shifts the tradeoff back towards the simpler elements. This view is supported to some extent by Yates, et.al. [74], who in commenting on future plans for addition of capability to the general purpose code, DAISY, state, "We feel there is plenty of room for improvement in the quality of plate and solid elements.

...In trying more sophisticated plate elements we found none that would improve accuracy without extreme penalties in formation time and reliability."

The curved finite element technology discussed above has remained for the most part in the research stage and has not been widely used by the practical designer and shell analyst. A partial assessment of the utilization of curved finite elements in large scale, general purpose computer codes can be made on the basis of a critical review published in [21]. The ASKA, NASTRAN, DAISY, STARDYNE, STRUDL-II and MARC codes were critically reviewed by experienced users. NASTRAN, DAISY, and STARDYNE have no curved elements for general shell analysis, but rather rely on the "facet" type of element. ASKA has both the SHEBA-3 and SHEBA-6 elements of Argyris and Scharpf [69]. Meijers, the ASKA reviewer [75], states: "SHEBA shell elements are very complicated, require an extremely high amount of computer time and are very restricted in their application to practical problems." STRUDL-II has both triangular and quadrilateral, shallow shell elements; however, the reviewer, Chu [76], states: "...it has also been found that the results obtained from the shell elements, SSCR and SSCT, are not reliable." MARC has implemented one of the family of triangular elements developed by Dupuis and Goel [71]. The reviewer, Ayres [77], reports on satisfactory experience with a three-noded element with nine degrees of freedom per node. The element has been used for

elastic-plastic and creep problems associated with the design of high-temperature pressure vessels. It is interesting to note that the 27 degree of freedom element (T3) implemented in the MARC code was considered to be inferior to more sophisticated 54 degree of freedom elements (T1 and T2) by the element developers [71] on the basis that the T3 elements lead to worse numerical results for a given amount of computer time and generally require relatively fine meshes for convergence.

C. Historical Review-Finite Difference Energy Method

The finite difference method is generally associated with the concept of directly approximating the spatial derivatives in the partial differential equations of equilibrium which govern the behavior of a physical system. In recent years a variational method for deriving difference equations has come into use which is more closely allied to the finite element method than is the traditional method of finite differences. In the finite difference energy method the domain of interest is subdivided into a set of subareas by means of a finite difference mesh. For each subarea the strain energy density is expressed in terms of displacement components and their derivatives. After approximating the derivatives with finite difference relations, the strain energy of the system together with the work done by applied loads can be summed over the domain to form the total potential energy. As in the finite element method, the use of the minimum potential energy theorem results in a set of algebraic equations in the unknown nodal displacements. The imposition of discrete boundary conditions and the solution of the algebraic equations can be accomplished via the same matrix methods employed in finite element analysis.

The method has been used by mathematicians for many years to solve elliptic partial differential equations. The work by Courant, Friedricks and Lewy [78] in 1928 is often cited in the literature as being the earliest published use of the method. Forsythe and Wasow [79] in their 1960 text discuss variational methods for setting up difference equations and they cite,as important, the 1953 paper by McNeal [80] which dealt with using network analyzers for solving Laplace's equation.

As was the case with the finite element method, the finite difference energy method was first used to solve structural problems in the aircraft industry. Williams [81], in his 1960 text on Aircraft Structures, discusses the "method of individual displacements" which was combined with an energy approach to solve beam and plate problems. Although the method had in the past yielded useful results via hand calculations, Williams emphasized its great potential for exploiting the capabilities of the digital computers then emerging.

Griffen and Kellogg [82] computerized the method for the solution of axially symmetric and plane elasticity problems and noted that the difference equations obtained were closely related to those obtained by finite element methods.

Havner and Stanton [83] discussed variationally-derived finite difference equations in mixed boundary value problems of plane thermoelastic stress and strain.

As they point out, one possible disadvantage of the variational formulation of difference equations is that prescribed traction and mixed boundary conditions are not explicitly satisfied for a given finite difference network. These boundary conditions arise as distinct conditions only in the continuum problem and are not established separately from the field equations in minimizing the discretized form of the energy function. Hence, the accuracy of the variational approach at or near the boundary might be questioned. The Havner and Stanton paper provides a partial answer to this question for a specific class of problems. A detailed study was made of the boundary discretization error and it was shown that a variationally derived difference equation at the boundary can be represented as a linear combination of the corresponding natural boundary condition and field equation, converging to the discretized natural boundary condition with decreasing grid size. It was also demonstrated numerically that effective control of the boundary discretization error could be obtained with only local changes in grid spacing.

In the mid 1960's a group of researchers at the Lockheed Missiles and Space Company initiated a continuing effort to apply the finite difference energy method to a wide range of axisymmetric and general thin shell problems. Bushnell and his coworkers have developed the method for the analysis of stress, vibration and buckling of ring-

stiffened shells of revolution with various wall instructions. A series of computer codes with the acronym BOSOR (Buckling of Shells of Revolution) have resulted. Almroth and his coworkers have concurrently developed the method for the analysis of general shells, including stress, vibration, buckling and plasticity effects. A series of computer codes with the acronym STAGS (Structural Analysis for General Shells) have evolved. Bushnell and Almroth [84] give a good overview of the BOSOR and STAGS codes and the numerical analysis on which they are based.

References [85-87] describe the initial application of the method to the buckling and free vibration analysis of cylindrical panels. In [88], a linear version of the STAGS code was extended to handle circular or elliptic cutouts in stiffened cylindrical panels. The addition of a capability to treat shells with non-orthogonal Gaussian coordinates was reported in [89] which deals with the nonlinear collapse of elliptic cones. References [90-93] detail various improvements in capability to the STAGS code which include: provision to allow both the temperature and material properties to vary over the surface and through the thickness of the shell, the addition of a bifurcation buckling branch to the code, the extension of the nonlinear version to shells of more general shape with cutouts of arbitrary contour, the addition of inelastic deformation, the capability to handle a finite difference

grid with variable nodal point spacing and the treatment of realistic types of shell wall construction including those which involve anisotropic materials.

STAGS is applicable to four-sided shell panels (or closed shells with two edges) with one rectangular cutout and discrete or smeared stiffeners. Additional cutouts or cutouts of more general shape are handled by specification of a zero modulus of elasticity in the appropriate area. It applies to any shell for which a reference surface and a suitable set of rectangular grid lines can be mathematically defined. In general applications, the user provides a subroutine describing the geometry, but subroutines are included for such standard geometries as cylinder, cone, annular and rectangular plate, sphere, paraboloid, elliptic cylinder, ellipsoid, torus, hyperboloid and elliptic cone. References [94-97] describe research efforts in which the STAGS code has been used to study the stability of various types of shells.

The BOSOR code has undergone an evolution similar to that of STAGS and references [98-109] detail its development. Since the BOSOR code is based on a one-dimensional discretization and deals with the more restrictive class of shell of revolution problems, the history of its development and details of its analytical capabilities will not be discussed.

In the development of the STAGS analysis, various two-dimensional discretization schemes are explored [84]. The shell panel is covered with mesh lines parallel to the shell coordinate lines and the unknowns of the system are the tangential displacements u and v and the normal displacement w. Figure 1 shows three finite-difference schemes that are discussed in [84]. Figure 1a shows the "whole-station" scheme in which u, v and w are all located at grid points defined by intersections of the coordinate lines. For a typical interior "element" there are nine nodal points which define the u, v and w displacement fields and the "element area" over which membrane and bending energies are integrated is shaded. The energy integration for all schemes is by one point quadrature in which the functional values and derivatives of displacement are evaluated at the integration point (centroid of area). The whole station scheme of Figure 1a has been discarded because it leads to "jumpy" solutions in some cases and fails completely in cases where the mesh spacing varies.

Figure 1b shows the "whole-station" scheme in which membrane and bending energies are integrated over different areas. Although this scheme has exhibited good numerical behavior it is restricted to shells of such a wall construction that no coupling exists between membrane and bending energies.

The scheme shown in Figure 1c is termed "half-station" because the u and v displacement components are defined at points which lie halfway between the mesh points at which w components of displacement are defined. For a typical interior "element" there are nine nodal points which define the w displacement field and four which define the u, v displacement field. This scheme also gives good numerical results and is applicable to all forms of wall construction since it is not necessary to integrate over different elements of area for membrane and bending energies. The scheme is equivalent to a rectangular finite element in which the u, v displacements vary bi-linearly and the w displacement varies biquadratically. Unlike conventional finite elements, however, the w displacement field extends beyond the region of integration into several adjacent elements.

The most obvious limitation of the finite difference energy method as presently implemented in the STAGS code is the restriction on the type of grid and shell shape which can be handled. Complex shell configurations are much easier to model with finite element methods.

Johnson [110] and Jensen [111] have both proposed less restrictive schemes for positioning the discrete points at which unknown displacements are defined. Johnson used Green's Theorem to derive difference relations at the centroid of a quadrilateral area which is defined in

a manner quite similar to the STAGS "half-station" scheme of Figure 1c. The Johnson mesh scheme is shown in Figure 2. As in the STAGS "half station" scheme, the u, v displacements are defined at the centroidal points of the four quadrilateral areas which are formed by the nine nodal points at which w displacements are defined. The u, v control points then define the quadrilateral element area over which integrations are performed. In generating a structural mesh, a row of u, v control points must be positioned so as to fall on the shell boundary, so that all of the element areas fall within the boundaries of the shell. This is a departure from the STAGS "half-station" scheme where w control points are positioned on the boundary and the area of boundary elements are appropriately modified. The use of Green's Theorem to obtain finite difference approximations to the first derivatives of u and v at the element centroid is straightforward but the determination of difference relations for the second derivatives of w is quite complex and uses some simplifying assumptions which tend to restrict the generality of the mesh. The procedure relies on a somewhat cumbersome indexing system for the control points and two successive applications of Green's Theorem. The second derivative approximations for w are actually derived for points in the mesh other than the element centroid, but the assumption is made that the lengths of the line segments connecting

w control points are all of the same order of magnitude (Δ); hence the difference approximations hold also at the element centroid to within an error Δ. This method has been programmed for automatic computation and good results were obtained for several example problems.

Jensen [111] has done research on a procedure for generating the required difference relations in terms of the displacements of six arbitrarily placed neighboring nodes. The method is based on the use of the Taylor series expansion and requires special routines for locating and classifying the neighboring nodes, for calculating and storing the inverse nodal matrix for each class of node and for testing for singular nodal matrices, since the set of nearest neighbors in a given grid is sometimes insufficient to determine all the difference expressions needed. When the nodal matrix is singular the node must be reclassified, i.e., a new set of neighbors selected. Another complication is that nodal matrices for points on the boundary of the domain are constructed differently from those in the interior. Jensen experienced difficulties in automating the procedure and it was not implemented in a structural analysis.

In summary, the finite difference energy method has been developed into a powerful analysis tool for certain classes of shell structures, especially for problems involving geometric nonlinearities. It will be compared

to the finite element method in the following section and the advantages and disadvantages of both methods will be discussed.

D. Comparison of Finite Element Method And Finite Difference Energy Method

In recent years a number of papers have addressed the problem of comparing various finite element formulations with finite difference energy method formulations. The comparisons are based on a number of specific numerical examples which have been solved by both methods.

Forsberg [112] considered several sample problems including a cylindrical shell roof, a stiffened cylinder with a rectangluar cutout and a "pear-shaped" cylinder. For the cylindrical shell roof, comparisons were made between the STAGS finite difference energy method formulation [84] and four finite elements. The finite elements included two flat plates, a 20 degree of freedom quadrilateral [113], a 15 degree of freedom triangle [45], and two curved triangular elements [66,67] based on shallow shell theory, both with 36 degrees of freedom. The STAGS formulation had a more rapid rate of convergence to the analytical solution than the finite elements for both displacement and stress predictions.

In concluding his paper, Forsberg made the following points which apply to the analysis of general shells. For the linear static and dynamic analysis of irregular structures the finite element technique is ideal due to its inherent generality and flexibility in modeling. The finite

difference technique, though not able to treat as general a configuration, is applicable to a wide range of practical structures. The numerical studies indicated a comparable accuracy for the two methods for a given mesh size, however, the finite element method will have far more degrees of freedom and consequently will require considerably more computer time. For an equivalent problem size, the finite difference technique will still require less computer time because the time required to generate the stiffness equations is less. Finite elements have been more extensively used to study material nonlinearities while the finite difference approach has been more highly developed for problems involving geometric nonlinearity.

Hartung, in assessing capability for computer analysis of shell structures, surveyed all available codes and summarized current capability in [8] and reported on the results of comparative analyses for three sample problems representative of current engineering practice in [9]. Solutions were solicited from the structures community for analyses of linear stress, free vibration, bifurcation buckling, elastic and inelastic collapse, and linear and nonlinear transient response. In general there was good agreement among the codes for linear stress, free vibration and bifurcation buckling. The STAGS finite difference energy formulation was the only code for which a solution

was submitted to the elastic and inelastic collapse problems. The linear and nonlinear transient response solutions submitted were primarily from conventional finite difference methods. The agreement between solutions for the linear analysis was good for displacements and membrane strains and only fair for bending strains. The nonlinear results showed virtually no agreement. The conclusions drawn by Forsberg [112] in his comparison of finite element and finite difference energy methods were generally confirmed by the results of the comparative analyses of Hartung [9].

The most rigorous comparison between the finite element and finite difference energy techniques has been carried out by Bushnell [114]. In the previous comparisons by Forsberg and Hartung it was difficult to make quantitative assessments of computer run times because the analyses had been run on various computers and a variety of programming techniques had been used for essentially similar operations (e.g., solution of simultaneous equations). Bushnell inserted curved finite elements into the BOSOR3 computer code, a shell of revolution analyzer which is based on the finite difference energy method. Rates of convergence and computer times were established for linear stresses and displacements, bifurcation buckling loads and free vibration frequencies. The various discrete elements depicted in Figure 3 were compared with respect to convergence rate of mesh spacing, computer times required to form global stiffness, load

geometric and mass matrices, computer times required to factor and solve the systems of algebraic equations, and number of Gaussian integration points required for accurate formation of local matrices. The first three discrete elements shown in Figure 3 are curved finite elements with various displacement assumptions while the fourth is a finite difference element which is the one-dimensional analog of the STAGS "half-station" scheme (Figure 1c) previously discussed.

The rates of convergence were case dependent, the finite difference method showed better performance for vibration frequencies and stress problems not involving rapidly varying edge discontinuity stresses while the finite element method showed more rapidly convergent behavior for buckling loads and static problems involving high stress gradients at a clamped edge.

The finite difference element was clearly superior with respect to computer time. With the finite element models, two to six times as much computer time was required for formation of each of the stiffness, load-geometric and mass matrices. The extra time was associated with coordinate transformations, static reduction and evaluation of element energy density at more than one Gaussian integration point, operations which were not required for the finite difference analysis.

The behavior of the finite element models with a variation in the number of Gauss points used for numerical integration was also studied by Bushnell. The most rapidly convergent solution was obtained by using the minimum number of Gauss points required for eventual convergence to the correct solution. If too few points were used, the calculations converged to the wrong solution. None of the finite elements converged to the proper solution if only one Gauss point was used as was done with the finite difference energy model. The optimum number of Gauss points required for each of the discrete elements is shown in Figure 3.

Although the Bushnell study was restricted to comparisons of one-dimensional discrete elements, he did discuss in some detail the extrapolation of these results to the two-dimensional discrete elements required for the analysis of general shells. He cites four factors of prime importance in numerical analysis of practical structures: ease of application, computer time required to form the various matrices, computer time to decompose the stiffness matrix and solve for eigenvalues, and rate of convergence with increasing number of degrees of freedom.

With respect to ease of application the finite element method is far superior in two-dimensional problems involving irregular grids and arbitrary boundaries.

The saving in computer time for matrix formation which was noted in the one-dimensional case is expected to be even more of an advantage for the finite difference energy method in the two-dimensional case, especially for nonlinear problems. This advantage is anticipated because the order of the element matrices is larger for two-dimensional finite elements and the difference in number of Gauss points between the two methods is greater. For example the finite difference element has 17 degrees of freedom while the finite elements range from 20 to 63 (see Tables 1 and 2 and Figure 1). The number of required Gaussian integration points ranges from 4 for flat plate elements with low order displacement assumptions up to 25 and more for the higher order curved elements [61].

The computer time required to decompose the stiffness matrix and solve for eigenvalues is a significant portion of the total computer time in two-dimensional problems. The simplest finite element formulations lead to coupling over three lines of mesh points and have five unknowns at each node. The STAGS type of finite difference model involves coupling over five lines of mesh points with up to three unknowns per node. The numerical characteristics of these two nodal arrangements lead to computer time ratios which slightly favor the finite difference model. More sophisticated finite elements with midside nodes and/or more degrees of freedom per node require correspondingly

more computer time but presumably fewer elements would be required for convergence to a given degree of accuracy.

The computer times discussed above all depend on the mesh size required to reach a convergent solution. The convergence characteristics of the two methods varied from case to case in all of the comparative studies [9,112,114] and a fair statement would probably be that the two methods are about equal.

A recurring theme in each of the previously discussed comparative studies [8,9,112,114] and several other review articles [73,97] has been the advantage that finite element methods have in modeling complex structures. As Hartung [8] points out in his discussion of areas for further study, if finite difference methods are going to achieve the same versatility for modeling complex structures that the finite element method has achieved, then a capability for handling truly arbitrary meshes must be developed.

E. Objective And Synopsis Of Research

The objective of this research is to demonstrate that two well accepted matrix methods for thin shell structural analysis, the finite element method and the finite difference energy method, can be integrated into one unified analytical approach and effectively applied to the thermo-elastic analysis of anisotropic thin shells. Since its inception almost 20 years ago the finite element method has evolved into the most widely used tool for structural analysis, primarily due to its generality, i.e., its ability to model the complex geometries that occur in engineering practice. In recent years, the finite difference energy method has been developed to a very high degree, especially for problems involving geometric nonlinearities. Although the method has been demonstrated to have significant advantages over contemporary finite element formulations, it suffers from the modeling restrictions imposed by rectangular grid works. It is the intention of this research to demonstrate that this classic restriction can be removed and that the finite difference energy method can be cast in a formulation which is amenable to insertion in contemporary general purpose finite element computer codes.

In succeeding chapters the details of the analytical development are presented along with the results of several sample calculations. In Chapter II a tensorial description of the geometry of the shell reference surface is presented along with the thin shell theory of Sanders. Chapter III contains a general description of the application of the finite difference energy method to the analysis of thin shells. Chapter IV contains the details of the analytical development of the generalized finite difference element. In Chapter V the analytical results obtained with the element for a number of demonstration problems are compared to theoretical or experimental results and in some cases to the results obtained with finite element formulations. Chapter VI summarizes the results of this research and the Appendices contain the Tables and Illustrations along with further details of the numerical analysis.

CHAPTER II

SHELL THEORY

A. Surface Geometry

A description of the curvilinear surface geometry for shells of arbitrary curvature will be summarized in this section using tensor notation.* A detailed treatment of this subject is given by Green and Zerna [115] and Sokolnikoff [116].

It is assumed that the reference surface of the shell is defined by curvilinear Gaussian surface coordinates x^α which are contained in a three-dimensional Euclidean space defined by the basic Cartesian coordinates X^i (see Figure 4). The curvilinear coordinate lines, x^α = constant, $x^3 = 0$, are embedded in the shell reference surface and x^3 is the outward normal to the undeformed reference surface. The position vector of a point, P, on the reference surface is

---

*Remarks on notation:

1. Greek indices range over the values 1,2 while Latin indices have the values 1,2,3 unless otherwise noted.
2. Unless specifically suppressed a repeated index in a term represents a summation over the range of the index.
3. $(\ )_{,\alpha}$ denotes partial differentiation with respect to x^α.
4. $(\ )|_\alpha$ denotes covariant differentiation with respect to x^α.

denoted $\vec{r}$. The vectors $\vec{a}_1$ and $\vec{a}_2$ are the base vectors of the Gaussian surface coordinates and the unit normal vector to the reference surface is $\vec{e}_3$. The vectors $\vec{I}_i$ are the unit vectors in the X^i directions.

The position vector, $\vec{r}$, is related to basic coordinates by,

$$\vec{r} = X^i \vec{I}_i \tag{II.1}$$

The covariant base vectors $\vec{a}_\alpha$ are related to basic coordinates by,

$$\vec{a}_\alpha = X^i_{,\alpha} \vec{I}_i \tag{II.2}$$

The base vectors $\vec{a}_\alpha$ are not in general unit vectors, the unit vectors being given by,

$$\vec{e}_\alpha = \frac{\vec{a}_\alpha}{|\vec{a}_\alpha|} = \frac{\vec{a}_\alpha}{\sqrt{\vec{a}_\alpha \cdot \vec{a}_\alpha}} \quad \text{(no sum)} \tag{II.3}$$

The incremental arc length on the shell reference surface is measured by,

$$\begin{aligned} dS^2 &= d\vec{r} \cdot d\vec{r} \\ &= a_{\alpha\beta}\, dx^\alpha dx^\beta \end{aligned} \tag{II.4}$$

where $a^{\alpha\beta}$ is the metric tensor of the undeformed reference surface and the right hand expression of (II.4) is called

the first fundamental quadratic form of the surface.

The metric tensor is computed by,

$$a_{\alpha\beta} = \vec{a}_\alpha \cdot \vec{a}_\beta$$

$$= X^i_{,\alpha} X^i_{,\beta} \qquad \text{(II.5)}$$

An area element on the shell reference surface is,

$$dA = |\vec{a}_1 \times \vec{a}_2| dx^1 dx^2$$

$$= \sqrt{a}\, dx^1 dx^2 \qquad \text{(II.6)}$$

where a is the determinant of the metric tensor.

An alternate form of (II.4) is,

$$dS^2 = (A_1)^2 dx^1 dx^1 + 2A_1 A_2 \cos\Phi dx^1 dx^2 + (A_2)^2 dx^2 dx^2 \qquad \text{(II.7)}$$

where

$$A_\alpha = \sqrt{a_{\alpha\alpha}} \qquad \text{(no sum)} \qquad \text{(II.8)}$$

$$\cos\Phi = \frac{a_{12}}{\sqrt{a_{11} a_{22}}} \qquad \text{(II.9)}$$

$$\sin\Phi = \frac{\sqrt{a}}{\sqrt{a_{11} a_{22}}} \qquad \text{(II.10)}$$

The quantities A_α, known as the Lame´ parameters, are measures of arc length along the surface coordinate lines and Φ is the angle between the coordinate lines. For orthogonal coordinates, the angle Φ is 90 degrees and the component a_{12} is zero.

The contravariant base vectors are defined by,

$$\vec{a}^1 = \frac{1}{\sqrt{a}} \vec{a}_2 \times \vec{e}_3 \tag{II.11}$$

$$\vec{a}^2 = \frac{1}{\sqrt{a}} \vec{e}_3 \times \vec{a}_1 \tag{II.12}$$

where,

$$\vec{e}_3 = \frac{1}{\sqrt{a}} \vec{a}_1 \times \vec{a}_2 \tag{II.13}$$

The covariant and contravariant base vectors are related by,

$$\vec{a}_\alpha \cdot \vec{a}^\beta = \delta_\alpha^\beta \tag{II.14}$$

where,

$$\delta_\alpha^\beta = \begin{cases} 1 , & \alpha=\beta \\ 0 , & \alpha\neq\beta \end{cases} \tag{II.15}$$

The components of the associated metric tensor are,

$$a^{\alpha\beta} = \vec{a}^\alpha \cdot \vec{a}^\beta \tag{II.16}$$

The covariant and contravariant base vectors are transformed via the metric tensors. This operation is termed raising and lowering of indices and is given by,

$$\vec{a}^{\alpha} = a^{\alpha\beta}\vec{a}_{\beta} \tag{II.17}$$

$$\vec{a}_{\alpha} = a_{\alpha\beta}\vec{a}^{\beta} \tag{II.18}$$

The Christoffel symbols of the second kind are defined in terms of the metric tensor and base vectors to be,

$$\Gamma^{\alpha}_{\beta\gamma} = a^{\alpha\lambda}(\vec{a}_{\lambda}\cdot\vec{a}_{\beta,\gamma}) \tag{II.19}$$

The covariant form of the initial curvature tensor is defined by,

$$\Gamma^{3}_{\alpha\beta} = b_{\alpha\beta} = \vec{e}_{n}\cdot\vec{a}_{\alpha,\beta} \tag{II.20}$$

The quantities $b_{\alpha\beta}$ are known as the coefficients of the second fundamental form of the undeformed reference surface and they describe the initial curvature of the surface.

The indices of the tensor $b_{\alpha\beta}$ may also be raised and lowered via the metric tensor to give the mixed and contravariant forms,

$$b^{\alpha}_{\beta} = a^{\alpha\lambda} b_{\lambda\beta} = a_{\beta\lambda} b^{\lambda\alpha} \tag{II.21}$$

$$b^{\alpha\beta} = a^{\alpha\lambda} b^{\beta}_{\lambda} \tag{II.22}$$

The displacement vector at a point on the shell reference surface is,

$$\begin{aligned} \vec{u} &= u^{\alpha}\vec{a}_{\alpha} + w\,\vec{e}_{n} \\ &= u_{\alpha}\vec{a}_{\alpha} + w\,\vec{e}_{n} \end{aligned} \tag{II.23}$$

where u_{α} and u^{α} are the covariant and contravariant components of in-plane displacement.

The concept of covariant differentiation is utilized in the tensor analysis of the deformation of the shell reference surface. The covariant derivatives of the displacements u_{α} and u^{α} are,

$$u_{\alpha}|_{\nu} = u_{\alpha,\nu} - \Gamma^{\lambda}_{\alpha\nu} u_{\lambda} \tag{II.24}$$

$$u^{\alpha}|_{\nu} = u_{\alpha,\nu} + \Gamma^{\alpha}_{\lambda\nu} u^{\lambda} \tag{II.25}$$

and the covariant derivatives of the second order tensors $b_{\alpha\beta}$ and $b^{\alpha\beta}$ are,

$$b_{\alpha\beta}|_{\nu} = b_{\alpha\beta,\nu} - \Gamma^{\lambda}_{\alpha\nu} b_{\lambda\beta} - \Gamma^{\lambda}_{\beta\nu} b_{\alpha\lambda} \tag{II.26}$$

$$b^{\beta}_{\alpha}|_{\nu} = b^{\beta}_{\alpha,\nu} + \Gamma^{\beta}_{\lambda\nu} b^{\lambda}_{\alpha} - \Gamma^{\lambda}_{\alpha\nu} b^{\beta}_{\lambda} \tag{II.27}$$

The practical utilization of the above concepts is demonstrated in Appendix D wherein the tensors necessary to describe the geometry and deformation of the shell reference surface are computed for several classes of shell surfaces.

B. Deformation of the Shell

Strain displacement relations in arbitrary curvilinear coordinates have been derived by Sanders [117] for thin shells with small reference surface strains and moderately small rotations. The deformation of the shell is defined by the reference surface strain tensor $\gamma_{\alpha\beta}$ which accounts for stretching or membrane behavior and the curvature change tensor $\chi_{\alpha\beta}$ which accounts for bending behavior.

The strain tensor at an arbitrary point, Q, which lies off the shell reference surface (see Figure 4) is given by,

$$\overline{\gamma}_{\alpha\beta} = \gamma_{\alpha\beta} + x^3 \cdot \chi_{\alpha\beta} \tag{II.28}$$

where the reference surface tensors $\gamma_{\alpha\beta}$ and $\chi_{\alpha\beta}$ are defined by Sanders [117] to be (see also Oden [118]),

$$\gamma_{\alpha\beta} = \tfrac{1}{2}[u_\alpha|_\beta + u_\beta|_\alpha - 2b_{\alpha\beta}w] \tag{II.29}$$

$$\chi_{\alpha\beta} = \tfrac{1}{2}[\bullet_\alpha|_\beta + \bullet_\beta|_\alpha + b^\lambda_\beta\omega_{\alpha\lambda} + b^\lambda_\alpha\omega_{\beta\lambda}] \tag{II.30}$$

and

$$\bullet_\alpha = -[w_{,\alpha} + b^\lambda_\alpha u_\lambda] \tag{II.31}$$

$$\omega_{\alpha\beta} = \tfrac{1}{2}[u_\alpha|_\beta - u_\beta|_\alpha] \tag{II.32}$$

The quantities Θ_α are the covariant components of the rotation vector and describe the rotation of the normal to the deformed reference surface.

The displacement vector at an arbitrary point off the shell reference surface is then defined by,

$$\vec{\bar{u}} = \vec{u} + x^3 \cdot \vec{\Theta} \tag{II.33}$$

where

$$\vec{\Theta} = \Theta_\alpha \vec{a}^\alpha = \Theta^\alpha \vec{a}_\alpha \tag{II.34}$$

$$\vec{\Theta} = \Psi_\alpha \vec{e}_\alpha \tag{II.35}$$

The quantities Θ^α are the contravariant components and the quantities Ψ_α are the physical components of the rotation vector.

By use of (II.3), (II.8), (II.17) and (II.34), (II.35) the relationship between physical components and tensor components is found to be,

$$\Psi_\alpha = A_\alpha \Theta^\alpha \qquad \text{(no sum)} \tag{II.36}$$

$$\Psi_\alpha = A_\alpha a^{\alpha\beta} \Theta_\beta \qquad \text{(no sum on } \alpha\text{)} \tag{II.37}$$

Substituting (II.31) into (II.37) permits the physical components of the rotation vector to be expressed in terms of the covariant components of displacement,

$$\Psi_\alpha = -A_\alpha (a^{\alpha\beta} w_{,\beta} + b^{\alpha\lambda} u_\lambda) \qquad \text{(no sum on } \alpha\text{)} \qquad \text{(II.38)}$$

An alternate form of the rotation vector can be defined by,

$$\vec{\vartheta} = \vec{e}_n \times \vec{\theta}$$

$$= -\Psi_2 \vec{e}_1 + \Psi_1 \vec{e}_2 \qquad \text{(II.39)}$$

This form obeys the right hand rule and is more convenient for certain calculations such as the work done by externally applied concentrated or distributed moment loading.

CHAPTER III

GENERAL DESCRIPTION OF THE ANALYSIS METHOD

The strain energy for an arbitrary, thin shell segment may be expressed as [119],

$$U = \iiint U_o \sqrt{a}\, dx^3 dx^1 dx^2 \qquad \text{(III.1)}$$

where U_o is the strain energy density.

Introducing the stress tensor $\tau^{\alpha\beta}$ and the strain tensor $\gamma_{\alpha\beta}$, the strain energy density is [120],

$$U_o = \frac{1}{2} \bar{\tau}^{\alpha\beta} (\bar{\gamma}_{\alpha\beta} - \varepsilon_{\alpha\beta} \cdot \Delta T) \qquad \text{(III.2)}$$

where the bar indicates quantities at a point which lies off the shell reference surface, $\varepsilon_{\alpha\beta} \cdot \Delta T$ are thermal strains and,

$$\bar{\gamma}_{\alpha\beta} = \gamma_{\alpha\beta} + x^3 \cdot \chi_{\alpha\beta} \qquad \text{(III.3)}$$

The constitutive equations including thermal effects are,

$$\bar{\tau}^{\alpha\beta} = \mathbf{E}^{\alpha\beta\lambda\rho} (\gamma_{\lambda\rho} - \varepsilon_{\lambda\rho} \cdot \Delta T) \qquad \text{(III.4)}$$

where $\mathbf{E}^{\alpha\beta\lambda\rho}$ and $\varepsilon_{\lambda\rho}$ are the elastic material constants and ΔT is the rise in temperature above the reference state.

The strain-displacement relations of Sanders are,

$$\gamma_{\alpha\beta} = \frac{1}{2}[u_\alpha|_\beta + u_\beta|_\alpha - 2b_{\alpha\beta}w] \tag{III.5}$$

$$\chi_{\alpha\beta} = \frac{1}{2}[\Theta_\alpha|_\beta + \Theta_\beta|_\alpha + b^\lambda_\beta w_{\alpha\lambda} + b^\lambda_\alpha \omega_{\beta\lambda}] \tag{III.6}$$

By substitution of the constitutive equations (III.4) and strain-displacement relations (III.5) and (III.6) into (III.2) it is possible to express the strain energy density as a functional in terms of the reference surface displacements, the elastic material constants and the temperature rise,

$$U_o = U_o(u_\alpha, w, \mathbf{E}^{\alpha\beta\lambda\rho}, \varepsilon_{\lambda\rho}, \Delta T) \tag{III.7}$$

The potential energy π is then,

$$\pi = U - W \tag{III.8}$$

where W is the potential of the externally applied mechanical and inertial loadings.

The integrals appearing in the potential energy expression (III.1) may be evaluated by numerical integration. If the derivatives of displacement which occur in π are replaced by finite difference approximations and a

variational procedure is applied according to the Theorem of Minimum Potential Energy, a set of linear equations in terms of the displacement variables will be obtained. This set of equations can be expressed in the matrix form:

$$[\mathbf{M}]\{\ddot{q}\} + [\mathbf{K}]\{q\} = \{\mathbf{P}\} \qquad \text{(III.9)}$$

or in the absence of inertial loads,

$$[\mathbf{K}]\{q\} = \{\mathbf{P}\} \qquad \text{(III.10)}$$

where: $[\mathbf{M}]$ = Mass matrix

$[\mathbf{K}]$ = Stiffness matrix

$\{q\}$ = Vector of unknown displacements at discrete points of the finite difference network

$\{\mathbf{P}\}$ = Vector of externally applied thermal or mechanical loads

The solution of (III.9) or (III.10) will yield the time-dependent or static displacements at discrete grid points. The displacements can be converted to strains by using a finite difference form of the strain-displacement relations and the strains can in turn be converted to stresses through the constitutive equations. Equation (III.9) can also be solved for natural frequencies and mode shapes.

Advantages of the above procedure include:

1. Permits point-to-point variation over the shell reference surface of thickness, material properties, and thermal and mechanical loading.
2. Only first and second order derivatives of displacement appear in the potential energy formulation.
3. Only the essential displacement boundary conditions have to be satisfied, the natural force boundary conditions being approximately satisfied via the energy minimization.
4. The stiffness equations are amenable to rapid calculation on modern computers and they are banded; hence large order systems may be economically solved.
5. This approach is based on thin shell theory and should be more accurate than the use of flat finite elements. It should also be competitive with curved finite elements based on shell theory since these elements tend to have a large number of degrees of freedom and therefore the computational time associated with their use can be excessive.

CHAPTER IV

THEORETICAL DEVELOPMENT OF SHEFA* ELEMENT

A. General Remarks

A thermoelastic analysis method for thin walled shell structures will be formulated using the general tensor notation. After each step of the development the tensor equations will be expanded and recast in a matrix form. The matrix equations will retain all the generality of the tensor equations in that no specialized forms will be substituted which limit the application of the method to a specific class of shell shapes. The only specialized model developed will be that for the shell wall construction and it will be sufficiently general to treat a broad range of anisotropic material configurations including layered orthotropic walls, filament wound walls and angle ply laminates as well as more conventional single layer construction. The model treats the effects of nonlinear temperature gradients through the shell wall including material property temperature dependence and also the coupling between membrane and bending action which results from certain classes of shell wall construction or the use of an arbitrary reference surface (i.e., one not restricted to the shell middle surface).

---

*The term SHEFA is an acronym for SHell Element based on a Finite difference Approach.

The utility of the matrix notation will be evident as the development progresses. From the standpoint of the theoretician the tensor notation is attractive for its compactness and the ease with which large sets of equations can be manipulated, but the highly condensed form serves to hinder the visibility of the theoretical development. The matrix notation adopted herein serves to provide high visibility and results in a formulation that can be directly programmed for automatic computation without further manipulation. Since this is a matrix method of structural analysis, a specific partitioning of certain variables is necessary in order to facilitate the introduction of numerical approximations, coordinate transformations and transformations from tensor to physical components. Also, since the analysis method is based on a variational procedure, the matrix formulation of the energy equations is done in such a way as to make trivial the final variational operation to obtain the equations of motion.

B. Thin Shell Strain Energy

1. Strain Energy Density

The strain energy density for a thin shell is, [120],

$$U_o = \frac{1}{2} \bar{\tau}^{\alpha\beta}(\bar{\gamma}_{\alpha\beta} - \varepsilon_{\alpha\beta} \cdot \Delta T) \qquad \text{(IV.1)}$$

or in matrix form,

$$U_o = \frac{1}{2} \{\bar{\tau}\}^T[\{\bar{\gamma}\} - \{\varepsilon\} \cdot \Delta T] \qquad \text{(IV.2)}$$

where,

$\bar{\tau}^{\alpha\beta}$, $\bar{\gamma}_{\alpha\beta}$ = Stress, strain tensors at a point off the shell reference surface

$\varepsilon_{\alpha\beta}$ = Tensor of thermal expansion coefficients

ΔT = Temperature change from reference state

and

$$\{\bar{\tau}\}^T = [\bar{\tau}^{11}, \bar{\tau}^{22}, \bar{\tau}^{12}] \qquad \text{(IV.3)}$$

$$\{\bar{\gamma}\}^T = [\bar{\gamma}_{11}, \bar{\gamma}_{22}, 2\bar{\gamma}_{12}] \qquad \text{(IV.4)}$$

$$\{\varepsilon\}^T = [\varepsilon_{11}, \varepsilon_{22}, 2\varepsilon_{12}] \qquad \text{(IV.5)}$$

The thermoelastic constitutive equations relating the stress and strain tensors are:

$$\bar{\gamma}_{\alpha\beta} = \mathbf{F}_{\alpha\beta\lambda\rho}\,\bar{\tau}^{\lambda\rho} + \varepsilon_{\alpha\beta}\cdot\Delta T \qquad \text{(IV.6)}$$

$$\bar{\tau}^{\alpha\beta} = \mathbf{E}^{\alpha\beta\lambda\rho}\,\bar{\gamma}_{\lambda\rho} - \Omega^{\alpha\beta} \qquad \text{(IV.7)}$$

$$\Omega^{\alpha\beta} = \mathbf{E}^{\alpha\beta\lambda\rho}\,\varepsilon_{\lambda\rho}\cdot\Delta T \qquad \text{(IV.8)}$$

or in matrix form:

$$\{\bar{\gamma}\} = [\ \mathbf{F}\ ]\{\bar{\tau}\} + \{\varepsilon\}\cdot\Delta T \qquad \text{(IV.9)}$$

$$\{\bar{\tau}\} = [\ \mathbf{E}\ ]\{\bar{\gamma}\} - \{\Omega\} \qquad \text{(IV.10)}$$

$$\{\Omega\} = [\ \mathbf{E}\ ]\{\varepsilon\}\cdot\Delta T \qquad \text{(IV.11)}$$

$$[\ \mathbf{E}\ ] = [\ \mathbf{F}\ ]^{-1} \qquad \text{(IV.12)}$$

where

$\mathbf{E}^{\alpha\beta\lambda\rho}$, $\mathbf{F}_{\alpha\beta\lambda\rho}$ = material elastic constant tensors

and,

$$[\ \mathbf{E}\ ] = \begin{bmatrix} \mathbf{E}^{1111} & \mathbf{E}^{1122} & \mathbf{E}^{1112} \\ \mathbf{E}^{2211} & \mathbf{E}^{2222} & \mathbf{E}^{2212} \\ \mathbf{E}^{1211} & \mathbf{E}^{1222} & \mathbf{E}^{1212} \end{bmatrix} \qquad \text{(IV.13)}$$

$$[\ \mathbf{F}\ ] = \begin{bmatrix} \mathbf{F}_{1111} & \mathbf{F}_{1122} & 2\,\mathbf{F}_{1112} \\ \mathbf{F}_{2211} & \mathbf{F}_{2222} & 2\,\mathbf{F}_{2212} \\ 2\,\mathbf{F}_{1211} & 2\,\mathbf{F}_{1222} & 4\,\mathbf{F}_{1212} \end{bmatrix} \qquad \text{(IV.14)}$$

The strain tensor ($\bar{\gamma}_{\alpha\beta}$) at a point off of the reference surface is related to the reference surface strain tensor ($\gamma_{\alpha\beta}$) and curvature change tensor ($\chi_{\alpha\beta}$) by,

$$\bar{\gamma}_{\alpha\beta} = \gamma_{\alpha\beta} + x^3 \cdot \chi_{\alpha\beta} \tag{IV.15}$$

or in matrix form,

$$\{\bar{\gamma}\} = \{\gamma\} + x^3 \cdot \{\chi\} \tag{IV.16}$$

where:

$$\{\gamma\}^T = [\gamma_{11}, \gamma_{22}, 2\gamma_{12}] \tag{IV.17}$$

$$\{\chi\}^T = [\chi_{11}, \chi_{22}, 2\chi_{12}] \tag{IV.18}$$

x^3 = coordinate normal to reference surface (positive in direction of outward normal)

Substituting equations (IV.10) and (IV.16) into equation (IV.2) gives for the strain energy density,

$$\begin{aligned} U_o &= [\tfrac{1}{2}\{\gamma\}^T[\ \mathbf{E}\ ]\{\gamma\} + \tfrac{1}{2}\, x^3(\{\chi\}^T[\ \mathbf{E}\ ]\{\gamma\} + \{\gamma\}^T[\ \mathbf{E}\ ]\{\chi\}) \\ &\quad + \tfrac{1}{2}(x^3)^2\{\chi\}^T[\ \mathbf{E}\ ]\{\chi\}] + [-\{\Omega\}^T\{\gamma\} - x^3\{\Omega\}^T\{\chi\} \\ &\quad - \tfrac{1}{2}(\Delta T)^2\{\varepsilon\}^T[\ \mathbf{E}\ ]\{\varepsilon\}] \\ &= [U_o^M + U_o^C + U_o^B] + [U_o^{TM} + U_o^{TB} + C_1] \\ &= U_o^S + U_o^T \end{aligned} \tag{IV.19}$$

where,

U_o^S = Strain energy of the shell

U_o^T = Work done by thermal forces

$$U_o^M = \frac{1}{2}\{\gamma\}^T[\,\mathbf{E}\,]\{\gamma\} \qquad \text{(IV.20)}$$

= Strain energy due to membrane action

$$U_o^C = \frac{1}{2}\, x^3(\{\chi\}^T[\,\mathbf{E}\,]\{\gamma\} + \{\gamma\}^T[\,\mathbf{E}\,]\{\chi\}) \qquad \text{(IV.21)}$$

= Strain energy due to coupled membrane and bending action

$$U_o^B = \frac{1}{2}(x^3)^2\{\chi\}^T[\,\mathbf{E}\,]\{\chi\} \qquad \text{(IV.22)}$$

= Strain energy due to bending action

$$U_o^{TM} = -\{\Omega\}^T\{\gamma\} = -\{\varepsilon\}^T[\,\mathbf{E}\,]\{\gamma\}\cdot\Delta T \qquad \text{(IV.23)}$$

= Strain energy due to thermal membrane action

$$U_o^{TB} = -x^3\{\Omega\}^T\{\chi\} = -x^3\{\varepsilon\}^T[\,\mathbf{E}\,]\{\chi\}\cdot\Delta T \qquad \text{(IV.24)}$$

= Strain energy due to thermal bending action

$$C_1 = -\frac{1}{2}(\Delta T)^2\{\varepsilon\}^T[\,\mathbf{E}\,]\{\varepsilon\} \qquad \text{(IV.25)}$$

= Thermal constant which does not contribute to the stiffness equations*.

*Since C_1 is not a function of the displacements, it vanishes when the potential energy is minimized.

Thus,

$$U_o^S = \frac{1}{2}\left\{\begin{matrix}\gamma\\ \chi\end{matrix}\right\}^T \left[\begin{matrix}\mathbf{E} & x^3\cdot\mathbf{E}\\ x^3\cdot\mathbf{E} & (x^3)^2\cdot\mathbf{E}\end{matrix}\right] \left\{\begin{matrix}\gamma\\ \chi\end{matrix}\right\} \qquad \text{(IV.26)}$$

$$U_o^T = \frac{1}{2}\left\{\begin{matrix}\Omega\\ x^3\cdot\Omega\end{matrix}\right\}^T \left\{\begin{matrix}\gamma\\ \chi\end{matrix}\right\} \qquad \text{(IV.27)}$$

2. Shell Wall Model

Integrating through the shell wall,

$$\bar{U}_o = \int U_o dx^3$$

$$= \frac{1}{2}\left\{\begin{matrix}\gamma\\ \chi\end{matrix}\right\}^T \left[\begin{matrix}D & C\\ C & B\end{matrix}\right] \left\{\begin{matrix}\gamma\\ \chi\end{matrix}\right\} - \left\{\begin{matrix}N_T\\ M_T\end{matrix}\right\}^T \left\{\begin{matrix}\gamma\\ \chi\end{matrix}\right\}$$

$$= \frac{1}{2}\{\gamma\}^T[D]\{\gamma\} + \frac{1}{2}(\{\chi\}^T[C]\{\gamma\} + \{\gamma\}^T[C]\{\chi\})$$

$$+ \frac{1}{2}\{\chi\}^T[B]\{\chi\} - \{N_T\}^T\{\gamma\} - \{M_T\}^T\{\chi\} \qquad \text{(IV.28)}$$

where,

$$[D] = \int [\mathbf{E}]dx^3 \qquad \text{(IV.29)}$$

$$[C] = \int [\mathbf{E}]x^3dx^3 \qquad \text{(IV.30)}$$

$$[B] = \int [\mathbf{E}](x^3)^2dx^3 \qquad \text{(IV.31)}$$

$$\{N_T\} = \int \{\Omega\}dx^3 = \int [\mathbf{E}]\{\epsilon\}\cdot\Delta T\cdot dx^3 \qquad \text{(IV.32)}$$

$$\{M_T\} = \int \{\Omega\}x^3dx^3 = \int [\mathbf{E}]\{\epsilon\}\cdot\Delta T\cdot x^3dx^3 \qquad \text{(IV.33)}$$

The final form of the shell compliances (IV.29) - (IV.31) thermal forces (IV.32) and moments (IV.33) depends on the shell wall construction, the materials used, their degree of anisotropy and temperature dependence, the orientation of the natural material axes with respect to the shell coordinates, and the nature of the thermal environment.

For convenience, the symbol z will be used interchangeably with the normal coordinate, x^3, in the following analytical development (see Figure 5a).

A general model that will treat a broad range of shell walls and thermal environments is one that accounts for a layered construction with each layer being a different planarly orthotropic, temperature dependent material whose natural axes do not necessarily coincide with the Gaussian surface (shell) coordinates (see Figure 5).

For each orthotropic layer the physical material properties (with respect to the natural material axes) are,

$$[G]_m = \begin{bmatrix} \frac{E_{11}}{1-\nu_o^2} & \frac{\nu_{12}E_{22}}{1-\nu_o^2} & 0 \\ \frac{\nu_{21}E_{11}}{1-\nu_o^2} & \frac{E_{22}}{1-\nu_o^2} & 0 \\ 0 & 0 & E_{12} \end{bmatrix}, \quad \{\alpha\}_m = \begin{Bmatrix} \alpha_{11} \\ \alpha_{22} \\ 0 \end{Bmatrix} \tag{IV.34}$$

where,

$$\nu_o^2 = \nu_{12}\nu_{21} \tag{IV.35}$$

and by symmetry in the constitutive relations,

$$\nu_{12} = \nu_{21} \frac{E_{11}}{E_{22}} \tag{IV.36}$$

The spatial variation of temperature is assumed not to change with the local surface coordinates and to be constant through the thickness of each layer. Hence, nonlinear gradients through the shell thickness can be approximated by a series of finite steps. It is assumed that the temperature gradient through the shell wall is defined by a set of discrete temperatures, T_K, (K = 1,M), which are given at normal coordinate locations, z_K, (K = 1,M), (see Figure 6). This gradient is defined at the element level and is given at the element centroid location. The average layer temperature, T_n, must then be obtained by interpolation of the temperature gradient through the wall. It is further assumed that the material property matrices $[G]_m$ and $\{\alpha\}_m$ are temperature dependent and that they have been obtained by interpolating the appropriate set of material properties at the average layer temperature.

As an example, using linear interpolation the average layer temperature is,

$$T_n = T_K + (T_{K+1} - T_K) \frac{(z_C^n - z_K)}{(z_{K+1} - z_K)} \qquad \text{(IV.37)}$$

where

$$z_C^n = \frac{1}{2}(z_I^n + z_O^n) \qquad \text{(IV.38)}$$

Having computed the matrices $[G]_m$ and $\{\alpha\}_m$ for each layer in the material coordinate system (x_m^K) it is now necessary to rotate them through the anisotropic material orientation angle, ϕ, into the shell coordinates (x_S^K). The angle ϕ can change from layer to layer.

$$[G]_S = [T_P][G]_m[T_P]^T \qquad \text{(IV.39)}$$

$$\{\alpha\}_S = [T_Q]\{\alpha\}_m \qquad \text{(IV.40)}$$

where the transformation matrices (see [121]) are,

$$[T_P]^T = \begin{bmatrix} C^2 & S^2 & CS \\ S^2 & C^2 & -CS \\ -2CS & 2CS & C^2 - S^2 \end{bmatrix} \qquad \text{(IV.41)}$$

$$[T_Q] = \begin{bmatrix} C^2 & S^2 & -CS \\ S^2 & C^2 & CS \\ 2CS & -2CS & C^2 - S^2 \end{bmatrix} \qquad \text{(IV.42)}$$

$$C = \cos\phi, \; S = \sin\phi \qquad \text{(IV.43)}$$

The physical matrices $[G]_S$ and $\{\alpha\}_S$ in shell coordinates must now be transformed to tensor quantities to permit their use in the general tensor formulation. (See Section IV.D, equations (IV.323) and (IV.310)).

$$[\,\mathbf{E}\,] = [T_\sigma][G]_S[T_\gamma] \tag{IV.44}$$

$$\{\varepsilon\} = [T_\gamma]^{-1}\{\alpha\}_S \tag{IV.45}$$

where:

$$[T_\sigma] = \begin{bmatrix} \sqrt{\frac{a^{11}}{a_{11}}} & 0 & 0 \\ 0 & \sqrt{\frac{a^{22}}{a_{22}}} & 0 \\ 0 & 0 & \sqrt{\frac{a^{11}}{a_{22}}} \end{bmatrix} \tag{IV.46}$$

$$[T_\gamma] = \begin{bmatrix} \frac{1}{a_{11}} & 0 & 0 \\ 0 & \frac{1}{a_{22}} & 0 \\ 0 & 0 & \frac{1}{\sqrt{a_{11}a_{22}}} \end{bmatrix} \tag{IV.47}$$

Thus,

$$[\mathbf{E}] = \begin{bmatrix} \frac{1}{a_{11}}\sqrt{\frac{a^{11}}{a_{11}}}\,G_{11} & \frac{1}{a_{22}}\sqrt{\frac{a^{11}}{a_{11}}}\,G_{12} & \frac{1}{a_{11}}\sqrt{\frac{a^{11}}{a_{22}}}\,G_{13} \\ \frac{1}{a_{11}}\sqrt{\frac{a^{22}}{a_{22}}}\,G_{21} & \frac{1}{a_{22}}\sqrt{\frac{a^{22}}{a_{22}}}\,G_{22} & \frac{1}{a_{22}}\sqrt{\frac{a^{22}}{a_{11}}}\,G_{23} \\ \frac{1}{a_{11}}\sqrt{\frac{a^{11}}{a_{22}}}\,G_{31} & \frac{1}{a_{22}}\sqrt{\frac{a^{11}}{a_{22}}}\,G_{32} & \frac{1}{a_{22}}\sqrt{\frac{a^{11}}{a_{11}}}\,G_{33} \end{bmatrix}_S \qquad \text{(IV.48)}$$

$$\{\varepsilon\} = \begin{Bmatrix} \varepsilon_{11} \\ \varepsilon_{22} \\ 2\varepsilon_{12} \end{Bmatrix} = \begin{Bmatrix} a_{11}\alpha_{11} \\ a_{22}\alpha_{22} \\ \sqrt{a_{11}a_{22}}\;\alpha_{12} \end{Bmatrix}_S \qquad \text{(IV.49)}$$

Having completed the preliminary calculations for each layer, the integration of the material properties through the thickness can be performed to obtain the compliances for the shell wall.

$$[D] = \int [\mathbf{E}]dz$$

$$= \sum_{n=1}^{N} [\mathbf{E}]_n \int_{z_I^n}^{z_o^n} dz$$

$$= \sum_{n=1}^{N} [\mathbf{E}]_n (z_o^n - z_I^n) \qquad \text{(IV.50)}$$

$$[C] = \int [\mathbf{E}] z\, dz$$

$$= \sum_{n=1}^{N} [\mathbf{E}]_n \int_{z_I^n}^{z_o^n} z\, dz$$

$$= \frac{1}{2} \sum_{n=1}^{N} [\mathbf{E}]_n ((z_o^n)^2 - (z_I^n)^2) \qquad \text{(IV.51)}$$

$$[B] = \int [\mathbf{E}] z^2 dz$$

$$= \sum_{n=1}^{N} [\mathbf{E}] \int_{z_I^n}^{z_o^n} z^2 dz$$

$$= \frac{1}{3} \sum_{n=1}^{N} [\mathbf{E}]_n ((z_o^n)^3 - (z_I^n)^3) \qquad \text{(IV.52)}$$

The thermal forces and moments are,

$$\{N_T\} = \int \{\Omega\} dz$$

$$= \sum_{n=1}^{N} \{\Omega\}_n \int_{z_I^n}^{z_o^n} dz$$

$$= \sum_{n=1}^{N} [\mathbf{E}]_n \{\varepsilon\}_n (z_o^n - z_I^n) \cdot \Delta T \qquad \text{(IV.53)}$$

$$\{M_T\} = \int \{\Omega\} z \, dz$$

$$= \sum_{n=1}^{N} \{\Omega\}_n \int_{z_I^n}^{z_o^n} z dz$$

$$= \frac{1}{2} \sum_{n=1}^{N} [\mathbf{E}]_n \{\varepsilon\}_n \cdot ((z_o^n)^2 - (z_I^n)^2) \cdot \Delta T$$

(IV.54)

Inherent in the philosophy of usage of the above material model is the concept that spatial variations of temperature with the surface coordinates (x_s^1, x_s^2) are accounted for by the element discretization. Thus in selecting the nodal point mesh, care should be taken to insure that surface temperature variations and the consequent material degradation and thermal loading effects can be adequately

approximated. Similar care should be taken in selecting the layer discretization through the thickness. Discretization strategy requirements such as these are inherent in numerical methods of analysis, both finite element and finite difference, and should not be viewed as undue restrictions on the method of analysis.

3. Strain-Displacement and Curvature Displacement Relations

The reference surface strain tensor, $\gamma_{\alpha\beta}$, is related to the components of the reference surface displacement vector, $\vec{u} = u_\alpha \vec{a}^\alpha + w \vec{e}_n$ by,

$$\gamma_{\alpha\beta} = \frac{1}{2}(u_\alpha|_\beta + u_\beta|_\alpha - 2wb_{\alpha\beta}) \qquad \text{(IV.55)}$$

The tensor form can be expanded and recast in the following matrix form,

$$\{\gamma\} = [S]\{U\} \qquad \text{(IV.56)}$$

where,

$$\{U\}^T = [u_1|u_{1,1}|u_{1,2}|u_2|u_{2,1}|u_{2,2}|w] \qquad \text{(IV.57)}$$

$$\{\gamma\}^T = [\gamma_{11}, \gamma_{22}, 2\gamma_{12}] \qquad \text{(IV.58)}$$

$$[S] = \begin{bmatrix} -\Gamma_{11}^{1} & 1 & 0 & -\Gamma_{11}^{2} & 0 & 0 & -b_{11} \\ -\Gamma_{22}^{1} & 0 & 0 & -\Gamma_{22}^{2} & 0 & 1 & -b_{22} \\ -2\Gamma_{12}^{1} & 0 & 1 & -2\Gamma_{12}^{2} & 1 & 0 & -2b_{12} \end{bmatrix} \qquad \text{(IV.59)}$$

The curvature change tensor, $\chi_{\alpha\beta}$, is related to the displacement components by,

$$\chi_{\alpha\beta} = \frac{1}{2}(\Theta_{\alpha}|_{\beta} + \Theta_{\beta}|_{\alpha} + b_{\beta}^{\mu}\omega_{\alpha\mu} + b_{\alpha}^{\mu}\omega_{\beta\mu}) \qquad \text{(IV.60)}$$

where,

$$\Theta_{\alpha} = -(w_{,\alpha} + b_{\alpha}^{\mu}u_{\mu})$$

$$= \text{shell rotation tensor} \qquad \text{(IV.61)}$$

$$\omega_{\alpha\beta} = \frac{1}{2}(u_{\alpha}|_{\beta} - u_{\beta}|_{\alpha}) \qquad \text{(IV.62)}$$

The tensor form can be expanded and recast in the following matrix form,

$$\{\chi\} = [R]\{V\} \qquad \text{(IV.63)}$$

where,

$$\{V\}^T = [u_1|u_{1,1}|u_{1,2}|u_2|u_{2,1}|u_{2,2}|w_{,1}|w_{,2}|w_{,11}|w_{,12}|w_{,22}] \tag{IV.64}$$

$$\{\chi\}^T = [\chi_{11},\ \chi_{22},\ {}^2\chi_{12}] \tag{IV.65}$$

$$[R]^T = \left[\begin{array}{c|c|c}
b_1^1\Gamma_{11}^1+b_1^2\Gamma_{21}^1 & b_2^1\Gamma_{12}^1+b_2^2\Gamma_{22}^1 & b_1^1\Gamma_{12}^1+b_1^2\Gamma_{22}^1 \\
-b_1^1|_1 & -b_2^1|_2 & +b_2^1\Gamma_{11}^1+b_2^2\Gamma_{21}^1 \\
 & & -b_1^1|_2-b_2^1|_1 \\
\hline
-b_1^1 & 0 & -b_2^1 \\
\hline
\frac{1}{2}b_1^2 & -\frac{3}{2}b_2^1 & -\frac{3}{2}b_1^1+\frac{1}{2}b_2^2 \\
\hline
b_1^1\Gamma_{11}^2+b_1^2\Gamma_{21}^2 & b_2^1\Gamma_{12}^2+b_2^2\Gamma_{22}^2 & b_1^1\Gamma_{12}^2+b_1^2\Gamma_{22}^2 \\
-b_1^2|_1 & -b_2^2|_2 & +b_2^1\Gamma_{11}^2+b_2^2\Gamma_{21}^2 \\
 & & -b_1^2|_2-b_2^2|_1 \\
\hline
-\frac{3}{2}b_1^2 & \frac{1}{2}b_2^1 & -\frac{3}{2}b_2^2+\frac{1}{2}b_1^1 \\
\hline
0 & -b_2^2 & -b_1^2 \\
\hline
\Gamma_{11}^1 & \Gamma_{22}^1 & 2\Gamma_{12}^1 \\
\hline
\Gamma_{11}^2 & \Gamma_{22}^2 & 2\Gamma_{12}^2 \\
\hline
-1 & 0 & 0 \\
\hline
0 & 0 & -2 \\
\hline
0 & -1 & 0
\end{array}\right] \tag{IV.66}$$

The matrices [S] and [R] are functions of the shell geometry only and are completely general, not being restricted to any particular shell shape. If the [S] and [R] matrices are programmed for automatic computation in this form, various shell geometries can be handled at execution time by appropriate computation of the entries in [S] and [R]. For any particular class of shells of interest (e.g., cylindrical, spherical, conical) it is only necessary to compute the Christoffel symbols $\Gamma^{\alpha}_{\beta\rho}$, the second fundamental form b^{α}_{β}, and its covariant derivative $b^{\alpha}_{\beta}|_{\rho}$, and the metric tensor $a_{\alpha\beta}$, in order to completely define the [S] and [R] matrices. In Appendix E, Tables E.1 through E.5, concise summaries of these tensors are given for conical, cylindrical and spherical shells as well as for flat plates in both polar and Cartesian coordinates.

4. Finite Difference Approximation to Strain and Curvature Change Tensors

It is now necessary to introduce a finite approximation to the reference surface strain and curvature change tensors. The approximation will be a generalized finite difference procedure which will be developed in the same general way as a finite element. That is, the strain energy will be integrated over a finite region (element) and the total energy obtained by summing on the number of elements. The finite difference element differs from the conventional

finite element in that the displacement field for the normal component of displacement is defined such that it extends beyond the region of integration (element) into several adjacent elements. The displacement fields for the tangential components of displacement are contained within the region of integration.

The computational procedure is termed generalized because unlike conventional finite difference methods the discrete approximation formulated herein does not rely on nodal point meshes which coincide with shell surface coordinate lines, but rather it is developed for arbitrary grids. The removal of this classic restriction which is inherent in conventional finite difference methods makes this generalized finite difference scheme competitive with the finite element method in its ability to model complex geometries. The generalized finite difference element geometry is depicted in Figures 4 and 7.

The tangential components of displacement, u_1 and u_2, are assumed to be a bilinear function of the local element coordinates λ and μ. These displacement fields are defined over the region contained within the solid line of Figure 7, and include the discrete values of displacement, u_1^K and u_2^K, $K = 1,4$. This region is also the area over which the strain energy will be integrated; hence it is the "element area" in conventional finite element terminology. In matrix form, the displacement approximations are,

$$u_1 = [L]\{W_1\} \ , \quad u_2 = [L]\{W_2\} \tag{IV.67}$$

where,

$$[L] = \text{linear shape functions}^*$$

$$= [L_1, L_2, L_3, L_4] \tag{IV.68}$$

$$\{W_N\}^T = \text{discrete nodal point displacement vector}$$

$$= [u_N^1, u_N^2, u_N^3, u_N^4], \ N=1,2 \tag{IV.69}$$

and,

$$L_1 = \tfrac{1}{4}(1-\lambda)(1-\mu)$$

$$L_2 = \tfrac{1}{4}(1+\lambda)(1-\mu)$$

$$L_3 = \tfrac{1}{4}(1+\lambda)(1+\mu)$$

$$L_4 = \tfrac{1}{4}(1-\lambda)(1+\mu) \tag{IV.70}$$

The displacement gradients with respect to the element coordinates (λ,μ) are then obtained by differentiating (IV.67),

$$u_{N,\lambda} = [L_{,\lambda}]\{W_N\}$$

$$u_{N,\mu} = [L,\mu]\{W_N\} \qquad N=1,2 \tag{IV.71}$$

*The linear shape functions are described in detail in Appendix C.

In order to proceed with the discrete approximation it is necessary to obtain the displacement gradients with respect to the Gaussian surface coordinates. This can be accomplished by utilizing the isoparametric mapping techniques of Zienkiewicz and his coworkers, [23,24,29,30]. Let the Gaussian surface coordinates be bilinear functions of the local element coordinates (λ and μ) using the same shape functions as for the tangential displacements. In matrix form, this approximation is,

$$x^M = [L]\{x_K^M\} \tag{IV.72}$$

where,

$\{x_K^M\}^T$ = vector of nodal point Gaussian coordinates

$M = 1,2$ = coordinate direction

$K = 1,\ldots, 4$ = nodal point number

then by differentiating (IV.72),

$$x^M_{,\lambda} = [L_{,\lambda}]\{x_K^M\}$$

$$x^M_{,\mu} = [L_{,\mu}]\{x_K^M\} \tag{IV.73}$$

The spatial derivatives of the displacement functions with respect to local coordinates are related to the displacement gradients (referred to Gaussian surface coordinates x^1, x^2) by the familiar first order Jacobian matrix,

$$\begin{Bmatrix} u_{N,\lambda} \\ \\ u_{N,\mu} \end{Bmatrix} = [J_1] \begin{Bmatrix} u_{N,1} \\ \\ u_{N,2} \end{Bmatrix} \qquad \text{(IV.74)}$$

where,

$$[J_1] = \begin{bmatrix} x^1_{,\lambda} & x^2_{,\lambda} \\ \\ x^1_{,\mu} & x^2_{,\mu} \end{bmatrix} \qquad \text{(IV.75)}$$

By substituting (IV.73) into (IV.75) the Jacobian can be expressed in terms of the shape functions and nodal point Gaussian coordinates,

$$[J_1] = \begin{bmatrix} L_{,\lambda} \\ \hline L_{,\mu} \end{bmatrix} [x^1_k \,\vdots\, x^2_k] \,, \quad k=1,\ldots,4 \qquad \text{(IV.76)}$$

where by differentiation of (IV.70),

$$\begin{aligned} L_{1,\lambda} &= -\tfrac{1}{4}(1-\mu) \,, & L_{1,\mu} &= -\tfrac{1}{4}(1-\lambda) \\ L_{2,\lambda} &= \tfrac{1}{4}(1-\mu) \,, & L_{2,\mu} &= -\tfrac{1}{4}(1+\lambda) \\ L_{3,\lambda} &= \tfrac{1}{4}(1+\mu) \,, & L_{3,\mu} &= \tfrac{1}{4}(1+\lambda) \\ L_{4,\lambda} &= -\tfrac{1}{4}(1+\mu) \,, & L_{4,\mu} &= \tfrac{1}{4}(1-\lambda) \end{aligned} \qquad \text{(IV.77)}$$

The displacement gradients with respect to the Gaussian coordinates are then obtained from the inverse of (IV.74),

AD-A034 788 NAVAL SURFACE WEAPONS CENTER WHITE OAK LAB SILVER SP--ETC F/G 13/13
A GENERALIZED FINITE DIFFERENCE ELEMENT FOR THE THERMOELASTIC S--ETC(U)
JUN 76 R J EDWARDS

UNCLASSIFIED NSWC/WOL/TR-76-66 NL

2 OF 4
AD
A034788



$$\begin{Bmatrix} u_{N,1} \\ \\ u_{N,2} \end{Bmatrix} = [J_1]^{-1} \begin{Bmatrix} u_{N,\lambda} \\ \\ u_{N,\mu} \end{Bmatrix}$$

$$= [T^L] \{W_N\} \qquad \text{(IV.78)}$$

where the relations (IV.71) have been used to arrive at,

$$[T^L] = [J_1]^{-1} \begin{bmatrix} L_{,\lambda} \\ L_{,\mu} \end{bmatrix} \qquad \text{(IV.79)}$$

The matrix equation which relates the strain vector, $\{\gamma\}$, and displacement gradient vector, $\{U\}$, can now be recast in the following form. Let,

$$\{U\} = [F]\{W\} \qquad \text{(IV.80)}$$

Then by substituting (IV.80) into (IV.56),

$$\{\gamma\} = [S]\{U\}$$
$$= [S][F]\{W\} \qquad \text{(IV.81)}$$

where,

$$\{U\}^T = [u_1, u_{1,1}, u_{1,2}, u_2, u_{2,1}, u_{2,2}, w] \tag{IV.82}$$

$$\{W\}^T = [u_1^1, u_2^1, u_1^2, u_2^2, u_1^3, u_2^3, u_1^4, u_2^4 | w^5, w^6, \ldots, w^{13}] \tag{IV.83}$$

$$[F] = \left[\begin{array}{cccccccc|cc}
L_1 & 0 & L_2 & 0 & L_3 & 0 & L_4 & 0 & 0 & 0 \longrightarrow 0 \\
T_{11}^L & 0 & T_{12}^L & 0 & T_{13}^L & 0 & T_{14}^L & 0 & 0 & 0 \longrightarrow 0 \\
T_{21}^L & 0 & T_{22}^L & 0 & T_{23}^L & 0 & T_{24}^L & 0 & 0 & 0 \longrightarrow 0 \\
0 & L_1 & 0 & L_2 & 0 & L_3 & 0 & L_4 & 0 & 0 \longrightarrow 0 \\
0 & T_{11}^L & 0 & T_{12}^L & 0 & T_{13}^L & 0 & T_{14}^L & 0 & 0 \longrightarrow 0 \\
0 & T_{12}^L & 0 & T_{22}^L & 0 & T_{23}^L & 0 & T_{24}^L & 0 & 0 \longrightarrow 0 \\
0 & 0 & 0 & 0 & 0 & 0 & 0 & 0 & 1 & 0 \longrightarrow 0
\end{array}\right] \tag{IV.84}$$

The normal component of displacement, w, is assumed to be a biquadratic function of the local element coordinates α and β. The displacement field is defined over the region contained within the dashed line of Figure 7 and includes the discrete values of displacement w^k, $k = 5, 13$. The w displacement field thus extends beyond the "element area" into several adjacent elements.

In matrix form, the displacement approximation is,

$$w = [H]\{W_3\} \tag{IV.85}$$

where,

$$[H] = \text{quadratic shape functions*}$$
$$= [H_1, H_2, \ldots, H_9] \qquad \text{(IV.86)}$$

$$\{W_3\}^T = \text{discrete nodal point displacement vector}$$
$$= [w^5, w^6, \ldots, w^{13}] \qquad \text{(IV.87)}$$

and,

$$H_1 = (1-\alpha^2)(1-\beta^2)$$
$$H_2 = \tfrac{1}{4}\alpha(1-\alpha)\beta(1-\beta)$$
$$H_3 = -\tfrac{1}{2}(1-\alpha^2)\beta(1-\beta)$$
$$H_4 = -\tfrac{1}{4}\alpha(1+\alpha)\beta(1-\beta)$$
$$H_5 = \tfrac{1}{2}\alpha(1+\alpha)(1-\beta^2)$$
$$H_6 = \tfrac{1}{4}\alpha(1+\alpha)\beta(1+\beta)$$
$$H_7 = \tfrac{1}{2}(1-\alpha^2)\beta(1+\beta)$$
$$H_8 = -\tfrac{1}{4}\alpha(1-\alpha)\beta(1+\beta)$$
$$H_9 = -\tfrac{1}{2}\alpha(1-\alpha)(1-\beta^2) \qquad \text{(IV.88)}$$

---

*The quadratic shape functions are described in detail in Appendix C.

The displacement gradients with respect to the element coordinates (α,β) are obtained by differentiating (IV.85),

$$
\begin{aligned}
w_{,\alpha} &= [H_{,\alpha}]\{W_3\} \\
w_{,\beta} &= [H_{,\beta}]\{W_3\} \\
w_{,\alpha\alpha} &= [H_{,\alpha\alpha}]\{W_3\} \\
w_{,\alpha\beta} &= [H_{,\alpha\beta}]\{W_3\} \\
w_{,\beta\beta} &= [H_{,\beta\beta}]\{W_3\}
\end{aligned}
\qquad \text{(IV.89)}
$$

Again using the isoparametric mapping technique, let the shell coordinates be biquadratic functions of the element coordinates (α,β) using the same shape functions as for the normal displacement. In matrix form this approximation is,

$$x^M = [H]\{x_K^M\} \qquad \text{(IV.90)}$$

where,

$\{x_K^M\}$ = vector of nodal point shell coordinates

M = 1,2 = coordinate direction

K = 5,...,13 = nodal point number

Then by differentiating (IV.90),

$$
\begin{aligned}
x^M_{,\alpha} &= [H_{,\alpha}]\{x^M_K\} \\
x^M_{,\beta} &= [H_{,\beta}]\{x^M_K\} \\
x^M_{,\alpha\alpha} &= [H_{,\alpha\alpha}]\{x^M_K\} \qquad K=5,\ldots,13 \\
x^M_{,\alpha\beta} &= [H_{,\alpha\beta}]\{x^M_K\} \\
x^M_{,\beta\beta} &= [H_{,\beta\beta}]\{x^M_K\}
\end{aligned}
\tag{IV.91}
$$

The spatial derivatives of the normal displacement function with respect to local coordinates α,β are related to the displacement gradients (referred to shell coordinates x^1, x^2) by the second order Jacobian matrix,

$$
\begin{bmatrix} w_{,\alpha} \\ w_{,\beta} \\ \hline w_{,\alpha\alpha} \\ w_{,\alpha\beta} \\ w_{,\beta\beta} \end{bmatrix}
=
\left[\begin{array}{c|c} J_2 & \text{null} \\ \hline J_3 & J_4 \end{array}\right]
\begin{bmatrix} w_{,1} \\ w_{,2} \\ \hline w_{,11} \\ w_{,12} \\ w_{,22} \end{bmatrix}
= [J_5]
\left[\begin{array}{c} w_{,1} \\ w_{,2} \\ \hline w_{,11} \\ w_{,12} \\ w_{,22} \end{array}\right]
\tag{IV.92}
$$

where,

$$[J_5] = \left[\begin{array}{cc|ccc} x^1_{,\alpha} & x^2_{,\alpha} & 0 & 0 & 0 \\ x^1_{,\beta} & x^2_{,\beta} & 0 & 0 & 0 \\ \hline x^1_{,\alpha\alpha} & x^2_{,\alpha\alpha} & (x^1_{,\alpha})^2 & 2\cdot x^1_{,\alpha}\cdot x^2_{,\alpha} & (x^2_{,\alpha})^2 \\ x^1_{,\alpha\beta} & x^2_{,\alpha\beta} & x^1_{,\alpha}\cdot x^1_{,\beta} & x^1_{,\alpha}\cdot x^2_{,\beta} & x^2_{,\alpha}\cdot x^2_{,\beta} \\ & & & +x^1_{,\beta}\cdot x^2_{,\alpha} & \\ x^1_{,\beta\beta} & x^2_{,\beta\beta} & (x^1_{,\beta})^2 & 2\cdot x^1_{,\beta}\cdot x^2_{,\beta} & (x^2_{,\beta})^2 \end{array}\right] \qquad \text{(IV.93)}$$

By substituting (IV.91) into (IV.93) the Jacobian can be expressed in terms of the shape functions and nodal point coordinates,

$$[J_2] = \begin{bmatrix} H \\ \underline{H}_{,\alpha} \\ \underline{H}_{,\beta} \end{bmatrix} [x^1_K | x^2_K] , \qquad K=5,\ldots,13 \qquad \text{(IV.94)}$$

$$[J_3] = \begin{bmatrix} H \\ \underline{H}_{,\alpha\alpha} \\ \underline{H}_{,\alpha\beta} \\ H_{,\beta\beta} \end{bmatrix} [x^1_K | x^2_K] , \qquad K=5,\ldots,13 \qquad \text{(IV.95)}$$

$$[J_4] = \left[\begin{array}{c|c|c} (J_2)_{11}\cdot(J_2)_{11} & 2\cdot(J_2)_{11}\cdot(J_2)_{12} & (J_2)_{12}\cdot(J_2)_{12} \\ (J_2)_{11}\cdot(J_2)_{21} & (J_2)_{11}\cdot(J_2)_{22} & (J_2)_{12}\cdot(J_2)_{22} \\ & +(J_2)_{21}\cdot(J_2)_{12} & \\ (J_2)_{21}\cdot(J_2)_{21} & 2\cdot(J_2)_{21}\cdot(J_2)_{22} & (J_2)_{22}\cdot(J_2)_{22} \end{array}\right] \qquad \text{(IV.96)}$$

where by differentiation of (IV.88)

$$\begin{aligned} H_{1,\alpha} &= -2\alpha(1-\beta^2) \\ H_{2,\alpha} &= \tfrac{1}{4}\beta(1-\beta)(1-2\alpha) \\ H_{3,\alpha} &= \alpha\beta(1-\beta) \\ H_{4,\alpha} &= -\tfrac{1}{4}\beta(1-\beta)(1+2\alpha) \\ H_{5,\alpha} &= \tfrac{1}{2}(1-\beta^2)(1+2\alpha) \\ H_{6,\alpha} &= \tfrac{1}{4}\beta(1+\beta)(1+2\alpha) \\ H_{7,\alpha} &= -\alpha\beta(1+\beta) \\ H_{8,\alpha} &= -\tfrac{1}{4}\beta(1+\beta)(1-2\alpha) \\ H_{9,\alpha} &= -\tfrac{1}{2}(1-\beta^2)(1-2\alpha) \end{aligned} \qquad \text{(IV.97)}$$

$$H_{1,\beta} = -2\beta(1-\alpha^2)$$

$$H_{2,\beta} = \tfrac{1}{4}\alpha(1-\alpha)(1-2\beta)$$

$$H_{3,\beta} = -\tfrac{1}{2}(1-\alpha^2)(1-2\beta)$$

$$H_{4,\beta} = -\tfrac{1}{4}\alpha(1+\alpha)(1-2\beta)$$

$$H_{5,\beta} = -\alpha\beta(1+\alpha)$$

$$H_{6,\beta} = \tfrac{1}{4}\alpha(1+\alpha)(1+2\beta)$$

$$H_{7,\beta} = \tfrac{1}{2}(1-\alpha^2)(1+2\beta)$$

$$H_{8,\beta} = -\tfrac{1}{4}\alpha(1-\alpha)(1+2\beta)$$

$$H_{9,\beta} = \alpha\beta(1-\alpha) \qquad \text{(IV.98)}$$

and,

$$H_{1,\alpha\alpha} = -2(1-\beta^2)$$

$$H_{2,\alpha\alpha} = -\tfrac{1}{2}\beta(1-\beta)$$

$$H_{3,\alpha\alpha} = \beta(1-\beta)$$

$$H_{4,\alpha\alpha} = -\tfrac{1}{2}\beta(1-\beta)$$

$$H_{5,\alpha\alpha} = (1-\beta^2)$$

$$H_{6,\alpha\alpha} = \tfrac{1}{2}\beta(1+\beta)$$

$$H_{7,\alpha\alpha} = -\beta(1+\beta)$$

$$H_{8,\alpha\alpha} = \tfrac{1}{2}\beta(1+\beta)$$

$$H_{9,\alpha\alpha} = (1-\beta^2) \qquad \text{(IV.99)}$$

$$H_{1,\beta\beta} = -2(1-\alpha^2)$$

$$H_{2,\beta\beta} = -\frac{1}{2}\alpha(1-\alpha)$$

$$H_{3,\beta\beta} = (1-\alpha^2)$$

$$H_{4,\beta\beta} = \frac{1}{2}\alpha(1+\alpha)$$

$$H_{5,\beta\beta} = -\alpha(1+\alpha)$$

$$H_{6,\beta\beta} = \frac{1}{2}\alpha(1+\alpha)$$

$$H_{7,\beta\beta} = (1-\alpha^2)$$

$$H_{8,\beta\beta} = -\frac{1}{2}\alpha(1-\alpha)$$

$$H_{9,\beta\beta} = \alpha(1-\alpha) \qquad \text{(IV.100)}$$

$$H_{1,\alpha\beta} = 4\alpha\beta$$

$$H_{2,\alpha\beta} = \frac{1}{4}(1-2\alpha)(1-2\beta)$$

$$H_{3,\alpha\beta} = \alpha(1-2\beta)$$

$$H_{4,\alpha\beta} = -\frac{1}{4}(1+2\alpha)(1-2\beta)$$

$$H_{5,\alpha\beta} = -\beta(1+2\alpha)$$

$$H_{6,\alpha\beta} = \frac{1}{4}(1+2\alpha)(1+2\beta)$$

$$H_{7,\alpha\beta} = -\alpha(1+2\beta)$$

$$H_{8,\alpha\beta} = -\frac{1}{4}(1-2\alpha)(1+2\beta)$$

$$H_{9,\alpha\beta} = \beta(1-2\alpha) \qquad \text{(IV.101)}$$

The displacement gradients referred to shell coordinates are then obtained from the inverse of (IV.92),

$$\begin{bmatrix} w_{,1} \\ w_{,2} \\ w_{,11} \\ w_{,12} \\ w_{,22} \end{bmatrix} = [J_5]^{-1} \begin{bmatrix} w_{,\alpha} \\ w_{,\beta} \\ w_{,\alpha\alpha} \\ w_{,\alpha\beta} \\ w_{,\beta\beta} \end{bmatrix}$$

$$= [T^H]\{W_3\} \qquad \text{(IV.102)}$$

where the relations (IV.89) have been used to arrive at,

$$[T^H] = [J_5]^{-1} \begin{bmatrix} H_{,\alpha} \\ H_{,\beta} \\ H_{,\alpha\alpha} \\ H_{,\alpha\beta} \\ H_{,\beta\beta} \end{bmatrix} \qquad \text{(IV.103)}$$

A convenient form for the inverse of the Jacobian is,

$$[J_5]^{-1} = \left[\begin{array}{c|c} J_2^{-1} & \text{null} \\ \hline J_4^{-1} J_3 J_2^{-1} & J_4^{-1} \end{array}\right] \qquad \text{(IV.104)}$$

The matrix equation which relates the curvature vector, $\{\chi\}$, and displacement gradient vector, $\{V\}$, can now be recast in the following form. Let,

$$\{V\} = [E]\{W\} \tag{IV.105}$$

Then by substituting (IV.105) into (IV.63),

$$\{\chi\} = [R][E]\{W\} \tag{IV.106}$$

where

$$\{V\}^T = [u_1, u_{1,1}, u_{1,2}, u_2, u_{2,1}, u_{2,2} \mid w_{,1}, w_{,2}, w_{,11}, w_{,12}, w_{,22}] \tag{IV.107}$$

$$\{W\}^T = [u_1^1, u_2^1, u_1^2, u_2^2, u_1^3, u_2^3, u_1^4, u_{,2}^4 \mid w^5, w^6, \ldots, w^{13}] \tag{IV.108}$$

$$[E] = \left[\begin{array}{cccccccc|c} L_1 & 0 & L_2 & 0 & L_3 & 0 & L_4 & 0 & \\ T_{11}^L & 0 & T_{12}^L & 0 & T_{13}^L & 0 & T_{14}^L & 0 & \\ T_{21}^L & 0 & T_{22}^L & 0 & T_{23}^L & 0 & T_{24}^L & 0 & \\ 0 & L_1 & 0 & L_2 & 0 & L_3 & 0 & L_4 & \text{NULL} \\ 0 & T_{11}^L & 0 & T_{12}^L & 0 & T_{13}^L & 0 & T_{14}^L & \\ 0 & T_{21}^L & 0 & T_{22}^L & 0 & T_{23}^L & 0 & T_{24}^L & \\ \hline \multicolumn{8}{c|}{\text{NULL}} & T^H \end{array}\right] \tag{IV.109}$$

5. Coordinate Transformations

It is necessary at this point in the analytical development to introduce several coordinate transformations which will be useful in deriving the final physical form of structural matrices and load vectors. These transformations relate the tensor and physical components of the displacement or rotation vectors at an arbitrary point in the element domain to the element displacement vector. The element displacement vector consists of a specific partitioning of the discrete displacement components which are defined at the 13 nodal points shown in Figure 7. Equation (IV.83) defines the covariant tensor form of the element displacement vector; the physical form will be derived in this section. The shape function approximations (IV.67) and (IV.85) will be employed in several alternative matrix forms as required by various partitionings of the displacement variables.

The physical components of displacement, $\{w\}$, at an arbitrary point on the shell reference surface are related to the covariant components, $\{u\}$, by the transformation (see IV.285),

$$\{w\} = [T_u]\{u\} \tag{IV.110}$$

where,

$$\{w\}^T = [u,v,w] \tag{IV.111}$$

$$\{u\}^T = [u_1, u_2, w] \tag{IV.112}$$

$$[T_u] = \begin{bmatrix} A_1 a^{11} & A_1 a^{12} & 0 \\ A_2 a^{21} & A_2 a^{22} & 0 \\ 0 & 0 & 1 \end{bmatrix} \qquad \text{(IV.113)}$$

The covariant components of displacement, {u}, at an arbitrary point in the displacement field of an element are related to the covariant components, {w}, of the element displacement vector by the previously introduced shape functions (IV.67) and (IV.86) as follows.

Let,

$$\{u\} = [T_E]\{W\} \qquad \text{(IV.114)}$$

or in partitioned form,

$$\left\{\begin{array}{c} u_1 \\ u_2 \\ \hline w \end{array}\right\} = \left[\begin{array}{c|c} T_L & \text{NULL} \\ \hline \text{NULL} & H \end{array}\right] \left\{\begin{array}{c} W_{12} \\ \hline W_3 \end{array}\right\} \qquad \text{(IV.115)}$$

where by (IV.83),

$$\{W\}^T = [W_{12} \mid W_3]$$
$$= [u_1^1, u_2^1, \ldots, u_1^4, u_2^4 \mid w^5, \ldots, w^{13}] \qquad \text{(IV.116)}$$

and by use of (IV.67) and (IV.86),

$$[T_E] = \left[\begin{array}{cccccccc|c} L_1 & 0 & L_2 & 0 & L_3 & 0 & L_4 & 0 & \\ 0 & L_1 & 0 & L_2 & 0 & L_3 & 0 & L_4 & \text{NULL} \\ \hline & & & & \text{NULL} & & & & H_1,\ldots,H_9 \end{array}\right] \tag{IV.117}$$

The covariant tensor form of the element displacement vector, $\{W\}$, is related to the physical form, $\{\bar{W}\}$, by the transformation,

$$\{W\} = [T_W]\{\bar{W}\} \tag{IV.118}$$

where by the use of the inverse of (IV.113),

$$\begin{aligned} \{\bar{W}\}^T &= [\bar{W}_{12} \mid W_3] \\ &= [u^1, v^1, \ldots, u^4, v^4 \mid w^5, \ldots, w^{13}] \end{aligned} \tag{IV.119}$$

$$\begin{aligned} [T_W] &= \text{Diagonal } [T_{W_{12}} \mid T_{W_3}] \\ &= \text{Diagonal}[[T_W{}^1], \ldots, [T_W{}^4] \mid [T_W{}^5], \ldots, [T_W{}^{13}]] \end{aligned} \tag{IV.120}$$

$$[T_W^I] = \begin{bmatrix} A_1 & a_{21}/A_2 \\ a_{12}/A_1 & A_2 \end{bmatrix}, \quad I = 1,\ldots,4$$

$$= [1], \qquad I = 5,\ldots,13 \tag{IV.121}$$

The covariant tensor components of displacement, {u}, at an arbitrary point in the displacement field are then related to the physical components, $\{\bar{W}\}$, of the element displacement vector by substitution of (IV.118) into (IV.114) which gives,

$$\{u\} = [T_E][T_W]\{\bar{W}\} \tag{IV.122}$$

The physical components of displacement, {w}, at an arbitrary point in the displacement field are similarly related to the physical components, $\{\bar{W}\}$, of the element displacement vector by substituting (IV.122) into (IV.110) to give,

$$\{w\} = [T_u][T_E][T_W]\{\bar{W}\} \tag{IV.123}$$

Later in the analytical development the partitions of the above transformations which pertain to the in-plane components of displacement will be needed. These are obtained as follows.

Let the in-plane partition of (IV.110), (IV.115) and (IV.118) be,

$$\begin{Bmatrix} u \\ v \end{Bmatrix} = [T_v] \begin{Bmatrix} u_1 \\ u_2 \end{Bmatrix} \tag{IV.124}$$

$$\begin{Bmatrix} u_1 \\ u_2 \end{Bmatrix} = [T_L]\{W_{12}\} \tag{IV.125}$$

$$\{W_{12}\} = [T_{W_{12}}]\{\bar{W}_{12}\} \tag{IV.126}$$

Then by substitution of (IV.126) into (IV.125),

$$\begin{Bmatrix} u_1 \\ u_2 \end{Bmatrix} = [T_L][T_{W_{12}}]\{\bar{W}_{12}\} \tag{IV.127}$$

and by substitution of (IV.127) into (IV.124),

$$\begin{Bmatrix} u \\ v \end{Bmatrix} = [T_v][T_L][T_{W_{12}}]\{\bar{W}_{12}\} \tag{IV.128}$$

where

$$[T_v] = \begin{bmatrix} A_1 a^{11} & A_1 a^{12} \\ A_2 a^{21} & A_2 a^{22} \end{bmatrix} \tag{IV.129}$$

$$[T_L] = \begin{bmatrix} L_1 & 0 & L_2 & 0 & L_3 & 0 & L_4 & 0 \\ 0 & L_1 & 0 & L_2 & 0 & L_3 & 0 & L_4 \end{bmatrix} \tag{IV.130}$$

$$\{W_{12}\}^T = [u_1^1, u_2^1, \ldots, u_1^4, u_2^4] \tag{IV.131}$$

$$\{\bar{W}_{12}\}^T = [u^1, v^1, \ldots, u^4, v^4] \tag{IV.132}$$

$$[T_{W_{12}}] = \text{Diagonal } [[T_W{}^1], \ldots, [T_W{}^4]] \tag{IV.133}$$

The first derivatives of the normal displacement at an arbitrary point in the displacement field of an element are related to the discrete normal components, $\{W_3\}$, of the element displacement vector by extracting a partition of (IV.102) and using (IV.189) to give,

$$\begin{Bmatrix} w_{,1} \\ w_{,2} \end{Bmatrix} = [J_2]^{-1} \begin{Bmatrix} w_{,\alpha} \\ w_{,\beta} \end{Bmatrix}$$

$$= [J_2]^{-1} \begin{bmatrix} H_{,\alpha} \\ H_{,\beta} \end{bmatrix} \{W_3\}$$

$$= [T_H] \{W_3\} \tag{IV.134}$$

Utilizing the last two transformations it is possible to express the covariant components of the rotation vector, $\{\theta\}$, at an arbitrary point in the element domain in terms of the physical components, $\{\bar{W}\}$, of the element displacement vector as follows. The rotation vector is,

$$\vec{\theta} = \theta_1 \vec{a}^1 + \theta_2 \vec{a}^2 \tag{IV.135}$$

where by (II.31),

$$\theta_\alpha = -w_{,\alpha} - b_\alpha^\beta u_\beta \tag{IV.136}$$

Recasting in matrix form gives,

$$\{\theta\} = \begin{Bmatrix} \theta_1 \\ \theta_2 \\ 0 \end{Bmatrix} = -[\bar{b}] \begin{Bmatrix} u_1 \\ u_2 \\ 0 \end{Bmatrix} - \begin{Bmatrix} w_{,1} \\ w_{,2} \\ 0 \end{Bmatrix} \tag{IV.137}$$

where,

$$[\bar{b}] = \begin{bmatrix} b_1^1 & b_1^2 & 0 \\ b_2^1 & b_2^2 & 0 \\ 0 & 0 & 0 \end{bmatrix} \tag{IV.138}$$

Since by (IV.125),

$$\begin{Bmatrix} u_1 \\ \hline u_2 \\ \hline 0 \end{Bmatrix} = \begin{bmatrix} T_L \\ \hline \text{------} \\ \text{NULL} \end{bmatrix} \{W_{12}\}$$

$$= [\bar{T}_L]\{W_{12}\} \qquad \text{(IV.139)}$$

and by (IV.134),

$$\begin{Bmatrix} w_{,1} \\ \hline w_{,2} \\ \hline 0 \end{Bmatrix} = \begin{bmatrix} T_H \\ \hline \text{------} \\ \text{NULL} \end{bmatrix} \{W_3\}$$

$$= [\bar{T}_H]\{W_3\} \qquad \text{(IV.140)}$$

then substituting (IV.139) and (IV.140) into (IV.137) results in the transformation,

$$\{\bullet\} = -[\bar{b}][\bar{T}_L]\{W_{12}\} - [\bar{T}_H]\{W_3\}$$

$$= [-[\bar{b}][\bar{T}_L] \,|\, -[\bar{T}_H]] \left\{\begin{matrix} W_{12} \\ \hline W_3 \end{matrix}\right\}$$

$$= [T_\bullet]\{W\} \qquad \text{(IV.141)}$$

Transforming (IV.141) to physical components by use of (IV.118) gives,

$$\{\Theta\} = [T_\Theta][Tw]\{\bar{W}\} \tag{IV.142}$$

In a similar manner the physical components of the rotation vector, $\{\Psi\}$, at an arbitrary point in the element displacement field may be expressed in terms of the physical components, $\{\bar{W}\}$, of the element displacement vector.

The physical rotation vector is,

$$\vec{\Theta} = \Psi_1 \vec{e}_1 + \Psi_2 \vec{e}_2 \tag{IV.143}$$

where by (II.38),

$$\Psi_1 = - A_1[a^{11}w_{,1} + a^{12}w_{,2} + b^{11}u_1 + b^{12}u_2] \tag{IV.144}$$

$$\Psi_2 = - A_2[a^{21}w_{,1} + a^{22}w_{,2} + b^{21}u_1 + b^{22}u_2] \tag{IV.145}$$

Recasting in matrix form gives,

$$\{\Psi\} = \begin{Bmatrix} \Psi_1 \\ \\ \Psi_2 \end{Bmatrix} = [d_v] \begin{Bmatrix} u_1 \\ \\ u_2 \end{Bmatrix} + [d_w] \begin{Bmatrix} w_{,1} \\ \\ w_{,2} \end{Bmatrix} \tag{IV.146}$$

where,

$$[d_v] = \left[\begin{array}{c} d_v^1 \\ \hline d_v^2 \end{array}\right] = \left[\begin{array}{c|c} -A_1 b^{11} & -A_1 b^{12} \\ \hline -A_2 b^{21} & -A_2 b^{22} \end{array}\right] \qquad \text{(IV.147)}$$

$$[d_w] = \left[\begin{array}{c} d_w^1 \\ \hline d_w^2 \end{array}\right] = \left[\begin{array}{c|c} -A_1 a^{11} & -A_1 a^{12} \\ \hline -A_2 a^{21} & -A_2 a^{22} \end{array}\right] \qquad \text{(IV.148)}$$

Then by substitution of (IV.125) and (IV.134) into (IV.146),

$$\{\Psi\} = [d_v][T_L]\{W_{12}\} + [d_w][T_H]\{W_3\} \qquad \text{(IV.149)}$$

or alternatively,

$$\{\Psi\} = [[d_v][T_L] \quad [d_w][T_H]] \left\{\begin{array}{c} W_{12} \\ \hline W_3 \end{array}\right\}$$

$$= [T_\Psi]\{W\} \qquad \text{(IV.150)}$$

Transforming (IV.150) to physical components by use of (IV.118) gives,

$$\{\Psi\} = [T_\Psi][T_W]\{\bar{W}\} \qquad \text{(IV.151)}$$

Another form of the rotation vector which is defined by $\vec{\vartheta} = \vec{e}_n \times \vec{\omega}$ (see II.39), is more useful in deriving physical load vectors. It also can be expressed in terms of the

physical components, $\{\bar{W}\}$, of the element displacement vector as follows.

The alternate form of the physical rotation vector is,

$$\vec{\vartheta} = -\Psi_2 \vec{e}_1 + \Psi_1 \vec{e}_2 \qquad \text{(IV.152)}$$

Recasting in matrix form and using (IV.144) and (IV.145) yields,

$$\{\vartheta\} = \begin{Bmatrix} \vartheta_1 \\ \\ \vartheta_2 \end{Bmatrix} = [C_v] \begin{Bmatrix} u_1 \\ \\ u_2 \end{Bmatrix} + [C_w] \begin{Bmatrix} w_{,1} \\ \\ w_{,2} \end{Bmatrix} \qquad \text{(IV.153)}$$

where,

$$[C_v] = \left[\begin{array}{c} C_v^1 \\ \hline C_v^2 \end{array}\right] = \left[\begin{array}{c|c} A_2 b^{21} & A_2 b^{22} \\ \hline -A_1 b^{11} & -A_1 b^{12} \end{array}\right] \qquad \text{(IV.154)}$$

$$[C_w] = \left[\begin{array}{c} C_w^1 \\ \hline C_w^2 \end{array}\right] = \left[\begin{array}{c|c} A_2 a^{21} & A_2 a^{22} \\ \hline -A_1 a^{11} & -A_1 a^{12} \end{array}\right] \qquad \text{(IV.155)}$$

Then by substituting (IV.125) and (IV.134) into (IV.153),

$$\{\vartheta\} = [C_v][T_L]\{W_{12}\} + [C_w][T_H]\{W_3\} \qquad \text{(IV.156)}$$

or alternatively,

$$\{\vartheta\} = [[C_v][T_L] \vdots [C_w][T_H]] \begin{Bmatrix} W \\ -\bar{W}_3^{12}- \end{Bmatrix}$$

$$= [T_\vartheta]\{W\} \qquad \text{(IV.157)}$$

Transforming (IV.157) to physical components by use of (IV.118) results in,

$$\{\vartheta\} = [T_\vartheta][T_W]\{\bar{W}\} \qquad \text{(IV.158)}$$

6. Element Stiffness Matrix

In section IV.B.1, it was shown that the strain energy density for a thin shell is the sum of energies associated with membrane, bending and coupled membrane and bending action. From (IV.19),

$$U_o^S = U_o^M + U_o^C + U_o^B$$

$$= \tfrac{1}{2}\{\gamma\}^T[\mathbf{E}]\{\gamma\} + \tfrac{1}{2}x^3(\{\chi\}^T[\mathbf{E}]\{\gamma\} + \{\gamma\}^T[\mathbf{E}]\{\chi\})$$

$$+ \tfrac{1}{2}(x^3)^2\{\chi\}^T[\mathbf{E}]\{\chi\} \qquad \text{(IV.159)}$$

In section IV.B.2, an analytical model for the shell wall construction was introduced and the strain energy density was integrated through the shell wall to obtain the

strain energy density per unit area. From (IV.28),

$$\bar{U}_o^S = \int U_o^S \, dx^3$$

$$= \frac{1}{2}\{\gamma\}^T[D]\{\gamma\} + \frac{1}{2}(\{\chi\}^T[C]\{\gamma\} + \{\gamma\}^T[C]\{\chi\})$$

$$+ \frac{1}{2}\{\chi\}^T[B]\{\chi\} \qquad \text{(IV.160)}$$

In section IV.B.3, matrix forms of the strain-displacement and curvature-displacement relations were introduced in which, for later convenience in the analytical development, the shell geometry was effectively isolated from the displacements and displacement gradients. In section IV.B.4, a finite difference approximation to the strain and curvature tensors was described. The method closely parallels that used for the development of conventional finite elements except that the concept of displacement fields which overlap into several adjacent elements was introduced. By substitution of (IV.81) and (IV.106) into (IV.160) the strain energy for the finite difference element now takes the form,

$$U_e^S = \frac{1}{2}\int\int \{W\}^T \Big[[F]^T[S]^T[D][S][F]$$

$$+ [E]^T[R]^T[C][S][F] + [F]^T[S]^T[C][R][E]$$

$$+ [E]^T[R]^T[B][R][E]\Big]\{W\}\sqrt{a}\; dx^1dx^2$$

$$= \frac{1}{2}\{W\}^T\,[\mathbf{K}_e]\{W\} \qquad \text{(IV.161)}$$

Transforming the tensor form of the element displacement vector, $\{W\}$, which appears in (IV.161) to the physical form, $\{\bar{W}\}$, by use of (IV.118) results in,

$$U_e^S = \frac{1}{2}\{\bar{W}\}^T[T_W]^{-T}[\mathbf{K}_e][T_W]\{\bar{W}\}$$

$$= \frac{1}{2}\{\bar{W}\}^T[\overline{\mathbf{K}}_e]\{\bar{W}\} \qquad \text{(IV.162)}$$

As outlined in Chapter III, the equations of motion (III.9) and (III.10) are arrived at by use of the Theorem of Minimum Potential Energy. By minimizing the strain energy (IV.162) with respect to the discrete variables of the element displacement vector, $\{\bar{W}\}$, the physical form of the element stiffness matrix is found to be,

$$[\overline{\mathbf{K}}_e] = [T_W]^T[\mathbf{K}_e][T_W] \quad . \qquad \text{(IV.163)}$$

where the tensor form of the element stiffness matrix is given by,

$$[\mathbf{K}_e] = \int\int[K_M+K_C^T+K_C+K_B]\sqrt{a}\ \ dx^1\ \ dx^2 \qquad \text{(IV.164)}$$

and by inspection of (IV.161),

$$[K_M] = [F]^T[S]^T[D][S][F]$$

$$[K_C] = [F]^T[S]^T[C][R][E]$$

$$[K_B] = [E]^T[R]^T[B][R][E] \qquad \text{(IV.165)}$$

The subscripts M, B, C refer to stiffnesses associated with membrane, bending and coupled membrane and bending energies.

The integration of expression (IV.164) can be approximated by Gaussian quadrature and gives,

$$[\mathbf{K}_e] = \int_{-1}^{1}\int_{-1}^{1} [K_M+K_C^T+K_C+K_B]\sqrt{a}\cdot|J_1|d\lambda d\mu$$

$$= \sum_{i=1}^{M}\sum_{j=1}^{M} H_i H_j [f_k(\lambda_j,\mu_i)] \qquad \text{(IV.166)}$$

where,

$$[f_k(\lambda_j,\mu_i] = \left[[K_M+K_C^T+K_C+K_B]\cdot\sqrt{a}\cdot|J_1|\right]_{\lambda=\lambda_j,\mu=\mu_i}$$

(IV.167)

H_i, H_j = Weighting coefficients

λ_j, μ_i = Abscissae of the integration points

$|J_1|$ = Determinant of the Jacobian matrix (IV.75)

The weighting coefficients and the positions of the integration points are given in Table 3 for integration orders M=1 through M=5, [24].

The system stiffness matrix appearing in (III.9) and (III.10) is then obtained by summation of the element stiffness matrices (IV.163).

7. Element Thermal Load Vector

In section IV.B.1, it was shown that the thermal work density for a thin shell is the sum of strain energies associated with thermal membrane forces and thermal bending forces. From (IV.19),

$$U_o^T = U_o^{TM} + U_o^{TB}$$

$$= - \Delta T\{\varepsilon\}^T[\,\mathbf{E}\,]\{\gamma\} - \Delta T\{\varepsilon\}^T[\,\mathbf{E}\,]\{\chi\}\cdot x^3 \qquad \text{(IV.168)}$$

In section IV.B.2,an analytical model for the shell wall construction was introduced and the work density was integrated through the shell wall to obtain the thermal work density per unit area. From (IV.28),

$$\bar{U}_o^T = \int U_o^T \, dx^3$$

$$= - \{N_T\}^T\{\gamma\} - \{M_T\}^T\{\chi\} \qquad \text{(IV.169)}$$

In sections IV.B.4 and IV.B.5,a numerical approximation to the reference surface strain and curvature tensors was developed. By substitution of (IV.81) and (IV.106) into (IV.169) the thermal work for the finite difference element can now be expressed in the form,

$$U_e^T = \int\int \left[\{N_T\}^T[S][F] + \{M_T\}^T[R][E]\right]\{W\}\sqrt{a}\, dx^1\, dx^2$$

$$= \{\mathbf{P}_T\}_e^T\{W\} \qquad \text{(IV.170)}$$

Transforming the tensor form of the element displacement vector, $\{W\}$, which appears in (IV.170) to the physical form, $\{\bar{W}\}$, by use of (IV.118) results in,

$$U_e^T = \{\mathbf{P}_T\}_e^T[T_W]\{\bar{W}\}$$

$$= \{\mathbf{P}_T\}_e^T\{\bar{W}\} \qquad \text{(IV.171)}$$

By minimizing the thermal work (IV.171) with respect to the discrete variables of the element displacement vector, $\{\bar{W}\}$, the physical form of the element thermal load vector is found to be,

$$\{\bar{\mathbf{P}}_T\}_e = [T_W]^T\{\mathbf{P}_T\}_e \qquad \text{(IV.172)}$$

where the tensor form of the element thermal load vector is given by,

$$\{\mathbf{P}_T\}_e = \int\int \{P_T^M + P_T^B\}\sqrt{a}\, dx^1\, dx^2 \qquad \text{(IV.173)}$$

and by inspection of (IV.170)

$$\{P_T^M\} = [F]^T[S]^T\{N_T\}$$

$$\{P_T^B\} = [E]^T[R]^T\{M_T\} \qquad \text{(IV.174)}$$

The superscripts M, B refer to thermal loads associated with membrane and bending energies.

The integration of expression (IV.173) can be approximated by Gaussian quadrature and gives,

$$\{\mathbf{P}_T\}_e = \int_{-1}^{1}\int_{-1}^{1}\{P_T^M + P_T^B\}\sqrt{a} \cdot |J_1| \cdot d\lambda d\mu$$

$$= \sum_{i=1}^{M}\sum_{j=1}^{M} H_i H_j \left\{f_{P_T}(\lambda_j,\mu_i)\right\} \qquad \text{(IV.175)}$$

where,

$$\{f_{P_T}(\lambda_j,\mu_i)\} = \left\{\{P_T^M + P_T^B\}\sqrt{a} \cdot |J_1|\right\}_{\lambda=\lambda_j,\mu=\mu_i} \qquad \text{(IV.176)}$$

The thermal contribution to the system load vector appearing in (III.10) is then obtained by summation of the element thermal load vectors (IV.172).

C. Potential Energy of Mechanical and Inertial Loads

1. Total Work Potential

The total potential energy of various mechanical and inertial loadings is,

$$U^W_{TOT} = \sum_{I=1}^{N_p} (U^p_e)_I + \sum_{J=1}^{N_F} U^F_J + \sum_{K=1}^{N_Q} U^Q_K + \sum_{L=1}^{N_e} (U^g_e + U^I_e)_L \qquad \text{(IV.177)}$$

The work term U^p_e is due to a uniformly distributed surface load ($\vec{p}$) acting on the element reference surface, N_p is the number of elements with surface loading and,

$$U^p_e = \int \int (\vec{p} \cdot \vec{u}) \sqrt{a}\, dx^1\, dx^2 \qquad \text{(IV.178)}$$

where

$$\vec{p} = p_1 \vec{e}_1 + p_2 \vec{e}_2 + p_n \vec{e}_n \qquad \text{(IV.179)}$$

$$\vec{u} = u\, \vec{e}_1 + v\, \vec{e}_2 + w\, \vec{e}_n \qquad \text{(IV.180)}$$

= Physical displacement vector at reference surface (see IV.110)

The work term U^F_J is due to a concentrated force ($\vec{F}$) acting at a discrete nodal point (J), N_F is the number of concentrated loads acting and,

$$U_J^F = (\vec{F} \cdot \vec{u})_J \tag{IV.181}$$

where

$$\vec{F}_J = (F_1 \vec{e}_1 + F_2 \vec{e}_2 + F_n \vec{e}_n)_J \tag{IV.182}$$

$$\vec{u}_J = (u \vec{e}_1 + v \vec{e}_2 + w \vec{e}_n)_J \tag{IV.183}$$

= Physical displacement vector at nodal point J

The work term U^Q is due to a concentrated moment $(\vec{Q})$ acting at a discrete nodal point (K), N_Q is the number of concentrated moments acting and,

$$U_K^Q = (\vec{Q} \cdot \vec{\vartheta})_K \tag{IV.184}$$

where,

$$\vec{Q}_K = (Q_1 \vec{e}_1 + Q_2 \vec{e}_2)_K \tag{IV.185}$$

$$= (\vartheta_1 \vec{e}_1 + \vartheta_2 \vec{e}_2)_K \tag{IV.186}$$

= Physical rotation vector at nodal point K

The work term U_e^g is due to a gravity force $(\vec{F}_g)$ acting over the volume of the element, N_E is the total number of elements and,

$$U_e^g = \iiint (\vec{F}_g \cdot \vec{\bar{u}}) \sqrt{a}\, dx^1\, dx^2\, dx^3 \qquad \text{(IV.187)}$$

An approximation to (IV.187) is,

$$U_e^g \approx \iint (\bar{w}_e \vec{g} \cdot \vec{\bar{u}}) \sqrt{a}\, dx^1\, dx^2 \qquad \text{(IV.188)}$$

where

$\bar{w}_e$ = element weight per unit area

$\vec{g}$ = gravity vector

$$\vec{\bar{u}} = \bar{u}\,\vec{e}_1 + \bar{v}\,\vec{e}_2 + w\,\vec{e}_n \qquad \text{(IV.189)}$$

= physical displacement vector at a point off the reference surface

The work term U_e^I is due to inertial loads acting over the volume of the element and is obtained by applying the well known principle of D'Alembert,

$$U_e^I = -\int_V \rho \left(\frac{\partial^2 \vec{\bar{u}}}{\partial t^2} \cdot \vec{\bar{u}}\right) dV \qquad \text{(IV.190)}$$

where,

ρ = mass density

2. Element Mass Matrix

The potential energy of inertia forces is by (IV.190),

$$U_e^I = -\int_V U_o^I \, dV \tag{IV.191}$$

where,

$$U_o^I = \rho \left(\frac{d^2\vec{\bar{u}}}{\partial t^2} \cdot \vec{\bar{u}}\right) \tag{IV.192}$$

and by (II.33),

$$\vec{\bar{u}} = (u_\alpha + x^3 \bullet_\alpha)\vec{a}^\alpha + w\,\vec{e}_n \tag{IV.193}$$

Expanding the work potential density, U_o, and recasting in matrix form gives,

$$U_o^I = \rho\{\ddot{\bar{u}}_1, \ddot{\bar{u}}_2, \ddot{w}\}^T \begin{bmatrix} a^{11} & a^{12} & 0 \\ a^{21} & a^{22} & 0 \\ 0 & 0 & 1 \end{bmatrix} \begin{Bmatrix} \bar{u}_1 \\ \bar{u}_2 \\ w \end{Bmatrix}$$

$$= \rho\{\ddot{\bar{u}}\}^T[a_M]\{\bar{u}\} \tag{IV.194}$$

where the relation, $\vec{a}^\alpha \cdot \vec{a}^\beta = a^{\alpha\beta}$, has been used.

In terms of reference surface displacements, $\{u\}$, and rotations, $\{\bullet\}$, the work potential is by use of (IV.193),

$$U_e^I = \int_V [U_o^{IT} + U_o^{IC} + U_o^{IR}]dV \qquad \text{(IV.195)}$$

where,

$$U_o^{IT} = \rho\{\ddot{u}\}^T[a_M]\{u\} \qquad \text{(IV.196)}$$

= translation work density

$$U_o^{IR} = \rho(x^3)^2 \{\ddot{\bullet}\}^T[a_M]\{\bullet\} \qquad \text{(IV.197)}$$

= rotational work density

$$U_o^{IC} = \rho \cdot x^3[\{\ddot{\bullet}\}^T[a_M]\{u\} + \{\ddot{u}\}[a_M]\{\bullet\}] \qquad \text{(IV.198)}$$

= coupled translational and rotational work density

$$\{u\}^T = [u_1, u_2, w] \qquad \text{(IV.199)}$$

$$\{\bullet\}^T = [\bullet_1, \bullet_2, 0] \qquad \text{(IV.200)}$$

$$\{\bar{u}\} = \{u\} + x^3\{\bullet\} \qquad \text{(IV.201)}$$

Considering first the translational inertia (IV.196) and introducing the transformation (IV.122) from {u} to the physical components, $\{\bar{W}\}$, of the element displacement vector results in,

$$U_I^T = \iiint \rho\{\ddot{\bar{W}}\}^T[T_W][T_E]^T[a_M][T_E][T_W]\{\bar{W}\}\sqrt{a}\, dx^1\, dx^2\, dx^3$$

$$= \{\ddot{\bar{W}}\}^T[\bar{M}_e^T]\{\bar{W}\} \qquad \text{(IV.202)}$$

By minimizing the inertial expression (IV.202) with respect to the discrete variables of the element displacement vector, $\{\bar{W}\}$, the element mass matrix due to translational inertia is obtained in the form,

$$[\bar{M}_e^T] = \iint [\bar{M}^T]\bar{m}_e\sqrt{a}\, dx^1 dx^2 \qquad \text{(IV.203)}$$

where,

$$[\bar{M}^T] = [T_W]^T[T_E]^T[a_M][T_E][T_W] \qquad \text{(IV.204)}$$

$$\bar{m}_e = \bar{m}_{ns} + \int \rho dx^3$$

$$= \bar{m}_{ns} + \sum_{n=1}^{N} \rho_n(z_o^n - z_I^n) \qquad \text{(IV.205)}$$

m_e = total mass per unit area

$\bar{m}_{ns}$ = non-structural mass per unit area*

z_o, z_I = layer thickness coordinates (see Figure 5b)

N = number of layers through shell wall

The integration of expression (IV.203) can be approximated by Gaussian quadrature and gives for the mass matrix due to translational inertia,

*The non-structural mass per unit area term is provided as a convenience to the analyst. It is useful in accounting for the inertial effects of appendages to the shell.

$$[\bar{M}_e^T] = \int_{-1}^{1}\int_{-1}^{1} [\bar{M}^T]\bar{m}_e \cdot \sqrt{a} \cdot |J_1| d\lambda d\mu$$

$$= \sum_{i=1}^{M}\sum_{j=1}^{M} H_i H_j [f_{M^T}(\lambda_j, \mu_i)] \qquad \text{(IV.206)}$$

where,

$$[f_{M^T}(\lambda_j, \mu_i)] = \left[[\bar{M}^T]\bar{m}_e \cdot \sqrt{a} \cdot |J_1| \right]_{\lambda=\lambda_j, \mu=\mu_i} \qquad \text{(IV.207)}$$

Considering next the rotational inertia (IV.197) and introducing the transformation (IV.142) from $\{\bullet\}$ to the physical components, $\{\bar{W}\}$, of the element displacement vector results in,

$$U_I^R = \iiint \rho(x^3)^2 \{\ddot{\bar{W}}\}^T [T_W]^T [T_\bullet]^T [a_M] [T_\bullet] [T_W] \{\bar{W}\} \sqrt{a}\, dx^1 dx^2 dx^3$$

$$= \{\ddot{\bar{W}}\}^T [M_e^R] \{\bar{W}\} \qquad \text{(IV.208)}$$

By minimizing the inertial work expression (IV.208) with respect to the discrete variables of the element displacement vector, $\{\bar{W}\}$, the element mass matrix due to translational inertia is obtained in the form,

$$[\bar{M}_e^R] = \iint [\bar{M}^R]\bar{m}_e^R \sqrt{a}\, dx^1 dx^2 \qquad \text{(IV.209)}$$

where,

$$[\bar{M}^R] = [T_W]^T[T_\bullet]^T[a_M][T_\bullet][T_W] \tag{IV.210}$$

$$\bar{m}_e^R = \int \rho (x^3)^2 \, dx^3$$

$$= \frac{1}{3} \sum_{n=1}^{N} \rho_n ((z_o^n)^3 - (z_I^n)^3) \tag{IV.211}$$

Integrating (IV.209) by Gaussian quadrature gives,

$$[\bar{M}_e^R] = \int_{-1}^{1} \int_{-1}^{1} [\bar{M}^R] \bar{m}_e^R \cdot \sqrt{a} \cdot |J_1| \, d\lambda d\mu$$

$$= \sum_{i=1}^{M} \sum_{j=1}^{M} H_i H_j [f_{M^R}(\lambda_j, \mu_i)] \tag{IV.212}$$

where,

$$[f_{M^R}(\lambda_j, \mu_i)] = \left[[\bar{M}^R] \bar{m}_e^R \cdot \sqrt{a} \cdot |J_1| \right]_{\lambda=\lambda_j, \mu=\mu_i} \tag{IV.213}$$

Considering now the coupling between translational and rotational inertia (IV.198) and using the transformations (IV.122) and (IV.142) gives,

$$U_I^c = \iiint \rho \, x^3 \Big[\{\ddot{\bar{W}}\}^T [T_W]^T [T_\bullet]^T [a_M][T_E][T_W]\{\bar{W}\}$$

$$+ \{\ddot{\bar{W}}\}^T [T_W]^T [T_E]^T [a_M][T_\bullet]\{\bar{W}\} \Big] \sqrt{a} \, dx^1 dx^2 \, dx^3$$

$$= \{\ddot{\bar{W}}\}^T \left[[\bar{M}_e^c] + [\bar{M}_e^c]^T \right] \{\bar{W}\} \tag{IV.214}$$

By minimizing the inertial work expression (IV.214) with respect to the discrete variables of the element displacement vector, $\{\bar{W}\}$, the element mass matrix due to coupling between translational and rotational inertia is obtained in the form,

$$[\bar{M}_e^c] = \iint [\bar{M}^c]\bar{m}_e^c \sqrt{a}\ dx^1\ dx^2 \qquad \text{(IV.215)}$$

where,

$$[\bar{M}^c] = [T_W]^T[T_\bullet]^T[a_M][T_E][T_W] \qquad \text{(IV.216)}$$

$$\bar{m}_e^c = \int \rho \cdot x^3 dx^3$$

$$= \frac{1}{2}\sum_{n=1}^{N} \rho_n((z_o^n)^2 - (z_I^n)^2) \qquad \text{(IV.217)}$$

Integrating (IV.215) by Gaussian quadrature gives,

$$[\bar{M}_e^c] = \int_{-1}^{1}\int_{-1}^{1} [\bar{M}^c]\bar{m}_e^c \cdot \sqrt{a} \cdot |J_1| d\lambda d\mu$$

$$= \sum_{i=1}^{M}\sum_{j=1}^{M} H_i H_j [f_{M^c}(\lambda_j, \mu_i)] \qquad \text{(IV.218)}$$

where,

$$[f_{M^C}(\lambda_j,\mu_i)] = \left[[\bar{M}^C]\bar{m}_e^C \cdot \sqrt{a} \cdot |J_1|\right]_{\lambda=\lambda_j,\mu=\mu_i} \qquad \text{(IV.219)}$$

The element mass matrix which accounts for the effects of translational inertia, rotational inertia and the coupling between translational and rotational inertia is then the summation of (IV.206), (IV.212) and (IV.218),

$$[\bar{\mathbf{M}}_e] = [\bar{M}_e^T] + [\bar{M}_e^C] + [\bar{M}_e^C]^T + [\bar{M}_e^R] \qquad \text{(IV.220)}$$

The system mass matrix appearing in (III.9) is then obtained by summation of the element mass matrices.

3. Element Surface Load Vector

The potential of a uniformly distributed surface load, $\vec{p}$, acting on the element reference surface is by (IV.178),

$$U_e^p = \iint (\vec{p}\cdot\vec{u})\sqrt{a}\, dx^1 dx^2 \qquad \text{(IV.221)}$$

Carrying out the dot product operation and recasting in matrix form results in,

$$U_e^p = \iint \{\bar{p}\}^T \{w\} \sqrt{a}\, dx^1 dx^2 \qquad \text{(IV.222)}$$

where by use of (IV.179) and (IV.180),

$$\{\bar{p}\}^T = [p_1 + p_2 \cos\Phi,\ p_2 + p_1 \cos\Phi,\ p_n] \qquad \text{(IV.223)}$$

$$\{w\}^T = [u,\ v,\ w] \qquad \text{(IV.224)}$$

since,

$$\vec{e}_i \cdot \vec{e}_j = 1 \ , \qquad i=j$$

$$\vec{e}_i \cdot \vec{e}_j = \cos\Phi \ , \qquad i \neq j$$

$$\cos\Phi = \frac{a_{12}}{\sqrt{a_{11}\, a_{22}}} \qquad \text{(IV.225)}$$

Introducing the transformation (IV.123) into (IV.222) results in,

$$U_e^p = \iint \{\bar{p}\}^T [T_u][T_E][T_W]\{\bar{W}\} \sqrt{a}\ dx^1\, dx^2$$

$$= \{\bar{P}_p\}_e^T \{\bar{W}\} \qquad \text{(IV.226)}$$

By minimizing the mechanical work expression (IV.226) with respect to the discrete variables of the element displacement vector, $\{\bar{W}\}$, the element load vector due to

surface loading is obtained in the form,

$$\{\bar{\mathbf{P}}_p\}_e = \iint \{P_p\} \sqrt{a}\ dx^1\ dx^2 \qquad \text{(IV.227)}$$

where

$$\{P_p\} = [T_W]^T[T_E]^T[T_W]^T\{\bar{p}\} \qquad \text{(IV.228)}$$

Integrating (IV.227) by Gaussian quadrature gives,

$$\{\bar{\mathbf{P}}_p\}_e = \int_{-1}^{1}\int_{-1}^{1} \{P_p\}\sqrt{a} \cdot |J_1| d\lambda d\mu$$

$$= \sum_{i=1}^{M}\sum_{j=1}^{M} H_i H_j \{f_{P_p}(\lambda_j,\mu_i)\} \qquad \text{(IV.229)}$$

where

$$\{f_{P_p}(\lambda_j,\mu_i)\} = \left\{\{P_p\} \cdot \sqrt{a} \cdot |J_1|\right\}_{\lambda=\lambda_j,\mu=\mu_i} \qquad \text{(IV.230)}$$

The surface load contribution to the system load vector appearing in (III.10) is then obtained by summation of the element surface load vectors.

4. Concentrated Force Vector

The potential of a concentrated force, $\vec{F}$, acting at a discrete nodal point, J, that lies within element K is by (IV.181),

$$U_J^F = (\vec{F} \cdot \vec{u})_J \tag{IV.231}$$

Carrying out the dot product operation recasting in matrix form results in,

$$U_J^F = \{\bar{F}\}_J^T \{W\}_J \tag{IV.232}$$

where by use of (IV.182) and (IV.183),

$$\{\bar{F}\}^T = [F_1 + F_2 \cos\Phi,\ F_2 + F_1 \cos\Phi,\ F_n] \tag{IV.233}$$

Introducing the transformation (IV.123) into (IV.232) results in,

$$U_J^F = \{\bar{P}_F\}_J^T \{\bar{W}\}_K \tag{IV.234}$$

where

$$\{\bar{P}_F\}_J = [Tw]_K^T [T_E]_J^T [Tu]_J^T \{\bar{F}\}_J \tag{IV.235}$$

By minimizing the mechanical work expression (IV.234) with respect to the discrete variables of the element displacement vector, $\{\bar{W}\}$, the element load vector due to a concentrated force (IV.235) is obtained. The subscript J locates the point of application of the concentrated force vector within the particular element K and is identified by the element connection sequence number which ranges from 1 to 13. The location of node J in the several coordinate systems associated with element K (see Figure 7) is,

$$\begin{aligned} x^1 &= x^1_J \quad , \quad x^2 = x^2_J \\ \lambda &= \lambda_J \quad , \quad \mu = \mu_J \\ \alpha &= \alpha_J \quad , \quad \beta = \beta_J \end{aligned} \tag{IV.236}$$

The discrete values of λ_J, μ_J and α_J, β_J which correspond to the element connection sequence numbers J=1,...,13 are given in Table 4. When the point J is one of the connection points 1 through 4, the values of α_J and β_J must be determined numerically from the known values of x^1_J and x^2_J by use of the shape function relations (IV.90),

$$\begin{aligned} x^1_J &= [H_L(\alpha_J, \beta_J)]\{x^1_L\} \\ & \qquad\qquad L=5,\ldots,13 \\ x^2_J &= [H_L(\alpha_J, \beta_J)]\{x^2_L\} \end{aligned} \tag{IV.237}$$

When the point J is one of the connection points 6 through 13, the values of λ_K and μ_K must be determined numerically from the known values of x_J^1 and x_J^2 by use of the shape function relations (IV.72),

$$x_J^1 = [L_L(\lambda_J,\mu_J)]\{x_L^1\}$$
$$L=1,\ldots,4$$
$$x_J^2 = [L_L(\lambda_J,\mu_J)]\{x_L^2\} \qquad \text{(IV.238)}$$

The inverse functional relationship between α,β and x^1,x^2 or λ,μ and x^1,x^2 cannot be derived analytically but Newton's method can be used to rapidly converge on values of α_J, β_J or λ_J, μ_J when given the discrete values x_J^1, x_J^2. The details of this calculation are given in Appendix D.

For the convenience of the analyst, several alternative forms of force discretization will be derived.

A force resultant applied along one edge of an element's reference surface is with respect to the element edge coordinate system (see Figure 8),

$$\vec{N} = \tilde{N}_s\vec{e}_s + \tilde{N}_t\vec{e}_t + \tilde{N}_n\vec{e}_n \qquad \text{(IV.239)}$$

and with respect to the surface coordinate system,

$$\vec{N} = \tilde{N}_1\vec{e}_1 + \tilde{N}_2\vec{e}_2 + \tilde{N}_n\vec{e}_n \qquad \text{(IV.240)}$$

Let the unit vector tangent to the edge of the shell, $\vec{e}_t$, be located with respect to the surface coordinate, x^1, by the angle, ψ, which has the positive sense indicated in Figure 8. The tangent vector is then,

$$\vec{e}_t = \cos\psi\, \vec{e}_1 + \sin\psi\, \vec{e}_2 \qquad \text{(IV.241)}$$

and the unit vector normal to the edge of the shell is,

$$\vec{e}_s = \vec{e}_t \times \vec{e}_n = \sin\psi\, \vec{e}_1 - \cos\psi\, \vec{e}_2 \qquad \text{(IV.242)}$$

It follows that the transformation relating force resultant components in surface coordinates to components in edge coordinates is,

$$\begin{Bmatrix} \tilde{N}_1 \\ \tilde{N}_2 \\ \tilde{N}_n \end{Bmatrix} = \begin{bmatrix} \sin\psi & \cos\psi & 0 \\ -\cos\psi & \sin\psi & 0 \\ 0 & 0 & 1 \end{bmatrix} \begin{Bmatrix} \tilde{N}_s \\ \tilde{N}_t \\ \tilde{N}_n \end{Bmatrix} \qquad \text{(IV.243)}$$

The angle ψ may be approximated as follows. In the surface coordinate directions the incremental arc lengths between points L and M are (see Figure 8 and (II.7)),

$$\Delta S_1 = (A_1 x^1)_M - (A_1 x^1)_L \qquad \text{(IV.244)}$$

$$\Delta S_2 = (A_2 x^2)_M - (A_2 x^2)_L \qquad \text{(IV.245)}$$

The length of the element side is approximately,

$$\Delta S_K = [(\Delta S_1)^2 + 2(\Delta S_1 \Delta S_2)\cos\Phi + (\Delta S_2)^2]^{1/2} \qquad \text{(IV.246)}$$

where,

$$\cos\Phi = \left(\frac{a_{12}}{\sqrt{a_{11}\ a_{22}}}\right)_K \qquad \text{(IV.247)}$$

The angle ψ is then defined by,

$$\sin\psi_K = \frac{\Delta S_2}{\Delta S_K} \quad , \quad \cos\psi_K = \frac{\Delta S_1}{\Delta S_K} \qquad \text{(IV.248)}$$

The total force acting at the midside of the element (point K of Figure 8) is then,

$$\vec{F}_K = \Delta S_K(\vec{N})$$

$$= F_1 \vec{e}_1 + F_2 \vec{e}_2 + F_n \vec{e}_n \qquad \text{(IV.249)}$$

where

$$F_1 = \Delta S_K \cdot \tilde{N}_1 \quad \text{or} \quad \Delta S_K(\tilde{N}_S \sin\psi + \tilde{N}_t \cos\psi)$$

$$F_2 = \Delta S_K \cdot \tilde{N}_2 \quad \text{or} \quad \Delta S_K(-\tilde{N}_S \cos\psi + \tilde{N}_t \sin\psi)$$

$$F_n = \Delta S_K \cdot \tilde{N}_n \qquad \text{(IV.250)}$$

The calculation of the load vector for $\vec{F}_K$ then follows from (IV.233) and (IV.235).

The contribution from concentrated loads or force resultants to the system load vector appearing in (III.10) is then obtained by summation of the corresponding element load vectors.

5. Concentrated Moment Vector

The potential of a concentrated moment, $\vec{Q}$, acting at a discrete node, K, that lies within element J is by (IV.184),

$$U_K^Q = (\vec{Q} \cdot \vec{\vartheta})_K \tag{IV.251}$$

where by use of (II.38) and (II.21),

$\vec{\vartheta}_K$ = rotation vector at node K

$$\vartheta_1 = [A_2 a^{21} w_{,1} + A_2 a^{22} w_{,2} + \frac{A_2}{A_1} b_1^2 u + b_2^2 v] \tag{IV.252}$$

$$\vartheta_2 = -[A_1 a^{11} w_{,1} + A_1 a^{12} w_{,2} + b_1^1 u + \frac{A_1}{A_2} b_2^1 v] \tag{IV.253}$$

since from (IV.286)

$$u = A_1 u^1 \quad , \quad v = A_2 u^2 \tag{IV.254}$$

Carrying out the dot product operation and recasting in matrix form results in,

$$U_K^Q = \{\tilde{Q}\}_K^T \{\vartheta\}_K \tag{IV.255}$$

where by use of (IV.185) and (IV.186),

$$\{\tilde{Q}\}^T = [\tilde{Q}_1 + \tilde{Q}_2 \cos\Phi, \tilde{Q}_2 + \tilde{Q}_1 \cos\Phi] \tag{IV.256}$$

$$\{\vartheta\}^T = [\vartheta_1, \vartheta_2] \tag{IV.257}$$

Introducing the transformation (IV.157) into (IV.255) results in,

$$U_K^Q = \{\bar{P}_Q\}_K^T \{\bar{W}\}_K \tag{IV.258}$$

where

$$\{\bar{P}_Q\}_K = [T_W]_J^T [T_\vartheta]_K^T \{\tilde{Q}\}_K \tag{IV.259}$$

By minimizing the mechanical work expression (IV.258) with respect to the discrete variables of the element displacement vector, $\{\bar{W}\}$, the element load vector due to a concentrated moment (IV.259) is obtained.

The subscript K locates the point of application of the concentrated moment vector within the particular element J and is identified by the element connection sequence

number which ranges from 1 to 13. The location of node K in the several coordinate systems associated with element K (see Figure 7) is given in Table 4.

For the convenience of the analyst, several alternative forms of moment discretization will be derived as was done for the concentrated force vector.

A moment resultant applied along one edge of an element's reference surface is with respect to the element edge coordinate system (see Figure 8),

$$\vec{M} = \tilde{M}_s \vec{e}_s + \tilde{M}_t \vec{e}_t \qquad \text{(IV.260)}$$

and with respect to the surface coordinate system,

$$\vec{M} = \tilde{M}_1 \vec{e}_1 + \tilde{M}_2 \vec{e}_2 \qquad \text{(IV.261)}$$

Defining the vectors, $\vec{e}_s$ and $\vec{e}_t$, in the same manner as was done in the preceding section, it follows that the transformation relating moment resultants in surface coordinates to moment resultants in edge coordinates is,

$$\begin{Bmatrix} \tilde{M}_1 \\ \tilde{M}_2 \end{Bmatrix} = \begin{bmatrix} \sin\psi & \cos\psi \\ -\cos\psi & \sin\psi \end{bmatrix} \begin{Bmatrix} \tilde{M}_s \\ \tilde{M}_t \end{Bmatrix} \qquad \text{(IV.262)}$$

Approximating the angle ψ and the length of the element side, ΔS_K, as in the preceding section, the total moment

acting at the midside of the element (point K of Figure 8) is then,

$$\vec{Q}_K = \Delta S_K(\vec{M})$$

$$= \tilde{Q}_1 \vec{e}_1 + \tilde{Q}_2 \vec{e}_2 \qquad \text{(IV.263)}$$

where,

$$\tilde{Q}_1 = \Delta S_K \cdot \tilde{M}_1 \text{ or } \Delta S_K(\tilde{M}_s \sin\psi + \tilde{M}_t \cos\psi)$$

$$\tilde{Q}_2 = \Delta S_K \cdot \tilde{M}_2 \text{ or } \Delta S_K(-\tilde{M}_s \cos\psi + \tilde{M}_t \sin\psi) \qquad \text{(IV.264)}$$

The calculation of the load vector for $\vec{Q}_K$ then follows from (IV.256) and (IV.259).

The contribution from concentrated moments or moment resultants to the system load vector appearing in (III.10) is then obtained by summation of the corresponding element load vector.

6. Element Gravity Load Vector

The potential of a gravity force, $\vec{F}_g$, acting over the volume of the element is by (IV.188),

$$U_e^g \approx \iint (\bar{w}_e \vec{g} \cdot \vec{u}) \sqrt{a} \; dx^1 \, dx^2 \qquad \text{(IV.265)}$$

where,

$$\vec{g} = g_1 \vec{e}_1 + g_2 \vec{e}_2 + g_n \vec{e}_n \qquad \text{(IV.266)}$$

= gravity vector (g units)

$$\bar{w}_e = w_{NS} + \int \rho_w \, dx^3$$

$$= w_{NS} + \sum_{n=1}^{N} \rho_w (z_o^n - z_I^n) \qquad \text{(IV.267)}$$

= element weight per unit area

w_{NS} = non-structural weight per unit area

ρ_w = weight density

Carrying out the dot product operation in (IV.265) and recasting in matrix form results in,

$$U_e^g = \iint \{\bar{g}\}^T \{w\} \sqrt{a} \; dx^1 \, dx^2 \qquad \text{(IV.268)}$$

where by use of (IV.189) and (IV.266),

$$\{\bar{g}\}^T = \bar{w}_e [g_1 + g_2 \cos\phi \, , \; g_2 + g_1 \cos\phi \, , \; g_n] \qquad \text{(IV.269)}$$

Introducing the transformation (IV.123) into (IV.268) results in,

$$U_e^g = \iint \{\bar{g}\}^T [T_u][T_E][T_W]\{\bar{w}\} \sqrt{a} \; dx^1 \, dx^2$$

$$= \{\bar{P}_g\}_e^T \{\bar{w}\} \qquad \text{(IV.270)}$$

By minimizing the work expression (IV.270) with respect to the discrete variables of the element displacement vector, $\{\bar{W}\}$, the element load vector due to gravity loading is obtained in the form,

$$\{\bar{P}_g\}_e = \iint \{P_g\}\sqrt{a}\ dx^1\ dx^2 \qquad \text{(IV.271)}$$

where,

$$\{P_g\} = [T_W]^T[T_E]^T[T_u]^T\{\bar{g}\} \qquad \text{(IV.272)}$$

Integrating (IV.271) by Gaussian quadrature gives,

$$\{\bar{P}_g\}_e = \int_{-1}^{1}\int_{-1}^{1}\{P_g\}\sqrt{a}\cdot|J_1|d\lambda d\mu$$

$$= \sum_{i=1}^{M}\sum_{j=1}^{M} H_i H_j \{f_{P_g}(\lambda_j,\mu_i)\} \qquad \text{(IV.273)}$$

where,

$$\{f_{P_g}(\lambda_j,\mu_i)\} = \left\{\{P_g\}\sqrt{a}\cdot|J_1|\right\}_{\lambda=\lambda_j,\mu=\mu_i} \qquad \text{(IV.274)}$$

The gravity load contribution to the system load vector appearing in (III.10) is obtained by summation of the element gravity load vectors.

D. Calculation of Structural Response

In this section, transformations between tensor quantities and physical quantities are defined and the equations for calculating strains, stresses, forces and moments from the element displacement vector are developed.

The displacement vector at a point on the reference surface of the shell is from (II.23),

$$\vec{u} = u^{\alpha}\vec{a}_{\alpha} + w\vec{e}_{n} = u_{\alpha}\vec{a}^{\alpha} + w\vec{e}_{n} \qquad \text{(IV.275)}$$

where $\vec{a}_{\alpha}$ and $\vec{a}^{\alpha}$ are the covariant and contravariant base vectors of the Gaussian surface coordinates and $\vec{e}_{n}$ is the unit vector normal to the reference surface.

The unit vectors in the $\vec{a}_{\alpha}$ and $\vec{a}^{\alpha}$ directions are by (II.3), (II.5) and (II.18),

$$\vec{e}_{\alpha} = \frac{\vec{a}_{\alpha}}{A_{\alpha}} = \frac{a_{\alpha\beta}}{A_{\alpha}}\vec{a}^{\beta} \quad \text{(no sum on } \alpha\text{)} \qquad \text{(IV.276)}$$

where the Lame´ parameters are,

$$A_{\alpha} = \sqrt{a_{\alpha\alpha}} \quad \text{(no sum)} \qquad \text{(IV.277)}$$

By substitution of (IV.276) into (IV.275) the displacement vector can thus be written in the alternative physical forms,

$$\vec{u} = u^1 A_1 \vec{e}_1 + u^2 A_2 \vec{e}_2 + w \vec{e}_n \tag{IV.278}$$

$$\vec{u} = A_1(a^{11}u_1 + a^{12}u_2)\vec{e}_1 + A_2(a^{21}u_1 + a^{22}u_2)\vec{e}_2 + w \vec{e}_n \tag{IV.279}$$

$$\vec{u} = u \vec{e}_1 + v \vec{e}_2 + w \vec{e}_n \tag{IV.280}$$

The rotation vector at a point on the reference surface is by (II.34),

$$\vec{\Theta} = \Theta^\alpha \vec{a}_\alpha = \Theta_\alpha \vec{a}^\alpha \tag{IV.281}$$

By substitution of (IV.276) into (IV.281) it can be expressed in the alternative physical forms,

$$\vec{\Theta} = \Theta^1 A_1 \vec{e}_1 + \Theta^2 A_2 \vec{e}_2 \tag{IV.282}$$

$$= A_1(a^{11}\Theta_1 + a^{22}\Theta_2)\vec{e}_1 + A_2(a^{21}\Theta_1 + a^{22}\Theta_2)\vec{e}_2 \tag{IV.283}$$

$$= \Psi_1 \vec{e}_1 + \Psi_2 \vec{e}_2 \tag{IV.284}$$

The sign convention for reference surface displacements and rotations is shown in Figure 9.

From an inspection of (IV.278), (IV.279) and (IV.280) the physical components of the reference surface displacement vector, {w}, are related to the covariant components, {u}, and

contravariant components, $\{\tilde{u}\}$, by the transformations,

$$\{w\} = [T_u]\{u\} = [T^u]\{\tilde{u}\} \tag{IV.285}$$

or,

$$\begin{Bmatrix} u \\ v \\ w \end{Bmatrix} = \begin{bmatrix} A_1 a^{11} & A_1 a^{12} & 0 \\ A_2 a^{21} & A_2 a^{22} & 0 \\ 0 & 0 & 1 \end{bmatrix} \begin{Bmatrix} u_1 \\ u_2 \\ w \end{Bmatrix} = \begin{bmatrix} A_1 & 0 & 0 \\ 0 & A_2 & 0 \\ 0 & 0 & 1 \end{bmatrix} \begin{Bmatrix} u^1 \\ u^2 \\ w \end{Bmatrix} \tag{IV.286}$$

Conversely,

$$\{u\} = [T_u]^{-1}\{w\} = [T_w]\{w\}$$
$$\{\tilde{u}\} = [T^u]^{-1}\{w\} = [T^w]\{w\} \tag{IV.287}$$

or

$$\begin{Bmatrix} u_1 \\ u_2 \\ w \end{Bmatrix} = \begin{bmatrix} A_1 & \frac{a_{21}}{A_2} & 0 \\ \frac{a_{12}}{A_1} & A_2 & 0 \\ 0 & 0 & 1 \end{bmatrix} \begin{Bmatrix} u \\ v \\ w \end{Bmatrix} \tag{IV.288}$$

$$\begin{Bmatrix} u^1 \\ u^2 \\ w \end{Bmatrix} = \begin{bmatrix} \frac{1}{A_1} & 0 & 0 \\ 0 & \frac{1}{A_2} & 0 \\ 0 & 0 & 1 \end{bmatrix} \begin{Bmatrix} u \\ v \\ w \end{Bmatrix} \qquad \text{(IV.288 cont.)}$$

The displacement vector at a point located a distance z from the reference surface is by (II.33) and (II.34),

$$\begin{aligned} \vec{\bar{u}} &= \vec{u} + z\,\vec{\Theta} \\ &= (u^\alpha + z\,\Theta^\alpha)\vec{a}_\alpha + w\,\vec{e}_n \\ &= (u_\alpha + z\,\Theta_\alpha)\vec{a}^\alpha + w\,\vec{e}_n \end{aligned} \qquad \text{(IV.289)}$$

Introducing the unit vectors (IV.276) into (IV.289) leads to the alternative physical forms,

$$\vec{\bar{u}} = (u^1 + z\Theta^1)A_1\,\vec{e}_1 + (u^2 + z\Theta^2)A_2\,\vec{e}_2 + w\,\vec{e}_n \qquad \text{(IV.290)}$$

$$\begin{aligned} \vec{\bar{u}} = {} & [A_1(a^{11}u_1 + a^{21}u_2) + z\cdot A_1(a^{11}\Theta_1 + a^{21}\Theta_2)]\vec{e}_1 \\ & + [A_2(a^{12}u_1 + a^{22}u_2) + z\cdot A_2(a^{12}\Theta_1 + a^{22}\Theta_2)]\vec{e}_2 \\ & + w\,\vec{e}_n \end{aligned} \qquad \text{(IV.291)}$$

$$\vec{\bar{u}} = (u + z\Psi_1)\vec{e}_1 + (v + z\Psi_2)\vec{e}_2 + w\,\vec{e}_n \qquad \text{(IV.292)}$$

$$\vec{\bar{u}} = \bar{u}\,\vec{e}_1 + \bar{v}\,\vec{e}_2 + \bar{w}\,\vec{e}_n \qquad \text{(IV.293)}$$

From inspection of (IV.292) and (IV.293) the reference surface displacements and rotations are related to the displacements off the reference surface by,

$$\{\bar{w}\} = \{w\} + z\,\{\Psi\} \tag{IV.294}$$

or

$$\begin{Bmatrix} \bar{u} \\ \bar{v} \\ \bar{w} \end{Bmatrix} = \begin{Bmatrix} u \\ v \\ w \end{Bmatrix} + z \begin{Bmatrix} \Psi_1 \\ \Psi_2 \\ 0 \end{Bmatrix} \tag{IV.295}$$

where the physical components of the rotation vector are related to the tensor components by inspection of (IV.290) and (IV.291),

$$\{\Psi\} = [T_u]\{\Theta\} = [T^u]\{\tilde{\Theta}\} \tag{IV.296}$$

or

$$\begin{Bmatrix} \Psi_1 \\ \Psi_2 \\ 0 \end{Bmatrix} = \begin{bmatrix} A_1 a^{11} & A_1 a^{12} & 0 \\ A_2 a^{21} & A_2 a^{22} & 0 \\ 0 & 0 & 1 \end{bmatrix} \begin{Bmatrix} \Theta_1 \\ \Theta_2 \\ 0 \end{Bmatrix} = \begin{bmatrix} A_1 & 0 & 0 \\ 0 & A_2 & 0 \\ 0 & 0 & 1 \end{bmatrix} \begin{Bmatrix} \Theta^1 \\ \Theta^2 \\ 0 \end{Bmatrix} \tag{IV.297}$$

Conversely,

$$\{ \mathbf{e} \} = [T_u]^{-1}\{\nu\} = [T_w]\{\Psi\}$$

$$\{ \tilde{\mathbf{e}} \} = [T^u]^{-1}\{\Psi\} = [T^w]\{\Psi\} \qquad \text{(IV.298)}$$

or

$$\begin{Bmatrix} \mathbf{e}_1 \\ \mathbf{e}_2 \\ 0 \end{Bmatrix} = \begin{bmatrix} A_1 & \frac{a_{21}}{A_2} & 0 \\ \frac{a_{12}}{A_1} & A_2 & 0 \\ 0 & 0 & 1 \end{bmatrix} \begin{Bmatrix} \Psi_1 \\ \Psi_2 \\ 0 \end{Bmatrix}$$

$$\begin{Bmatrix} \mathbf{e}^1 \\ \mathbf{e}^2 \\ 0 \end{Bmatrix} = \begin{bmatrix} \frac{1}{A_1} & 0 & 0 \\ 0 & \frac{1}{A_2} & 0 \\ 0 & 0 & 1 \end{bmatrix} \begin{Bmatrix} \Psi_1 \\ \Psi_2 \\ 0 \end{Bmatrix} \qquad \text{(IV.299)}$$

The physical components of the strain tensor at a point off the reference surface are related to the covariant tensor components by the well known transformation (see [27]),

$$\{\bar{e}\} = [T_\gamma]\{\bar{\gamma}\} \qquad \text{(IV.300)}$$

or

$$\begin{Bmatrix} \bar{e}_{11} \\ \bar{e}_{22} \\ \bar{e}_{12} \end{Bmatrix} = \begin{bmatrix} 1/a_{11} & 0 & 0 \\ 0 & 1/a_{22} & 0 \\ 0 & 0 & 1/\sqrt{a_{11}a_{12}} \end{bmatrix} \begin{Bmatrix} \bar{\gamma}_{11} \\ \bar{\gamma}_{22} \\ 2\bar{\gamma}_{12} \end{Bmatrix} \tag{IV.301}$$

and conversely,

$$\{\bar{\gamma}\} = [T_\gamma]^{-1} = [T_e]\{\bar{e}\} \tag{IV.302}$$

or

$$\begin{Bmatrix} \bar{\gamma}_{11} \\ \bar{\gamma}_{22} \\ 2\bar{\gamma}_{12} \end{Bmatrix} = \begin{bmatrix} a_{11} & 0 & 0 \\ 0 & a_{22} & 0 \\ 0 & 0 & \sqrt{a_{11}a_{22}} \end{bmatrix} \begin{Bmatrix} \bar{e}_{11} \\ \bar{e}_{22} \\ \bar{e}_{12} \end{Bmatrix} \tag{IV.303}$$

Similarly, the physical components of the reference surface strain tensor and curvature change (or bending strain) tensor are,

$$\{e\} = [T_\gamma]\{\gamma\} \tag{IV.304}$$

$$\{\kappa\} = [T_\gamma]\{\chi\} \tag{IV.305}$$

Conversely,

$$\{\gamma\} = [T_\gamma]^{-1}\{e\} = [T_e]\{e\} \tag{IV.306}$$

$$\{\chi\} = [T_\gamma]^{-1}\{\kappa\} = [T_e]\{\kappa\} \tag{IV.307}$$

The coefficient of thermal expansion tensor $\{\varepsilon\}$ and physical vector $\{\alpha\}$ are also related by the same transformations,

$$\{\alpha\} = [T_\gamma]\{\varepsilon\} \tag{IV.308}$$

or

$$\begin{Bmatrix} \alpha_{11} \\ \alpha_{22} \\ \alpha_{12} \end{Bmatrix} = [T_\gamma] \begin{Bmatrix} \varepsilon_{11} \\ \varepsilon_{22} \\ \varepsilon_{12} \end{Bmatrix} \tag{IV.309}$$

Conversely,

$$\{\varepsilon\} = [T_\gamma]^{-1}\{\alpha\} = [T_e]\{\alpha\} \tag{IV.310}$$

The physical components of the stress tensor are related to the contravariant tensor components by the well known transformation (see [27]),

$$\{\bar{\sigma}\} = [T_\tau]\{\bar{\tau}\} \tag{IV.311}$$

or

$$\begin{Bmatrix} \bar{\sigma}_{11} \\ \bar{\sigma}_{22} \\ \bar{\sigma}_{12} \end{Bmatrix} = \begin{bmatrix} \sqrt{\frac{a_{11}}{a^{11}}} & 0 & 0 \\ 0 & \sqrt{\frac{a_{22}}{a^{22}}} & 0 \\ 0 & 0 & \sqrt{\frac{a_{22}}{a^{11}}} \end{bmatrix} \begin{Bmatrix} \bar{\tau}^{11} \\ \bar{\tau}^{22} \\ \bar{\tau}^{12} \end{Bmatrix} \tag{IV.312}$$

Conversely,

$$\{\bar{\tau}\} = [T_\tau]^{-1}\{\bar{\sigma}\} = [T_\sigma]\{\bar{\sigma}\} \tag{IV.313}$$

or

$$\begin{Bmatrix} \bar{\tau}^{11} \\ \bar{\tau}^{22} \\ \bar{\tau}^{12} \end{Bmatrix} = \begin{bmatrix} \sqrt{\frac{a^{11}}{a_{11}}} & 0 & 0 \\ 0 & \sqrt{\frac{a^{22}}{a_{22}}} & 0 \\ 0 & 0 & \sqrt{\frac{a^{11}}{a_{22}}} \end{bmatrix} \begin{Bmatrix} \bar{\sigma}_{11} \\ \bar{\sigma}_{22} \\ \bar{\sigma}_{12} \end{Bmatrix} \tag{IV.314}$$

The sign convention for stresses is shown in Figure 9.

The tensor form of the constitutive equations are thus related to the physical form as follows. The tensor form is by (IV.10) and (IV.11),

$$\{\bar{\tau}\} = [\mathbf{E}]\{\bar{\gamma}\} - \{\Omega\} \tag{IV.315}$$

where,

$$\{\Omega\} = [\,\mathbf{E}\,]\{\varepsilon\}\cdot\Delta T \qquad \text{(IV.316)}$$

Transforming to physical quantities by use of (IV.302) (IV.310) and (IV.313) gives,

$$\{\bar{\sigma}\} = [T_\tau][\,\mathbf{E}\,][T_e]\{\bar{e}\}-[T_\tau][\,\mathbf{E}\,][T_e]\{\alpha\}\cdot\Delta T \qquad \text{(IV.317)}$$

or

$$\{\bar{\sigma}\} = [G]\{\bar{e}\} - \{Q\} \qquad \text{(IV.318)}$$

where,

$$\{Q\} = [G]\{\alpha\}\cdot\Delta T \qquad \text{(IV.319)}$$

By inspection of (IV.317) through (IV.319) the following relations thus hold,

$$[G] = [T_\tau][\,\mathbf{E}\,][T_e] \qquad \text{(IV.320)}$$

or

$$[G] = \begin{bmatrix} a_{11}\sqrt{\frac{a_{11}}{a_{11}}}\,\mathbf{E}^{1111} & a_{22}\sqrt{\frac{a_{11}}{a_{11}}}\,\mathbf{E}^{1122} & a_{11}\sqrt{\frac{a_{22}}{a_{11}}}\,\mathbf{E}^{1112} \\ a_{11}\sqrt{\frac{a_{22}}{a_{22}}}\,\mathbf{E}^{2211} & a_{22}\sqrt{\frac{a_{22}}{a_{22}}}\,\mathbf{E}^{2222} & a_{22}\sqrt{\frac{a_{11}}{a_{22}}}\,\mathbf{E}^{2212} \\ a_{11}\sqrt{\frac{a_{22}}{a_{11}}}\,\mathbf{E}^{1211} & a_{22}\sqrt{\frac{a_{22}}{a_{11}}}\,\mathbf{E}^{1222} & a_{22}\sqrt{\frac{a_{11}}{a_{11}}}\,\mathbf{E}^{1212} \end{bmatrix}$$

(IV.321)

and,

$$\{Q\} = [T_\tau]\{\Omega\} \tag{IV.322}$$

Conversely,

$$[\,\mathbf{E}\,] = [T_\sigma][G][T_\gamma] \tag{IV.323}$$

or,

$$[\,\mathbf{E}\,] = \begin{bmatrix} \frac{1}{a_{11}}\sqrt{\frac{a^{11}}{a_{11}}}\,G_{11} & \frac{1}{a_{22}}\sqrt{\frac{a^{11}}{a_{11}}}\,G_{12} & \frac{1}{a_{11}}\sqrt{\frac{a^{11}}{a_{22}}}\,G_{13} \\ \frac{1}{a_{11}}\sqrt{\frac{a^{22}}{a_{22}}}\,G_{21} & \frac{1}{a_{22}}\sqrt{\frac{a^{22}}{a_{22}}}\,G_{22} & \frac{1}{a_{22}}\sqrt{\frac{a^{22}}{a_{11}}}\,G_{23} \\ \frac{1}{a_{11}}\sqrt{\frac{a^{11}}{a_{22}}}\,G_{31} & \frac{1}{a_{22}}\sqrt{\frac{a^{11}}{a_{22}}}\,G_{32} & \frac{1}{a_{22}}\sqrt{\frac{a^{11}}{a_{11}}}\,G_{33} \end{bmatrix} \tag{IV.324}$$

and

$$\{\Omega\} = [T_\sigma]\{Q\} \tag{IV.325}$$

The physical strain components, $\{\bar{e}\}$, at an arbitrary point located a distance z from the shell reference surface are from (II.28),

$$\{\bar{e}\} = \{e\} + z\{\kappa\} \tag{IV.326}$$

The physical reference surface strain components, $\{e\}$, are related to the physical components, $\{\bar{W}\}$, of the element displacement vector by substituting the transformations (IV.81) and (IV.118) into equation (IV.300),

$$\{e\} = [T_\gamma][S][F][T_W]\{\bar{W}\} \qquad \text{(IV.327)}$$

The physical bending strain components, $\{\kappa\}$, are related to the physical components, $\{\bar{W}\}$, of the element displacement vector by substituting the transformation (IV.106) and (IV.118) into (IV.305),

$$\{\kappa\} = [T_\gamma][R][E][T_W]\{\bar{W}\} \qquad \text{(IV.328)}$$

Substituting (IV.327) and (IV.328) into (IV.326) gives for the total strains,

$$\{\bar{e}\} = [T_\gamma][S][F][T_W]\{\bar{W}\} + z[T_\gamma][R][E][T_W]\{\bar{W}\} \qquad \text{(IV.329)}$$

and the strains associated with stress are,

$$\{\bar{e}_s\} = \{\bar{e}\} - \{\alpha\}\cdot\Delta T \qquad \text{(IV.330)}$$

Substituting (IV.329) into the constitutive equation (IV.318) gives for the physical stress components,

$$\{\bar{\sigma}\} = [G][T_\gamma][S][F][T_W]\{\bar{W}\}$$

$$+ z[G][T_\gamma][R][E][T_W]\{\bar{W}\}$$

$$- [G]\{\alpha\}\cdot\Delta T \qquad \text{(IV.331)}$$

The force resultants acting on a differential element of the shell reference surface (see Figure 10) are defined to be,

$$\{\bar{N}\} = \int \{\bar{\sigma}\}dx^3 \qquad \text{(IV.332)}$$

where

$$\{\bar{N}\}^T = [\bar{N}_1, \bar{N}_2, \bar{N}_{12}] \qquad \text{(IV.333)}$$

Substituting (IV.331) into (IV.332) and integrating through the shell thickness gives,

$$\{\bar{N}\} = [\bar{D}][T_\gamma][S][F][T_W]\{\bar{W}\}$$

$$+ [\bar{C}][T_\gamma][R][E][T_W]\{\bar{W}\} - \{\bar{N}_T\} \qquad \text{(IV.334)}$$

where,

$$[\bar{D}] = \int [G]dx^3 \qquad \text{(IV.335)}$$

$$[\bar{C}] = \int [G]x^3dx^3 \qquad \text{(IV.336)}$$

$$\{\bar{N}_T\} = \int [G]\{\alpha\}\cdot\Delta T\cdot dx^3 \qquad \text{(IV.337)}$$

The moment resultants acting on a differential element of the shell reference surface (see Figure 10) are defined by,

$$\{\bar{M}\} = \int \{\bar{\sigma}\} x^3 dx^3 \qquad \text{(IV.338)}$$

where

$$\{\bar{M}\}^T = [\bar{M}_1, \bar{M}_2, \bar{M}_{12}] \qquad \text{(IV.339)}$$

Substituting (IV.331) into (IV.338) and integrating through the shell thickness gives,

$$\{\bar{M}\} = [\bar{C}][T_\gamma][S][F][T_W]\{\bar{W}\}$$

$$+ [\bar{B}][T_\gamma][R][E][T_W]\{\bar{W}\} - \{\bar{M}_T\} \qquad \text{(IV.340)}$$

where,

$$[B] = \int [G] \cdot (x^3)^2 dx^3 \qquad \text{(IV.341)}$$

$$\{\bar{M}_T\} = \int [G]\{\alpha\} \cdot \Delta T \cdot x^3 \, dx^3 \qquad \text{(IV.342)}$$

The physical shell wall compliances (IV.335), (IV.336), (IV.341) and physical thermal forces and moments (IV.337) and (IV.342) are computed in the same manner as the corresponding tensor quantities were computed in equations (IV.50) through (IV.54) except [G] is substituted for [**E**], and $\{\alpha\}$ is substituted for $\{\varepsilon\}$.

E. Boundary Conditions

When a variational procedure is used to obtain a stationary value of the total potential energy, the Euler differential equations of equilibrium and the "natural" force boundary conditions are obtained. For the solution of a specific structural problem the "essential" displacement boundary conditions must be imposed on the equilibrium equations (see [122]).

Analogously, the minimum potential energy principle used herein to derive the matrix equations of motion requires only that the essential displacement boundary conditions be satisfied through imposition of constraints on the appropriate nodal point degrees of freedom. Force boundary conditions are satisfied through application of the consistent external loads which were derived in section IV.C. The term "consistent" was coined by Archer [123] in referring to mass matrices which have been derived from strain energy considerations and employ the same displacement functions as were used in deriving the stiffness matrix. Consistent mass matrices and load vectors are distinguished from lumped approaches where the analyst using engineering judgement apportions the mass or loading among the discrete nodes of the element.

The displacement boundary conditions in thin shell problems consist of either enforced translational components and/or rotational components. Since the translations appear as nodal point degrees of freedom it is a straight

forward procedure to impose this type of constraint, the procedure being a standard operation in finite element technology (see [37], [38]).

The imposition of prescribed values of rotation, however, is not so straightforward since the shell rotations do not appear as nodal point degrees of freedom in the analysis. At an arbitrary point on the shell reference surface the components of the rotation vector may be expressed explicitly as a function of the reference surface displacements and their spatial derivatives at the arbitrary point. By use of the same interpolating functions used to formulate the element stiffness matrix, the rotation components may be expressed as a function of the discrete nodal displacements at neighboring grid points. The resulting equations of constraint thus involve multiple degrees of freedom at several discrete nodal points. The derivation of the multipoint constraint equations required to impose a prescribed value of rotation is described below. The procedure for imposing multipoint constraints is detailed in [37] and [38].

The physical rotation vector at a point, K, lying along one side of the reference surface of element J is with respect to the element edge coordinate system (see Figure 8),

$$\vec{\vartheta}_K = (\vartheta_s \vec{e}_s + \vartheta_t \vec{e}_t)_K \qquad \text{(IV.343)}$$

and with respect to the surface coordinate system,

$$\vec{\vartheta}_K = (\vartheta_1 \vec{e}_1 + \vartheta_2 \vec{e}_2)_K \qquad \text{(IV.344)}$$

Let the unit vector tangent to the edge of the shell, $\vec{e}_t$, be located with respect to the surface coordinate, x^1, by the angle, ψ, which has the positive sense indicated in Figure 8. The tangent vector is then,

$$\vec{e}_t = \cos\psi \vec{e}_1 + \sin\psi \vec{e}_2 \qquad \text{(IV.345)}$$

and the unit vector normal to the edge of the shell is,

$$\vec{e}_s = \vec{e}_t \times \vec{e}_n = \sin\psi \vec{e}_1 - \cos\psi \vec{e}_2 \qquad \text{(IV.346)}$$

It follows that the transformation relating rotation components in surface coordinates to rotation components in edge coordinates is,

$$\begin{Bmatrix} \vartheta_1 \\ \vartheta_2 \end{Bmatrix} = \begin{bmatrix} \sin\psi & \cos\psi \\ -\cos\psi & \sin\psi \end{bmatrix} \begin{Bmatrix} \vartheta_s \\ \vartheta_t \end{Bmatrix} \qquad \text{(IV.347)}$$

The angle ψ may be approximated as outlined in section IV.C.4, equations (IV.245) through (IV.248).

The rotation vector at a discrete node which lies within element number J and is identified by element connection point K is,

$$\vec{\vartheta}_K = [\vartheta_1 \vec{e}_1 + \vartheta_2 \vec{e}_2]_K \qquad \text{(IV.348)}$$

where by (II.38) and (II.39),

$$(\vartheta_1)_K = (A_2(a^{21}w_{,1}+a^{22}w_{,2}+b^{21}u_1+b^{22}u_2))_K \qquad \text{(IV.349)}$$

$$(\vartheta_2)_K = (-A_1(a^{11}w_{,1}+a^{12}w_{,2}+b^{11}u_1+b^{12}u_2))_K \qquad \text{(IV.350)}$$

Introducing the transformation (IV.156) and (IV.126) into (IV.349) gives,

$$(\vartheta_1)_K = [c_v^1][T_L]_K[T_{w_{12}}]_J\{\bar{W}_{12}\}_J + [c_w^1]_K[T_H]_K\{W_3\}_J \qquad \text{(IV.351)}$$

$$(\vartheta_2)_K = [c_v^2][T_L]_K[T_{w_{12}}]_J\{\bar{W}_{12}\}_J + [c_w^2]_K[T_H]_K\{W_3\}_J \qquad \text{(IV.352)}$$

For specified values of rotation components in the shell coordinate system (i.e., $\vartheta_1 = \vartheta_1^\circ$ and/or $\vartheta_2 = \vartheta_2^\circ$) at node K of element J, the two equations of multipoint constraint relating the shell rotations to the physical displacement components at the other nodes within element J are,

$$(\vartheta_1^o)_K - [\bar{C}_v^1]_K\{\bar{W}_{12}\}_J - [\bar{C}_w^1]_K\{W_3\}_J = 0 \qquad \text{(IV.353)}$$

$$(\vartheta_2^o)_K - [\bar{C}_v^2]_K\{W_{12}\}_J - [\bar{C}_w^2]_K\{W_3\}_J = 0 \qquad \text{(IV.354)}$$

where for $\alpha = 1,2$,

$$[\bar{C}_v^\alpha]_K = [C_v^\alpha]_K[T_L(\lambda_K,\mu_K)][T_w]_J \qquad \text{(IV.355)}$$

$$[\bar{C}_w^\alpha]_K = [C_w^\alpha]_K[T_H(\alpha_K,\beta_K)] \qquad \text{(IV.356)}$$

For specified values of rotation components in the element edge coordinate system (i.e., $\vartheta_s = \vartheta_s^o$ and/or $\vartheta_t = \vartheta_t^o$) the two equations of multipoint constraint are,

$$(\vartheta_s^o)_K \sin\psi_K + (\vartheta_t)\cos\psi_K - [\bar{C}_v^1]_K\{\bar{W}_{12}\}_J - [\bar{C}_w^1]\{W_3\} = 0 \qquad \text{(IV.357)}$$

$$-(\vartheta_s^o)_K \cos\psi_K + (\vartheta_t)_K \sin\psi_K - [\bar{C}_v^2]_K\{\bar{W}_{12}\}_J - [\bar{C}_w^2]\{W_3\} = 0 \qquad \text{(IV.358)}$$

CHAPTER V

ANALYTICAL RESULTS

A. Introduction

The SHEFA finite difference element formulated in Chapter IV was installed in the NASTRAN* general purpose, finite element computer program [37,38]. A series of demonstration problems were solved to verify the accuracy and convergence characteristics of the element in a variety of applications and to demonstrate the generality of the element via several problems that are most efficiently modeled with arbitrary meshes. The SHEFA solutions were verified against theoretical or experimental results and in some cases the results obtained with various finite element formulations were available for comparison.

The 12 demonstration problems are summarized in Table 5. Problem 1, the stretching of an isotropic square plate under parabolically distributed edge loads, was selected to study the membrane behavior of the element. Problems 2 through 5 are a study of the bending behavior of the SHEFA element for an isotropic square plate with two different boundary conditions (fixed and simply supported edges) and two lateral loadings (concentrated load at center

---

*NASTRAN is an acronym formed from NASA Structural Analysis.

and uniformly distributed load). Problems 6 through 8 demonstrate the versatility of the wall model and the accuracy of the element when applied to the bending of plates with anisotropic wall construction. The plate of problem 6 has a single layer, orthotropic wall and that for problem 7 has an anisotropic composite wall composed of ten orthotropic plies alternately oriented at +30° and -30° to the plate axes. The anisotropic wall construction for problem 8 is two orthotropic plies alternately oriented at 0° and 90° to the plate axes. The unsymmetrical nature of this layup causes coupling between membrane and bending action and results in both bending and stretching of the plate when it is subjected to a uniform lateral load. Problem 9 illustrates the modeling versatility of the SHEFA element in accommodating a non-rectangular grid pattern which follows the natural boundaries of a cantilevered, rhombic plate under uniform load. With problem 10 the ability of the SHEFA element to predict severe displacement and stress gradients was demonstrated for the case of localized bending of a cylindrical shell by a concentrated line load. Problem 11 further demonstrates the versatility of the SHEFA wall model in treating the effects of thermal stresses due to a nonlinear radial temperature gradient through the wall of a cylindrical shell, including the effects of temperature dependent material properties. The stress concentrations caused by a circular cutout in a cylindrical shell subjected to axial tension loading were studied in problem 12. This problem requires a very fine

grid adjacent to the hole in order to predict the severe stress gradients caused by the cutout. For efficiency in modeling, an arbitrary mesh which does not coincide with the shell coordinate lines was used which further demonstrates the generality of the SHEFA element.

The computation of the SHEFA element stiffness matrix was discussed in Section IV.B.6 where it was shown that the total stiffness matrix is the sum of stiffnesses associated with membrane (K_M), bending (K_B) and coupled membrane and bending (K_C) energies. The integration of the energy per unit area over the surface of the element is approximated by Gaussian quadrature, the weighting coefficients and positions of the integration points being given in Table 3 for integration orders 1 through 5.

The finite difference energy method, as implemented by Bushnell and Almroth [84] for rectangular meshes, uses first order integration (one integration point) with satisfactory results. As pointed out in Section I.D, the use of one point integration offers a significant computational advantage over the finite element method which requires at least four integration points for flat plate elements with low order displacement assumptions and up to 25 points for the higher order curved shell elements. For example, the curved quadrilateral with 36 degrees of freedom by Key and Beisinger [62] uses 5 x 5 Gaussian quadrature (25 integration points) and the curved triangular element with 36 degrees of freedom by

Cowper, et. al. [69] uses a newly developed 13 point integration formula.

In performing the calculations for the membrane plate study (Problem 1) it was determined that 2 x 2 Gaussian quadrature (four integration points) was required to accurately evaluate the membrane stiffness, K_M. The plate bending study (Problems 2-5) confirmed that one integration point was adequate for the accurate evaluation of the bending stiffness, K_B. Accordingly, the computations for the remaining demonstration problems were performed using four point integration for the membrane stiffness and one point integration for the bending stiffness and load vectors. In the case where coupling occurred between membrane and bending energies (Problem 8), four point integration was also used for the coupling stiffness, K_C. The generalized finite difference energy method, in having to employ four point integration for a portion of the element stiffness calculations, thus incurs a computational penalty when compared to the conventional finite difference energy method. Since the membrane stiffness is not as complicated as the bending stiffness, the penalty is somewhat mitigated. Furthermore, the generalized method retains a computational advantage when compared to the finite element method, since the number of integration points required is still fewer than the number required by the curved shell elements.

B. Membrane Plate Study

Problem 1, a flat plate subjected to parabolically distributed end loads as shown in Figure 11, was used by Gallagher [57] to evaluate the membrane behavior of a rectangular shell element previously discussed in Chapter I (see Table 1). The calculations by Gallagher were repeated with the SHEFA element and the results of both discrete methods were compared to the analytical solution by Timoshenko and Goodier [124]. This solution is based on an assumed stress function and the use of the Principle of Least Work. As Gallagher points out, the analytical solution is not exact since it is based on only three undetermined parameters in the assumed stress function but it does represent a highly accurate basis for comparison.

The three mesh refinements used to study the convergence of deflections and stresses are shown in Figure 12. Also shown are the discretized nodal point loads used to approximate the parabolic edge load. Due to double symmetry only one quadrant of the plate was analyzed. The boundary conditions on the quadrant meshed and the plate dimensions and material properties are shown in Figure 11.

The distribution of displacements occurring on the loaded edge, at the points labeled 1 through 9 in Figure 12, are tabulated in Table 6. The results obtained with the SHEFA element are virtually the same as the results of Gallagher for all three meshes. At the point of maximum

displacement (point 1) the numerical results for even the coarsest grid work are nearly identical to the classical solution. The improvement in the overall distribution of displacements with mesh refinement is due in part to the improvement in load discretization which accompanies a refinement in mesh.

The distribution of stresses at the centroids of elements closest to the loaded edge, points labeled a through n in Figure 12, are tabulated in Table 7. Again, the results obtained with the SHEFA element are very nearly the same as the results of Gallagher for all three meshes. For the coarsest mesh the stresses are not as accurate as the displacements but the finer grids give stress results which are very close to the classical solution.

C. Isotropic Plate Bending Study

Clough and Tocher [125] conducted a thorough plate bending study of the relative accuracy provided by seven different finite elements. Three rectangular and four triangular plate bending elements were considered. The convergence of the central deflection was studied for each element using eight different isotropic, rectangular plate systems and five different mesh patterns.

A portion of this study (Problems 2-5) was repeated with the SHEFA element for an isotropic, square plate with two different boundary conditions (fixed and simply supported edges) and two lateral loadings (concentrated load at center and uniformly distributed load). Due to double symmetry only one quadrant of the plate was analyzed. The boundary conditions on the quadrant meshed, the plate dimensions, the loadings and the material properties are shown in Figure 13.

The convergence of the central deflection was studied by using a series of progressively finer N x N mesh patterns in the analysis of each case. The mesh size "N" refers to the number of elements along one side of a quadrant of the plate. Typical element patterns and nodal point arrangements for an N of seven are shown in Figure 14 for the simply supported edge condition and in Figure 15 for the fixed edge boundary condition. In both Figures 14 and 15 some nodes lie outside of the physical confines of the plate

quadrant being analyzed. Only w degrees of freedom are defined at these points and they are eliminated in the solution process via the multipoint constraints used to impose specified values of shell rotations (see Section IV.E).

Figures 16 through 19 show the convergence of the central deflection with refinement in the mesh size. The quantity plotted in these figures is the deflection coefficient, a dimensionless number which is related to the central deflection w_c, the plate dimension a, the loading P or q and the flexural rigidity D, which is defined by

$$D = \frac{Et^3}{12(1-\nu^2)} \qquad (V.1)$$

where,

E = Modulus of elasticity

ν = Poisson's ratio

t = plate thickness

Figures 20 through 23 show the convergence of the central deflection with an increase in the number of simultaneous equations that must be solved for a given mesh size. These figures are a replot of Figures 16-19 wherein the mesh size has been converted to the equivalent number of degrees of freedom associated with each element type after boundary conditions are imposed. This type of plot is more representative of the computational effort expended in obtaining a data point.

The "exact" deflection coefficients shown in Figures 16-23 are from the classical plate bending solutions by Timoshenko [128]. Error bands of $\pm$ 5% with respect to the classical solution are shown as a basis of comparison. In all cases the SHEFA element exhibited smoothly convergent behavior toward the classical solution. Acceptable accuracy was achieved with a mesh size of five or twenty degrees of freedom. The convergence was somewhat faster for the simply supported plates (Figures 16,17,20,21) than for the fixed edge plates (Figures 18,19,22,23).

The slower convergence of the fixed edge case is due to the method of imposing rotational constraints that is required by the finite difference energy method (see Section IV.E). Since the rotations do not appear as nodal point degrees of freedom they must be enforced through a multipoint constraint relation involving displacement components at several neighboring nodes adjacent to the boundary. The discretization of the boundary conditions could probably be improved by a local refinement of the mesh spacing in the vicinity of the boundary.

For both edge conditions the concentrated load cases (Figures 17,19,21,23) converged faster than the uniform load cases (Figures 16,18,20,22). This is to be expected since the discretization of the concentrated load is exact, while the uniform load is approximated by concentrated forces at the w nodes. The discretization of the uniform load for the coarser meshes is fairly crude and causes the slower convergence.

Along with the results of the SHEFA element, the results of four elements from the Clough and Tocher study are also plotted in Figures 16-23. The "ACM" element is the Adini-Clough-Melosh rectangle based on a 12 term polynomial displacement assumption. The "M" element is the Melosh rectangle which is based on physical reasoning and the use of beam displacement functions. The "P" element is the Papenfuss rectangle which is based on an incomplete bicubic polynomial displacement assumption which completely satisfies displacement and slope compatibility along the edges. The "HCT" element is the Hsieh-Clough-Tocher triangle which is formed from three subtriangles in such a way as to lead to full slope and displacement compatibility between adjacent elements. The mesh patterns for the HCT triangle were the same as for the rectangular elements except two triangles were used to represent each rectangle. The M, P and ACM rectangular plate bending elements are not of much interest from a practical viewpoint since they are restricted in their ability to model complex shapes. However, they do serve to show the effect of the assumed displacement functions on convergence for elements with the same number of degrees of freedom. The M and ACM elements converge quite rapidly but the P element converges to an overly stiff result.

The HCT triangular plate bending element is of practical interest since it has been proposed as a facet element for the analysis of thin shells of arbitrary shape by Clough and Johnson [45]. The flexural stiffness of the

facet element is represented by the HCT triangle and for the membrane stiffness a plane stress element [12] is used. Except for the simply supported plate under a concentrated load, the HCT element is converging faster than the SHEFA element on a mesh size basis (Figures 16-19). However, on a degree of freedom basis the SHEFA element is converging faster than the HCT element for the simply supported plates (Figures 20,21) and at about the same rate as HCT for the fixed edge plates (Figures 22,23).

For the case of the simply-supported plate under uniform load (Figures 16 and 20), the results of the KB1 and KB6 quadrilateral shell elements by Key and Beisinger [61, 62] and the results of the Q-19 quadrilateral plate bending element [126] are also plotted. The KB6 shell element (see Table 1) has 36 degrees of freedom and employs 12 term polynomial assumptions for the displacements u, v and w. The KB1 element, having 28 degrees of freedom. employs bilinear assumptions for the displacements u, v and rotations ψ_1, ψ_2 and bicubic assumptions for w. The Q-19 flat plate element by Clough and Fellipa [127] is a quadrilateral based on four triangles of the HCT type. It provides for slope and displacement compatibility between adjacent elements and has 12 degrees of freedom remaining after 7 internal degrees of freedom are removed by static condensation. For this case the KB6 and Q-19 elements converge faster than the SHEFA element on both a mesh size and a degree of freedom basis. The KB1

element converges faster than SHEFA on a mesh size basis and at about the same rate as SHEFA on a degree of freedom basis. The rapidly convergent behavior of the KB6 and Q-19 elements in comparison to the SHEFA element is in part associated with the manner of discretization of the uniform load and also is due to a greater sophistication in element formulation.

D. Anisotropic Plate Bending Study

Three anisotropic square plates with uniform lateral loading (Problems 6-8 of Table 5), for which analytical solutions are available, were selected to demonstrate the versatility of the SHEFA wall model. Due to double symmetry only one quadrant of the plates was analyzed. The boundary conditions on the quadrant meshed, the plate dimensions, the loading, the wall constructions and the material properties are shown in Figure 13. Problems 6 and 7 are simply supported plates while problem 8 has a boundary condition termed hinge-restrained, a form of simple support in which the in-plane components of displacement are also constrained. The wall construction for problem 6 is one orthotropic layer while that of problem 7 is an anisotropic composite wall composed of 10 orthotropic plies of equal thickness alternately oriented at -30° and +30° to the plate axes as shown in Figure 13. Problem 8 has an anisotropic composite wall consisting of two orthotropic plies of equal thickness alternately oriented at 0° and 90° to the plate axes and is also shown in Figure 13. The asymmetry in the cross-ply construction causes coupling between membrane and bending action and results in both bending and stretching of the plate when it is subjected to uniform lateral loading.

The convergence of the central deflection was studied by using a series of NxN mesh patterns as was done for the isotropic plate bending problems. Figures 24 through 26 show the convergence of the central deflection with refinement in the mesh size. The quantity plotted is a dimensionless deflection coefficient which is defined in each figure. It is a function of the central deflection w_c, the plate dimensions a and t, the uniform loading q and the orthotropic material properties,

E_{11}, E_{22} = Modulus of elasticity in the 1,2 material directions shown in Figure 13

G_{12} = Shear modulus in 1-2 plane

ν_{12}, ν_{21} = Poisson's ratios in the 1-2 plane

Due to symmetry in the constitutive relations the orthotropic Poisson's ratios are related by,

$$\nu_{12} = \nu_{21} \frac{E_{11}}{E_{22}} \qquad (V.2)$$

The "exact" deflection coefficient shown in Figure 24 is the classical plate bending solution by Lekhnitski [129]. The "exact" deflection coefficients shown in Figures 25 and 26 are by Fortier [130] who used the Ritz method and

trigonometric displacement assumptions to arrive at convergent solutions for a variety of unsymmetrically layered, anisotropic, square plates. In all three cases the SHEFA element showed a smooth convergence toward the "exact" solution and acceptable accuracy was obtained with a mesh size of five.

For the case of the single layer orthotropic wall the results of the Q-19 quadrilateral plate bending element [126] are also plotted. The comparison between the Q-19 and SHEFA results is essentially the same as for the corresponding isotropic plate (Problem 2).

E. Arbitrary Mesh Example - Bending of Rhombic Cantilever Plate

The bending of a rhombic cantilever plate by a uniform pressure load was also included in the Clough and Tocher Study [125]. The plate geometry, loading and isotropic material properties are shown in Figure 27. The finite element analyses by Clough and Tocher were all conducted with an 8x6 mesh which is shown by the dotted lines of Figure 27. The sloping boundaries of the plate were treated as stepped in the rectangular element analyses while the triangular elements fitted the boundaries exactly. Experimental results were available for the points labeled 1 through 6 in Figure 27. The finite element displacements at these points were obtained by interpolation of the nodal point deflection data and the results are tabulated in Figure 27 for the ACM, M and P rectangular elements and the HCT triangular element.

In order to obtain a representative comparison between the finite element and SHEFA solutions, a mesh size of 13x13 was selected as shown in Figure 28. This mesh has approximately the same number of degrees of freedom as the finite element meshes and also has nodes at the points where experimental deflections were measured so that comparisons can be made without interpolating. The w degrees of freedom at the nodes which lie outside of

the plate domain are eliminated via the multipoint constraints used to enforce the fixed edge boundary condition. The element layout of Figure 28, which follows the natural boundaries of the rhombic plate, illustrates the arbitrary meshing capability of the SHEFA element.

The SHEFA and finite element deflections together with the experimental results are tabulated in Figure 27. As discussed previously in the isotropic plate bending study, the M, P and ACM rectangles are not of practical interest but the HCT triangle is a representative facet type element for thin shell analysis. All of the numerical solutions are in good agreement with the experimental results, the P element being somewhat stiff as pointed out previously. The SHEFA and HCT results are about the same. The distribution of displacement predicted by the SHEFA element along the edges normal to the fixed support and along the plate centerline are shown in Figure 29. The experimental measurements are also shown.

F. Cylindrical Shell Bending Study

A curved shell problem, in which flexural behavior is significant, is the cylindrical shell with a uniformly distributed, circumferential line load as shown in Figure 30. Since this is an axisymmetric problem with a plane of symmetry, only a portion of the shell need be meshed. The boundary conditions on the portion meshed, the shell dimensions and the isotropic material properties are also shown in Figure 30. The convergence of the deflection under the load was studied by using a series of progressively finer 3xN mesh patterns. A typical example of the element pattern and nodal point arrangement for an N of 20 is shown in Figure 31. As described previously in section V.C, the w degrees of freedom at nodes lying outside the shell boundary are eliminated when the boundary conditions are imposed.

Figure 32 shows the convergence of the deflection under the load with a refinement in the mesh size. The quantity plotted is a dimensionless deflection coefficient which depends on the deflection under the load w_o, the loading P, the flexural rigidity D which is given by (V.1) and a parameter β which is defined by,

$$\beta^4 = \frac{Et}{4R^2D} = \frac{3(1-\nu)}{R^2t^2} \qquad (V.3)$$

The "exact" deflection coefficient shown in Figure 32 is from the classical solution by Timoshenko [128] of the governing differential equation for symmetrical deformation of circular cylindrical shells. Acceptable accuracy was achieved even for the coarsest mesh size (N=4). One solution, for a mesh of 8, was available for the rectangular shell element of Gallagher [57]. It also is shown in Figure 32 and is virtually the same as the SHEFA solution.

In Figure 33 the variation of normal displacement along the length of the shell is plotted in non-dimensional form. The deflection (w) and length coordinate (Z) are normalized with respect to the deflection under the load (w_o) and the half length of the shell (L). The SHEFA deflections for the 3x20 mesh are superimposed on the classical solution by Timoshenko. The agreement between the two predictions is excellent. The slight departure between the two solutions near the boundary is to be expected since the Timoshenko solution is for an infinite cylinder while the SHEFA solution is for a finite length cylinder with simply supported ends.

The variation of the meridional moment resultant along the length of the shell is plotted in non-dimensional form in Figure 34. The moment resultant (M) and length coordinate (Z) are normalized with respect to the moment resultant under the load (M_o) and the half length of the shell (L). The SHEFA results for the 3x20 mesh are shown

along with the classical solution. Again, the agreement between the two solutions is excellent and there is no departure between the two solutions near the boundary because the moment decays more rapidly than does the deflection.

G. Cylindrical Shell Thermal Stress Study

A curved shell problem that further demonstrates the versatility of the SHEFA wall model is the unrestrained cylindrical shell shown in Figure 35. It has a non-linear radial temperature gradient through the shell wall that is everywhere constant with respect to the surface coordinates. Since the problem is axisymmetric and has a plane of symmetry, only a portion of the shell was meshed. The boundary conditions on the portion meshed and the shell dimensions are also shown in Figure 35. The mesh used for analysis is shown in Figure 36 and the isotropic material properties, which are a function of temperature, are shown in Figure 37. The temperature distribution through the shell wall is shown in Figure 38. The shell wall was divided into 20 equal layers in order to model the effects of the material property temperature dependence and the thermal gradient on the compliances (IV.50)-(IV.52) and the thermal forces (IV.53) and thermal moments (IV.54).

Since the shell is completely unrestrained the stress distribution at locations sufficiently removed from the ends of the shell is governed by membrane shell theory. In a membrane state of stress the total strains (IV.329) in both the circumferential and meridional directions

are constant through the thickness, but the strains associated with stress (IV.330) of course vary through the thickness, since the free thermal strains vary according to the temperature distribution.

The variation of meridional and circumferential stresses through the thickness of the shell is shown in Figure 39. The SHEFA results at the extreme outer and inner fibers and at the center of each layer are superimposed on the results obtained with membrane shell theory. The SHEFA stress distribution is for elements near the center of the shell where end effects have decayed to zero. The theoretical results were obtained with an analysis method [131] based on membrane shell theory and employing a layered shell wall model to account for material property temperature dependence and thermal gradient effects. The results with both methods were essentially identical.

H. Arbitrary Mesh Example - Cylindrical Shell With Circular Cutout

A curved shell problem with severe stress concentrations is that of a cylindrical shell with a circular cutout loaded in axial tension as shown in Figure 40. The problem has two planes of symmetry which require the analysis of only one-quarter of the shell with appropriate boundary conditions. However, a very fine grid adjacent to the hole is required in order to predict the severe stress gradients caused by the cutout. If the entire quadrant of the shell were meshed, a problem with several thousand degrees of freedom would have to be solved. Since the perturbations in the membrane stress field due to the hole decay rapidly, it is only necessary to mesh a small portion of the shell quadrant. The theoretical solution by Van Dyke [132] indicates that the stress concentrations at the hole decay to a membrane state in about three to four hole radii. Accordingly, a portion equal to about seven hole radii on a side was selected for analysis. The boundary conditions on the portion meshed, the shell dimensions and the isotropic material properties are shown in Figure 40.

Two element discretizations were used in studying the stress concentrations at the hole, a 10x10 mesh and a 20x20 mesh. The element pattern and nodal point arrangement is shown in Figure 41 for the 20x20 mesh. An enlargement of this mesh in the vicinity of the hole is shown in Figure 42. An irregular grid work was used in which the mesh lines correspond roughly to a polar coordinate system about the hole rather than following the shell coordinate lines.

The predicted stress concentrations at the two points on the hole boundary labeled A and B in Figure 40 are given in Table 8 for an applied axial stress of 10,000 psi. The hoop stress peaks at point A and the axial stress peaks at point B. Outer and inner surface stresses as well as membrane and bending stresses are tabulated for two analytical solutions, four finite element solutions and the two SHEFA solutions. The analytical solutions are by Van Dyke [132] and Lekkerkerker [133]. Solutions are also available for the KB1 and KB6 quadrilateral shell elements by Key and Beisinger [61,62]. They used two element discretizations which cover a full quadrant of the shell. The coarse mesh had 176 nodal points, 148 elements and the fine mesh had 589 nodal points, 533 elements. In the KB6 analyses the number of degrees of freedom was 1534 for the coarse mesh and 5301

for the fine mesh, while for the KB1 analyses, the numbers were about ten percent smaller. The two SHEFA meshes, covering a smaller portion of the shell quadrant as shown in Figure 40, had 100 elements, 265 nodal points and 329 degrees of freedom for the 10x10 mesh and 400 elements, 925 nodal points and 1263 degrees of freedom for the 20x20 mesh. If the discrete element meshes are all compared on the basis of the smaller region of analysis used for the SHEFA calculations, the mesh gradations were such that the two finite element meshes each have about 20 percent fewer elements but more degrees of freedom than the SHEFA meshes.

The two SHEFA analyses were essentially the same and the results lie within the spread of the two analytical solutions except for the bending components of the stresses which are slightly higher than the Lekkerkerker prediction. Since stresses are only computed at the centroids of the SHEFA elements, the values in Table 8 were obtained by extrapolation.

The two KB6 analyses showed an increase in the stresses in going from the coarse mesh to the fine mesh. The fine mesh results were approximately the same as the Van Dyke solution. The two KB1 analyses also showed an increase in the stresses for the finer mesh and the results are approximately the same as those obtained by Lekkerkerker. The KB1 and KB6 stresses in Table 8 were also obtained by extrapolation of element centroidal stress data.

AD-A034 788 NAVAL SURFACE WEAPONS CENTER WHITE OAK LAB SILVER SP--ETC F/G 13/13
A GENERALIZED FINITE DIFFERENCE ELEMENT FOR THE THERMOELASTIC S--ETC(U)
JUN 76 R J EDWARDS

UNCLASSIFIED NSWC/WOL/TR-76-66 NL

3 OF 4
AD
A034788



VI. CONCLUSIONS

Two well established matrix methods for thin shell structural analysis, the finite element method and the finite difference energy method, have been integrated into one unified analytical approach and have been effectively applied to the thermoelastic analysis of anisotropic thin shells. The finite element method is a widely used tool for structural analysis of thin shells due to its ability to model the complex geometries that occur in engineering practice. In recent years, it has been demonstrated that the finite difference energy method offers significant advantages over contemporary finite element formulations, especially for problems involving geometrical nonlinearities. However, the method suffers from the modeling restrictions imposed by rectangular grid works which must follow the shell coordinate lines. The results of this research demonstrate that this classic restriction can be removed and that a generalized finite difference energy method can be developed for arbitrary quadrilateral meshes. Furthermore, the formulation is amenable to installation in contemporary, general purpose, finite element computer programs.

The SHEFA generalized finite difference element for the thermoelastic analysis of anisotropic thin shells has been developed. The shell reference surface geometry is described in terms of curvilinear surface coordinates using tensor

notation. The deformation of the shell is described by the linear strain and curvature change tensors of Sanders. A shell wall model has been developed that is sufficiently general to treat a broad range of wall constructions including layered orthotropic walls, filament wound walls and angle ply composite walls as well as more conventional monocoque construction. The model treats the effects of nonlinear temperature gradients through the shell wall, including material property temperature dependence, and also accounts for coupling between membrane and bending action. Isoparametric mapping techniques have been used to establish a finite difference approximation of the strain and curvature tensors in terms of displacement variables at arbitrarily placed discrete nodes on the shell reference surface. The potential energy of the structural system is then formed in terms of the nodal variables and the equations of motion are obtained by use of the Minimum Potential Energy Theorem.

A series of twelve demonstration problems were solved to verify the accuracy and convergence characteristics of the element in a variety of applications and to demonstrate the generality of the element via several problems that are most efficiently modeled with arbitrary meshes. The SHEFA predictions were verified against classical analytical solutions or experimental results and in some cases were compared to the results obtained with finite element formulations. Based on the limited comparisons of this

study, the performance of the SHEFA element was found to be comparable to the facet element of Clough and Johnson [45] and the curved rectangular shell element of Gallagher [57]. Some flat finite elements and the quadrilateral elements for axisymmetric shells of Key and Beisinger [61,62] were found to be more rapidly convergent for plate bending problems. However, the SHEFA element gave results comparable to the more sophisticated finite element formulations of Key and Beisinger for the case of an axially loaded cylindrical shell with a circular cutout.

APPENDIX A

TABLES

TABLE 1
CURVED, THIN SHELL, FINITE ELEMENTS WITH FOUR SIDES

DEVELOPER	REF. NO.	NO. OF NODES	NO. D.O.F.	NO. OF POLYNOMIAL TERMS w	u,v	ψ_1, ψ_2	SHELL THEORY	SURFACE APPROXIMATION	DISPLACEMENT CONTINUITY SATISFIED	RIGID BODY MODES SATISFIED	ELEMENT PLANFORM
1. BOGNER, ET. AL.	51	4	48	16	16		UNKNOWN	CYLINDRICAL	YES	NO	RECTANGLE
2. CANTIN & CLOUGH	52	4	24	16	4		NOVOZHILOV	CYLINDRICAL	NO	YES	RECTANGLE
3. OLSON & LINDBERG	53	4	28	12	8		LOVE	CYLINDRICAL	NO	YES(1)	RECTANGLE
4. YANG & KIM	54	4	48	16	16		UNKNOWN	CONICAL	YES	NO	TRAPEZOID
5. CONNOR & BREBBIA	55	4	20	12	4		MARGUERRE(2)	QUADRATIC	NO	NO	PARALLELOGRAM
6. BERGAN & CLOUGH	56	4	20	10	4		MARGUERRE(2)	CUBIC	YES	YES(1)	RECTANGLE
7. GALLAGHER & YANG	57,58	4	24	16	4		NOVOZHILOV	PRINCIPAL CURVATURES	NO	NO	RECTANGLE
8. GREENE, ET. AL.	59	4	40	16	16		NOVOZHILOV	QUADRATIC	YES	NO	RECTANGLE
9. WEMPNER, ET. AL.	60	4	20	4	4	4	WEMPNER(3)	GAUSSIAN	NO	NO	PARALLELOGRAM
10. KEY & BEISINGER	61,62	4	36	12	12		WASHIZU(3)	AXISYMMETRIC	YES	YES(1)	QUADRILATERAL
11. JONES	63	4	48	16	16		MARGUERRE(2)	QUADRATIC	YES	NO	EIGHT-SIDED POLYGON

(1) REPRESENTATION OF RIGID BODY MODES DEMONSTRATED NUMERICALLY VIA EIGENVALUES OF STIFFNESS MATRIX.

(2) SHALLOW SHELL THEORY

(3) THESE SHELL THEORIES ALSO INCLUDE TRANSVERSE SHEAR DEFORMATIONS BUT A DISCRETE EQUIVALENT OF THE KIRCHOFF HYPOTHESIS IS INTRODUCED TO ASSURE THAT THE KIRCHOFF THEORY IS APPROACHED IN THE LIMIT AS THE MESH IS REFINED.

TABLE 2
CURVED, THIN SHELL, FINITE ELEMENTS WITH THREE SIDES

DEVELOPER	REF. NO.	NO. OF NODES	NO. D.O.F.	NO. OF POLYNOMIAL TERMS w	u,v	ψ_1, ψ_2	SHELL THEORY	SURFACE APPROXI-MATION	DISPLACEMENT CONTINUITY SATISFIED	RIGID BODY MODES SATISFIED
1. UTKU	64	3	15	3	3	3	MARGUERRE(2)	QUADRATIC	YES	NO
2. STRICKLAND & LODEN	65	3	15	9	3		NOVOZHILOV(2)	QUADRATIC	NO	NO
3. BONNES, ET. AL.	66	6	36	12	12		REISSNER(2)	QUADRATIC	NO	NO
4. COWPER, ET. AL.	67,70	3	36	21	10		NOVOZHILOV(2)	GUASSIAN	YES	YES(1)
5. DHATT	68	3	27	9	10	6	REISSNER,(2,3) WASHIZU	QUADRATIC	YES	YES(1)
6. ARGYRIS & SCHARPF	69	6	63	21	21		ARGYRIS	NINE POINT LAGRANGIAN	YES	YES
7. COWPER, ET. AL.	70	3	36	21	10		DONNELL-VLASOV, KOITER-SANDERS	GAUSSIAN	YES	YES(1)
8. DUPUIS & GOEL	71	3	54	18	18		KOITER	TEN POINT LAGRANGIAN	YES	YES
9. THOMAS & GALLAGHER	72	4	36	10	10		KOITER	GAUSSIAN	YES	NO

(1) REPRESENTATION OF RIGID BODY MODES DEMONSTRATED NUMERICALLY VIA EIGENVALUES OF STIFFNESS MATRIX.

(2) SHALLOW SHELL THEORY

(3) THESE SHELL THEORIES ALSO INCLUDE TRANSVERSE SHEAR DEFORMATIONS BUT A DISCRETE EQUIVALENT OF THE KIRCHOFF HYPOTHESIS IS INTRODUCED TO ASSURE THAT THE KIRCHOFF THEORY IS APPROACHED IN THE LIMIT AS THE MESH IS REFINED.

TABLE 3

ABSCISSAE OF INTEGRATION POINTS

AND WEIGHT COEFFICIENTS FOR

THE GAUSSIAN QUADRATURE FORMULA

$$\int_{-1}^{1} f(x)dx = \sum_{i=1}^{N} H_i \, f(a_i)$$

N	± a	H
1	0.0	1.0
2	0.57735 02691 89626	1.0
3	0.77459 66692 41483	0.55555 55555 55556
	0.0	0.88888 88888 88889
4	0.86113 63115 94053	0.34785 48451 37454
	0.33998 10435 84856	0.65214 51548 62546
5	0.90617 98459 38664	0.23692 68850 56189
	0.53846 93101 05683	0.47862 86704 99366
	0.0	0.56888 88888 88889

TABLE 4

CORRESPONDENCE BETWEEN ELEMENT INTERPOLATING COORDINATES AND ELEMENT CONNECTION NUMBER

ELEMENT CONNECTION NUMBER, K	INTERPOLATING COORDINATES			
	λ_K	μ_K	α_K	β_K
1	−1	−1	DETERMINE NUMERICALLY* FROM: $x^1_k = [H_L(\alpha_k,\beta_k)] \{x^1_L\}$ $x^2_k = [H_L(\alpha_k,\beta_k)] \{x^2_L\}$ $k = 1, \ldots, 4$ $L = 5, \ldots, 13$	
2	1	−1		
3	1	1		
4	−1	1		
5	0	0	0	0
6	DETERMINE NUMERICALLY* FROM: $x^1_k = [L_L(\lambda_k,\mu_k)] \{x^1_L\}$ $x^2_k = [L_L(\lambda_k,\mu_k)] \{x^2_L\}$ $k = 5, \ldots, 13$ $L = 1, \ldots, 4$		−1	−1
7			0	−1
8			1	−1
9			1	0
10			1	1
11			0	1
12			−1	1
13			−1	0

*A NUMERICAL METHOD FOR DETERMINING THE INVERSE FUNCTIONAL RELATIONSHIP BETWEEN SURFACE COORDINATES AND PARAMETRIC INTERPOLATING COORDINATES IS PRESENTED IN APPENDIX D.

TABLE 5

SUMMARY OF DEMONSTRATION PROBLEMS

PROBLEM NO.	PROBLEM DESCRIPTION	LOADING	BOUNDARY CONDITIONS	NO. OF LAYERS IN WALL
1	STRETCHING OF ISOTROPIC, SQUARE PLATE	PARABOLIC EDGE LOADS	2 FREE EDGES 2 LOADED EDGES	1
2	BENDING OF ISOTROPIC, SQUARE PLATE	UNIFORM PRESSURE	SIMPLE SUPPORT	1
3	BENDING OF ISOTROPIC, SQUARE PLATE	CONCENTRATED LOAD AT CENTER	SIMPLE SUPPORT	1
4	BENDING OF ISOTROPIC, SQUARE PLATE	UNIFORM PRESSURE	FIXED EDGES	1
5	BENDING OF ISOTROPIC, SQUARE PLATE	CONCENTRATED LOAD AT CENTER	FIXED EDGES	1
6	BENDING OF ORTHOTROPIC, SQUARE PLATE	UNIFORM PRESSURE	SIMPLE SUPPORT	1
7	BENDING OF ANISOTROPIC, SQUARE PLATE ($\pm 30^{\circ}$ ANGLE PLY COMPOSITE)	UNIFORM PRESSURE	SIMPLE SUPPORT	10
8	COMBINED BENDING AND STRETCHING OF ANISOTROPIC, SQUARE PLATE (CROSS PLY COMPOSITE)	UNIFORM PRESSURE	HINGE-RESTRAINED	2
9	BENDING OF ISOTROPIC, RHOMBIC PLATE	UNIFORM PRESSURE	3 FREE EDGES 1 FIXED EDGE	1
10	BENDING OF ISOTROPIC, CYLINDRICAL SHELL	LINE LOAD AROUND CIRCUMFERENCE	ENDS SIMPLY SUPPORTED	1
11	THERMAL STRESSES IN CYLINDRICAL SHELL WITH ISOTROPIC, TEMPERATURE DEPENDENT PROPERTIES	NONLINEAR RADIAL TEMPERATURE GRADIENT	FREE ENDS	20
12	STRESS CONCENTRATIONS IN ISOTROPIC CYLINDRICAL SHELL WITH CIRCULAR HOLE	AXIAL TENSION	END LOADS	1

TABLE 6
FLAT PLATE MEMBRANE BEHAVIOR
DISPLACEMENT SOLUTIONS

POINT NO.	DISPLACEMENT, u, (10^{-3} IN.)						
	ANALYTICAL SOLUTION	SHEFA SOLUTION			GALLAGHER SOLUTION		
		4-ELEMENT	16-ELEMENT	64-ELEMENT	4-ELEMENT	16-ELEMENT	64-ELEMENT
1	1.4764	1.4727	1.4756	1.4764	1.4729	1.4757	1.4769
2				1.4542			1.4550
3	1.3895		1.3891	1.3883		1.3892	1.3899
4				1.2813			1.2842
5	1.1428	1.1491	1.1442	1.1373	1.1490	1.1442	1.1425
6				0.9620			0.9712
7	0.7786		0.7873	0.7643		0.7873	0.7795
8				0.5462			0.5972
9	0.3674	0.4958	0.4161	0.3620	0.4956	0.4159	0.3862

TABLE 7
FLAT PLATE MEMBRANE BEHAVIOR
STRESS SOLUTIONS

	ANALYTICAL SOLUTION		SHEFA ELEMENT SOLUTION		GALLAGHER ELEMENT SOLUTION	
POINT	σ_y	σ_x	σ_y	σ_x	σ_y	σ_x
a	78.7	909.6	102.33	854.02	102.35	854.04
b	18.8	456.2	32.94	479.36	32.94	479.29
c	217.8	975.0	224.59	959.95	224.64	960.03
d	171.6	852.6	177.12	837.82	177.18	837.90
e	91.9	609.4	95.42	597.16	95.48	597.26
f	14.9	249.2	21.99	271.57	22.02	271.40
g	310.2	993.5	316.38	989.43	309.27	989.70
h	293.3	962.5	300.90	958.27	293.60	958.54
i	261.4	900.0	270.42	895.98	262.80	896.27
j	213.8	806.9	226.22	803.03	218.93	803.06
k	157.4	683.1	170.54	678.87	163.53	679.18
l	97.0	528.1	107.51	525.83	101.14	525.38
m	41.9	342.6	41.53	315.78	43.78	341.85
n	5.6	126.6	4.11	115.82	8.12	139.32

VALUES SHOWN ARE LB/IN.^{2}

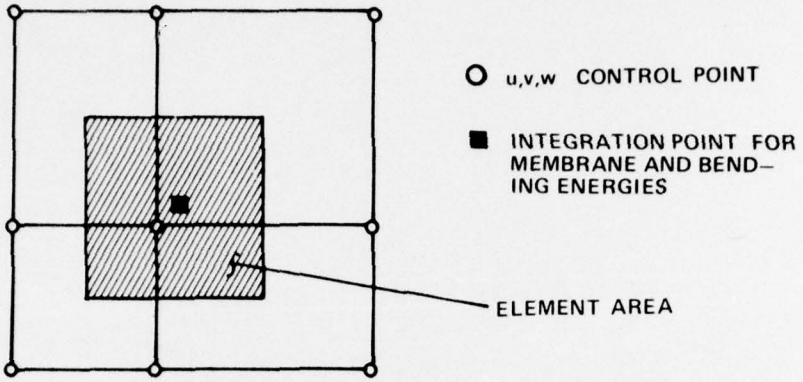
TABLE 8

STRESS CONCENTRATIONS IN AN AXIALLY LOADED CYLINDRICAL SHELL WITH A CIRCULAR HOLE

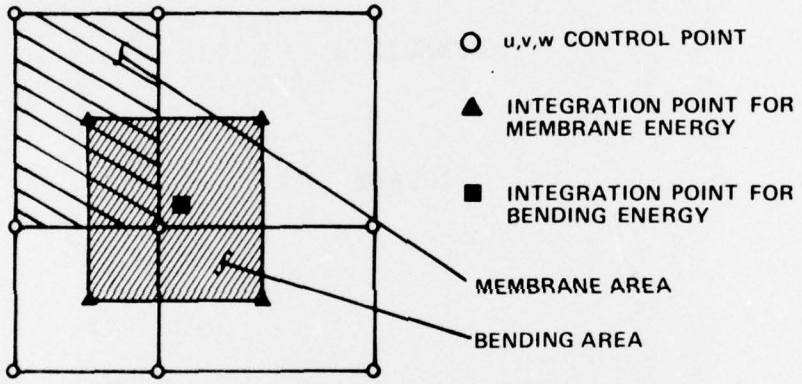
	STRESS LOCATION	STRESS DIRECTION	STRESSES AT HOLE DUE TO AN APPLIED AXIAL STRESS OF 10,000 PSI			
			OUTER SURFACE STRESS PSI	INNER SURFACE STRESS PSI	MEMBRANE STRESS PSI	BENDING STRESS PSI
VAN DYKE	A	HOOP	− 4410	− 20590	− 12500	8090
	B	AXIAL	30100	41900	36000	− 5900
LEKKER KERKER	A	HOOP	− 5500	− 22000	− 13750	8250
	B	AXIAL	33500	45600	39550	− 6050
SLADE-KB6 COARSE MESH	A	HOOP	− 2740	− 18860	− 10800	8060
	B	AXIAL	28900	39900	34400	− 5500
SLADE-KB6 FINE MESH	A	HOOP	− 3680	− 19920	− 11800	8120
	B	AXIAL	30400	41400	35900	− 5500
SLADE-KB1 COARSE MESH	A	HOOP	− 3970	− 19000	11485	7515
	B	AXIAL	30720	42020	36370	− 5650
SLADE-KB1 FINE MESH	A	HOOP	− 4690	− 21010	12850	8160
	B	AXIAL	33380	45060	39220	− 5840
SHEFA 10 X 10 MESH	A	HOOP	− 4000	− 20800	− 12400	8400
	B	AXIAL	31000	44000	37500	− 6500
SHEFA 20 X 20 MESH	A	HOOP	− 4400	− 21000	− 12700	8300
	B	AXIAL	31500	44500	38000	− 6500

APPENDIX B

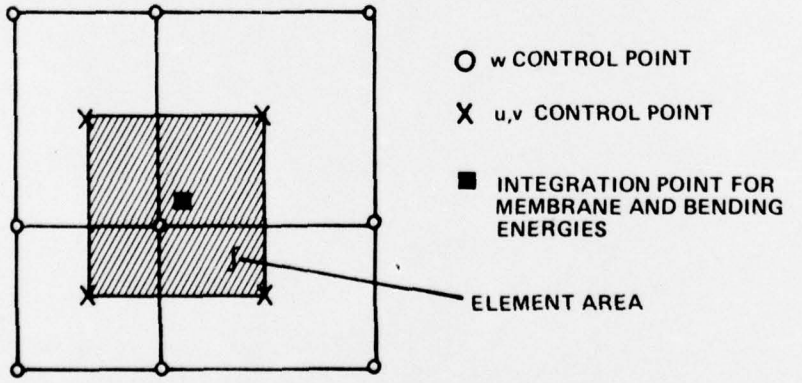
FIGURES



A. WHOLE–STATION SPACING WITH MEMBRANE AND BENDING ENERGIES INTEGRATED OVER SAME AREA



B. WHOLE STATION SPACING WITH MEMBRANE AND BENDING ENERGIES INTEGRATED OVER DIFFERENT AREAS



C. HALF–STATION SPACING WITH MEMBRANE AND BENDING ENERGIES INTEGRATED OVER THE SAME AREA

FIGURE 1 STAGS FINITE DIFFERENCE MESH SCHEMES

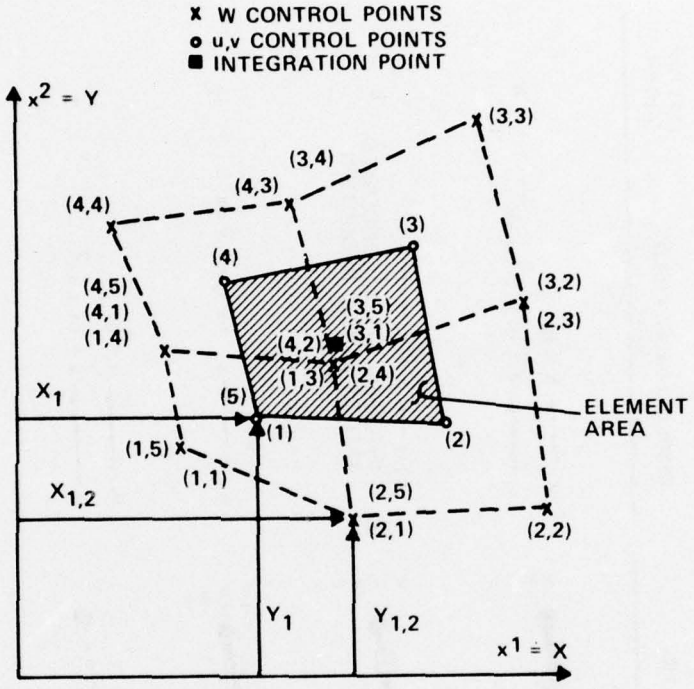


FIGURE 2 FINITE DIFFERENCE MESH SCHEME BY JOHNSON [110]

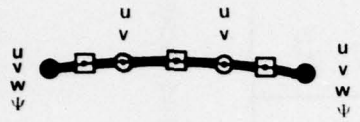
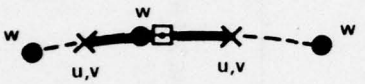
ELEMENT NUMBER	SCHEMATIC	DISPLACEMENT FIELD	MATRIX ORDER	GAUSS POINTS REQUIRED ⊡
1		u,v → a + bs w → a + bs + cs^2 + ds^3	8	2
2		u,v,w → a + bs + cs^2 + ds^3 ⊙ – INTERNAL D.O.F. CONDENSED OUT BY STATIC REDUCTION	8	3
3		u,v,w → a + bs + cs^2 + ds^3	12	3
4		u,v → a + bs w → a + bs + cs^2	7	1

FIGURE 3 DISCRETE ELEMENTS FOR COMPARATIVE STUDY BY BUSHNELL , [114]

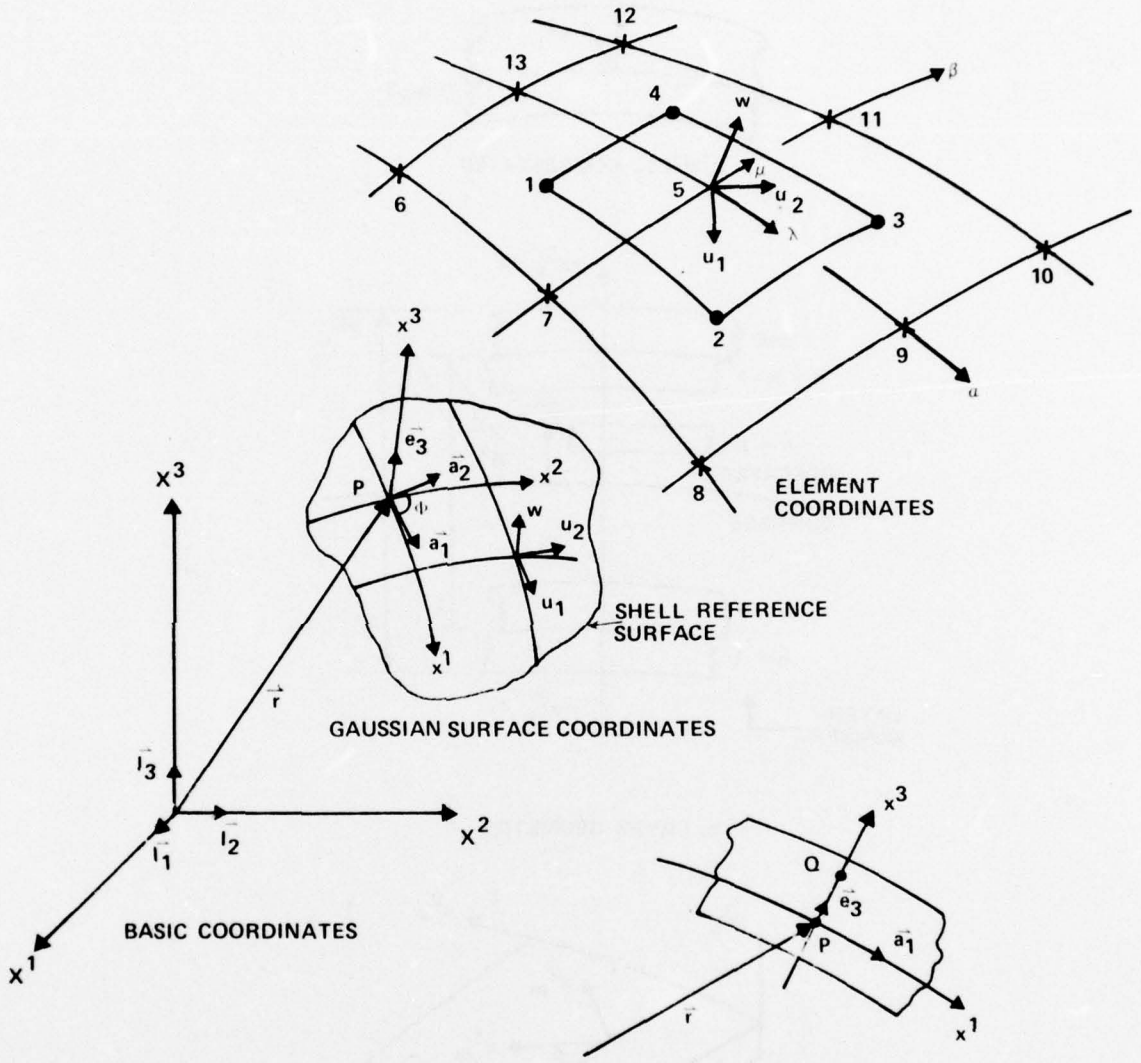
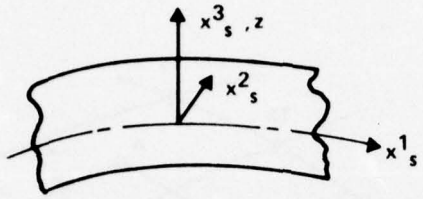
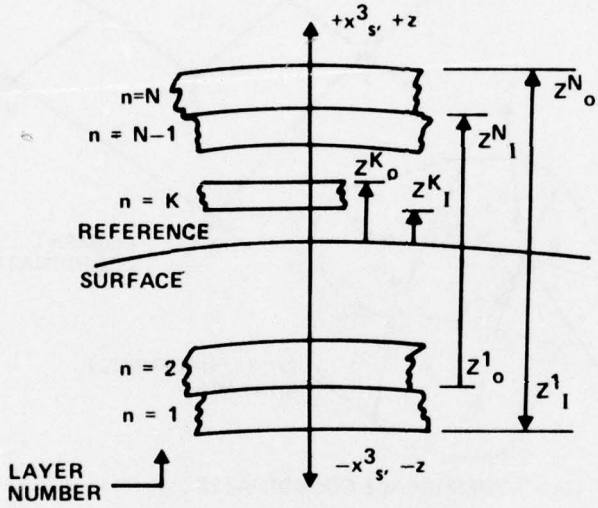


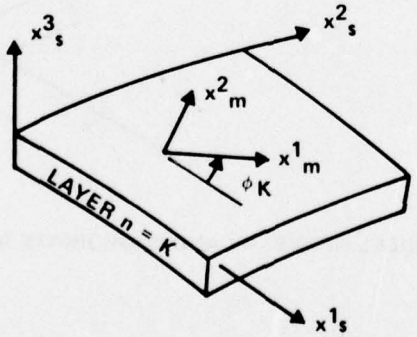
FIGURE 4 SHELL GEOMETRY AND COORDINATE SYSTEMS



a. SHELL COORDINATES



b. LAYER GEOMETRY



c. MATERIAL COORDINATES VERSUS SHELL COORDINATES

FIGURE 5 SHELL WALL MODEL

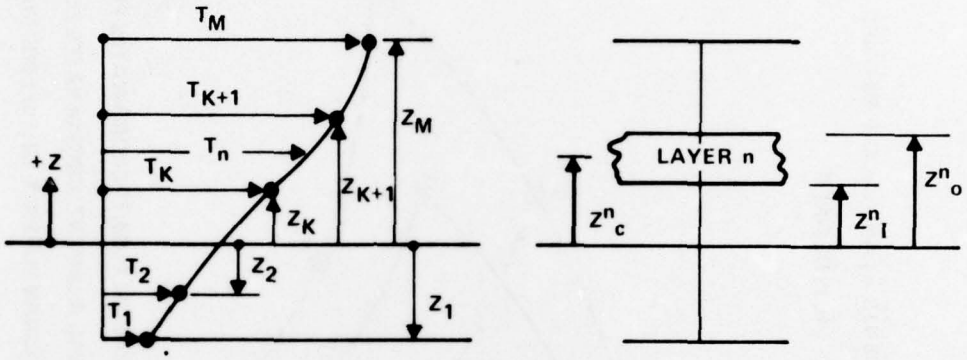
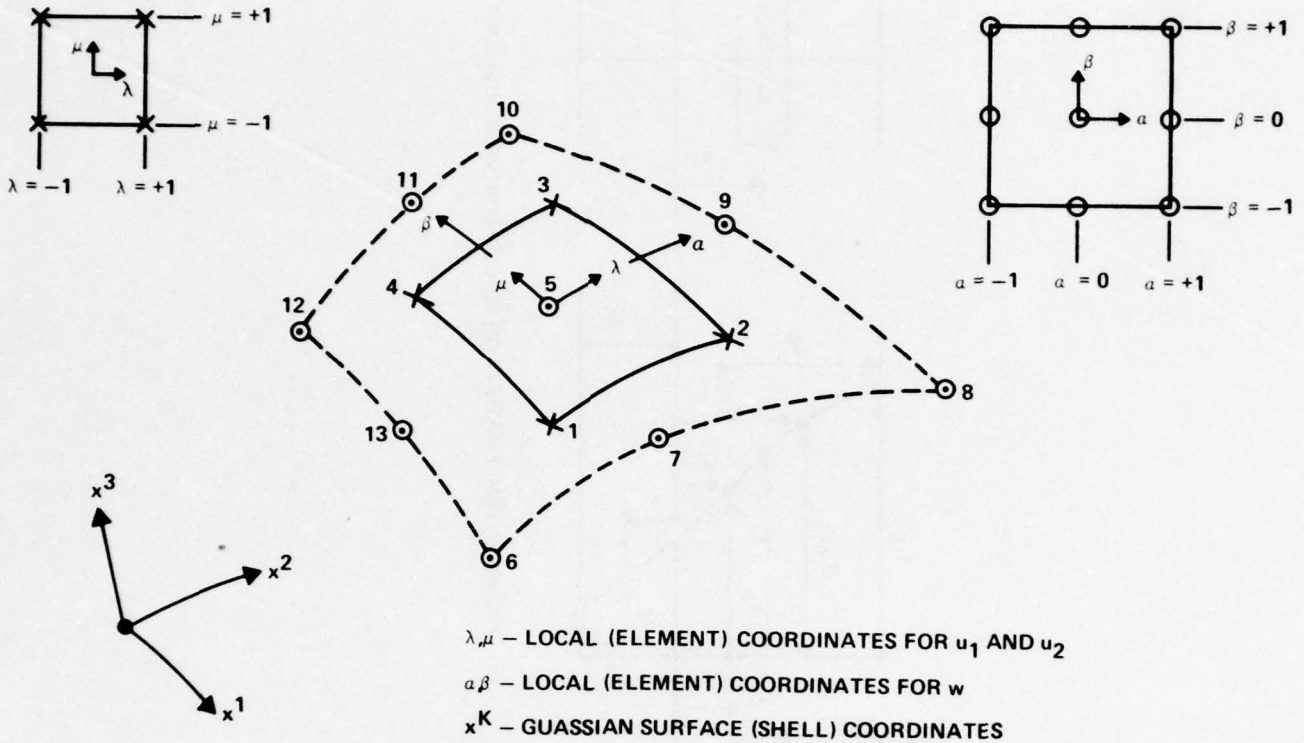


FIGURE 6 TEMPERATURE GRADIENT THROUGH SHELL WALL

X – POINTS AT WHICH TANGENTIAL DISPLACEMENTS, u_1 AND u_2, ARE DEFINED

◉ – POINTS AT WHICH NORMAL DISPLACEMENT , w, IS DEFINED



λ, μ – LOCAL (ELEMENT) COORDINATES FOR u_1 AND u_2

α, β – LOCAL (ELEMENT) COORDINATES FOR w

x^K – GUASSIAN SURFACE (SHELL) COORDINATES

FIGURE 7 SHEFA ELEMENT GEOMETRY

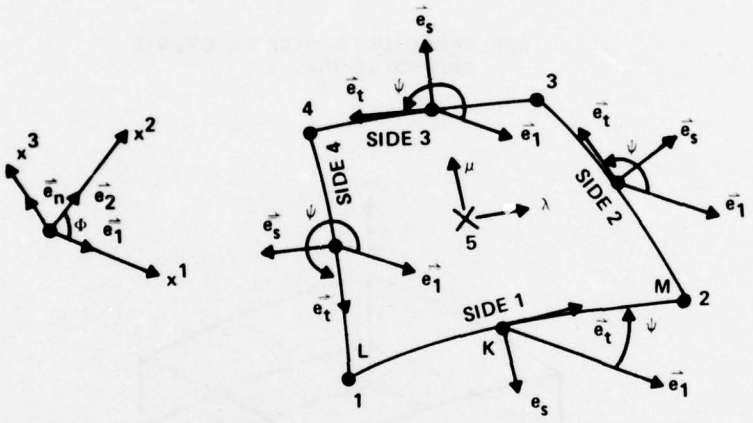
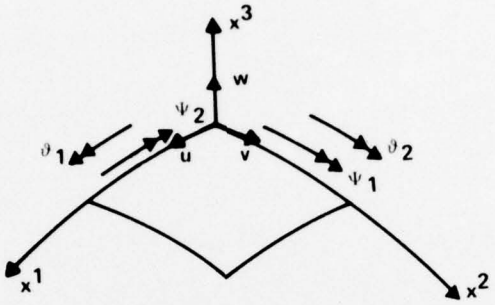
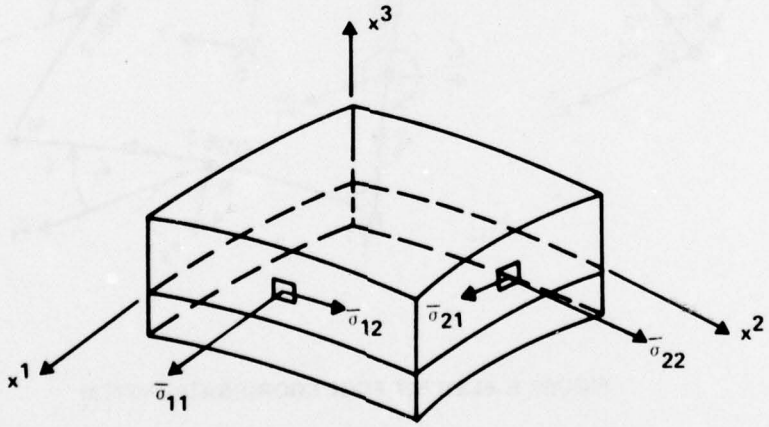


FIGURE 8 ELEMENT EDGE COORDINATE SYSTEM

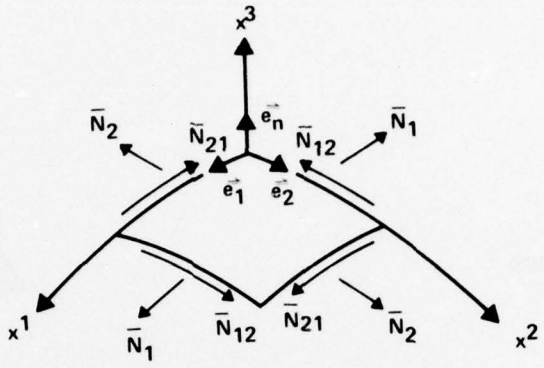


REFERENCE SURFACE DISPLACEMENTS
AND ROTATIONS

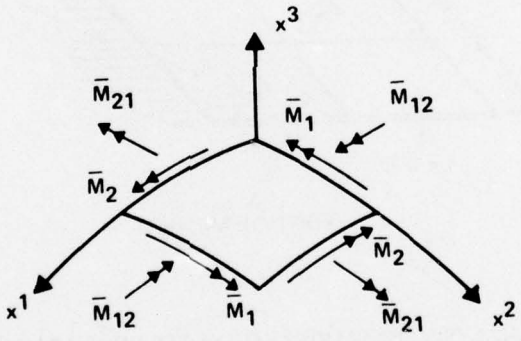


STRESSES

FIGURE 9 SIGN CONVENTIONS FOR DISPLACEMENTS, ROTATIONS AND STRESSES



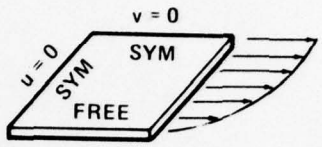
FORCE RESULTANTS



MOMENT RESULTANTS

FIGURE 10 SIGN CONVENTIONS FOR FORCE AND MOMENT RESULTANTS ACTING ON REFERENCE SURFACE

BOUNDARY CONDITIONS ON PORTION MESHED



MATERIAL PROPERTIES

$E = 10 \times 10^6$ PSI

$\nu = 0.3$

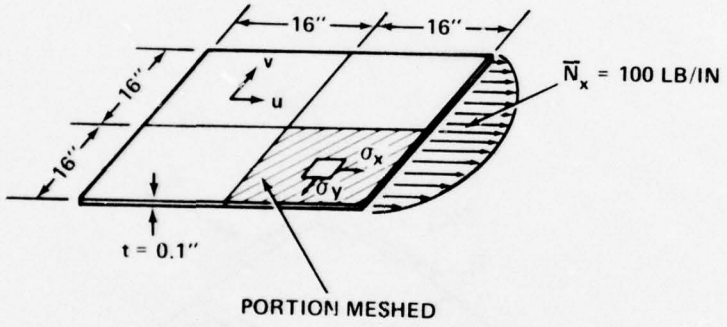


FIGURE 11 ANALYSIS CONDITIONS FOR PLATE UNDER PARABOLIC EDGE LOAD

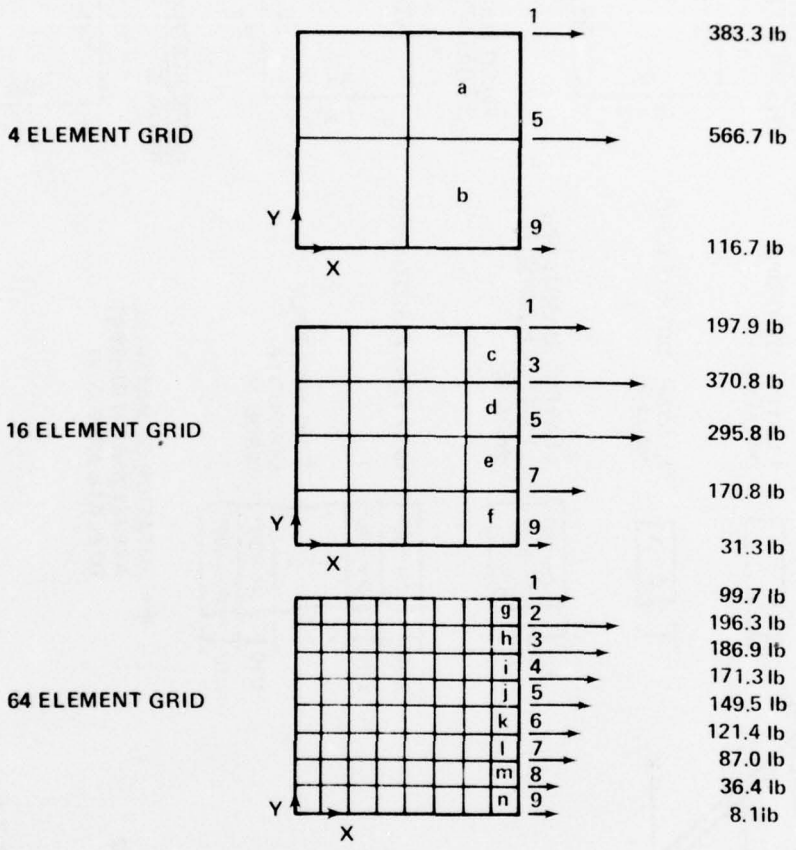
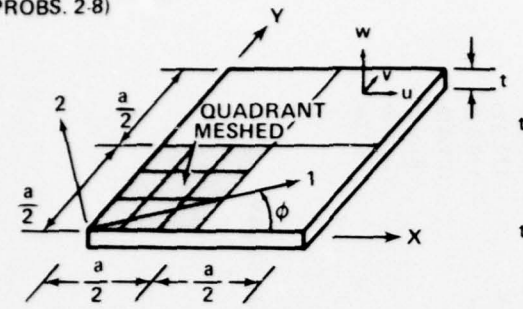


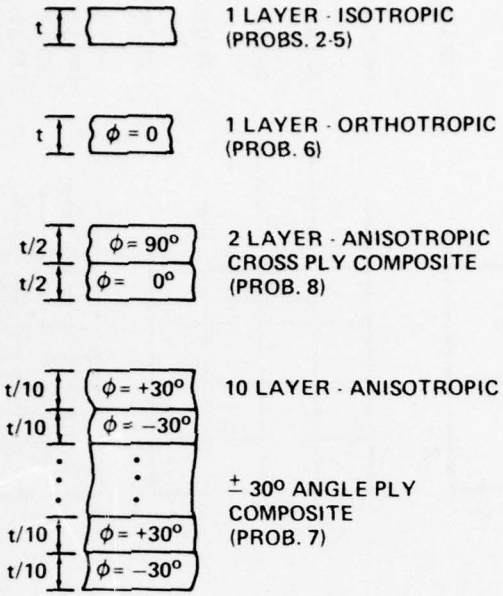
FIGURE 12 MESHES FOR MEMBRANE PLATE STUDY

PLATE GEOMETRY
(PROBS. 2-8)



a = 40 IN., t = 1.0 IN.

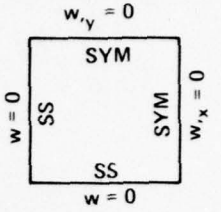
WALL CONSTRUCTIONS



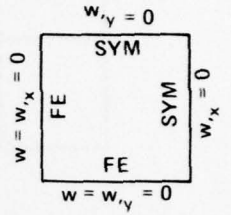
φ = ROTATION OF MATERIAL AXES (1-2) WITH RESPECT TO PLATE AXES (X-Y)

BOUNDARY CONDITIONS ON QUADRANT MESHED

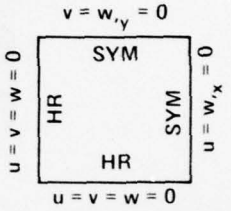
SIMPLE SUPPORT (SS)
(PROBS. 2,3,6,7)



FIXED EDGE (FE)
(PROBS. 4, 5)



HINGE-RESTRAINED (HR)
(PROB. 8)



LOAD CASES

P = 10000 LBS, (PROBS. 3,5)
= CONCENTRATED LOAD AT CENTER OF PLATE

q = 100 PSI, (PROBS. 2,4,6,7,8)
= UNIFORM PRESSURE LOAD

MATERIAL PROPERTIES

ISOTROPIC, (PROBS. 2-5):

$E = 10^7$ PSI, $\nu = 0.30$

ORTHOTROPIC, (PROB. 6):

$E_{11} = 4.338 \times 10^6$ PSI, $\nu_{21} = 0.02$

$E_{22} = 0.664 \times 10^6$ PSI

$G_{12} = 0.8075 \times 10^6$ PSI

ORTHOTROPIC LAMINAE, (PROBS. 7,8):

$E_{11} = 10^7$ PSI, $\nu_{12} = 0.25$

$E_{22} = G_{12} = 0.25 \times 10^6$ PSI

FIGURE 13 SUMMARY OF ANALYSIS CONDITIONS FOR PLATE BENDING PROBLEMS

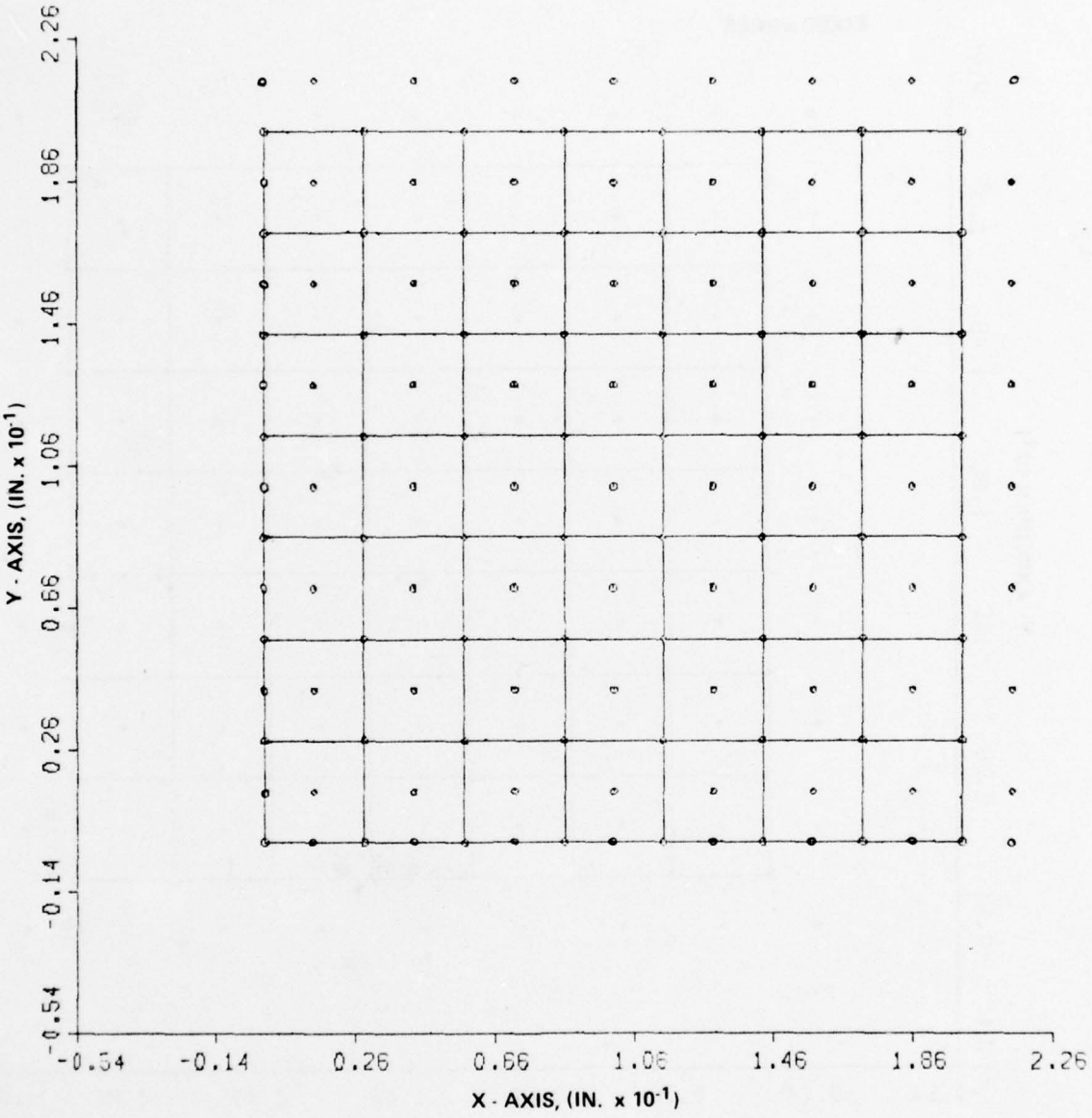


FIGURE 14 TYPICAL MESH FOR PLATE BENDING PROBLEMS WITH SIMPLY SUPPORTED EDGES

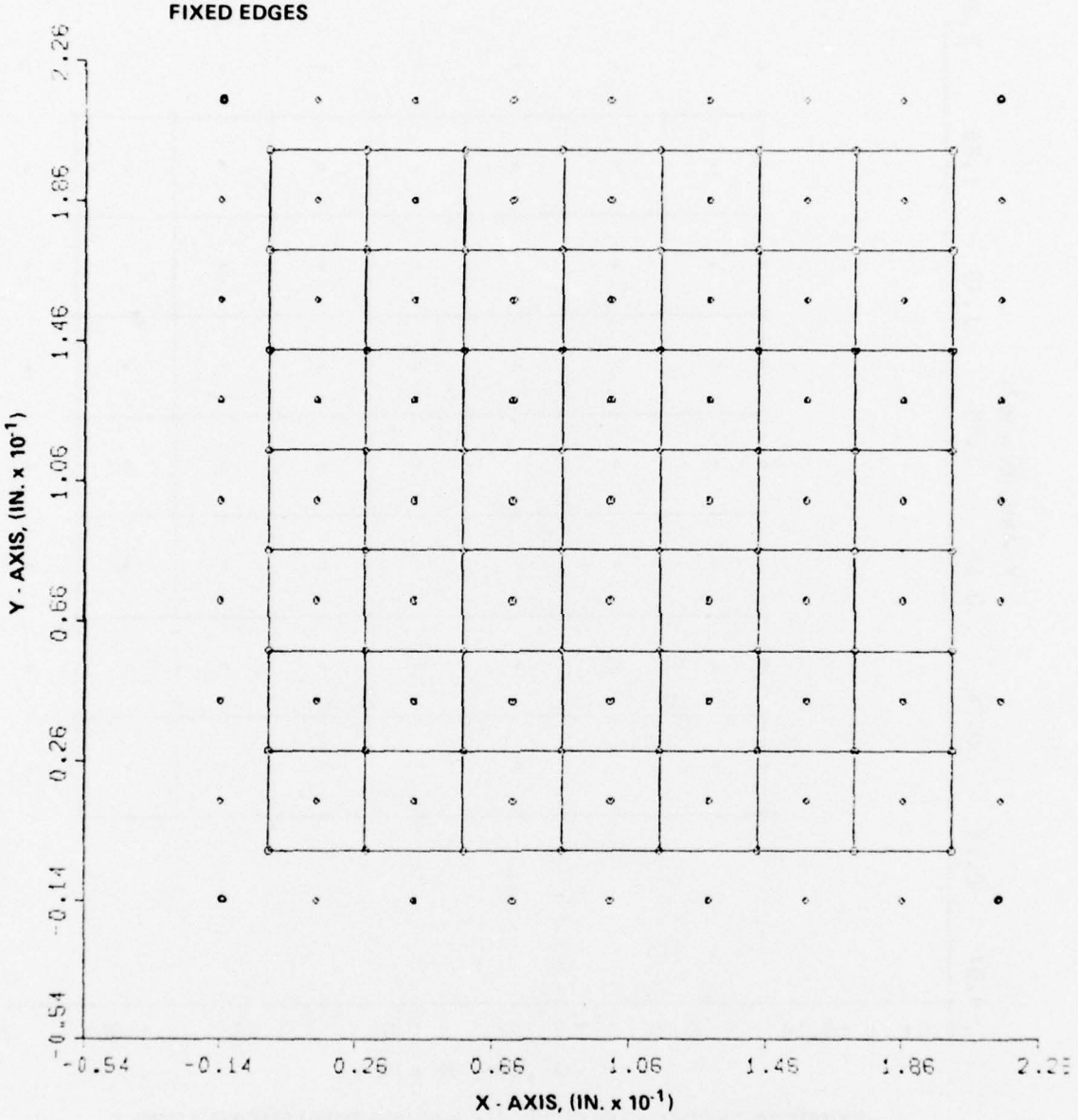


FIGURE 15 TYPICAL MESH FOR PLATE BENDING PROBLEMS WITH FIXED EDGES

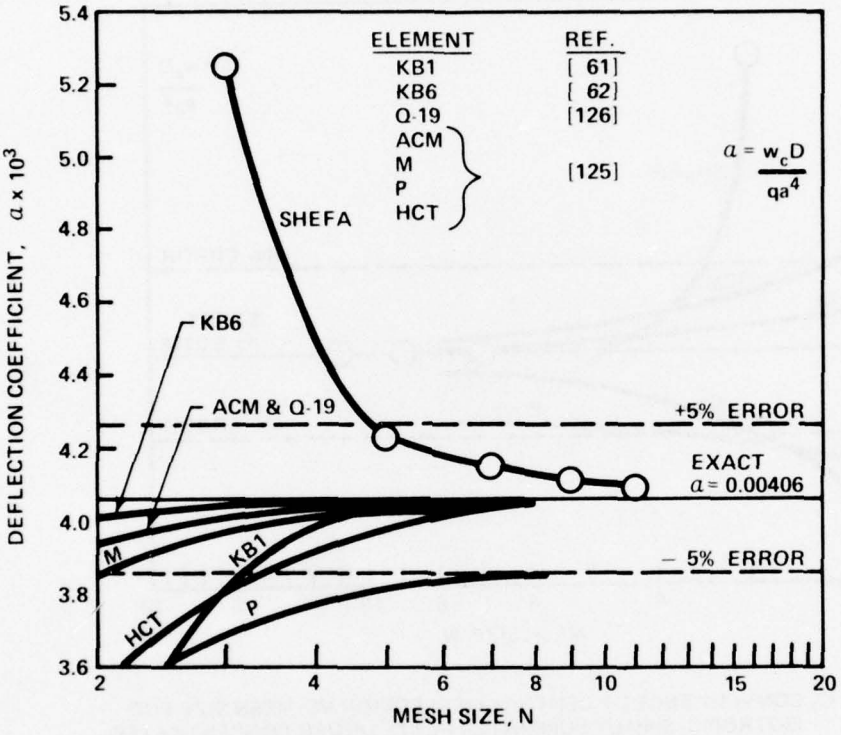


FIGURE 16 CONVERGENCE OF CENTRAL DEFLECTION VS. MESH SIZE FOR ISOTROPIC, SIMPLY-SUPPORTED PLATE UNDER UNIFORM LOAD

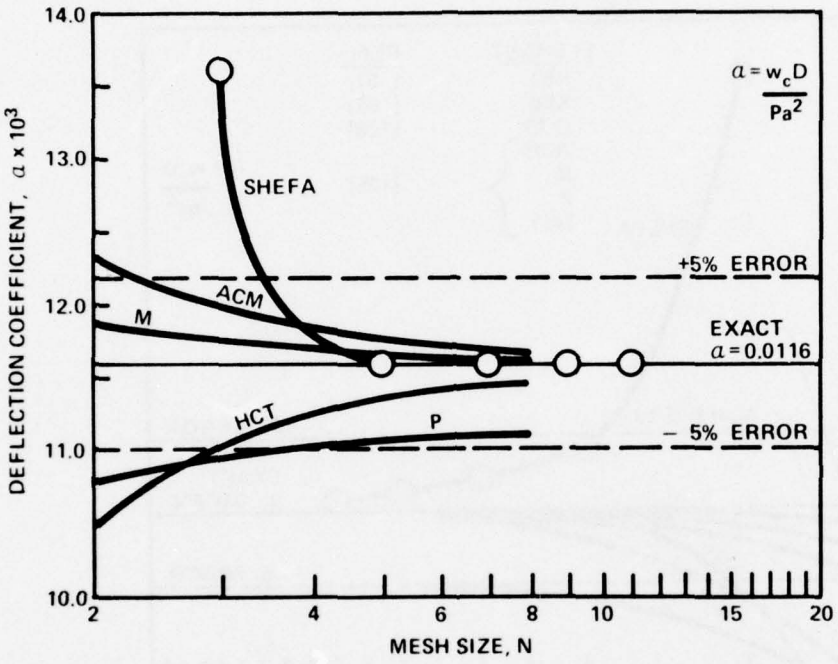


FIGURE 17 CONVERGENCE OF CENTRAL DEFLECTION VS. MESH SIZE FOR ISOTROPIC, SIMPLY-SUPPORTED PLATE UNDER CONCENTRATED LOAD

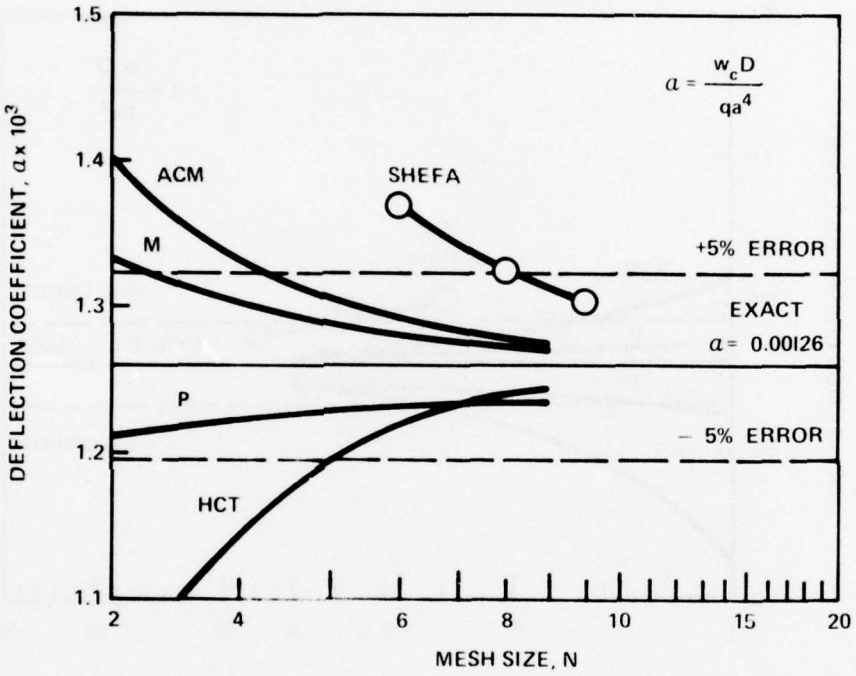


FIGURE 18 CONVERGENCE OF CENTRAL DEFLECTION VS. MESH SIZE FOR ISOTROPIC, CLAMPED PLATE UNDER UNIFORM LOAD

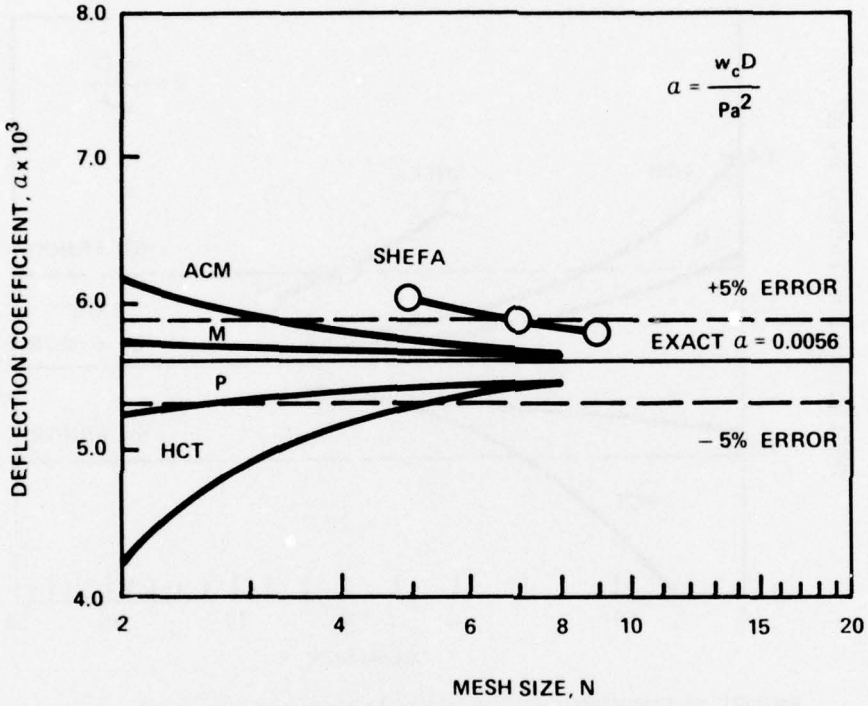


FIGURE 19 CONVERGENCE OF CENTRAL DEFLECTION VS. MESH SIZE FOR ISOTROPIC, CLAMPED PLATE UNDER CONCENTRATED LOAD

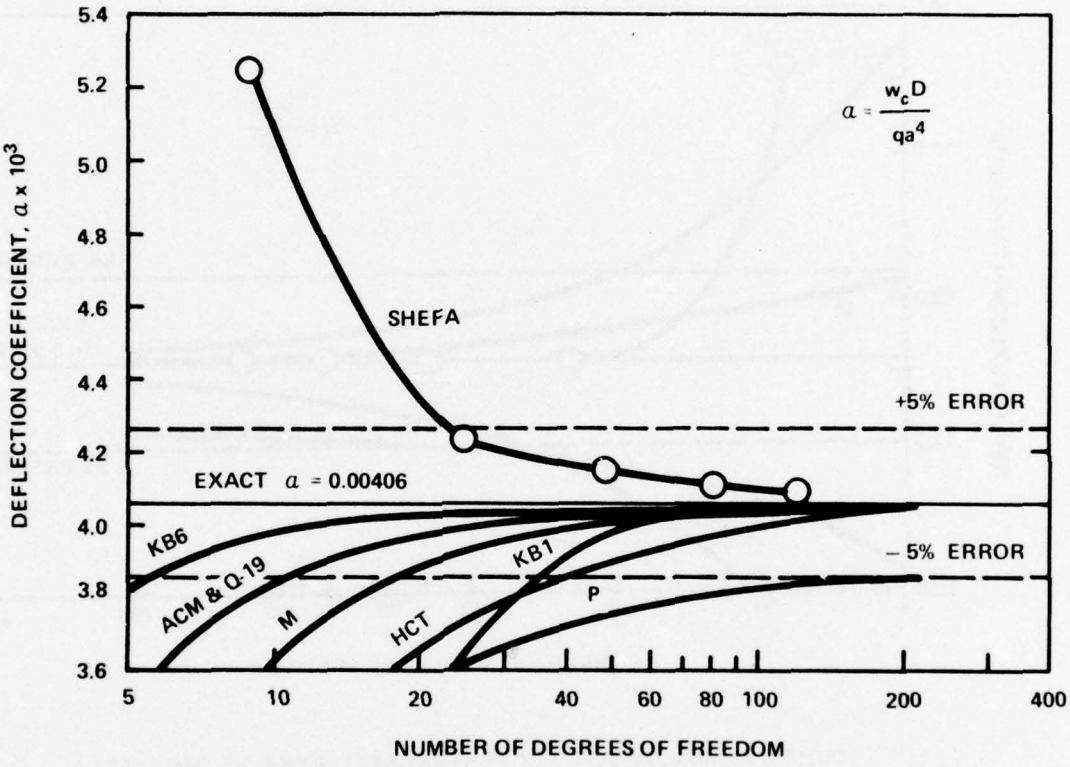


FIGURE 20 CONVERGENCE OF CENTRAL DEFLECTION VS. DEGREES OF FREEDOM FOR ISOTROPIC, SIMPLY-SUPPORTED PLATE UNDER UNIFORM LOAD

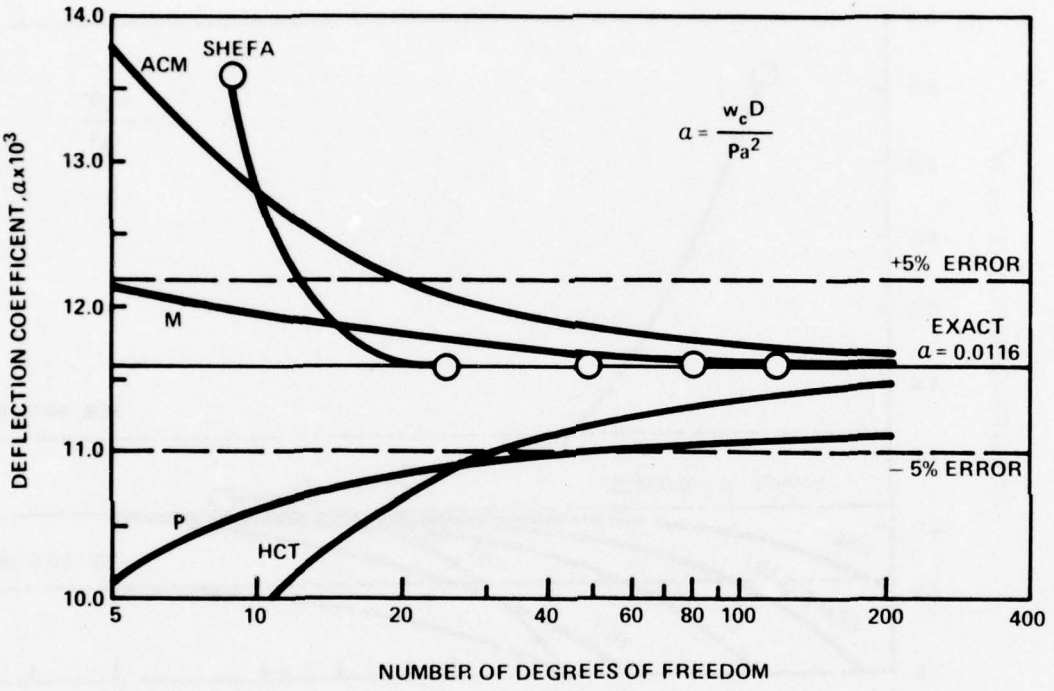


FIGURE 21 CONVERGENCE OF CENTRAL DEFLECTION VS. DEGREES OF FREEDOM FOR ISOTROPIC, SIMPLY-SUPPORTED PLATE UNDER CONCENTRATED LOAD

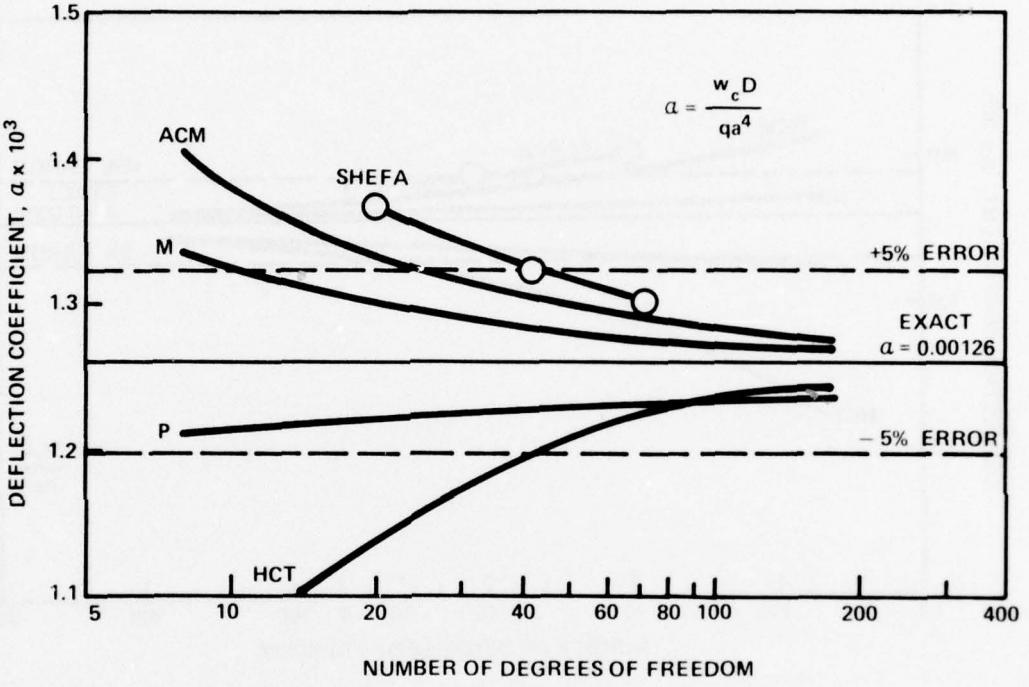


FIGURE 22 CONVERGENCE OF CENTRAL DEFLECTION VS. DEGREES OF FREEDOM FOR ISOTROPIC, CLAMPED PLATE UNDER UNIFORM LOAD

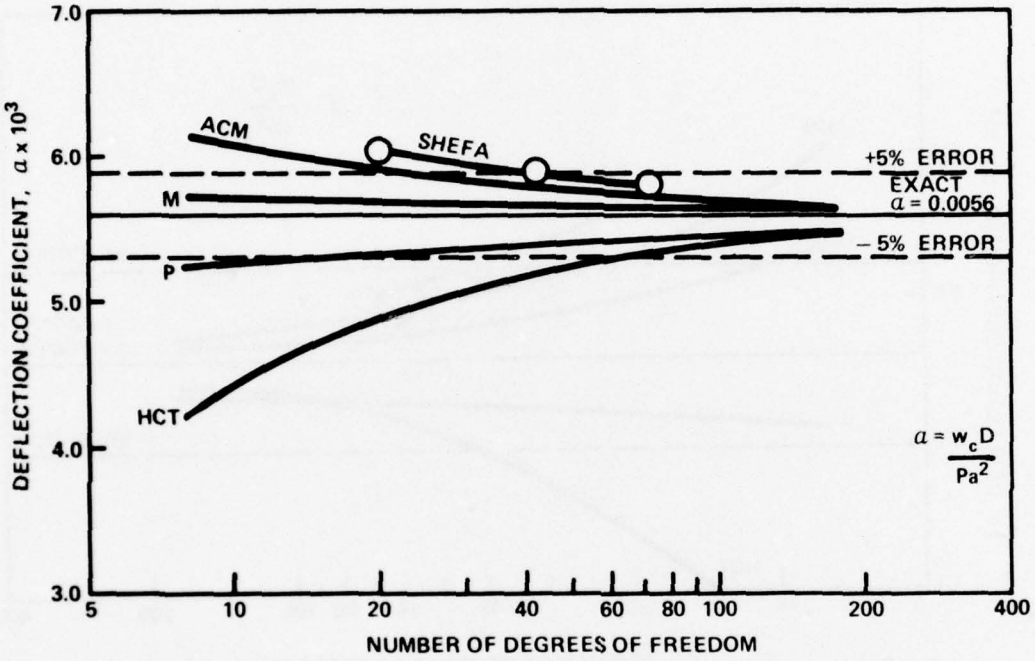


FIGURE 23 CONVERGENCE OF CENTRAL DEFLECTION VS. DEGREES OF FREEDOM FOR ISOTROPIC, CLAMPED PLATE UNDER CONCENTRATED LOAD

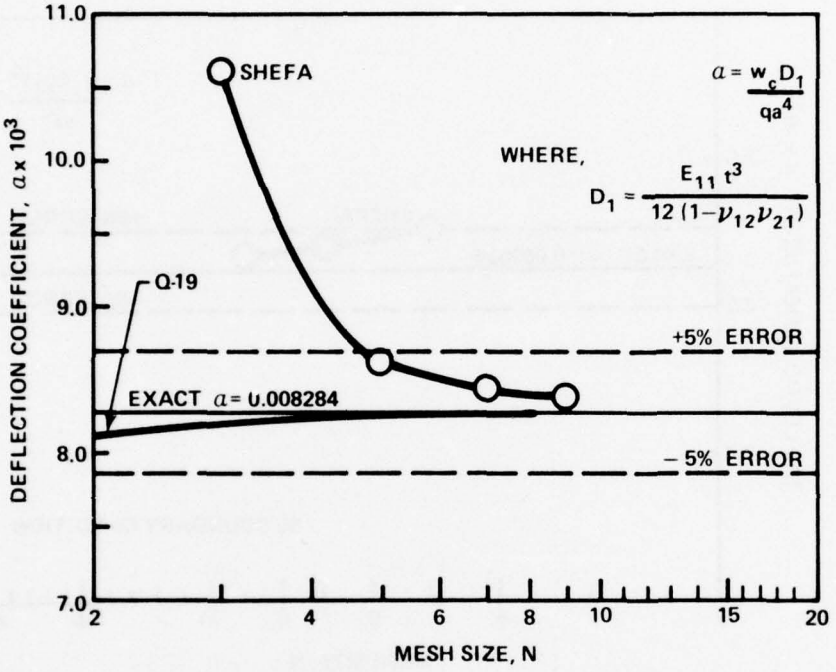


FIGURE 24 CONVERGENCE OF CENTRAL DEFLECTION VS. MESH SIZE FOR SIMPLY SUPPORTED ORTHOTROPIC PLATE UNDER UNIFORM LOAD

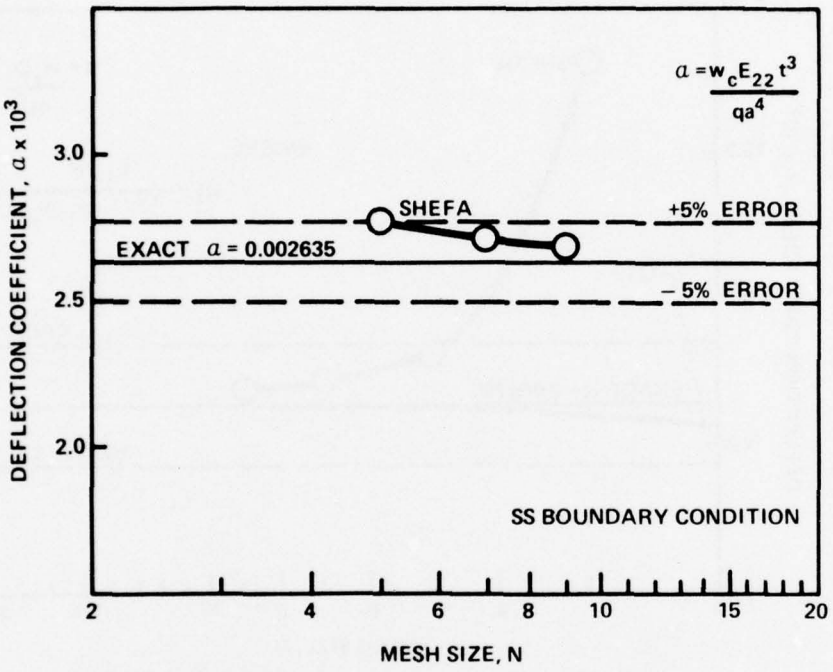


FIGURE 25 CONVERGENCE OF CENTRAL DEFLECTION VS. MESH SIZE FOR ANISOTROPIC PLATE (10 LAYER, ± 30° ANGLE-PLY COMPOSITE) UNDER UNIFORM LOAD

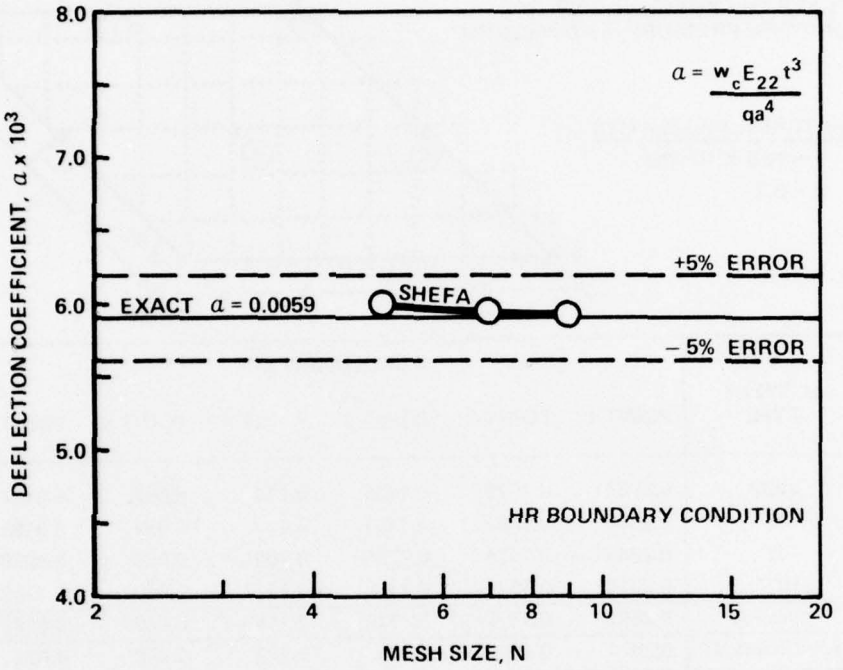
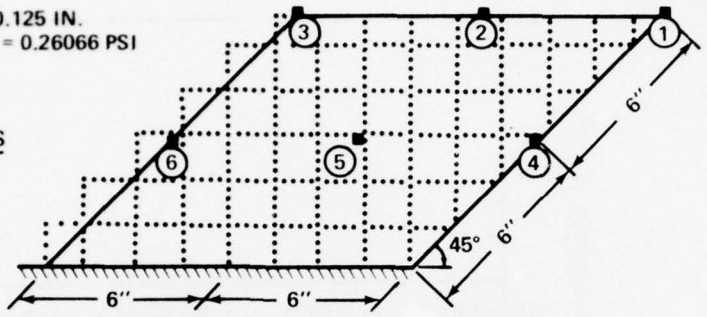


FIGURE 26 CONVERGENCE OF CENTRAL DEFLECTION VS. MESH SIZE FOR ANISOTROPIC PLATE (2 LAYER, CROSS PLY COMPOSITE) UNDER UNIFORM LOAD

PLATE THICKNESS, t = 0.125 IN.
UNIFORM PRESSURE, q = 0.26066 PSI

MATERIAL PROPERTIES
E = 10.5 X 10^6 PSI
ν = 0.3



ELEMENT TYPE	DEFLECTION AT POINT 1	POINT 2	POINT 3	POINT 4	POINT 5	POINT 6
ACM	0.2962	0.1979	0.1135	0.114	0.052	0.0197
M	0.2938	0.1965	0.1181	0.113	0.051	0.0198
P	0.2786	0.1874	0.1155	0.108	0.050	0.0210
HCT	0.2814	0.1879	0.1108	0.1112	0.0491	0.0182
SHEFA	0.2853	0.1897	0.1120	0.1159	0.0499	0.0182
EXPERIMENT	0.297	0.204	0.121	0.129	0.056	0.022

FIGURE 27 DEFLECTION OF UNIFORMLY LOADED RHOMBIC CANTILEVER

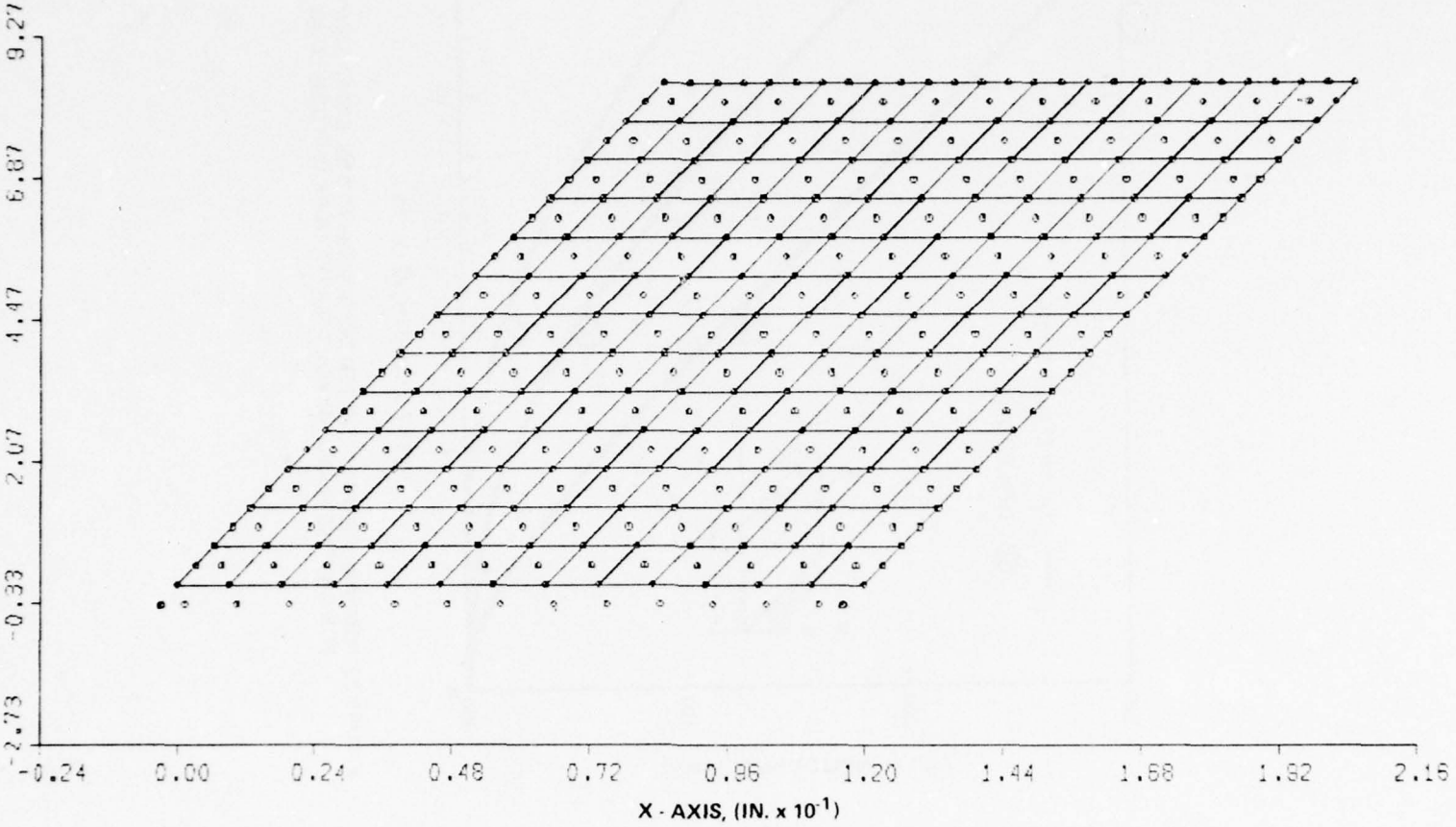


FIGURE 28 CANTILEVERED RHOMBIC PLATE, 13 x 13 MESH

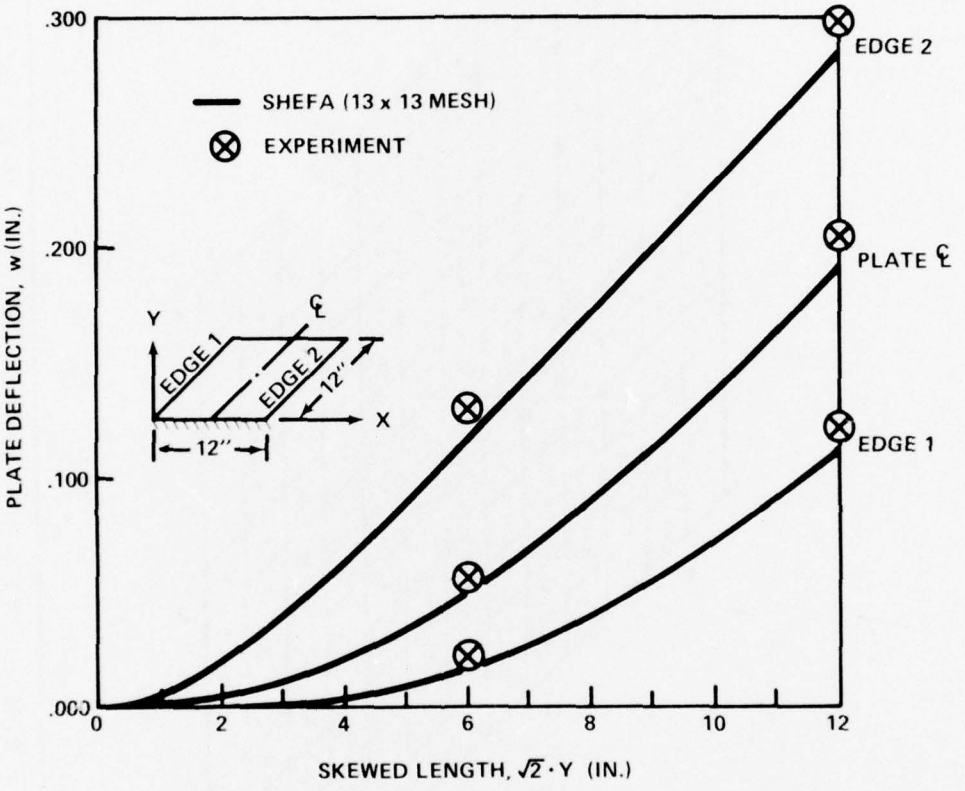


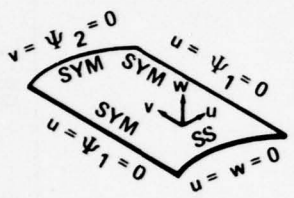
FIGURE 29 COMPARISON OF PREDICTED DISPLACEMENTS VS. EXPERIMENT FOR CANTILEVERED RHOMBIC PLATE UNDER UNIFORM LOAD

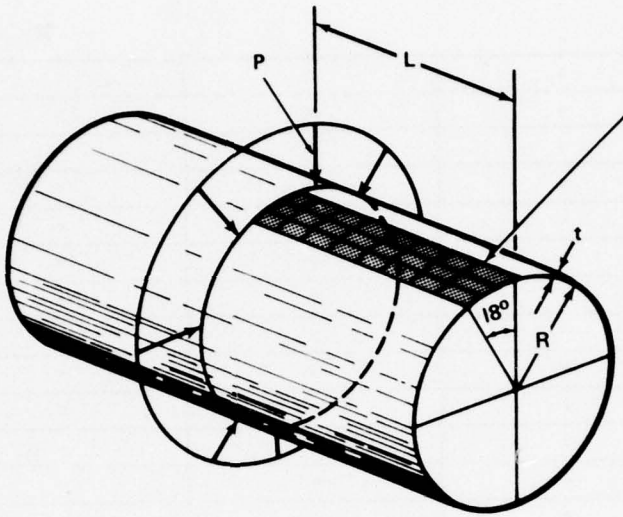
MATERIAL PROPERTIES

$E = 10 \times 10^6$ PSI

$\nu = 0.3$

BOUNDARY CONDITIONS ON PORTION MESHED





L = 3 IN.

R = 10 IN.

t = 0.1 IN.

FIGURE 30 SUMMARY OF ANALYSIS CONDITIONS FOR CYLINDRICAL SHELL WITH CIRCUMFERENTIAL LINE LOAD

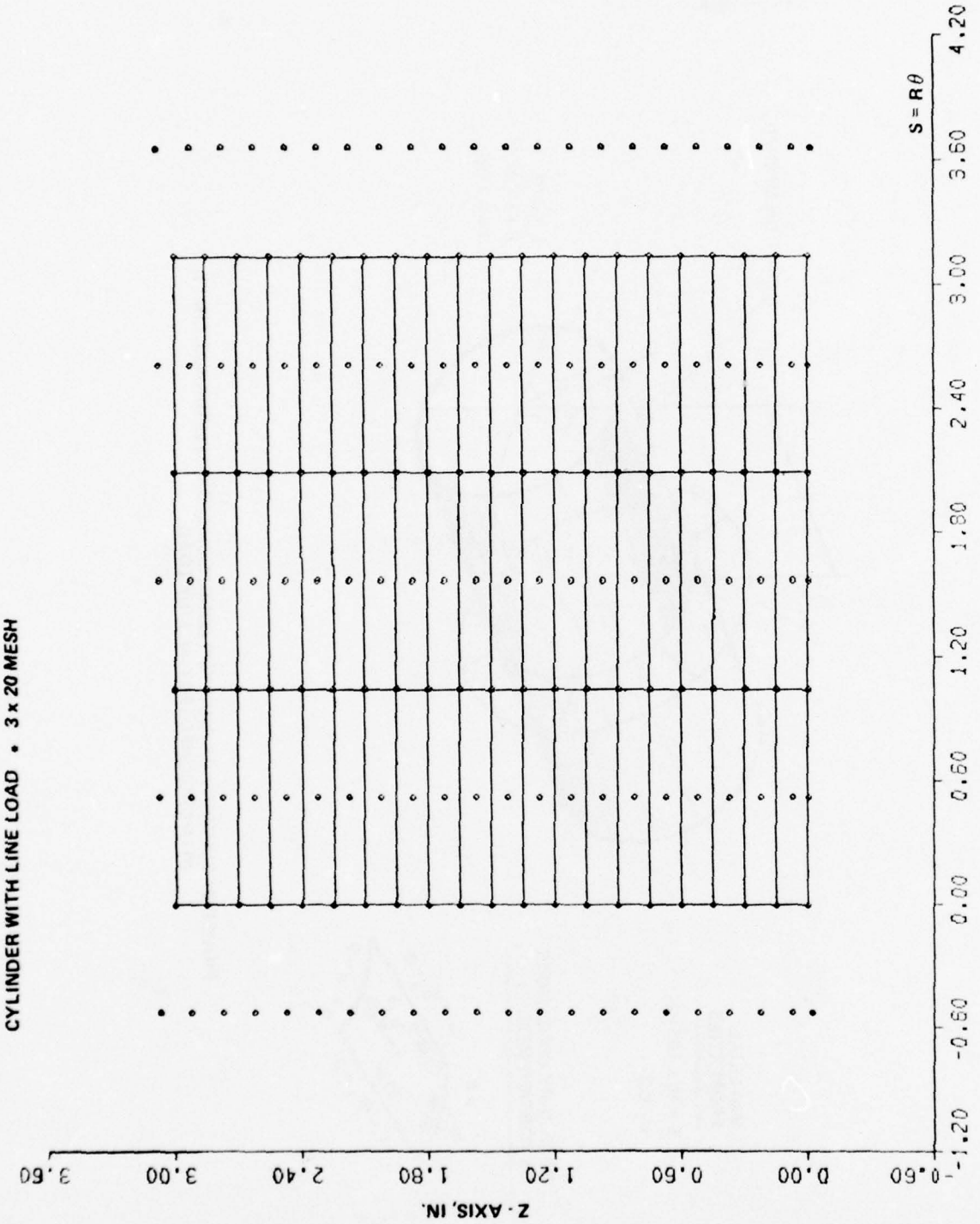


FIGURE 31 TYPICAL MESH FOR CYLINDRICAL SHELL BENDING PROBLEM

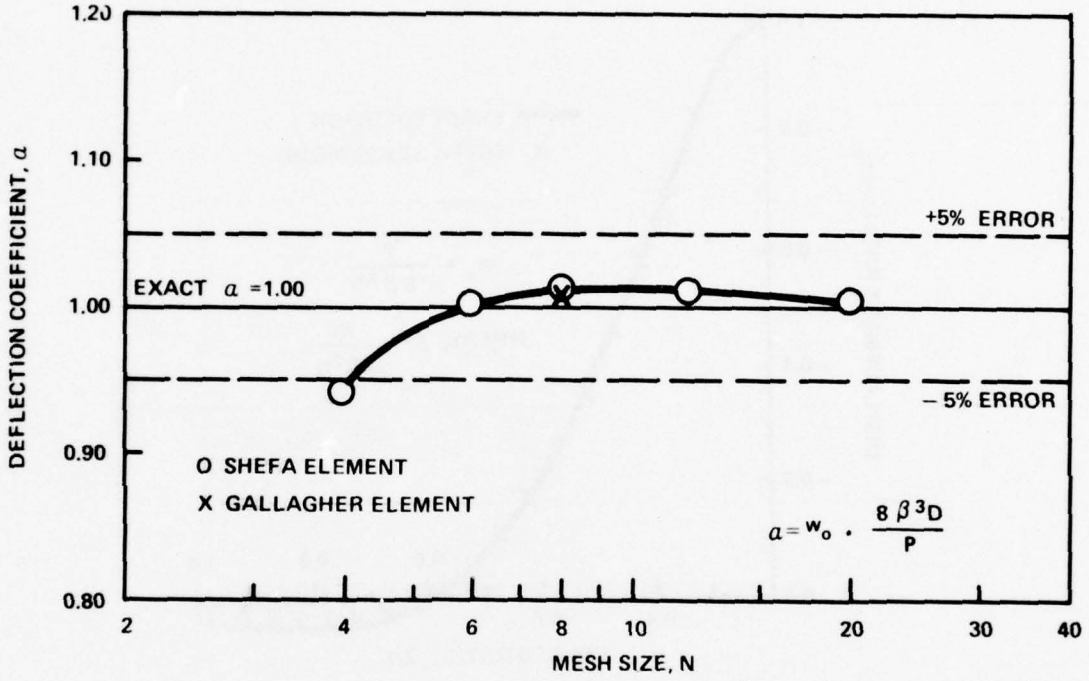


FIGURE 32 CONVERGENCE OF DEFLECTION UNDER LOAD VS. MESH SIZE FOR CYLINDRICAL SHELL WITH A LOAD UNIFORMLY DISTRIBUTED ALONG A CIRCULAR SECTION

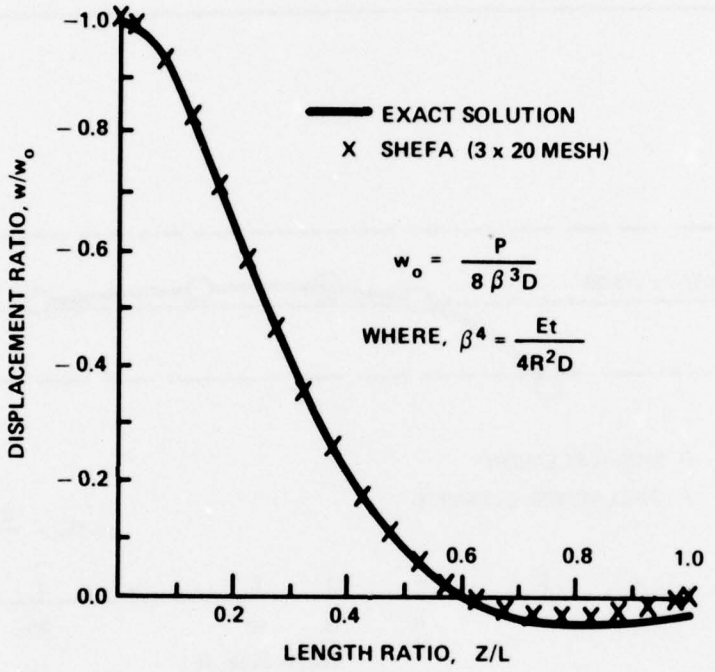


FIGURE 33 DISPLACEMENT DISTRIBUTION FOR CYLINDRICAL SHELL WITH A LOAD UNIFORMLY DISTRIBUTED ALONG A CIRCULAR SECTION

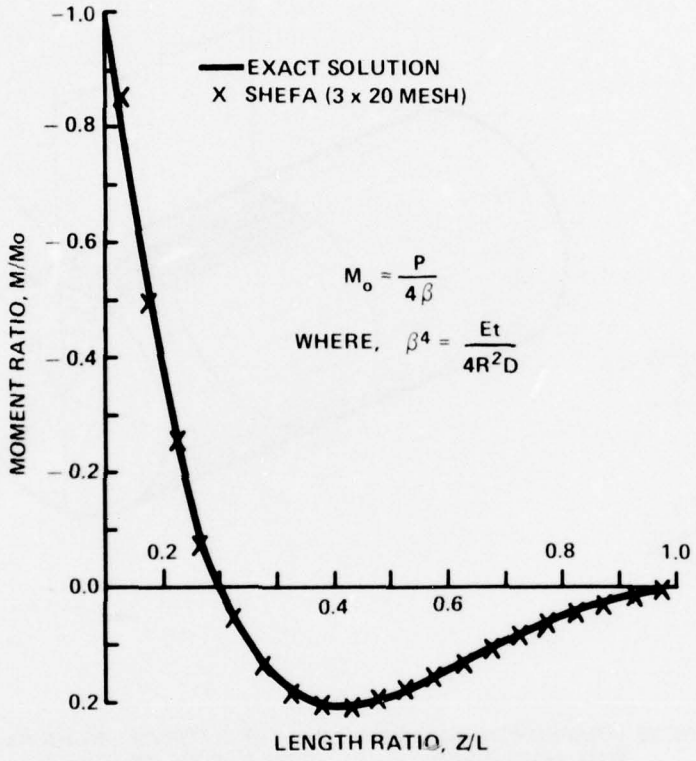
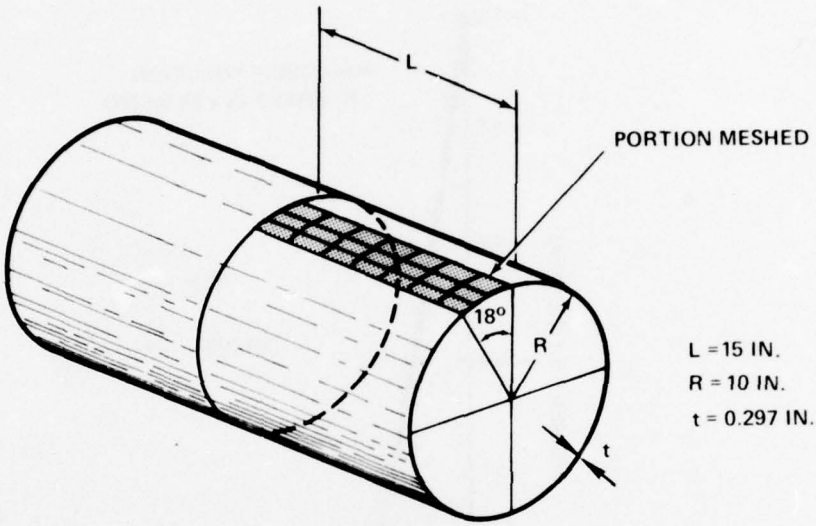


FIGURE 34 MOMENT DISTRIBUTION FOR CYLINDRICAL SHELL WITH A LOAD UNIFORMLY DISTRIBUTED ALONG A CIRCULAR SECTION



BOUNDARY CONDITIONS
ON PORTION MESHED

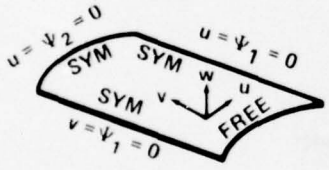


FIGURE 35 SUMMARY OF ANALYSIS CONDITIONS FOR CYLINDRICAL SHELL WITH NONLINEAR RADIAL TEMPERATURE GRADIENT

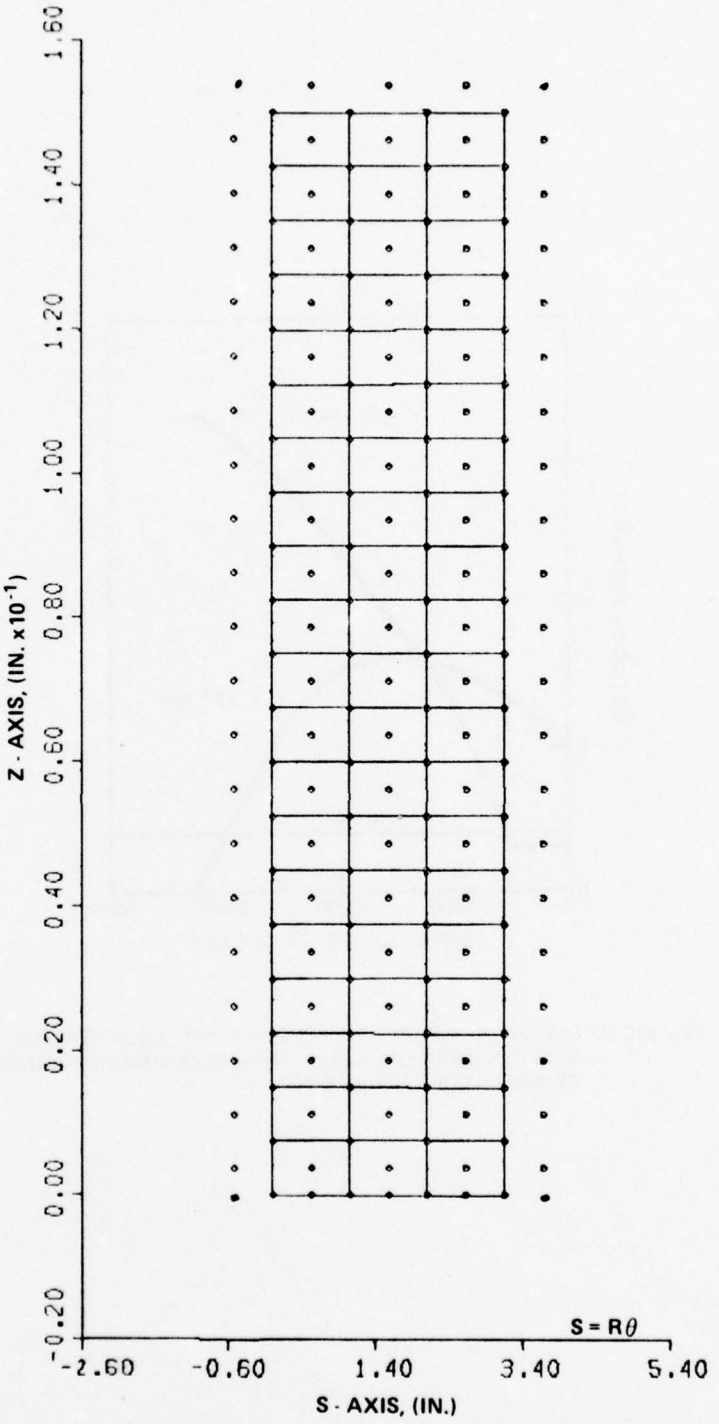


FIGURE 36 CYLINDER WITH NON LINEAR RADIAL TEMPERATURE GRADIENT, 3 x 20 MESH

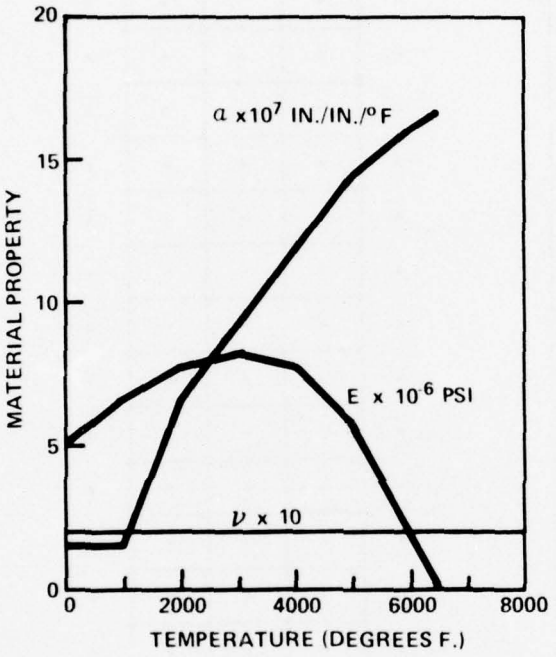


FIGURE 37 MATERIAL PROPERTY TEMPERATURE DEPENDENCE FOR CYLINDRICAL SHELL WITH NON LINEAR RADIAL TEMPERATURE GRADIENT

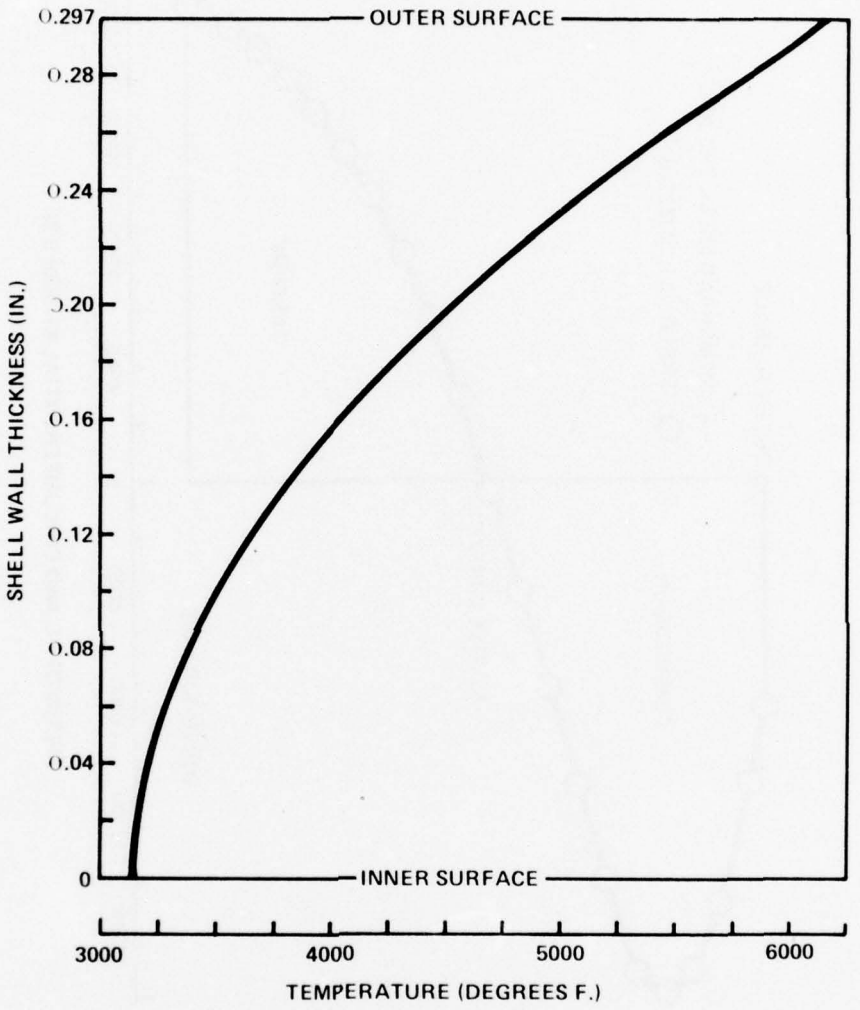


FIGURE 38 TEMPERATURE DISTRIBUTION THROUGH SHELL WALL FOR CYLINDRICAL SHELL WITH NONLINEAR RADIAL TEMPERATURE GRADIENT

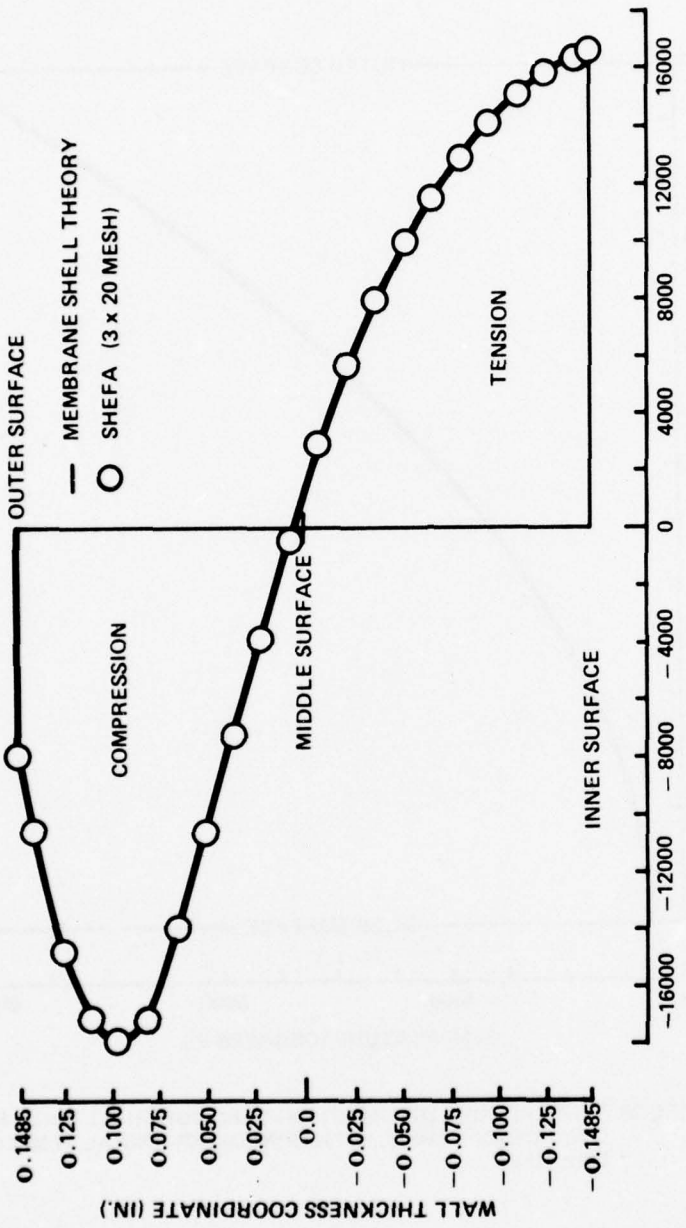


FIGURE 39 STRESS DISTRIBUTION THROUGH SHELL WALL FOR CYLINDRICAL SHELL WITH NON LINEAR RADIAL TEMPERATURE GRADIENT

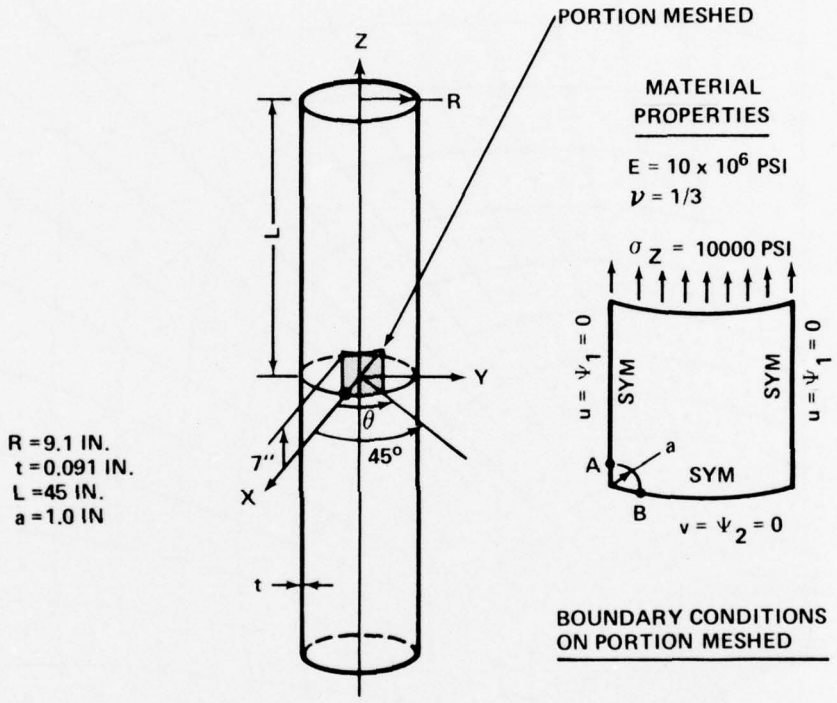


FIGURE 40 SUMMARY OF ANALYSIS CONDITIONS FOR CYLINDRICAL SHELL WITH CIRCULAR CUTOUT LOADED IN TENSION

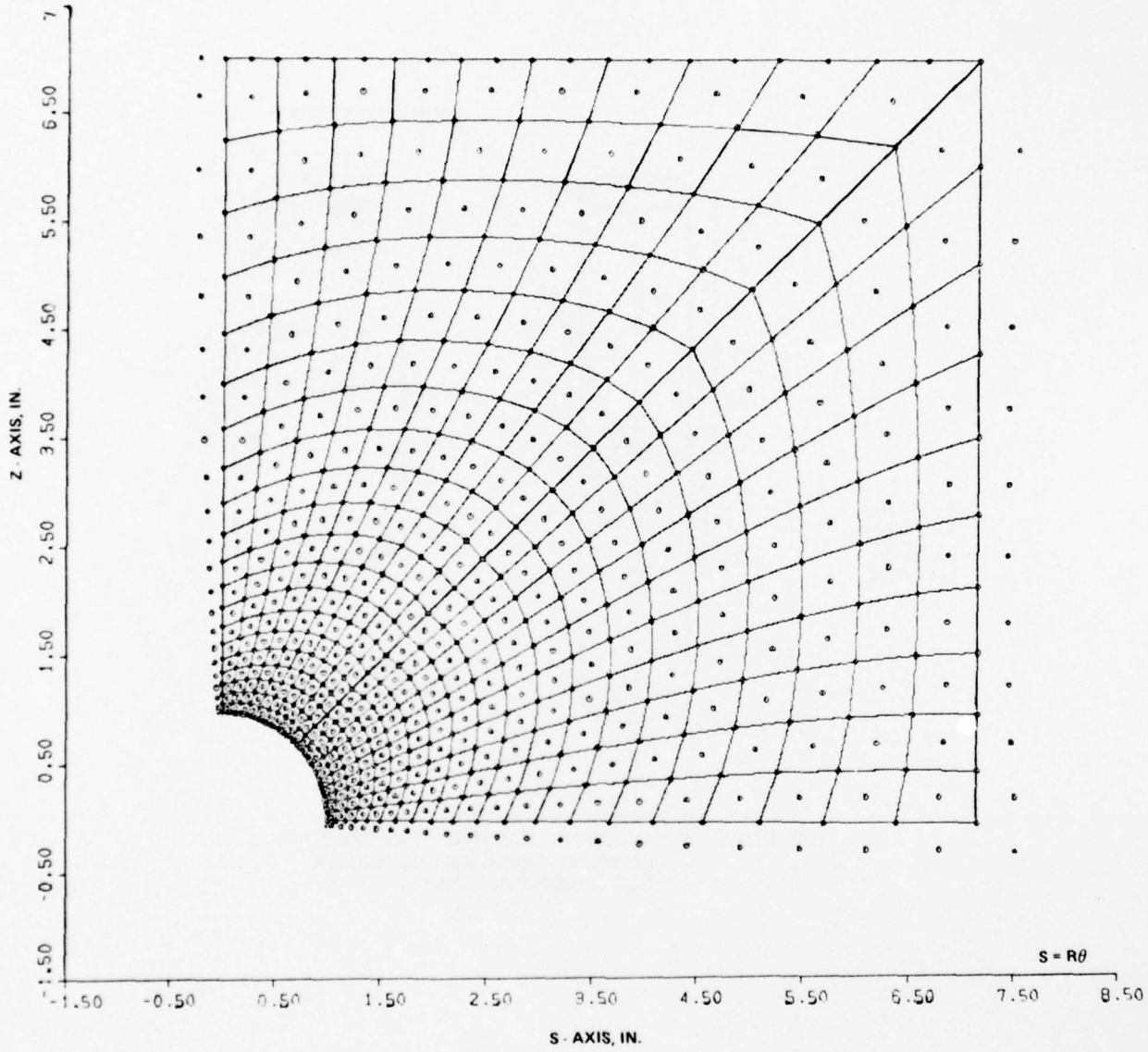


FIGURE 41 CYLINDRICAL SHELL WITH CIRCULAR CUTOUT 20 x 20 MESH

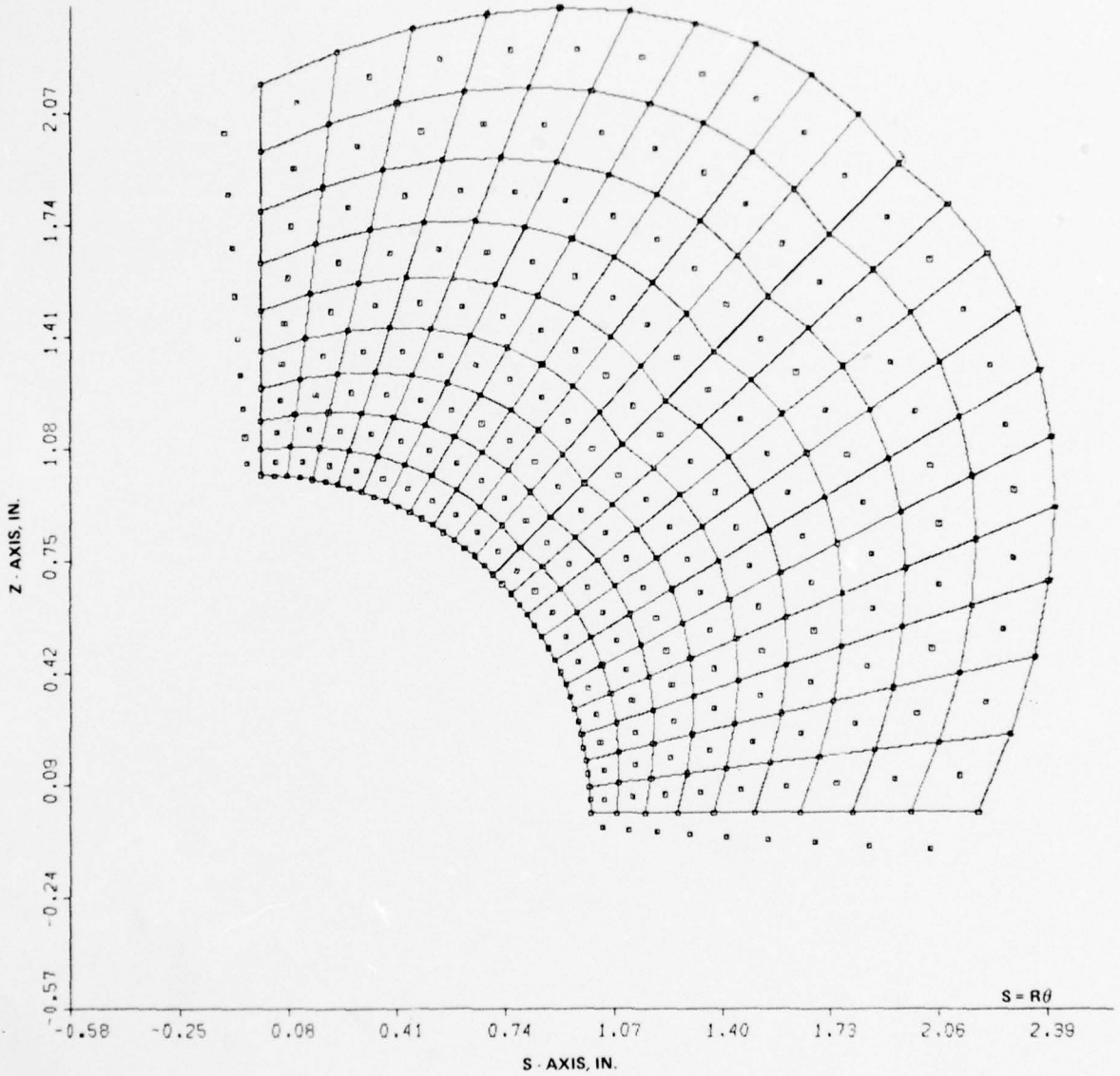


FIGURE 42 CYLINDRICAL SHELL WITH CIRCULAR CUTOUT, ENLARGEMENT OF 20 x 20 MESH IN VICINITY OF HOLE

APPENDIX C

DISCUSSION OF SHAPE FUNCTIONS

In this appendix the linear and quadratic shape functions will be derived in terms of curvilinear interpolating coordinates. The interpolating coordinates are defined at the local element level and are related to the Gaussian surface coordinates through transformations which were derived in Section IV.B.4.

It will be shown that the generalized interpolating procedure used to determine difference relations for arbitrary meshes reduces to the conventional finite difference formulas when the interpolating coordinates and surface coordinates are aligned.

1. Derivation of Linear Shape Functions

Let $\phi(\lambda,\mu)$ be an arbitrary function and expand it in a Taylor's series* about the centroid of the region shown in Figure C1-a,

$$\begin{aligned}\phi(\lambda,\mu) &= \phi^\circ + \lambda\phi,^\circ_\lambda + \mu\phi,^\circ_\mu \\ &\quad + \frac{1}{2}\left(\lambda^2\phi,^\circ_{\lambda\lambda} + 2\lambda\mu\phi,^\circ_{\lambda\mu} + \mu^2\phi,^\circ_{\mu\mu}\right) + O(\Delta)^3 \\ &= \phi^\circ + \lambda\phi,^\circ_\lambda + \mu\phi,^\circ_\mu + \lambda\mu\phi,^\circ_{\lambda\mu} + O(\Delta^2)\end{aligned} \tag{C.1}$$

---

* The notation ϕ° corresponds to $\phi(o,o)$ and $\phi,^\circ_\lambda$ ... corresponds to $\phi,_\lambda(o,o)$, ...

Recasting in matrix form,

$$\phi(\lambda,\mu) = \{P_1\}^T\{A\} \tag{C.2}$$

where

$$\{P_1\}^T = [1,\ \lambda,\ \mu,\ \lambda\mu] \tag{C.3}$$

$$\{A\}^T = [a_1,\ a_2,\ a_3,\ a_4]$$

$$= [\phi^\circ,\ \phi^\circ_{,\lambda},\ \phi^\circ_{,\mu},\ \phi^\circ_{,\lambda\mu}] \tag{C.4}$$

Evaluating $\phi(\lambda,\mu)$ at the four discrete points on the boundary of the region,

$$\begin{bmatrix} \phi^1 \\ \phi^2 \\ \phi^3 \\ \phi^4 \end{bmatrix} = \begin{bmatrix} 1 & -1 & -1 & 1 \\ 1 & 1 & -1 & -1 \\ 1 & 1 & 1 & 1 \\ 1 & -1 & 1 & -1 \end{bmatrix} \begin{bmatrix} a_1 \\ a_2 \\ a_3 \\ a_4 \end{bmatrix}$$

or,

$$\{\phi\} = [C]\ \{A\} \tag{C.5}$$

Solving for the generalized coordinates,

$$\{A\} = [C]^{-1}\{\phi\} \tag{C.6}$$

Substituting (C.6) into (C.2) results in the interpolating equation,

$$\phi(\lambda,\mu) = \{P_1\}^T[C]^{-1}\{\phi\}$$

$$= [L(\lambda,\mu)]\{\phi\} \tag{C.7}$$

where,

$$[C]^{-1} = \frac{1}{4}\begin{bmatrix} 1 & 1 & 1 & 1 \\ -1 & 1 & 1 & -1 \\ -1 & -1 & 1 & 1 \\ 1 & -1 & 1 & -1 \end{bmatrix} \tag{C.8}$$

$$[L(\lambda,\mu)] = [L_1, L_2, L_3, L_4]$$

$$= \{P_1\}^T[C]^{-1} \tag{C.9}$$

Equation (C.9) defines the linear shape functions used in Section IV.B.4 to approximate the tangential displacement fields.

2. Interpretation of Generalized Coordinates for Linear Shape Functions

The generalized coordinates associated with the linear shape functions are,

$$\{A\} = [C]^{-1}\{\phi\} \tag{C.10}$$

From (C.10) the following finite difference formulas are obtained,

$$a_1 = \phi^{\circ} = \frac{1}{4}\,(\phi^1 + \phi^2 + \phi^3 + \phi^4)$$

$$= [L(o,o)]\{\phi\} \tag{C.11}$$

$$a_2 = \phi_{,\lambda}^{\circ} = \frac{1}{2}\left(\frac{1}{2}(\phi^2+\phi^3) - \frac{1}{2}(\phi^4+\phi^1)\right)$$

$$= [L_{,\lambda}(o,o)]\{\phi\} \tag{C.12}$$

$$a_3 = \phi_{,\mu}^{\circ} = \frac{1}{2}\left(\frac{1}{2}(\phi^3 + \phi^4) - \frac{1}{2}(\phi^2+\phi^1)\right)$$

$$= [L_{,\lambda}(o,o)]\{\phi\} \tag{C.13}$$

$$a_4 = \phi_{,\lambda\mu}^{\circ} = \frac{1}{2}\left(\frac{1}{2}(\phi^3+\phi^1) - \frac{1}{2}(\phi^4+\phi^2)\right)$$

$$= [L_{,\lambda\mu}(o,o)]\{\phi\} \tag{C.14}$$

The generalized coordinates thus correspond to the familiar central difference formulas for approximating a variable and its spatial derivatives at the centroid of a square region. When the element boundaries in Figure C1-a coincide with the surface coordinate lines, the mapping plane is undistorted (λ,μ and x^1, x^2 are aligned) and the interpolating procedure used to determine difference relations for arbitrary meshes

reduces to the conventional finite difference approach using regular, coordinate line meshes.

3. Derivation of Quadratic Shape Functions

Let $\phi(\alpha,\beta)$ be an arbitrary function and expand it in a Taylor's series about the central point labeled 1 of the region shown in Figure C1-b,

$$\begin{aligned}\phi(\alpha,\beta) &= \phi^\circ + \alpha\phi^\circ_{,\alpha} + \beta\phi^\circ_{,\beta} \\ &+ \tfrac{1}{2}\left[\alpha^2\phi^\circ_{,\alpha\alpha} + 2\alpha\beta\phi^\circ_{,\alpha\beta} + \beta^2\phi^\circ_{,\beta\beta}\right] \\ &+ \tfrac{1}{6}\left[\alpha^3\phi^\circ_{,\alpha\alpha\alpha} + 3\alpha^2\beta\phi^\circ_{,\alpha\alpha\beta} + 3\alpha\beta^2\phi^\circ_{,\alpha\beta\beta} + \beta^3\phi^\circ_{,\beta\beta\beta}\right] \\ &+ \tfrac{1}{24}\left[\alpha^4\phi^\circ_{,\alpha\alpha\alpha\alpha} + 4\alpha^3\beta\phi^\circ_{,\alpha\alpha\alpha\beta} + 6\alpha^2\beta^2\phi_{,\alpha\alpha\beta\beta}\right. \\ &\quad \left. + 4\alpha\beta^3\phi^\circ_{,\alpha\beta\beta\beta} + \beta^4\phi^\circ_{,\beta\beta\beta\beta}\right] + O(\Delta^5) \\ &= \phi^\circ + \alpha\phi^\circ_{,\alpha} + \beta\phi^\circ_{,\beta} \\ &+ \tfrac{1}{2}\alpha^2\phi^\circ_{,\alpha\alpha} + \alpha\beta\phi^\circ_{,\alpha\beta} + \tfrac{1}{2}\beta^2\phi^\circ_{,\beta\beta} \\ &+ \tfrac{1}{2}\alpha^2\beta\phi^\circ_{,\alpha\alpha\beta} + \tfrac{1}{2}\alpha\beta^2\phi^\circ_{,\alpha\beta\beta} \\ &+ \tfrac{1}{4}\alpha^2\beta^2\phi^\circ_{,\alpha\alpha\beta\beta} + O(\Delta^3) \end{aligned} \tag{C.15}$$

Recasting in matrix form,

$$\phi(\alpha,\beta) = \{P_2\}^T\{B\} \tag{C.16}$$

where,

$$\{P_2\}^T = [1,\ \alpha,\ \beta,\ \alpha^2,\ \alpha\beta,\ \beta^2,\ \alpha^2\beta,\ \alpha\beta^2,\ \alpha^2\beta^2] \quad \text{(C.17)}$$

$$\{B\}^T = [b_1,\ b_2,\ \ldots,\ b_9]$$

$$= [\phi^\circ,\ \phi^\circ_{,\alpha},\ \phi^\circ_{,\beta},\ \tfrac{1}{2}\phi^\circ_{,\alpha\alpha},\ \phi^\circ_{,\alpha\beta},\ \tfrac{1}{2}\phi^\circ_{,\beta\beta},$$

$$\tfrac{1}{2}\phi^\circ_{,\alpha\alpha\beta},\ \tfrac{1}{2}\phi^\circ_{,\alpha\beta\beta},\ \tfrac{1}{4}\phi^\circ_{,\alpha\alpha\beta\beta}] \quad \text{(C.18)}$$

Evaluating $\phi(\alpha,\beta)$ at the nine discrete points defined over the region,

$$\begin{bmatrix} \phi^1 \\ \phi^2 \\ \phi^3 \\ \phi^4 \\ \phi^5 \\ \phi^6 \\ \phi^7 \\ \phi^8 \\ \phi^9 \end{bmatrix} = \begin{bmatrix} 1 & 0 & 0 & 0 & 0 & 0 & 0 & 0 & 0 \\ 1 & -1 & -1 & 1 & 1 & 1 & -1 & -1 & 1 \\ 1 & 0 & -1 & 0 & 0 & 1 & 0 & 0 & 0 \\ 1 & 1 & -1 & 1 & -1 & 1 & -1 & 1 & 1 \\ 1 & 1 & 0 & 1 & 0 & 0 & 0 & 0 & 0 \\ 1 & 1 & 1 & 1 & 1 & 1 & 1 & 1 & 1 \\ 1 & 0 & 1 & 0 & 0 & 1 & 0 & 0 & 0 \\ 1 & -1 & 1 & 1 & -1 & 1 & 1 & -1 & 1 \\ 1 & -1 & 0 & 1 & 0 & 0 & 0 & 0 & 0 \end{bmatrix} \begin{bmatrix} b_1 \\ b_2 \\ b_3 \\ b_4 \\ b_5 \\ b_6 \\ b_7 \\ b_8 \\ b_9 \end{bmatrix}$$

or,

$$\{\phi\} = [D]\ \{B\} \quad \text{(C.19)}$$

Solving for the generalized coordinates,

$$\{B\} = [D]^{-1}\{\phi\} \tag{C.20}$$

Substituting (C.20) into (C.16) results in the interpolating equation,

$$\begin{aligned}\phi(\alpha,\beta) &= \{P_2\}^T[D]^{-1}\{\phi\} \\ &= [H(\alpha,\beta)]\{\phi\}\end{aligned} \tag{C.21}$$

where,

$$[D]^{-1} = \frac{1}{4}\begin{bmatrix} 4 & 0 & 0 & 0 & 0 & 0 & 0 & 0 & 0 \\ 0 & 0 & 0 & 0 & 2 & 0 & 0 & 0 & -2 \\ 0 & 0 & -2 & 0 & 0 & 0 & 2 & 0 & 0 \\ -4 & 0 & 0 & 0 & 2 & 0 & 0 & 0 & 2 \\ 0 & 1 & 0 & -1 & 0 & 1 & 0 & -1 & 0 \\ -4 & 0 & 2 & 0 & 0 & 0 & 2 & 0 & 0 \\ 0 & -1 & 2 & -1 & 0 & 1 & -2 & 1 & 0 \\ 0 & -1 & 0 & 1 & -2 & 1 & 0 & -1 & 2 \\ 4 & 1 & -2 & 1 & -2 & 1 & -2 & 1 & -2 \end{bmatrix} \tag{C.22}$$

$$\begin{aligned}[H(\alpha,\beta)] &= [H_1, H_2, \ldots, H_9] \\ &= \{P_2\}^T[D]^{-1}\end{aligned} \tag{C.23}$$

Equation (C.23) defines the quadratic shape functions used in Section IV.B.4 to approximate the displacement field for the normal component of deflection.

4. Interpretation of Generalized Coordinates for Quadratic Shape Functions

The generalized coordinates associated with the quadratic shape functions are,

$$\{B\} = [D]^{-1}\{\phi\} \tag{C.24}$$

From (C.24) the following finite difference formulas are obtained,

$$b_1 = \phi^{\circ} = \phi^{1}$$

$$= [H(o,o)]\{\phi\} \tag{C.25}$$

$$b_2 = \phi^{\circ}_{,\alpha} = \frac{1}{2}(\phi^{5} - \phi^{9})$$

$$= [H_{,\alpha}(o,o)]\{\phi\} \tag{C.26}$$

$$b_3 = \phi^{\circ}_{,\beta} = \frac{1}{2}(\phi^{7} - \phi^{3})$$

$$= [H_{,\beta}(o,o]\{\phi\} \tag{C.27}$$

$$2b_4 = \phi^{\circ}_{,\alpha\alpha} = (\phi^{5} - 2\phi^{1} + \phi^{9})$$

$$= [H_{,\alpha\alpha}(o,o)]\{\phi\} \tag{C.28}$$

$$b_5 = \phi^{\circ}_{,\alpha\beta} = \frac{1}{4}(\phi^{2} - \phi^{4} + \phi^{6} - \phi^{8})$$

$$= [H_{,\alpha\beta}(o,c)\{\phi\} \tag{C.29}$$

$$2b_6 = \phi^{\circ}_{,\beta\beta} = (\phi^{7} - 2\phi^{1} + \phi^{3})$$

$$= [H_{,\beta\beta}(o,o)]\{\phi\} \qquad (C.30)$$

$$2b_7 = \phi^{\circ}_{,\alpha\alpha\beta} = \tfrac{1}{2}(-\phi^{2} + 2\phi^{3} - \phi^{4} + \phi^{6} - 2\phi^{7} + \phi^{8})$$

$$= [H_{,\alpha\alpha\beta}(o,o)]\{\phi\} \qquad (C.31)$$

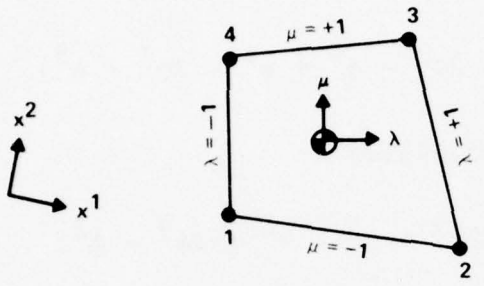
$$2b_8 = \phi^{\circ}_{,\alpha\beta\beta} = \tfrac{1}{2}(\phi^{4} - 2\phi^{5} + \phi^{6} - \phi^{8} + 2\phi^{9} - \phi^{2})$$

$$= [H_{,\alpha\beta\beta}(o,o)]\{\phi\} \qquad (C.32)$$

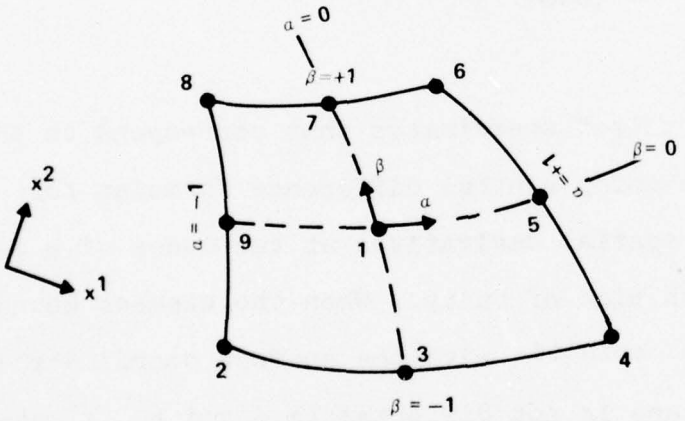
$$4b_9 = \phi^{\circ}_{,\alpha\alpha\beta\beta} = (\phi^{2} - 2\phi^{3} - \phi^{4} + 2\phi^{5} + \phi^{6} - 2\phi^{7} + \phi^{8} - 2\phi^{9} + 4\phi^{1})$$

$$= [H_{,\alpha\alpha\beta\beta}(o,o)]\{\phi\} \qquad (C.33)$$

The generalized coordinates thus correspond to the familiar three point central difference formulas for approximating spatial derivatives at the nodes of a square net with a mesh side of unity. When the element boundaries in Figure C1-b coincide with the surface coordinate lines, the mapping plane is not distorted (α,β and x^1, x^2 are aligned) and the interpolating procedure used to determine difference relations for arbitrary meshes reduces to the conventional finite difference approach using regular coordinate line meshes.



A. REGION OVER WHICH LINEAR SHAPE FUNCTIONS ARE DEFINED



B. REGION OVER WHICH QUADRATIC SHAPE FUNCTIONS ARE DEFINED

FIGURE C.1 SHAPE FUNCTION DOMAINS

APPENDIX D

INVERSE FUNCTIONAL RELATIONSHIP BETWEEN SURFACE COORDINATES AND PARAMETRIC INTERPOLATING COORDINATES

At a specific point in the shape function domain defined by the surface coordinates, x^1_*, x^2_*, it is sometimes necessary to know the corresponding values of the curvilinear interpolating coordinates, α_*, β_*, (see Figure D.1). Since the curvilinear interpolating coordinates cannot be explicitly related to the Gaussian surface coordinates for an arbitrary point in the shape function domain, it is necessary to resort to a numerical procedure.

1. Newton's Method

Any variable for which a number of discrete values are defined over some domain may be interpolated by the shape function relationship,

$$\phi(\alpha,\beta) = [N_L(\alpha,\beta)]\{\phi_L\} \qquad (D.1)$$

where,

$[N_L(\alpha,\beta)]$ = Shape functions

$\{\phi_L\}$ = Discrete values of the variable

α,β = Parametric interpolating coordinates

If x_*^1, x_*^2 are the surface coordinates of some point at which it is desired to know the corresponding local coordinates, α_*, β_*, then Newton's method may be employed to solve for α_*, β_* . The method is as follows.

Let the variation of surface coordinates over the element domain be approximated by the shape functions (see Figure D.1),

$$x^1 = [N_L(\alpha,\beta)]\ \{x_L^1\} \tag{D.2}$$

$$x^2 = [N_L(\alpha,\beta)]\ \{x_L^1\} \tag{D.3}$$

The nonlinear equations in α and β for which the roots are desired are then,

$$f_1(\alpha,\beta) = x_*^1 - [N_L]\{x_L^1\} = \Delta x^1 = 0 \tag{D.4}$$

$$f_2(\alpha,\beta) = x_*^2 - [N_L]\{x_L^2\} = \Delta x^2 = 0 \tag{D.5}$$

The iteration is then,

$$\alpha_k = \alpha_{K-1} + \Delta\alpha_K$$

$$\beta_k = \beta_{K-1} + \Delta\beta_K \tag{D.6}$$

The corrections ($\Delta\alpha_K$, $\Delta\beta_K$) are obtained from the equations,

$$\begin{bmatrix} f_{1,\alpha} & f_{1,\beta} \\ f_{2,\alpha} & f_{2,\beta} \end{bmatrix} \begin{Bmatrix} \Delta\alpha \\ \Delta\beta \end{Bmatrix} = \begin{Bmatrix} -f_1 \\ -f_2 \end{Bmatrix} \tag{D.7}$$

or in alternative notation,

$$\begin{bmatrix} x^1_{,\alpha} & x^1_{,\beta} \\ x^2_{,\alpha} & x^2_{,\beta} \end{bmatrix} \begin{Bmatrix} \Delta\alpha \\ \Delta\beta \end{Bmatrix} = \begin{Bmatrix} \Delta x^1 \\ \Delta x^2 \end{Bmatrix} \tag{D.8}$$

Since,

$$f_{1,\alpha} = -[N_{L,\alpha}]\{x^1_L\} = -x^1_{,\alpha}$$

$$f_{1,\beta} = -[N_{L,\beta}]\{x^1_L\} = -x^1_{,\beta}$$

$$f_{2,\alpha} = -[N_{L,\alpha}]\{x^2_L\} = -x^2_{,\alpha}$$

$$f_{2,\beta} = -[N_{L,\beta}]\{x^2_L\} = -x^2_{,\beta} \tag{D.9}$$

Solving (D.8) for the corrections,

$$\Delta\alpha = \frac{1}{J^T_o}[x^2_{,\beta}\cdot\Delta x^1 - x^1_{,\beta}\cdot\Delta x^2] \tag{D.10}$$

$$\Delta\beta = \frac{1}{J^T_o}[x^1_{,\alpha}\cdot\Delta x^2 - x^2_{,\alpha}\cdot\Delta x^1] \tag{D.11}$$

$$J^T_o = [x^1_{,\alpha}\cdot x^2_{,\beta} - x^1_{,\beta}\cdot x^2_{\alpha}] \tag{D.12}$$

For any desired point ($x^1 = x^1_*$, $x^2 = x^2_*$) the corresponding local coordinates ($\alpha = \alpha_*$, $\beta = \beta_*$) are determined by the iteration,

$$\begin{Bmatrix} \alpha \\ \beta \end{Bmatrix}_K = \begin{Bmatrix} \alpha \\ \beta \end{Bmatrix}_{K-1} + \begin{Bmatrix} \Delta\alpha \\ \Delta\beta \end{Bmatrix}_K \qquad \text{(D.13)}$$

The iteration is started with $\alpha_1 = 0$, $\beta_1 = 0$ and is assumed to converge to the desired values, α_*, β_*, when

$$\begin{Bmatrix} \alpha \\ \beta \end{Bmatrix}_K - \begin{Bmatrix} \alpha \\ \beta \end{Bmatrix}_{K-1} < \begin{Bmatrix} \varepsilon \\ \varepsilon \end{Bmatrix} \qquad \text{(D.14)}$$

For $\varepsilon = 10^{-6}$ the method usually converges in 3-6 iterations.

2. Procedure for Inverse Interpolation of the Linear Shape Functions

For efficiency in programming Newton's method for automatic computation the form will be slightly altered from that previously derived.

The variables Δx^i can be computed as follows,

$$\Delta x^i = x^i_* - [N_L]\{x^i_L\}$$

$$= x^i_* - [P_L]\{A^i_L\} \qquad \begin{matrix} i = 1,2 \\ L = 1,\ldots,4 \end{matrix} \qquad (D.15)$$

where the index i corresponds to the two surface coordinates, the index L corresponds to the four labeled nodes of Figure D.1-a and:

$$\{x^i_L\}^T = [x^i_1,\ x^i_2,\ x^i_3,\ x^i_4] \qquad (D.16)$$

$$[P_L] = [1,\ \alpha,\ \beta,\ \alpha\beta] \qquad (D.17)$$

$$\{A^i_L\}^T = [a^i_1,\ a^i_2,\ a^i_3,\ a^i_4] \qquad (D.18)$$

$$a^i_1 = \tfrac{1}{4}(x^i_1 + x^i_2 + x^i_3 + x^i_4)$$

$$a^i_2 = \tfrac{1}{4}(-x^i_1 + x^i_2 + x^i_3 - x^i_4)$$

$$a^i_3 = \tfrac{1}{4}(-x^i_1 - x^i_2 + x^i_3 + x^i_4)$$

$$a^i_4 = \tfrac{1}{4}(x^i_1 - x^i_2 + x^i_3 - x^i_4) \qquad (D.19)$$

Substituting (D.17), (D.18) and (D.19) into (D.15),

$$\Delta x^i = x^i_* - a^i_1 - a^i_2\alpha - a^i_3\beta - a^i_4\alpha\beta \qquad (D.20)$$

The variables $x^i_{,\alpha}$ and $x^i_{,\beta}$ are computed as follows,

$$x^i_{,\alpha} = [N_{L,\alpha}]\{x^i_L\}$$

$$= [P_{L,\alpha}]\{A^i_L\} \qquad (D.21)$$

$$x^i_{,\beta} = [N_{L,\beta}]\{x^i_L\}$$

$$= [P_{L,\beta}]\{A^i_L\} \qquad (D.22)$$

where,

$$[P_{L,\alpha}] = [0,\ 1,\ 0,\ \beta] \qquad (D.23)$$

$$[P_{L,\beta}] = [0,\ 0,\ 1,\ \alpha] \qquad (D.24)$$

hence,

$$x^i_{,\alpha} = a^i_2 + a^i_4\beta \qquad (D.25)$$

$$x^i_{,\beta} = a^i_3 + a^i_4\alpha \qquad (D.26)$$

The corrections $\Delta\alpha$ and $\Delta\beta$ can now be computed by,

$$\Delta\alpha = \frac{1}{J^T_o}[x^2_{,\beta}\cdot\Delta x^1 - x^1_{,\beta}\cdot\Delta x^2] \qquad (D.27)$$

$$\Delta\beta = \frac{1}{J^T_o}[x^1_{,\alpha}\cdot\Delta x^2 - x^2_{,\alpha}\cdot\Delta x^1] \qquad (D.28)$$

$$J^T_o = [x^1_{,\alpha}\cdot x^2_{,\beta} - x^1_{,\beta}\cdot x^2_{,\alpha}] \qquad (D.29)$$

The iteration for α_*, β_* is then,

$$\alpha_K = \alpha_{K-1} + \Delta\alpha$$

$$\beta_K = \beta_{K-1} + \Delta\beta \qquad \text{(D.30)}$$

3. Procedure for Inverse Interpolation of Quadratic Shape Functions

The variables Δx^i are computed as follows,

$$\Delta x^i = x^i_* - [N_L]\{x^i_L\}$$

$$= x^i_* - [P_L]\{A^i_L\} \qquad \begin{matrix} i = 1,2 \\ L = 1,\ldots, 9 \end{matrix} \qquad \text{(D.31)}$$

where the index i corresponds to the two surface coordinates, the index L corresponds to the nine labeled nodes of Figure D.1-b, and:

$$\{x^i_L\} = [x^i_1, x^i_2,\ldots, x^i_9] \qquad \text{(D.32)}$$

$$[P_L] = [1,\alpha,\beta,\alpha^2,\alpha\beta,\beta^2,\alpha^2\beta,\alpha\beta^2,\alpha^2\beta^2] \qquad \text{(D.33)}$$

$$\{A^i_L\}^T = [a^i_1, a^i_2,\ldots, a^i_9] \qquad \text{(D.34)}$$

$$a^i_1 = x^i_1$$

$$a^i_2 = \tfrac{1}{2}(x^i_5 - x^i_9)$$

$$a^i_3 = \tfrac{1}{2}(x^i_7 - x^i_3)$$

$$a_4^i = \frac{1}{2}(x_5^i - 2x_1^i + x_9^i)$$

$$a_5^i = \frac{1}{4}(x_2^i - x_4^i + x_6^i - x_8^i)$$

$$a_6^i = \frac{1}{2}(x_7^i - 2x_1^i + x_3^i)$$

$$a_7^i = \frac{1}{4}(-x_2^i + 2x_3^i - x_4^i + x_6^i - 2x_7^i + x_8^i)$$

$$a_8^i = \frac{1}{4}(x_4^i - 2x_5^i + x_6^i - x_8^i + 2x_9^i - x_2^i)$$

$$a_9^i = \frac{1}{4}(x_2^i - 2x_3^i + x_4^i - 2x_5^i + x_6^i - 2x_7^i + x_8^i - 2x_9^i + 4x_1^i)$$

(D.35)

Substituting (D.33), (D.34) and (D.35) into (D.31),

$$\Delta x^i = x_*^i - a_1^i - a_2^i\alpha - a_3^i\beta - a_4^i\alpha^2 - a_5^i\alpha\beta - a_6^i\beta^2 - a_7^i\alpha^2\beta - a_8^i\alpha\beta^2 - a_9^i\alpha^2\beta^2 \quad \text{(D.36)}$$

The variables $x^i_{,\alpha}$ and $x^i_{,\beta}$ are computed as follows,

$$x^i_{,\alpha} = [N_{L,\alpha}]\{x_L^i\} = [P_{L,\alpha}]\{A_L^i\} \quad \text{(D.37)}$$

$$x^i_{,\beta} = [N_{L,\beta}]\{x_L^i\} = [P_{L,\beta}]\{x_L^i\} \quad \text{(D.38)}$$

where,

$$[P_{L,\alpha}] = [0,1,0,2\alpha,\beta,0,2\alpha\beta,\beta^2,2\alpha\beta^2] \tag{D.39}$$

$$[P_{L,\beta}] = [0,0,1,0,\alpha,2\beta,\alpha^2,2\alpha\beta,2\alpha^2\beta] \tag{D.40}$$

hence,

$$x^1_{,\alpha} = a^i_2 + 2a^i_4\alpha + a^i_5\beta + 2a^i_7\alpha\beta + a^i_8\beta^2 + 2a^i_9\alpha\beta^2 \tag{D.41}$$

$$x^i_{,\beta} = a^i_3 + a^i_5\alpha + 2a^i_6\beta + a^i_7\alpha^2 + 2a^i_8\alpha\beta + 2a^i_9\alpha^2\beta \tag{D.42}$$

The corrections $\Delta\alpha$ and $\Delta\beta$ can now be computed by,

$$\Delta\alpha = \frac{1}{J^T_o}[x^2_{,\beta}\cdot\Delta x^1 - x^1_{,\beta}\cdot\Delta x^2] \tag{D.43}$$

$$\Delta\beta = \frac{1}{J^T_o}[x^1_{,\alpha}\cdot\Delta x^2 - x^2_{,\alpha}\cdot\Delta x^1] \tag{D.44}$$

$$J^T_o = [x^1_{,\alpha}\cdot x^2_{,\beta} - x^1_{,\beta}\cdot x^2_{,\alpha}] \tag{D.45}$$

The iteration for α_*, β_* is then,

$$\alpha_K = \alpha_{K-1} + \Delta\alpha$$

$$\beta_K = \beta_{K-1} + \Delta\beta \tag{D.46}$$

4. SUBROUTINE LISTING

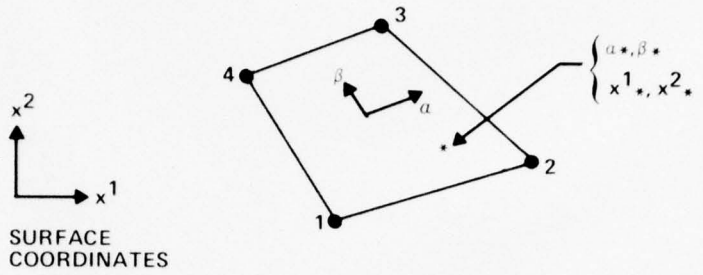
```
      SUBROUTINE ISOINV(ICASE,X1S,X2S,ELNO,LS,MS,AS,BS,IPRINT)
C*************************************************************************
C**
C**   SUBROUTINE FOR DETERMINING THE INVERSE FUNCTIONAL RELATIONSHIP
C**   BETWEEN ISOPARAMETRIC INTERPOLATING COORDINATES AND SPATIAL
C**   COORDINATES USING A NEWTON - RAPHSON ITERATION METHOD
C**   **********     R J EDWARDS   *   DEC 1974
C**
C**   X1S , X2S = SPATIAL COORDINATES INPUT TO SUBROUTINE
C**   ELNO = ELEMENT NUMBER
C**   LS , MS = LINEAR INTERPOLATING COORDINATES CORRESPONDING TO
C                X1S , X2S
C**   AS , BS = QUADRATIC INTERPOLATING COORDINATES CORRESPONDING TO
C                X1S , X2S
C**
C**   ICASE = -1 RETURN LS = LAMBDA-STAR , MS = MU-STAR
C**   ICASE = +1 RETURN AS = ALPHA-STAR , BS = BETA-STAR
C**   ICASE =  0 RETURN BOTH LS , MS AND AS , BS
C**
C**   IPRINT = 0 , DO NOT PRINT SUMMARY DATA
C**   IPRINT = 1 , PRINT SUMMARY DATA
C**
C*************************************************************************
      COMMON/ISODAT/ CX1(13),CX2(13),IGX(13)
      REAL LS,MS,LI,MI
      DATA EPSILN/0.000001/, ITLIM/30/
      IF(ICASE) 100,100,200
C*************************************************************************
C**
C*    ITERATION FOR INVERSE INTERPOLATION OF BI-LINEAR SHAPE FUNCTIONS
C**
C*************************************************************************
  100 CONTINUE
      X1 =CX1(1)
      X2 =CX1(2)
      X3 =CX1(3)
      X4 =CX1(4)
      Y1 =CX2(1)
      Y2 =CX2(2)
      Y3 =CX2(3)
      Y4 =CX2(4)
      A1 = 0.25*( X1 + X2 + X3 + X4)
      A2 = 0.25*(-X1 + X2 + X3 - X4)
      A3 = 0.25*(-X1 - X2 + X3 + X4)
      A4 = 0.25*( X1 - X2 + X3 - X4)
      B1 = 0.25*( Y1 + Y2 + Y3 + Y4)
      B2 = 0.25*(-Y1 + Y2 + Y3 - Y4)
      B3 = 0.25*(-Y1 - Y2 + Y3 + Y4)
      B4 = 0.25*( Y1 - Y2 + Y3 - Y4)
      LS = 0.0
      MS = 0.0
```

```
      IT = 0
  110 LI = LS
      MI = MS
      DELX1 = X1S - A1 - A2*LI - A3*MI - A4*LI*MI
      DELX2 = X2S - B1 - B2*LI - B3*MI - B4*LI*MI
      X1L = A2 + A4*MI
      X1M = A3 + A4*LI
      X2L = B2 + B4*MI
      X2M = B3 + B4*LI
      DETJ = X1L*X2M - X1M*X2L
      IF(ABS(DETJ).LT.EPSILN) GO TO 130
      DETJI = 1.0/DETJ
      DELL = DETJI * (X2M*DELX1 - X1M*DELX2)
      DELM = DETJI * (X1L*DELX2 - X2L*DELX1)
      LS = LI + DELL
      MS = MI + DELM
      ADELL = ABS(DELL)
      ADELM = ABS(DELM)
      IT = IT + 1
      IF(IT-ITLIM) 120,120,150
C**
C*****     CONVERGENCE TEST
  120 IF(ADELL.GT.EPSILN .OR.  ADELM.GT.EPSILN) GO TO 110
C**
      GO TO 200
  130 WRITE(6,1000) (CX1(I),I=1,13),(CX2(I),I=1,13),X1L,X1M,X2L,X2M,DETJ
      RETURN
  150 WRITE(6,2000) ELNO,X1S,X2S,LI,MI,LS,MS,X1L,X1M,X2L,X2M,DETJ,
     1              DELL,DELM
      IF(IT.LT.(ITLIM+4)) GO TO 110
      RETURN
  200 IF(IPRINT) 201,201,202
  202 WRITE(6,5000) ELNO,X1S,X2S,IT,LS,MS
  201 IF(ICASE) 300,251,251
C*******************************************************************
C**
C*   ITERATION FOR INVERSE INTERPOLATION OF BI-QUADRATIC SHAPE FUNCTIONS
C**
C*******************************************************************
  251 CONTINUE
      X1 =CX1(5)
      X2 =CX1(6)
      X3 =CX1(7)
      X4 =CX1(8)
      X5 =CX1(9)
      X6 =CX1(10)
      X7 =CX1(11)
      X8 =CX1(12)
      X9 =CX1(13)
      Y1 =CX2(5)
      Y2 =CX2(6)
      Y3 =CX2(7)
      Y4 =CX2(8)
      Y5 =CX2(9)
```

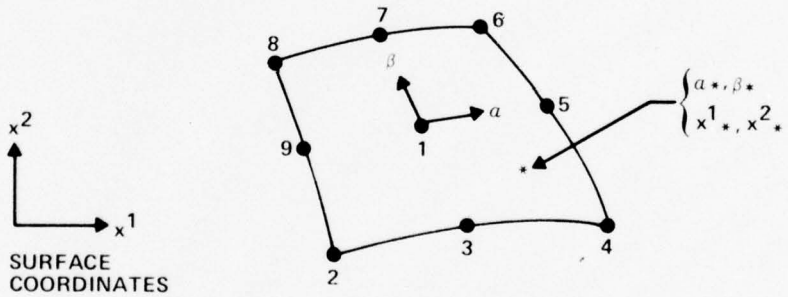
```
      Y6 =CX2(10)
      Y7 =CX2(11)
      Y8 =CX2(12)
      Y9 =CX2(13)
      X12 = 2.*X1
      X32 = 2.*X3
      X52 = 2.*X5
      X72 = 2.*X7
      X92 = 2.*X9
      Y12 = 2.*Y1
      Y32 = 2.*Y3
      Y52 = 2.*Y5
      Y72 = 2.*Y7
      Y92 = 2.*Y9
      C1 = X1
      C2 = 0.50*(X5-X9)
      C3 = 0.50*(X7-X3)
      C4 = 0.50*(X5-X12+X9)
      C5 = 0.25*( X2 - X4 + X6 - X8)
      C6 = 0.50*( X7 - X12 + X3)
      C7 = 0.25*(-X2 + X32 - X4 + X6 - X72 + X8)
      C8 = 0.25*( X4 - X52 + X6 - X8 + X92 - X2)
      C9 = 0.25*( X2 - X32 + X4 - X52 + X6 - X72 + X8 - X92) + X1
      D1 = Y1
      D2 = 0.50*(Y5-Y9)
      D3 = 0.50*(Y7-Y3)
      D4 = 0.50*(Y5 - Y12 + Y9)
      D5 = 0.25*(Y2 - Y4 + Y6 - Y8)
      D6 = 0.50*(Y7 - Y12 + Y3)
      D7 = 0.25*(-Y2 + Y32 - Y4 + Y6 - Y72 + Y8)
      D8 = 0.25*( Y4 - Y52 + Y6 - Y8 + Y92 - Y2)
      D9 = 0.25*( Y2 - Y32 +Y4 - Y52 + Y6 - Y72 + Y8 - Y92) + Y1
      AS = 0.0
      BS = 0.0
      IT = 0
  210 AI = AS
      BI = BS
      A2 = AI*AI
      B2 = BI*BI
      AB = AI*BI
      A2B = A2*BI
      AB2 = AI*B2
      A2B2 = A2*B2
      TA = 2.0*AI
      TB = 2.0*BI
      TAB = 2.0*AB
      TAB2 = 2.0*AB2
      TA2B = 2.0*A2B
      DELX1 = X1S - C1 - C2*AI - C3*BI - C4*A2 - C5*AB - C6*B2
     1              - C7*A2B - C8*AB2 - C9*A2B2
      DELX2 = X2S - D1 -D2*AI - D3*BI -D4*A2 - D5*AB - D6*B2
     1              - D7*A2B - D8*AB2 - D9*A2B2
      X1A =C2 + C4*TA + C5*BI + C7*TAB + C8*B2 + C9*TAB2
      X1B = C3 + C5*AI + C6*TB + C7*A2 + C8*TAB + C9*TA2B
```

```
      X2A = D2 + D4*TA + D5*BI + D7*TAB + D8*B2 + D9*TAB2
      X2B = D3 + D5*AI + D6*TB + D7*A2 + D8*TAB + D9*TA2B
      DETJ = X1A*X2B - X1B*X2A
      IF(ABS(DETJ).LT.EPSILN) GO TO 230
      DETJI = 1.0/DETJ
      DELA = DETJI * (X2B*DELX1 - X1B*DELX2)
      DELB = DETJI * (X1A*DELX2 - X2A*DELX1)
      AS = AI + DELA
      BS = BI + DELB
      ADELA = ABS(DELA)
      ADELB = ABS(DELB)
      IT = IT + 1
      IF(IT-ITLIM) 220,220,250
C**
C*****     CONVERGENCE TEST
  220 IF(ADELA.GT.EPSILN .OR.  ADELB.GT.EPSILN) GO TO 210
C**
      GO TO 300
  230 WRITE(6,3000) (CX1(I),I=1,13),(CX2(I),I=1,13),X1A,X1B,X2A,X2B,DETJ
      RETURN
  250 WRITE(6,4000) ELNO ,X1S,X2S,AI,BI,AS,BS,X1A,X1B,X2A,X2B,DETJ
     1             ,DELA,DELB
      IF(IT.LT.(ITLIM+4)) GO TO 210
      RETURN
  300 IF(IPRINT) 301,301,302
  302 WRITE(6,6000) ELNO,X1S,X2S,IT,AS,BS
  301 RETURN
 1000 FORMAT(1H0,//,5X,67HTHE DETERMINANT OF THE INVERSION MATRIX (JACOB
     1IAN) IS EQUAL TO ZERO ,
     2         //7X,8HX1(I) = ,1PE15.6,/,15X,6E15.6,
     3        ///7X,8HX2(I) = ,1PE15.6,/,15X,6E15.6,
     4        ///5X,6HX1L = ,E20.8,5X,6HX1M = ,E20.8,5X,6HX2L = ,E20.8,
     5        /,5X,6HX2M = ,E20.8,5X,7HDETJ = ,E20.8,//)
 3000 FORMAT(1H0,//,5X,67HTHE DETERMINANT OF THE INVERSION MATRIX (JACOB
     1IAN) IS EQUAL TO ZERO ,
     2         //7X,8HX1(I) = ,1PE15.6,/,15X,6E15.6,
     3        ///7X,8HX2(I) = ,1PE15.6,/,15X,6E15.6,
     4        ///5X,6HX1A = ,E20.8,5X,6HX1B = ,E20.8,5X,6HX2A = ,E20.8,
     5        /,5X,6HX2B = ,E20.8,5X,7HDETJ = ,E20.8,//)
 5000 FORMAT(1H0,//,5X,69HTHE ITERATION TO FIND LAMBDA, MU CONVERGED WIT
     1H THE FOLLOWING RESULTS,
     2 //5X,9HEL.NO. = ,I8,5X,6HX1S = ,1PE15.6,5X,6HX2S = ,1PE15.6,
     3 //5X,12HITERATION = ,I5,5X,9HLAMBDA = ,E15.6,5X,5HMU = ,E15.6,//)
 6000 FORMAT(1H0,//,5X,69HTHE ITERATION TO FIND ALPHA,BETA CONVERGED WIT
     1H THE FOLLOWING RESULTS,
     2 //5X,9HEL.NO. = ,I8,5X,6HX1S = ,1PE15.6,5X,6HX2S = ,1PE15.6,
     3 //5X,12HITERATION = ,I5,5X,8HALPHA = ,E15.6,5X,7HBETA = ,E15.6,/)
 2000 FORMAT(1H0,4X,49HTHE ITERATION TO FIND LAMBDA,MU DID NOT CONVERGE
     1 //5X,9HEL.NO. = ,I8,5X,6HX1S = ,1PE15.6,5X,6HX2S = ,1PE15.6,
     2 //5X,5HLI = ,E20.8,5X,5HMI = ,E20.8,5X,
     3  /5X,5HLS = ,E20.8,5X,5HMS = ,E20.8,
     4 //5X,6HX1L = ,E20.8,5X,6HX1M = ,E20.8,5X,
     5  /5X,6HX2L = ,E20.8,5X,6HX2M = ,E20.8,5X,7HDETJ = ,E20.8,
     6 //5X,9HDEL(L) = ,E20.8,5X,9HDEL(M) = ,E20.8,//)
```

```
4000 FORMAT(1H0,4X,49HTHE ITERATION TO FIND ALPHA,BETA DID NOT CONVERGE
     1 //5X,9HEL.NO. = ,I8,5X,6HX1S = ,1PE15.6,5X,6HX2S = ,1PE15.6,
     2 //5X,5HAI = ,E20.8,5X,5HBI = ,E20.8,5X,
     3  /5X,5HAS = ,E20.8,5X,5HBS = ,E20.8,
     4 //5X,6HX1A = ,E20.8,5X,6HX1B = ,E20.8,5X,
     5  /5X,6HX2A = ,E20.8,5X,6HX2B = ,E20.8,5X,7HDETJ = ,E20.8,
     6 //5X,9HDEL(A) = ,E20.8,5X,9HDEL(B) = ,E20.8,//)
      END
```



A. LINEAR SHAPE FUNCTION DOMAIN



B. QUADRATIC SHAPE FUNCTION DOMAIN

FIGURE D.1 SHAPE FUNCTION DOMAINS

APPENDIX E

SHELL REFERENCE SURFACE GEOMETRIES

The tensors necessary to describe the geometry and deformation of the shell reference surface are presented in this Appendix for several classes of shell surfaces. The equations for a conical reference surface are developed in detail to demonstrate the practical utilization of the general tensor formulation of Chapter II. The equations for cylindrical and spherical surfaces and those for flat plates in both polar and rectangular coordinates are only summarized since the detailed development closely parallels that of the conical surface example.

1. Conical Shell Geometry

Gridpoints on the shell reference surface are defined in the cylindrical coordinate system* (see Figure E.1),

$$\begin{Bmatrix} X^1 \\ X^2 \\ X^3 \end{Bmatrix}_G = \begin{Bmatrix} R \\ \Theta \\ Z \end{Bmatrix} \qquad \text{(E.1)}$$

*The coordinate system subscripts G, B and S refer to gridpoint coordinates, basic coordinates and surface coordinates respectively.

The cone angle α and base radius R_B are also specified. The following geometrical parameter may then be calculated,

$$L = \frac{R_B}{\tan \alpha} \tag{E.2}$$

At an arbitrary point P on the shell reference surface,

$$\left\{ \begin{matrix} x^1 \\ x^2 \\ x^3 \end{matrix} \right\}_B = \left\{ \begin{matrix} X \\ Y \\ Z \end{matrix} \right\} = \left\{ \begin{matrix} R\cos\theta \\ R\sin\theta \\ Z \end{matrix} \right\} = \left\{ \begin{matrix} (L-x^2)\tan\alpha\cos x^1 \\ (L-x^2)\tan\alpha\sin x^1 \\ Z \end{matrix} \right\} \tag{E.3}$$

where the Gaussian surface coordinates are,

$$\left\{ \begin{matrix} x^1 \\ x^2 \\ x^3 \end{matrix} \right\}_S = \left\{ \begin{matrix} \theta \\ Z \\ z \end{matrix} \right\} \tag{E.4}$$

The position vector of point P is,

$$\begin{aligned} \vec{r} &= X^K \vec{I}_K \\ &= (L-Z)\tan\alpha\cos\theta\, \vec{I}_1 \\ &+ (L-Z)\tan\alpha\sin\theta\, \vec{I}_2 + Z\, \vec{I}_3 \end{aligned} \tag{E.5}$$

The base vectors of the surface coordinates are then,

$$\vec{a}_\alpha = \vec{r}_{,\alpha} \tag{E.6}$$

hence,

$$\vec{a}_1 = -R \sin\theta \, \vec{I}_1 + R \cos\theta \, \vec{I}_2$$

$$\vec{a}_2 = -\tan\alpha\cos\theta \, \vec{I}_1 - \tan\alpha\sin\theta \, \vec{I}_2 + (1) \, \vec{I}_3 \tag{E.7}$$

The metric tensor is given by,

$$a_{\alpha\beta} = \vec{a}_\alpha \cdot \vec{a}_\beta \tag{E.8}$$

hence,

$$a_{11} = R^2$$

$$a_{12} = a_{21} = 0$$

$$a_{22} = \frac{1}{\cos^2\alpha} \tag{E.9}$$

The metric tensor, its determinant and the associated metric tensor are thus,

$$a_{\alpha\beta} = \begin{bmatrix} R^2 & 0 \\ 0 & \frac{1}{\cos^2\alpha} \end{bmatrix} \tag{E.10}$$

$$a = |a_{\alpha\beta}| = \frac{R^2}{\cos^2\alpha} \tag{E.11}$$

$$a^{\alpha\beta} = \begin{bmatrix} \frac{1}{R^2} & 0 \\ 0 & \cos^2\alpha \end{bmatrix} \tag{E.12}$$

The incremental arc lengths in the base vector directions are,

$$dS_1 = A_1 dx^1 = Rd\theta \tag{E.13}$$

$$dS_2 = A_2 dx^2 = \frac{1}{\cos\alpha}\, dz \tag{E.14}$$

and the incremental arc length on the shell reference surface is,

$$dS^2 = a_{\alpha\beta}\, dx^\alpha dx^\beta$$

$$= (Rd\theta)^2 + (\frac{1}{\cos\alpha}\, dz)^2 \tag{E.15}$$

The unit vectors in the base vector directions are,

$$\vec{e}_\alpha = \frac{\vec{a}_\alpha}{A_\alpha} \quad \text{(no sum)} \tag{E.16}$$

thus,

$$\vec{e}_1 = -\sin\theta\,\vec{I}_1 + \cos\theta\,\vec{I}_2 \tag{E.17}$$

$$\vec{e}_2 = -\sin\alpha\cos\theta\,\vec{I}_1 - \sin\alpha\sin\theta\,\vec{I}_2 + \cos\alpha\,\vec{I}_3 \tag{E.18}$$

The unit normal vector is,

$$\vec{e}_n = \vec{e}_1 \times \vec{e}_2$$

$$= \cos\alpha\cos\theta\,\vec{I}_1 + \cos\alpha\sin\theta\,\vec{I}_2 + \sin\alpha\,\vec{I}_3 \tag{E.19}$$

The transformation relating unit vectors in surface coordinates and unit vectors in basic coordinates is then,

$$\begin{Bmatrix} \vec{e}_1 \\ \vec{e}_2 \\ \vec{e}_n \end{Bmatrix} = [T_{SB}] \begin{Bmatrix} \vec{I}_1 \\ \vec{I}_2 \\ \vec{I}_3 \end{Bmatrix} \tag{E.20}$$

where,

$$[T_{SB}] = \begin{bmatrix} -S_\theta & C_\theta & 0 \\ -S_\alpha C_\theta & -S_\alpha S_\theta & C_\alpha \\ C_\alpha C_\theta & C_\alpha S_\theta & S_\alpha \end{bmatrix} \qquad \text{(E.21)}$$

$$C_\alpha = \cos\alpha, \quad S_\alpha = \sin\alpha$$
$$C_\theta = \cos\theta, \quad S_\theta = \sin\theta \qquad \text{(E.22)}$$

Conversely,

$$\begin{Bmatrix} \vec{I}_1 \\ \vec{I}_2 \\ \vec{I}_3 \end{Bmatrix} = [T_{SB}]^{-1} \begin{Bmatrix} \vec{e}_1 \\ \vec{e}_2 \\ \vec{e}_n \end{Bmatrix}$$

$$= [T_{SB}]^T \begin{Bmatrix} \vec{e}_1 \\ \vec{e}_2 \\ \vec{e}_n \end{Bmatrix} \qquad \text{(E.23)}$$

since,

$$[T_{SB}]^T[T_{SB}] = [I] \qquad \text{(E.24)}$$

where [I] is the identity matrix.

It follows that the transformation relating shell displacement components to basic displacement components is,

$$\begin{Bmatrix} u_\theta \\ u_S \\ u_n \end{Bmatrix} = [T_{SB}] \begin{Bmatrix} u_X \\ u_Y \\ u_Z \end{Bmatrix} \tag{E.25}$$

and conversely,

$$\begin{Bmatrix} u_X \\ u_Y \\ u_Z \end{Bmatrix} = [T_{SB}]^T \begin{Bmatrix} u_\theta \\ u_S \\ u_n \end{Bmatrix} \tag{E.26}$$

The Christoffel symbols of the second kind are defined by,

$$\Gamma^{\alpha}_{\beta\alpha} = a^{\alpha\lambda}(\vec{a}_\lambda \cdot \vec{a}_{\beta,\alpha}) \tag{E.27}$$

where,

$$\begin{aligned} \vec{a}_{1,1} &= -R\cos\theta\,\vec{I}_1 - R\sin\theta\,\vec{I}_2 \\ \vec{a}_{1,2} &= \vec{a}_{2,1} = \tan\alpha\sin\theta\,\vec{I}_1 - \tan\alpha\cos\theta\,\vec{I}_2 \\ \vec{a}_{2,2} &= 0 \end{aligned} \tag{E.28}$$

hence,

$$\Gamma^1_{11} = a^{11}(\vec{a}_1 \cdot \vec{a}_{1,1}) + a^{12}(\vec{a}_2 \cdot \vec{a}_{1,1})$$
$$= 0$$
$$\Gamma^1_{12} = a^{11}(\vec{a}_1 \cdot \vec{a}_{1,2}) + a^{12}(\vec{a}_2 \cdot \vec{a}_{1,2})$$
$$= -\frac{\tan\alpha}{R} = \Gamma^1_{21}$$
$$\Gamma^1_{22} = a^{11}(\vec{a}_1 \cdot \vec{a}_{2,2}) + a^{12}(\vec{a}_2 \cdot \vec{a}_{2,2})$$
$$= 0$$
$$\Gamma^2_{11} = a^{21}(\vec{a}_1 \cdot \vec{a}_{1,1}) + a^{22}(\vec{a}_2 \cdot \vec{a}_{1,1})$$
$$= R \sin\alpha \cos\alpha$$
$$\Gamma^2_{12} = a^{21}(\vec{a}_1 \cdot \vec{a}_{1,2}) + a^{22}(\vec{a}_2 \cdot \vec{a}_{1,2})$$
$$= 0 = \Gamma^2_{21}$$
$$\Gamma^2_{22} = a^{21}(\vec{a}_1 \cdot \vec{a}_{2,2}) + a^{22}(\vec{a}_2 \cdot \vec{a}_{2,2})$$
$$= 0 \qquad \text{(E.29)}$$

The covariant form of the initial curvature tensor is defined by,

$$b_{\alpha\beta} = \vec{e}_n \cdot \vec{a}_{\alpha,\beta} \qquad \text{(E.30)}$$

hence,

$$b_{11} = -R\cos\alpha$$
$$b_{21} = b_{12} = 0$$
$$b_{22} = 0 \qquad \text{(E.31)}$$

The mixed form of the initial curvature tensor is defined by,

$$b_{\alpha}^{\rho} = a^{\rho\beta} b_{\alpha\beta} \tag{E.32}$$

or in matrix form,

$$\begin{bmatrix} b_1^1 & b_2^1 \\ b_1^2 & b_2^2 \end{bmatrix} = \begin{bmatrix} a^{11} & a^{12} \\ a^{21} & a^{22} \end{bmatrix} \mathbf{x} \begin{bmatrix} b_{11} & b_{12} \\ b_{21} & b_{22} \end{bmatrix} \tag{E.33}$$

hence,

$$b_{\alpha}^{\rho} = \begin{bmatrix} -\frac{\cos\alpha}{R} & 0 \\ 0 & 0 \end{bmatrix} \tag{E.34}$$

The covariant derivatives of the covariant initial curvature tensor are,

$$b_{\alpha\beta}|_{\lambda} = b_{\alpha\beta,\lambda} - \Gamma_{\alpha\lambda}^{\mu} b_{\mu\beta} - \Gamma_{\beta\lambda}^{\mu} b_{\alpha\mu} \tag{E.35}$$

or in matrix form,

$$\begin{bmatrix} b_{11}|_\lambda & b_{12}|_\lambda \\ b_{21}|_\lambda & b_{22}|_\lambda \end{bmatrix} = \begin{bmatrix} b_{11,\lambda} & b_{12,\lambda} \\ b_{21,\lambda} & b_{22,\lambda} \end{bmatrix} -$$

$$\begin{bmatrix} \Gamma^1_{1\lambda} & \Gamma^2_{1\lambda} \\ \Gamma^1_{2\lambda} & \Gamma^2_{2\lambda} \end{bmatrix} \begin{bmatrix} b_{11} & b_{12} \\ b_{21} & b_{22} \end{bmatrix} -$$

$$\begin{bmatrix} b_{11} & b_{12} \\ b_{21} & b_{22} \end{bmatrix} \begin{bmatrix} \Gamma^1_{1\lambda} & \Gamma^1_{2\lambda} \\ \Gamma^2_{1\lambda} & \Gamma^2_{2\lambda} \end{bmatrix} \qquad (E.36)$$

thus,

$$b_{\alpha\beta}|_1 = \begin{bmatrix} 0 & -\sin\alpha \\ -\sin\alpha & 0 \end{bmatrix} \qquad (E.37)$$

$$b_{\alpha\beta}|_2 = \begin{bmatrix} -\sin\alpha & 0 \\ 0 & 0 \end{bmatrix} \qquad (E.38)$$

The covariant derivatives of the mixed initial curvature tensor are,

$$b^\alpha_\beta|_\lambda = a^{\alpha\mu} b_{\beta\mu}|_\lambda \qquad (E.39)$$

or in matrix form,

$$\begin{bmatrix} b^1_1|_\lambda & b^1_2|_\lambda \\ b^2_1|_\lambda & b^2_2|_\lambda \end{bmatrix} = \begin{bmatrix} a^{11} & a^{12} \\ a^{21} & a^{22} \end{bmatrix} \begin{bmatrix} b_{11}|_\lambda & b_{12}|_\lambda \\ b_{21}|_\lambda & b_{22}|_\lambda \end{bmatrix} \tag{E.40}$$

hence,

$$b^\alpha_\beta|_1 = \begin{bmatrix} 0 & -\frac{\sin\alpha}{R^2} \\ -\sin\alpha\cos^2\alpha & 0 \end{bmatrix} \tag{E.41}$$

$$b^\alpha_\beta|_2 = \begin{bmatrix} -\frac{\sin\alpha}{R^2} & 0 \\ 0 & 0 \end{bmatrix} \tag{E.42}$$

A concise summary of the above analytical development for the conical shell geometry is contained in Table E.1.

2. Cylindrical Shell Geometry

Gridpoint coordinates on the shell reference surface are defined in the cylindrical system (see Figure E.2),

$$\begin{Bmatrix} X^1 \\ X^2 \\ X^3 \end{Bmatrix}_G = \begin{Bmatrix} R \\ \theta \\ z \end{Bmatrix} \tag{E.43}$$

At an arbitrary point P on the shell reference surface,

$$\left\{\begin{matrix} X^1 \\ X^2 \\ X^3 \end{matrix}\right\}_B = \left\{\begin{matrix} X \\ Y \\ \cancel{Z} \end{matrix}\right\} = \left\{\begin{matrix} R\cos\theta \\ R\sin\theta \\ Z \end{matrix}\right\} = \left\{\begin{matrix} R\cos x^1 \\ R\sin x^1 \\ x^2 \end{matrix}\right\} \tag{E.44}$$

where the Gaussian surface coordinates are,

$$\left\{\begin{matrix} x^1 \\ x^2 \\ x^3 \end{matrix}\right\}_S = \left\{\begin{matrix} \theta \\ \cancel{Z} \\ z \end{matrix}\right\} \tag{E.45}$$

The position vector of point P is,

$$\vec{r} = X^K \vec{I}_K$$

$$= R\cos\theta\, \vec{I}_1 + R\sin\theta\, \vec{I}_2 + \cancel{Z}\, \vec{I}_3 \tag{E.46}$$

Proceeding as in the conical shell example, the equations summarized in Table E.2 are obtained.

3. Spherical Shell Geometry

Gridpoint coordinates on the shell reference surface are defined in the spherical system (see Figure E.3).

$$\begin{Bmatrix} X^1 \\ X^2 \\ X^3 \end{Bmatrix}_G = \begin{Bmatrix} R \\ \Theta \\ \phi \end{Bmatrix} \tag{E.47}$$

At an arbitrary point P on the shell reference surface,

$$\begin{Bmatrix} X^1 \\ X^2 \\ X^3 \end{Bmatrix}_B = \begin{Bmatrix} X \\ Y \\ Z \end{Bmatrix} = \begin{Bmatrix} R\sin\Theta\cos\phi \\ R\sin\Theta\sin\phi \\ R\cos\Theta \end{Bmatrix} = \begin{Bmatrix} R\sin x^1\cos x^2 \\ R\sin x^1\sin x^2 \\ R\cos x^1 \end{Bmatrix} \tag{E.48}$$

where the Gaussian surface coordinates are,

$$\begin{Bmatrix} x^1 \\ x^2 \\ x^3 \end{Bmatrix}_S = \begin{Bmatrix} \Theta \\ \phi \\ z \end{Bmatrix} \tag{E.49}$$

The position vector of point P is,

$$\begin{aligned} \vec{r} &= X^K \vec{I}_K \\ &= R\sin\Theta\cos\phi\ \vec{I}_1 + R\sin\Theta\sin\phi\ \vec{I}_2 + R\cos\Theta\ \vec{I}_3 \end{aligned} \tag{E.50}$$

Proceeding as in the conical shell example, the equations summarized in Table E.3 are obtained.

4. Plate Geometry in Polar Coordinates

Gridpoint coordinates on the plate reference surface are defined in the cylindrical system (see Figure E.4),

$$\left\{ \begin{array}{c} X^1 \\ X^2 \\ X^3 \end{array} \right\}_G = \left\{ \begin{array}{c} R \\ \Theta \\ Z_P \end{array} \right\} \tag{E.51}$$

At an arbitrary point P on the plate reference surface,

$$\left\{ \begin{array}{c} X^1 \\ X^2 \\ X^3 \end{array} \right\}_B = \left\{ \begin{array}{c} X \\ Y \\ Z_P \end{array} \right\} = \left\{ \begin{array}{c} R\cos\Theta \\ R\sin\Theta \\ Z_P \end{array} \right\} = \left\{ \begin{array}{c} x^1\cos x^2 \\ x^1\sin x^2 \\ Z_P \end{array} \right\} \tag{E.52}$$

where the Gaussian surface coordinates are,

$$\left\{ \begin{array}{c} x^1 \\ x^2 \\ x^3 \end{array} \right\}_S = \left\{ \begin{array}{c} R \\ \Theta \\ z \end{array} \right\} \tag{E.53}$$

The position vector of point P is,

$$\vec{r} = X^K \vec{I}_K$$

$$= R\cos\theta\, \vec{I}_1 + R\sin\theta\, \vec{I}_2 + Z_P \vec{I}_3 \qquad \text{(E.54)}$$

Proceeding as in the conical shell example, the equations summarized in Table E.4 are obtained.

5. Plate Geometry in Cartesian Coordinates

Gridpoint coordinates on the plate reference surface are defined in the Cartesian system (see Figure E.5),

$$\left\{ \begin{array}{c} X^1 \\ X^2 \\ X^3 \end{array} \right\}_G = \left\{ \begin{array}{c} X \\ Y \\ Z_P \end{array} \right\} \qquad \text{(E.55)}$$

At an arbitrary point P on the plate reference surface,

$$\left\{ \begin{array}{c} X^1 \\ X^2 \\ X^3 \end{array} \right\}_B = \left\{ \begin{array}{c} X \\ Y \\ Z_P \end{array} \right\} = \left\{ \begin{array}{c} x^1 \\ x^2 \\ Z_P \end{array} \right\} \qquad \text{(E.56)}$$

where the Gaussian surface coordinates are,

$$\left\{ \begin{array}{c} x^1 \\ x^2 \\ x^3 \end{array} \right\}_S = \left\{ \begin{array}{c} X \\ Y \\ Z \end{array} \right\} \qquad \text{(E.57)}$$

The position vector of point P is,

$$\vec{r} = X^K \vec{I}_K$$

$$= X \vec{I}_1 + Y \vec{I}_2 + Z_P \vec{I}_3 \qquad \text{(E.58)}$$

Proceeding as in the conical shell example, the equations summarized in Table E.5 are obtained.

AD-A034 788 NAVAL SURFACE WEAPONS CENTER WHITE OAK LAB SILVER SP--ETC F/G 13/13
A GENERALIZED FINITE DIFFERENCE ELEMENT FOR THE THERMOELASTIC S--ETC(U)
JUN 76 R J EDWARDS

UNCLASSIFIED NSWC/WOL/TR-76-66 NL

4 OF 4
AD
A034788



END

DATE
FILMED
2-77

TABLE E.1

SUMMARY OF CONICAL SHELL GEOMETRY

SURFACE COORDINATES:

$$\begin{Bmatrix} x^1 \\ x^2 \\ x^3 \end{Bmatrix} = \begin{Bmatrix} \theta \\ Z \\ z \end{Bmatrix}.$$

INCREMENTAL ARC LENGTHS:

$$\begin{Bmatrix} dS_1 \\ dS_2 \\ dS \end{Bmatrix} = \begin{Bmatrix} R d\theta \\ dZ/\cos\alpha \\ \sqrt{(R d\theta)^2 + (dZ/\cos\alpha)^2} \end{Bmatrix}$$

METRIC TENSORS:

$$a_{\alpha\beta} = \begin{bmatrix} R^2 & 0 \\ 0 & \dfrac{1}{\cos^2\alpha} \end{bmatrix} \quad a^{\alpha\beta} = \begin{bmatrix} \dfrac{1}{R^2} & 0 \\ 0 & \cos^2\alpha \end{bmatrix} \quad a = |a_{\alpha\beta}| = \frac{R^2}{\cos^2\alpha}$$

CHRISTOFFEL SYMBOLS:

$$\Gamma^1_{\alpha\beta} = \begin{bmatrix} 0 & -\dfrac{\tan\alpha}{R} \\ -\dfrac{\tan\alpha}{R} & 0 \end{bmatrix}, \quad \Gamma^2_{\alpha\beta} = \begin{bmatrix} R\sin\alpha\cos\alpha & 0 \\ 0 & 0 \end{bmatrix}$$

CURVATURE TENSORS:

$$b_{\alpha\beta} = \begin{bmatrix} -R\cos\alpha & 0 \\ 0 & 0 \end{bmatrix} \quad b^\alpha_\beta = \begin{bmatrix} -\dfrac{\cos\alpha}{R} & 0 \\ 0 & 0 \end{bmatrix}$$

COVARIANT DERIVATIVES OF CURVATURE TENSORS:

$$b_{\alpha\beta}|_1 = \begin{bmatrix} 0 & -\sin\alpha \\ -\sin\alpha & 0 \end{bmatrix}, \quad b_{\alpha\beta}|_2 = \begin{bmatrix} -\sin\alpha & 0 \\ 0 & 0 \end{bmatrix}$$

$$b^\alpha_\beta|_1 = \begin{bmatrix} 0 & -\dfrac{\sin\alpha}{R^2} \\ -\sin\alpha\cos^2\alpha & 0 \end{bmatrix}, \quad b^\alpha_\beta|_2 = \begin{bmatrix} -\dfrac{\sin\alpha}{R^2} & 0 \\ 0 & 0 \end{bmatrix}$$

COORDINATE TRANSFORMATIONS:

$$\begin{Bmatrix} u_\theta \\ u_S \\ u_n \end{Bmatrix} = [T_{SB}] \begin{Bmatrix} u_X \\ u_Y \\ u_Z \end{Bmatrix}, \quad \begin{Bmatrix} u_X \\ u_Y \\ u_Z \end{Bmatrix} = [T_{SB}]^T \begin{Bmatrix} u_\theta \\ u_S \\ u_n \end{Bmatrix}$$

WHERE,

$$[T_{SB}] = \begin{bmatrix} -\sin\theta & \cos\theta & 0 \\ -\sin\alpha\cos\theta & -\sin\alpha\sin\theta & \cos\alpha \\ \cos\alpha\cos\theta & \cos\alpha\sin\theta & \sin\alpha \end{bmatrix}$$

TABLE E.2

SUMMARY OF CYLINDRICAL SHELL GEOMETRY

SURFACE COORDINATES:

$$\begin{Bmatrix} x^1 \\ x^2 \\ x^3 \end{Bmatrix} = \begin{Bmatrix} \theta \\ Z \\ z \end{Bmatrix}$$

INCREMENTAL ARC LENGTHS:

$$\begin{Bmatrix} dS_1 \\ dS_2 \\ dS \end{Bmatrix} = \begin{Bmatrix} Rd\theta \\ dZ \\ \sqrt{(Rd\theta)^2 + (dZ)^2} \end{Bmatrix}$$

METRIC TENSORS:

$$a_{\alpha\beta} = \begin{bmatrix} R^2 & 0 \\ 0 & 1 \end{bmatrix}, \quad a^{\alpha\beta} = \begin{bmatrix} 1/R_2 & 0 \\ 0 & 1 \end{bmatrix}, \quad a = |a_{\alpha\beta}| = R^2$$

CHRISTOFFEL SYMBOLS:

$$\Gamma^1_{\alpha\beta} = \Gamma^2_{\alpha\beta} = \begin{bmatrix} 0 & 0 \\ 0 & 0 \end{bmatrix}$$

CURVATURE TENSORS:

$$b_{\alpha\beta} = \begin{bmatrix} -R & 0 \\ 0 & 0 \end{bmatrix}, \quad b^{\alpha}_{\beta} = \begin{bmatrix} -1/R & 0 \\ 0 & 0 \end{bmatrix}$$

COVARIANT DERIVATIVES OF CURVATURE TENSORS:

$$b_{\alpha\beta}|_1 = b_{\alpha\beta}|_2 = b^{\alpha}_{\beta}|_1 = b^{\alpha}_{\beta}|_2 = \begin{bmatrix} 0 & 0 \\ 0 & 0 \end{bmatrix}$$

COORDINATE TRANSFORMATIONS:

$$\begin{Bmatrix} u_\theta \\ u_Z \\ u_n \end{Bmatrix} = [T_{SB}] \begin{Bmatrix} u_X \\ u_Y \\ u_Z \end{Bmatrix}, \quad \begin{Bmatrix} u_X \\ u_Y \\ u_Z \end{Bmatrix} = [T_{SB}]^T \begin{Bmatrix} u_\theta \\ u_Z \\ u_n \end{Bmatrix}$$

WHERE,

$$[T_{SB}] = \begin{bmatrix} -\sin\theta & \cos\theta & 0 \\ 0 & 0 & 1 \\ \cos\theta & \sin\theta & 0 \end{bmatrix}$$

TABLE E.3

SUMMARY OF SPHERICAL SHELL GEOMETRY

SURFACE COORDINATES:

$$\begin{Bmatrix} x^1 \\ x^2 \\ x^3 \end{Bmatrix} = \begin{Bmatrix} \theta \\ \phi \\ Z \end{Bmatrix}$$

INCREMENTAL ARC LENGTHS:

$$\begin{Bmatrix} dS_1 \\ dS_2 \\ dS \end{Bmatrix} = \begin{Bmatrix} R d\theta \\ R \sin\theta \, d\theta \\ \sqrt{(R d\theta)^2 + (R \sin\theta \, d\phi)^2} \end{Bmatrix}$$

METRIC TENSORS:

$$a_{\alpha\beta} = \begin{bmatrix} R^2 & 0 \\ 0 & R^2 \sin^2\phi \end{bmatrix}, \quad a^{\alpha\beta} = \begin{bmatrix} \frac{1}{R^2} & 0 \\ 0 & \frac{1}{R^2 \sin^2\phi} \end{bmatrix}, \quad a = |a_{\alpha\beta}| = R^4 \sin^2\phi$$

CHRISTOFFEL SYMBOLS:

$$\Gamma^1_{\alpha\beta} = \begin{bmatrix} 0 & 0 \\ 0 & -\sin\theta\cos\theta \end{bmatrix}, \quad \Gamma^2_{\alpha\beta} = \begin{bmatrix} 0 & \cot\theta \\ \cot\theta & 0 \end{bmatrix}$$

CURVATURE TENSORS:

$$b_{\alpha\beta} \doteq \begin{bmatrix} -R & 0 \\ 0 & -R \sin^2\theta \end{bmatrix}, \quad b^{\alpha}_{\beta} = \begin{bmatrix} -\frac{1}{R} & 0 \\ 0 & -\frac{1}{R} \end{bmatrix}$$

COVARIANT DERIVATIVES OF CURVATURE TENSORS:

$$b_{\alpha\beta}|_1 = b_{\alpha\beta}|_2 = b^{\alpha}_{\beta}|_1 = b^{\alpha}_{\beta}|_2 = \begin{bmatrix} 0 & 0 \\ 0 & 0 \end{bmatrix}$$

COORDINATE TRANSFORMATIONS:

$$\begin{Bmatrix} u_\theta \\ u_\phi \\ u_n \end{Bmatrix} = [T_{SB}] \begin{Bmatrix} u_X \\ u_Y \\ u_Z \end{Bmatrix}, \quad \begin{Bmatrix} u_X \\ u_Y \\ u_Z \end{Bmatrix} = [T_{SB}]^T \begin{Bmatrix} u_\theta \\ u_\phi \\ u_n \end{Bmatrix}$$

WHERE,

$$[T_{SB}] = \begin{bmatrix} \cos\theta\cos\phi & \cos\theta\sin\phi & -\sin\theta \\ -\sin\phi & \cos\phi & 0 \\ \sin\theta\cos\phi & \sin\theta\sin\phi & \cos\theta \end{bmatrix}$$

TABLE E.4

SUMMARY OF PLATE GEOMETRY IN POLAR COORDINATES

SURFACE COORDINATES:

$$\begin{Bmatrix} x^1 \\ x^2 \\ x^3 \end{Bmatrix} = \begin{Bmatrix} r \\ \theta \\ z \end{Bmatrix}$$

INCREMENTAL ARC LENGTHS:

$$\begin{Bmatrix} dS_1 \\ dS_2 \\ dS \end{Bmatrix} = \begin{Bmatrix} dR \\ Rd\theta \\ \sqrt{(dR)^2 + (Rd\theta)^2} \end{Bmatrix}$$

METRIC TENSORS:

$$a_{\alpha\beta} = \begin{bmatrix} 1 & 0 \\ 0 & R^2 \end{bmatrix}, \quad a^{\alpha\beta} = \begin{bmatrix} 1 & 0 \\ 0 & \frac{1}{R^2} \end{bmatrix}, \quad a = |a_{\alpha\beta}| = R^2$$

CHRISTOFFEL SYMBOLS:

$$\Gamma^1_{\alpha\beta} = \begin{bmatrix} 0 & 0 \\ 0 & -R \end{bmatrix}, \quad \Gamma^2_{\alpha\beta} = \begin{bmatrix} 0 & \frac{1}{R} \\ \frac{1}{R} & 0 \end{bmatrix}$$

CURVATURE TENSORS:

$$b_{\alpha\beta} = b^{\alpha}_{\beta} = \begin{bmatrix} 0 & 0 \\ 0 & 0 \end{bmatrix}$$

COVARIANT DERIVATIVES OF CURVATURE TENSORS:

$$b_{\alpha\beta}|_1 = b_{\alpha\beta}|_2 = b^{\alpha}_{\beta}|_1 = b^{\alpha}_{\beta}|_2 = \begin{bmatrix} 0 & 0 \\ 0 & 0 \end{bmatrix}$$

COORDINATE TRANSFORMATIONS:

$$\begin{Bmatrix} u_r \\ u_\theta \\ u_n \end{Bmatrix} = [T_{sb}] \begin{Bmatrix} u_X \\ u_Y \\ u_Z \end{Bmatrix}, \quad \begin{Bmatrix} u_X \\ u_Y \\ u_Z \end{Bmatrix} = [T_{SB}]^T \begin{Bmatrix} u_r \\ u_\theta \\ u_n \end{Bmatrix}$$

WHERE,

$$[T_{SB}] = \begin{bmatrix} \cos\theta & \sin\theta & 0 \\ -\sin\theta & \cos\theta & 0 \\ 0 & 0 & 1 \end{bmatrix}$$

TABLE E.5

SUMMARY OF PLATE GEOMETRY IN CARTESIAN COORDINATES

SURFACE COORDINATES:

$$\begin{Bmatrix} x^1 \\ x^2 \\ x^3 \end{Bmatrix} = \begin{Bmatrix} X \\ Y \\ Z \end{Bmatrix}$$

INCREMENTAL ARC LENGTHS:

$$\begin{Bmatrix} dS_1 \\ dS_2 \\ dS \end{Bmatrix} = \begin{Bmatrix} dX \\ dY \\ \sqrt{(dX)^2 + (dY)^2} \end{Bmatrix}$$

METRIC TENSORS:

$$a_{\alpha\beta} = \begin{bmatrix} 1 & 0 \\ 0 & 1 \end{bmatrix}, \quad a^{\alpha\beta} = \begin{bmatrix} 1 & 0 \\ 0 & 1 \end{bmatrix}, \quad a = |a_{\alpha\beta}| = 1$$

CHRISTOFFEL SYMBOLS:

$$\Gamma^1_{\alpha\beta} = \Gamma^2_{\alpha\beta} = \begin{bmatrix} 0 & 0 \\ 0 & 0 \end{bmatrix}$$

CURVATURE TENSORS:

$$b_{\alpha\beta} = b^{\alpha}_{\beta} = \begin{bmatrix} 0 & 0 \\ 0 & 0 \end{bmatrix}$$

COVARIANT DERIVATIVES OF CURVATURE TENSORS:

$$b_{\alpha\beta}|_1 = b_{\alpha\beta}|_2 = b^{\alpha}_{\beta}|_1 = b^{\alpha}_{\beta}|_2 = \begin{bmatrix} 0 & 0 \\ 0 & 0 \end{bmatrix}$$

COORDINATE TRANSFORMATIONS:

$$\begin{Bmatrix} u_X \\ u_Y \\ u_n \end{Bmatrix} = \begin{bmatrix} 1 & 0 & 0 \\ 0 & 1 & 0 \\ 0 & 0 & 1 \end{bmatrix} \begin{Bmatrix} u_X \\ u_Y \\ u_Z \end{Bmatrix}$$

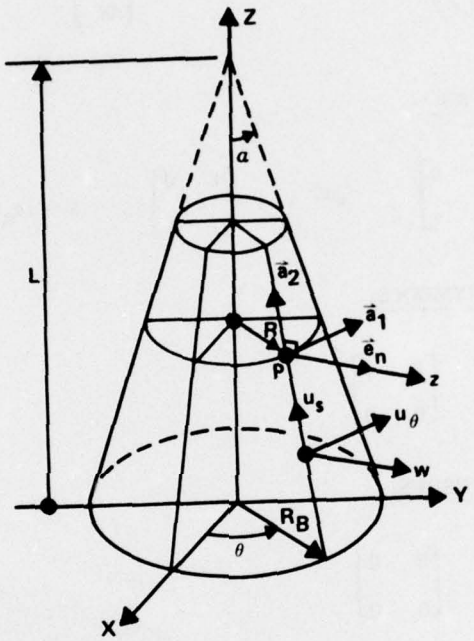


FIGURE E.1 CONICAL REFERENCE SURFACE

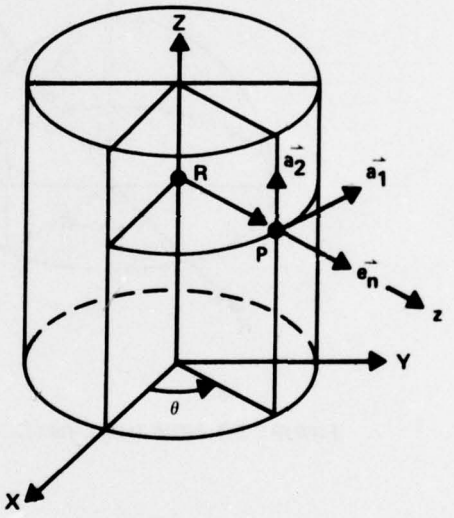


FIGURE E. 2 CYLINDRICAL REFERENCE SURFACE

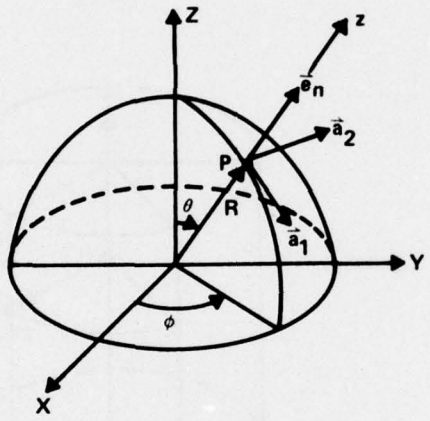


FIGURE E.3 SPHERICAL REFERENCE SURFACE

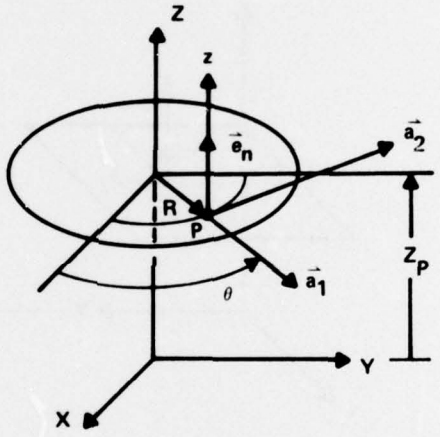


FIGURE E.4 PLATE REFERENCE SURFACE IN POLAR COORDINATES

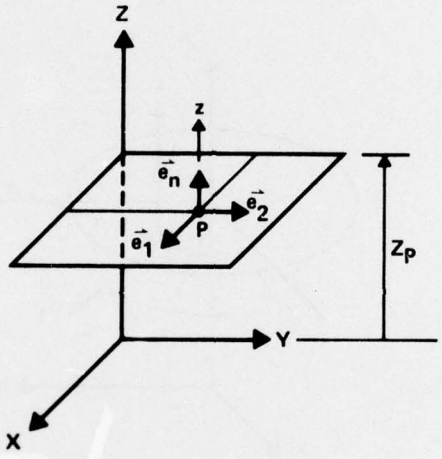


FIGURE E.5 PLATE REFERENCE SURFACE IN CARTESIAN COORDINATES

REFERENCES

1. Melosh, R. J., "Development of the Stiffness Method to Define Bounds on Elastic Behavior of Structures," Ph.D. Thesis, University of Washington, Seattle, Washington, 1962.

2. McLay, R. W., "An Investigation Into the Theory of the Displacement Method of Analysis for Linear Elasticity," Ph.D. Thesis, University of Washington, Seattle, Washington, 1963.

3. Fraejis de Veubeke, B. M., Editor, "Matrix Methods of Structural Analysis," AGARDograph 72, Pergamon Press Limited, Oxford, 1964.

4. Key, S. W., "A Convergence Investigation of the Direct Stiffness Method," Ph.D. Thesis, University of Washington, Seattle, Washington, 1966.

5. Johnson, M. W., Jr. and McLay, R. W., "Convergence of the Finite Element Method in the Theory of Elasticity," J. Applied Mechanics, Ser. E, Vol. 35, No. 2, 1968.

6. Dunne, P. C., "Complete Polynomial Displacement Fields for Finite Element Method," Aeron. J. Roy. Soc., Vol. 72, 1968.

7. Arantes e Oliveira, E. R. de, "Completeness and Convergence in the Finite Element Method," Proc. 2D Conf. Matrix Methods Struct. Mech., AFFDL-TR-68-150, Dec. 1969.

8. Hartung, R. F., "An Assessment of Current Capability for Computer Analysis of Shell Structures," AFFDL-TR-71-54, Apr. 1971.

9. Hartung, R. F. and Ball, R. E., "A Comparison of Several Computer Solutions to Three Structural Shell Analysis Problems," AFFDL-TR-73-15, Apr. 1973.

10. Oden, J. T., "Finite Elements of Non-Linear Continua," McGraw Hill Book Company, New York, 1972.

11. Argyris, J. H. and Kelsey, S., "Energy Theorems and Structural Analysis," Butterworths Scientific Publications, London, 1960.

12. Turner, M. J., Clough, R. W., Martin, H. C. and Topp, L. J., "Stiffness and Deflection Analysis of Complex Structures," J. Aeronaut. Sci., Vol. 23, Sep. 1956.

13. Clough, R. W., "The Finite Element Method in Plane Stress Analysis," J. Structural Division, ASCE, Proceedings of 2nd Conference on Electronic Computation, 1960.

14. Gallagher, R. H., "A Correlation Study of Methods of Matrix Structural Analysis," AGARDograph 69, Pergamon Press Limited, Oxford, 1964.

15. Przemieniecki, J. S., Et.Al., Editors, "Matrix Methods in Structural Mechanics - Proceedings of the Conference Held at Wright-Patterson Air Force Base, Ohio 26-28 October 1965," AFFDL-TR-66-80, Nov. 1966.

16. Berke, L., Et.Al., Editors, "Proceedings of the Second Conference on Matrix Methods in Structural Mechanics," AFFDL-TR-68-150, Dec. 1969.

17. Rowan, W. H. and Hackett, R. M., Editors, "Proceedings of the Symposium on Application of Finite Element Methods in Civil Engineering, Vanderbilt University, November 13-14, 1969," American Society of Civil Engineers, 1969.

18. Fraejis de Veubeke, B. M., Editor, "Proceedings of IUTAM Symposium on High-Speed Computing of Elastic Structures," Liege, Belgium, Aug. 1970.

19. Hartung, R. F., Editor, "Computer Oriented Analysis of Shell Structures - Proceedings of a Conference Held at Lockheed Missiles and Space Company, Palo Alto, California, August 10-14, 1970," AFFDL-TR-71-79, Jun. 1971.

20. Bader, R. M., Et.Al., Editors, "Proceedings of the Third Conference on Matrix Methods in Structural Mechanics," AFFDL-TR-71-160, Dec. 1973.

21. Fenves, S. J., Et.Al., Editors, "Numerical and Computer Methods in Structural Mechanics - Proceedings of the Conference Held at Urbana, Illinois, September 8-10, 1971," Academic Press, Inc., New York, 1973.

22. Pilkey, W., Et.Al., Editors, "Structural Mechanics Computer Programs: Surveys, Assessments and Availability (Proceedings of a Symposium Held at the University of Maryland, June 1974)," University Press of Virginia, Charlottesville, 1974.

23. Zienkiewicz, O. C. and Cheung, Y. K., "The Finite Element Method in Structural and Continuum Mechanics," McGraw Hill Publishing Company Limited, London, 1968.

24. Zienkiewicz, O. C., "The Finite Element Method in Engineering Science," McGraw Hill Publishing Company Limited, London,1971.

25. Oden, J. T., Clough, R. W., and Yamamoto, Y., Editors, "Advances in Computational Methods in Structural Mechanics and Design (Proceedings of 2nd U.S.-Japan Seminar on Matrix Methods of Structural Analysis and Design)," University of Alabama Press, Huntsville, Alabama, 1972.

26. Gallagher, R. H., "Finite Element Analysis: Fundamentals," Prentice-Hall, Inc., Englewood Cliffs, New Jersey, 1974.

27. Fung, Y. C., "Foundations of Solid Mechanics," Prentice Hall, Inc., Englewood Cliffs, New Jersey, 1965.

28. Irons, B. M., "Engineering Application of Numerical Integration in Stiffness Method," AIAA Journal, Nov. 1966.

29. Ergatoudis, I., Irons, B. M. and Zienkiewicz, O. C., "Curved, Isoparametric Quadrilateral Elements for Finite Element Analysis," Int. J. Solids Structures, Vol. 4, 1968.

30. Zienkiewicz, O. C., "Isoparametric and Allied Numerically Integrated Elements - A Review," Numerical and Computer Methods in Structural Mechanics, Academic Press Inc., 1973.

31. Ahmad, S., Irons, B. M. and Zienkiewicz, O. C., "Curved Thick Shell and Membrane Elements with Particular Reference to Axisymmetric Problems," Proc. 2nd. Conf. Matrix Methods Struct. Mech., AFFDL-TR-68-150, Dec. 1969.

32. Ahmad, S., Irons, B. M. and Zienkiewicz, "Analysis of Thick and Thin Shell Structures by Curved Finite Elements," Int. J. Num. Methods in Eng., Vol. 2, 1970.

33. Gallagher, R. H., "Analysis of Plate and Shell Structures," Proc. Symp. Application Finite Element Method in Civil Engr., ASCE, 1969.

34. Gallagher, R. H., "Applications of Finite Element Analysis," Proc. 2nd U.S.-Japan Seminar on Matrix Methods Struct. Anal. and Design, Univ. Alabama Press, Huntsville, 1972.

35. Melosh, R. J. and Christiansen, H. N., "Structural Analysis and Matrix Interpretive System (SAMIS) Program: Technical Report," JPL Technical Memorandum No. 33-311, Nov. 1966.

36. Lang, T. E., "Structural Analysis and Matrix Interpretive System (SAMIS) User Report," JPL Technical Memorandum No. 33-305, Mar. 1967.

37. McNeal, R. H., Editor, "The NASTRAN Theoretical Manual," NASA SP-221(01), Dec. 1972.

38. McCormick, C. W., Editor, "The NASTRAN User's Manual," NASA SP-222(01), Jun. 1972.

39. Batt, J. R. and Jordan, S., "MAGIC III: An Automated General Purpose System for Structural Analysis- Vol. I: Engineer's Manual," AFFDL-TR-72-42, Jul. 1972.

40. Jordan, S., and Batt, J. R., "MAGIC III: An Automated General Purpose System for Structural Analysis- Vol. II: User's Manual," AFFDL-TR-72-42, Jul. 1972.

41. Bathe, K. J. and Wilson, E. L., "Thick Shells," Structural Mechanics Computer Programs: Surveys, Assessments and Availability, University Press of Virginia, Charlottesville, 1974.

42. Pawsey, S. F. and Clough, R. W., "Improved Numerical Integration of Thick Shell Finite Elements," Int. J. Num. Methods in Eng., Vol. 3, 1971.

43. Zienkiewicz, O. C., Taylor, R. L. and Too, J. M., "Reduced Integration Techniques in General Analysis of Plates and Shells," Int. J. Num. Methods in

44. Wilson, E. L., Taylor, R. L., Doherty, W. P. and Ghaboussi, J., "Incompatible Displacement Models," Numerical and Computer Methods in Structural Mechanics," Academic Press, Inc., 1973.

45. Clough, R. W. and Johnson, C. P., "A Finite Element Approximation for the Analysis of Thin Shells," Int. J. of Solids Structures, Vol. 4, 1968.

46. Mebane, P. M. and Stricklin, J. A. "Implicit Rigid Body Motion in Curved Finite Elements," AIAA Journal, Vol. 9, No. 2, Feb. 1971.

47. Fonder, G. and Clough, R. W., "Explicit Addition of Rigid-Body Motions in Curved Finite Elements," AIAA Journal, Vol. 11, No. 3, Mar. 1973.

48. Stanton, E. L., "A Design Study for the Addition of Higher Order Parametric Discrete Elements to NASTRAN," NASA TM X-2637, Sep. 1972.

49. Stanton, E. L. and Palacol, E. L., "Anisotropic Parametric Plate Discrete Elements," McDonnel Douglas Astronautics Co. Paper WD 1656, Mar. 1972.

50. Dawe, D. J., "Curved Finite Elements in the Analysis of Shell Structures," Vol. 5, Part J, Proc. First Int. Conf. on Struct. Mech. in Reactor Technology, Berlin, 1971.

51. Bogner, F., Fox R. and Schmit, L., "A Cylindrical Shell Discrete Element," AIAA Journal, Vol. 5, No. 4, Apr. 1967.

52. Cantin, R. and Clough, R., "A Curved Cylindrical Shell Discrete Element," AIAA Journal, Vol. 6, No. 5, May 1968.

53. Olson, M. and Lindberg, G., "Vibration Analysis of Cantilevered Curved Plates Using a New Cylindrical Shell Finite Element," Proc. 2nd Conf. Matrix Methods Struct. Mech., AFFDL-TR-68-150, Dec. 1969.

54. Yang, T. Y. and Kim, H. W., "Asymmetrical Bending and Vibration of a Conical Shell Finite Element," Purdue Univ. Tech. Report No. 73-5-2, May 1973.

55. Connor, J. and Brebbia, C., "Stiffness Matrix for Shallow Rectangular Shell Element," Proc. ASCE, J. Engr. Mech. Div., No. EM2, Apr. 1968.

56. Bergan, P. G. and Clough, R. W., "Large Deflection Analysis of Plates and Shallow Shells Using the Finite Element Method," Int. J. Num. Methods in Engr., V. 5, 1973.

57. Gallagher, R. H., "The Development and Evaluation of Matrix Methods for Thin Shell Structural Analysis," Ph.D. Thesis, State University of New York, Buffalo, New York, 1966.

58. Gallagher, R. H. and Yang, H., "Elastic Instability Predictions for Doubly Curved Shells," Proc. 2nd. Conf. Matrix Methods Struct. Mech., AFFDL-TR-68-150, Dec. 1969.

59. Greene, B., Jones, R. and Strome, D., "Dynamic Analysis of Shells Using Doubly-Curved Finite Elements," Proc. 2nd Conf. Matrix Methods Struct. Mech., AFFDL-TR-68-150, Dec. 1969.

60. Wempner, G., Oden, J. T. and Kross, D., "Finite Element Analysis of Thin Shells," Proc. ASCE, J. Engr. Mech. Div., No. EM6, Dec. 1968.

61. Key, S. W. and Beisinger, Z., "The Analysis of Thin Shells With Transverse Shear Strains by the Finite Element Method," Proc. 2nd Conf. Matrix Methods Struct. Mech., AFFDL-TR-68-150, Dec. 1969.

62. Key, S. W. and Beisinger, Z. E., "SLADE: A Computer Program for the Static Analysis of Thin Shells," Sandia Laboratories Report No. SC-RR-69-369, Nov. 1970.

63. Jones, R. F., "Shell and Plate Analysis by Finite Elements," Proc. ASCE, J. Struct. Div., No. ST5, May 1973.

64. Utku, S., "Stiffness Matrices for Thin Triangular Elements of Nonzero Gaussian Curvature," AIAA Journal Vol. 5, No. 9, Sep. 1967.

65. Strickland, G. and Loden, W., "A Doubly-Curved Triangular Shell Element," Proc. of 2nd Conf. on Matrix Methods in Struct. Mech., AFFDL-TR-68-150, Dec. 1969.

66. Bonnes, G., Dhatt, G., Giroux, Y. and Robichaud, L., "Curved Triangular Elements for the Analysis of Shells," Proc. of 2nd Conf. on Matrix Methods in Struct. Mech., AFFDL-TR-68-150, Dec. 1969.

67. Cowper, G. R., Lindberg, G. M. and Olson, M., "A Shallow Shell Finite Element of Triangular Shape," Int. J. Solids Structures, Vol. 6, Aug. 1970.

68. Dhatt, G., "Numerical Analysis of Thin Shells by Curved Triangular Elements Based on Discrete-Kirchoff Hypothesis," Proc. Symp. Application Finite Element Methods in Civil Engr.," ASCE, 1969.

69. Argyris, J. H. and Scharpf, D., "The SHEBA Family of Shell Elements for the Matrix Displacement Method," Aeronaut. J., Oct. 1968.

70. Cowper, G. R., Lindberg, G. M. and Olson, M. D., "Comparison of Two High-Precision Triangular Finite Elements for Arbitrary Deep Shells," Proc. 3rd Conf. on Matrix Methods in Struct. Mech., AFFDL-TR-71-160, Dec. 1973.

71. Dupuis, G. and Goel, J., "A Curved Finite Element for Thin Elastic Shells," Int. J. Solids and Structures, Vol. 6, 1970.

72. Thomas, G. and Gallagher, R. H., "A Triangular Thin Shell Finite Element: Linear Analysis," NASA CR-1972.

73. Bushnell, D., "Thin Shells," Structural Mechanics Computer Programs: Surveys, Assessments and Availability, University Press of Virginia, Charlottesville, 1974.

74. Yates, D. N., Sable, W. W. and Vinson, T. J., "The DAISY Code," Numerical and Computer Methods in Structural Mechanics, Academic Press Inc., 1973.

75. Meijers, P., "Review of the ASKA Program," Numerical and Computer Methods in Structural Mechanics, Academic Press, Inc., 1973.

76. Chu, S. L., "Analysis and Design Capabilities of STRUDL Program," Numerical and Computer Methods in Structural Mechanics, Academic Press Inc., 1973.

77. Ayres, D. J., "Elastic-Plastic and Creep Analysis Via the MARC Finite Element Computer Program," Numerical and Computer Methods in Structural Mechanics, Academic Press Inc., 1973.

78. Courant, R., Friedricks, K. and Lewy, H., "On the Partial Difference Equations of Mathematical Physics," Math. Ann., Vol. 100, 1928.

79. Forsythe, G. E. and Wasow, R. W., "Finite-Difference Methods for Partial Differential Equations," John Wiley and Sons, Inc. New York,1960.

80. McNeal, R. H., "An Asymmetrical Finite Difference Network," Quart. Appl. Math., Vol. 11, 1953.

81. Williams, D., "An Introduction to the Theory of Aircraft Structures," Edward Arnold Publishers, Ltd., London, 1960.

82. Griffen, D. S. and Kellogg, R. B., "A Numerical Solution for Axially Symmetrical and Plane Elasticity Problems," Int. J. Solids Structures, Vol. 3, 1967.

83. Havner, K. S. and Stanton, E. L., "On Energy-Derived Difference Equations in Thermal Stress Problems," J. Franklin Inst., Vol. 284, Aug. 1967.

84. Bushnell, D. and Almroth, B. O., "Finite-Difference Energy Method for Nonlinear Shell Analysis," Computer Oriented Analysis of Shell Structures, AFFDL-TR-71-79, Jun. 1971.

85. Almroth, B. O., Brogan, F. A. and Pittner, E. V., "Buckling Analysis of Segmental Orthotropic Cylinders Under Nonuniform Stress Distribution," Lockheed Missiles and Space Company Report M-77-65-4, Vol. VIII, Jul. 1965.

86. Almroth, B. O. and Brogan, F. A., "Buckling of Cylinders with Cutouts," AIAA Journal, Vol. 8, No. 2, Feb. 1970.

87. Brogan, F. A., Forsberg, K. and Smith, S., "Experimental and Analytical Investigation of the Dynamic Behavior of a Cylinder with a Cutout " AIAA Paper No. 68-318, AIAA/ASME 9th Structures, Structural Dynamics and Materials Conference, Apr. 1968.

88. Brogan, F. A. and Stern, P., "Analysis of Stiffened Shells with Cutouts," Lockheed Missiles and Space Company Report N-3M-69-1, 1969.

89. Almroth, B. O., Brogan, F. A. and Marlowe, M. B., "Collapse Analysis for Elliptic Cones," AIAA Journal, Vol. 9, Jan. 1971.

90. Almroth, B. O., Brogan, F. A. and Zele, F., "Nosetip Design Analysis and Test (NDAT) Program-User's Manual for the STAGS Computer Code," SAMSO-TR-71-95, Dec. 1970.

91. Almroth, B. O., Brogan, F. A., Meller, E. and Zele, F., "User's Manual for the STAGS Computer Code," Lockheed Missiles and Space Company Report D266611, Apr. 1972.

92. Almroth, B. O., Brogan, F. A. and Marlowe, M. B., "Collapse Analysis for Shells of General Shape, Volume I: Analysis," AFFDL-TR-71-8, Vol. I, Aug. 1972.

93. Almroth, B. O., Brogan, F. A., Meller, E., Zele, F. and Petersen, H. T., "Collapse Analysis for Shells of General Shape, Volume II: User's Manual for the STAGS-A Computer Code," AFFDL-TR-71-8, Vol. II, Mar. 1973.

94. Brogan, F. A. and Almroth, B. O., "Practical Methods for Elastic Collapse Analysis for Shell Structures," AIAA Paper No. 71-359, AIAA/ASME 12th Structures, Structural Dynamic and Materials, Conference, Apr. 1971.

95. Almroth, B. O. and Brogan, F. A., "Bifurcation Buckling as an Approximation of the Collapse Load for General Shells," AIAA Journal Vol. 10, Apr. 1972.

96. Almroth, B. O., Brogan, F. A. and Marlowe, M. B., "Stability Analysis of Cylinders with Circular Cutouts," AIAA Journal, Vol. 11, Nov. 1973.

97. Almroth, B. O. and Felippa, C. A., "Structural Stability," Structural Mechanics Computer Programs: Surveys, Assessments and Availability, University Press of Virginia, Charlottesville, 1974.

98. Almroth, B. O., Bushnell, D. and Sobel, L. H., "Buckling of Shells of Revolution with Various Wall Constructions, Vol. 1 - Numerical Results," NASA CR-1049, May 1968.

99. Bushnell, D., Almroth, B. O. and Sobel, L. H., "Buckling of Shells of Revolution with Various Wall Constructions, Vol. 2 - Basic Equations and Method of Solution," NASA CR-1050, May 1968.

100. Bushnell, D., Almroth, B. O. and Sobel, L. H., "Buckling of Shells of Revolution with Various Wall Constructions, Vol. 3-User's Manual for BOSOR," NASA CR-1051, May 1968.

101. Almroth, B. O. and Bushnell, D., "Computer Analysis of Various Shells of Revolution," AIAA Journal, Vol. 6, Oct. 1968.

102. Bushnell, D., "Nonlinear Analysis for Axisymmetric Elastic Stresses in Ring-Stiffened, Segmented Shells of Revolution," Proc. AIAA/ASME 10th Structures, Structural Dynamics and Materials Conference, New Orleans, Louisiana, Apr. 1969

103. Bushnell, D., "Analysis of Buckling and Vibration of Ring-Stiffened, Segmented Shells of Revolution," Int. Journal Solids Structures, Vol. 6, 1970.

104. Bushnell, D., "Stress, Buckling and Vibration of Prismatic Shells," AIAA Journal, Vol. 9, Oct. 1971.

105. Bushnell, D., "Analysis of Complex Shells of Revolution Under Combined Mechanical and Thermal Loads," AIAA Journal, Vol. 9 Mar. 1971.

106. Bushnell, D., "Stress, Stability and Vibration of Complex Branched Shells of Revolution: Analysis and User's Manual for BOSOR4," Lockheed Missiles and Space Company Report D243605, Mar. 1972.

107. Bushnell, D., "Effect of Ring Out-of-Plane Bending Stiffness on Thermal Buckling Prediction for Ring-Stiffened Cylinders," AIAA Journal, Vol. 9, Aug. 1972.

108. Bushnell, D., "Nonsymmetric Buckling of Cylinders with Axisymmetric Thermal Discontinuities," AIAA Journal, Vol. 11, Sep. 1973.

109. Bushnell, D., "Evaluation of Various Analytical Models for Buckling and Vibration of Stiffened Shells," AIAA Journal, Vol. 11, Sep. 1973.

110. Johnson, D. E., "A Difference-Based Variational Method for Shells," Int. Journal Solids Structures, Vol. 6, 1970.

111. Jensen, P. S., "Finite Difference Techniques for Variable Grids," Computer Oriented Analysis of Shell Structures, AFFDL-TR-71-79, Jun. 1971.

112. Forsberg, K. J., "An Evaluation of Finite Difference and Finite Element Techniques for Analysis of General Shells," Proc. IUTAM Conf. on High Speed Computing of Elastic Structures, Liege, Belgium, Aug. 1970.

113. Loden, W. A., "User's Manual for the REXBAT Program," Lockheed Missiles and Space Company Report 6-80-70-24, Aug. 1970.

114. Bushnell, D., "Finite Difference Energy Models Versus Finite Element Models: Two Variational Approaches in One Computer Program," Numerical and Computer Methods in Structural Mechanics," Academic Press Inc., 1973.

115. Green, A. E. and Zerna, W., "Theoretical Elasticity," Clarendon Press, Oxford, 1954.

116. Sokolnikoff, I. S., "Tensor Analysis, Theory and Applications to Geometry and Mechanics of Continua," John Wiley and Sons, Inc., New York, 1951.

117. Sanders, J. L., Jr., "Nonlinear Theories for Thin Shells," Harvard University Technical Report No. 10, Feb. 1961.

118. Oden, J. T., "Calculation of Stiffness Matrices for Finite Elements of Thin Shells of Arbitrary Shape," AIAA Journal, May 1968.

119. Langhaar, H. L., "Energy Methods in Applied Mechanics," John Wiley and Sons, Inc., New York, 1962.

120. Zudans, Z., "New Formulation and Evaluation of Elastic Shell Theory," Ph.D. Thesis, University of Pennsylvania, Philadelphia, Pennsylvania, 1966.

121. Reuter, R. C., Jr., "Concise Property Transformation Relations for an Anisotropic Lamina," J. Composite Materials, Apr. 1971.

122. Rivello, R. M., "Theory and Analysis of Flight Structures," McGraw Hill Book Company, New York, 1969.

123. Archer, J. S., "Consistent Mass Matrix for Distributed Mass Systems," Proc. ASCE, Vol. 89, Aug. 1963.

124. Timoshenko, S. and Goodier, J. N., "Theory of Elasticity," McGraw-Hill Book Company, New York, 1951.

125. Clough, R. W. and Tocher, J. L., "Finite Element Stiffness Matrices for Analysis of Plate Bending," Matrix Methods in Structural Mechanics, AFFDL-TR-66-80, Nov. 1966.

126. Rai, I. S. and Sandhu, R. S., "Finite Element Analysis of Anisotropic Plates Using Q-19 Element," AFFDL-TR-74-120, Part I, Oct. 1974

127. Clough, R. W. and Fellippa, C. A., "A Refined Quadrilateral Element for Analysis of Plate Bending," 2D Conf. Matrix Methods Struct. Mech., AFFDL-TR-68-150, Dec. 1969.

128. Timoshenko, S. and Woinowsky-Krieger, S., "Theory of Plates and Shells," McGraw-Hill Book Company, New York, 1959.

129. Lekhnitski, S. G., "Anisotropic Plates," Gordon and Breach, Science Publishers, New York, 1968.

130. Fortier, R. C., "A Study Into the Behavior of Unsymmetrically Layered Anisotropic Plates," Ph.D. Thesis, Northeastern University, Boston, Massachusetts, 1972

131. Gilliam, P. "Thermal Stresses in an Orthotropic, Nonhomogeneous Thin Shell of Revolution," TRW Inc., Informal Technical Memorandum, Mar. 1972.

132. Van Dyke, P., "Stresses About a Circular Hole in a Cylindrical Shell," AIAA Journal, Vol. 3, No. 9, Sep. 1965.

133. Lekkerkerker, J. G., "Stress Concentration Around Circular Holes in Cylindrical Shells," Proc. Eleventh Int. Congress Applied Mechanics, Springer-Verlag, Berlin, 1964.

DISTRIBUTION LIST

	Copies
AVCO Corporation 201 Lowell Street Wilmington, Massachusetts 01887	
Attn: Dr. D. E. Johnson	1
Dr. A. A. Pallone	1
Advanced Ballistic Missile Defense Agency Commonwealth Building 1300 Wilson Boulevard Arlington, Virginia 22209	
Attn: Mr. V. Kupelian	1
Aeronautical Research Associates of Princeton, Inc. 50 Washington Road Princeton, New Jersey 08540	
Attn: Dr. T. McDonough	1
Aerospace Corporation P.O. Box 92957 Los Angeles, California 90009	
Attn: Mr. D. Geiler	1
Mr. R. Hallse	1
Mr. J. McClelland	1
Dr. E. Meyer	1
Mr. R. Mortensen	1
Army Ballistic Research Laboratories Aberdeen Proving Ground, Maryland 21005	
Attn: Dr. W. J. Gillich	1
Dr. N. J. Huffington, Jr.	1
Mr. E. Quigley	1
Army Materials and Mechanics Research Center Watertown, Massachusetts 92172	
Attn: Mr. J. F. Dignam	1
Aerotherm-Acurex Corporation 485 Clyde Avenue Mountain View, California 94040	
Attn: Dr. D. Baker	1
Air Force Flight Dynamics Laboratory Wright Patterson Air Force Base, Ohio 45433	
Attn: Mr. R. Bader	1
MR. J. Johnson	1

Air Force Materials Laboratory
Wright-Patterson Air Force Base, Ohio 45433
Attn: Mr. T. Cooper (MXA) 1
Dr. W. Kessler (MBC) 1
Mr. C. Pratt (MXS) 1
Mr. D. Schmidt (MBC) 1

Air Force Office of Scientific Research
Building 410
Bolling Air Force Base, Washington, D.C. 20332
Attn: Mr. W. J. Walker 1

Air Force Weapons Laboratory
Kirtland Air Force Base
Albuquerque, New Mexico 87117
Attn: LTCOL D. Ericson 1

Battelle Columbus Laboratories
505 King Avenue
Columbus, Ohio 43201
Attn: Dr. M. Lemcoe 1
Dr. H. D. Moran 1
Mr. B. R. Noton 1

Office of the Chief of Naval Operations
Department of the Navy
Washington, D. C. 20350
Attn: Mr. R. Blaise (OP-620E) 1

Office of the Chief of Naval Research
800 North Quincy Street
Arlington, Virginia 22217
Attn: Dr. N. Perrone (Code 439) 1

Office of the Chief of Research and Development
Department of the Army
Washington, D. C. 20310
Attn: Dr. J. Bryant (DARS-ARS-PM) 1

Defense Documentation Center
Cameron Station
Alexandria, Virginia 22314 12

Director, Defense Nuclear Agency
Washington, D. C. 20305
Attn: Mr. J. Moulton 1

Effects Technology, Inc.
P.O. Box 30400
5383 Hollister Avenue
Santa Barbara, California 93105
Attn: Mr. J. Green 1
Dr. R. F. Parisse 1

Embassy of Australia
1601 Massachusetts Avenue
Washington, D. C. 20036
Attn: Dr. G. A. Morgan 1

General Electric Company
Re-entry & Environment Systems Division
Valley Forge Space Center
P.O. Box 8555
Philadelphia, Pennsylvania 19101
Attn: Mr. A. Garber 1
Mr. H. R. Minnich 1

ITT Research Institute
10 West 35th Street
Chicago, Illinois 60616
Attn: Mr. S. Bortz 1

The Johns Hopkins University
Applied Physics Laboratory
8621 Georgia Avenue
Silver Spring, Maryland 20910
Attn: Mr. W. Caywood 1
Mr. R. M. Rivello 1

Kaman Sciences Corporation
1700 Garden of the Gods Road
Colorado Springs, Colorado 80907
Attn: Mr. F. Barberra 1

Lockheed Missiles & Space Company, Inc.
3251 Hanover Street
Palo Alto, California 94304
Attn: Dr. D. Bushnell 1
Dr. R. F. Hartung 1

Lockheed Missiles & Space Company, Inc.
P.O. Box 504
1111 Lockheed Way
Sunnyvale, California 94088
Attn: Mr. A. Mietz 1
Mr. R. Teter 1

Los Alamos Scientific Laboratory
Los Alamos, New Mexico 87544
Attn: Dr. J. Taylor 1

Martin-Marietta Corporation
Orlando Division
P.O. Box 5837
Orlando, Florida 32805
Attn: Mr. G. Fotieo 1
Mr. L. Kinnaird 1

Materials Sciences Corporation
Blue Bell Office Campus
Merion Towle Building
Blue Bell, Pennsylvania 19422
Attn: Dr. W. Rosen 1

McDonnell Douglas Astronautics Company
5301 Bolsa Avenue
Huntington Beach, California 92647
Attn: Mr. L. Greszczuk 1
Mr. J. Jortner 1
Dr. J. C. Peck 1
Dr. R. Reck 1
Mr. F. Stone 1

McDonnell Douglas Astronautics Company
1136 Washington Boulevard
St. Louis, Missouri 63166
Attn: Mr. R. L. Johnson 1

NASA Goddard Space Flight Center
Greenbelt, Maryland
Attn: Dr. J. B. Mason 1
Dr. W. Case 1

NASA Langley Research Center
Hampton, Virginia 23665
Attn: Dr. R. Anderson (MS-188) 1
Dr. P. Cooper (MS-208) 1
Dr. A. K. Noor (MS-362) 1
Dr. J. P. Raney 1
Mr. W. B. Stephens (MS-190) 1
Dr. D. Weidman (MS-188C) 1

National Aeronautics and Space Administration
Scientific and Technical Information Facility
P.O. Box 33
College Park, Maryland 20740 1

Commander, Naval Air Systems Command
Department of the Navy
Washington, D. C. 20361
Attn: Mr. W. Volz (AIR-320C) 1

Director, Naval Research Laboratory
Washington, D. C. 20375
Attn: Dr. P. Mast 1
Dr. I. Wolock 1

Commander
Naval Air Development Center
Warminster, Pennsylvania 18974
Attn: Dr. T. Hess 1
Dr. S. L. Huang 1
Dr. R. K. Lobb 1
Mr. T. Neu 1

Commander
David W. Taylor Naval Ship Research &
Development Center
Bethesda, Maryland 20034
Attn: Dr. B. Cuthill 1
Dr. G. Everstine 1
Mr. M. Hurwitz 1
Dr. R. F. Jones 1
Mr. J. McKee 1
Mr. P. Matula 1

Chief of Naval Material
Department of the Navy
Arlington, Virginia 20360
Attn: Dr. R. Allgier (MAT-0321 1
Mr. S. Jacobson (MAT-03422) 1

Naval Postgraduate School
Monterey, California 93940
Attn: Dr. R. Ball 1

Commander
Naval Weapons Center
China Lake, California 93557
Attn: Mr. E. L. Jeter 1
Mr. J. Serpanos 1

Commander, Naval Sea Systems Command
Department of the Navy
Washington, D. C. 20362
Attn: Mr. M. Kinna (SEA-0352) 1
Mr. S. Marcus (SEA-03B0 1
Mr. L. Pasiuk (SEA-03513) 1
Mr. G. Sorkin (SEA-035) 1

Commander
Naval Underwater Systems Center
New London, Connecticut 06320
Attn: Mr. A. Carlson 1

Nuclear Regulatory Commission
7920 Norfolk Avenue
Bethesda, Maryland 20014
Attn: Dr. S. Klein (LMFBR) 1

Oak Ridge National Laboratory
P.O. Box X
Oak Ridge, Tennessee 37830
Attn: Dr. W. P. Eatherly 1

Philco-Ford Corporation
Aeronutronic Division
Ford Road
Newport Beach, California 92663
Attn: Mr. W. Smallwood 1

Prototype Development Associates, Inc.
1740 Garry Avenue, Suite 201
Santa Ana, California 92705
Attn: Dr. J.G. Crose 1
Dr. J. McDonald 1
Dr. D. McGovern 1
Mr. J. Schutzler 1
Dr. E. Stanton 1

R & D Associates
525 Wilshire Boulevard
Santa Monica, California 90403
Attn: Dr. A. Field 1

Sandia Laboratories
P.O. Box 5800
Albuquerque, New Mexico 87115
Attn: Dr. S. Key 1
Dr. T. G. Priddy 1

SMU Institute of Technology
Civil and Mechanical Engineering Dept.
Dallas, Texas 75275
Attn: Dr. R. M. Jones 1

Office of the Secretary of Defense
Director of Defense Research & Engineering
Pentagon
Washington, D. C. 20301
Attn: Mr. J. Persh (OAD/ET) 1

Director, Strategic Systems Project Office (PM-1)
Department of the Navy
Washington, D. C. 20376
Attn: SP-272 1

Southern Research Institute
2000 Ninth Avenue, South
Birmingham, Alabama 35205
Attn: Mr. J. Koenig 1
Dr. C. D. Pears 1

Space & Missile System Organization
Worldway Postal Center
P.O. Box 92960
Los Angeles, California 90045
Attn: MAJ L. Hudak 1
MAJ J. McCormack 1

Project Manager, Trident Systems Project (CNM-PM2)
Department of the Navy
Washington, D. C. 20360
Attn: Mr. J. L. Crone (PM-2-001) 1

TRW Systems Group
One Space Park Boulevard
Redondo Beach, California 90200
Attn: Mr. J. Bird 1
Mr. A. Hausrath 1
Mr. R. Winje 1

University of California at Los Angeles
Mechanics and Structures Department
Los Angeles, California 90024
Attn: Dr. S. B. Dong 1

University of Delaware
Mechanical and Aerospace Engineering Dept.
Newark, Delaware 19711
Attn: Dr. J. R. Vinson 1

University of Maryland
College Park, Maryland
Attn: Dr. B. Berger (ENME) 1
Dr. P. Cuniff (ENME) 1
Dr. B. Donaldson (ENAE) 1
Dr. W. Fourney (ENME) 1
Dr. C. Heins (ENCE) 1
Dr. H. G. Schaeffer (ENAE) 1
Dr. W. Walston (ENME) 1
Dr. W. B. Widhelm (BSAD) 1
Dr. J. Yang (ENME) 1

Weiler Research, Inc.
2672 Bayshore Frontage Road, Suite 524
Mountain View, California 94040
Attn: Dr. F. Weiler 1

NDW-NSWC(W)-5605/1 (Rev. 1-75)

TO AID IN UPDATING THE DISTRIBUTION LIST FOR NAVAL SURFACE WEAPONS CENTER, WHITE OAK LABORATORY TECHNICAL REPORTS PLEASE COMPLETE THE FORM BELOW:

TO ALL HOLDERS OF NSWC/WOL/TR 76-66
by R. J. Edwards, Code WA-21

DO NOT RETURN THIS FORM IF ALL INFORMATION IS CURRENT

A. FACILITY NAME AND ADDRESS *(OLD) (Show Zip Code)*

NEW ADDRESS *(Show Zip Code)*

B. ATTENTION LINE ADDRESSES:

C.

☐ REMOVE THIS FACILITY FROM THE DISTRIBUTION LIST FOR TECHNICAL REPORTS ON THIS SUBJECT.

D.
NUMBER OF COPIES DESIRED _____

GPO 885-970

DEPARTMENT OF THE NAVY
NAVAL SURFACE WEAPONS CENTER
WHITE OAK, SILVER SPRING, MD. 20910

OFFICIAL BUSINESS
PENALTY FOR PRIVATE USE, $300

POSTAGE AND FEES PAID
DEPARTMENT OF THE NAVY
DOD 316

COMMANDER
NAVAL SURFACE WEAPONS CENTER
WHITE OAK, SILVER SPRING, MARYLAND 20910

ATTENTION: CODE WA-21